TRENDS IN STREAMFLOW FROM OLD GROWTH FORESTED WATERSHEDS IN THE WESTERN CASCADES

by

Kathleen M. Moore

A RESEARCH PAPER

submitted to

THE GEOSCIENCES DEPARTMENT

in partial fulfillment of the
requirements for the
degree of

MASTER OF SCIENCE

GEOGRAPHY PROGRAM

May 2010

Directed by
Dr. J. A. Jones

Acknowledgements

I thank my advisor Julia Jones for her excellent direction, encouragement, and constant support. I thank my committee members Barbara Bond and Chris Daly for their help and guidance. I would like to express special thanks to Chris Thomas for sharing his wavelet analysis program with me and teaching me the basics of Matlab. I am also grateful to Jay Alder for his assistance with Fortran, as well as his help with formatting. Finally, I thank my fiancé Evan for his help with Matlab programming, editing, and most importantly his support and patience.

Table of Contents

Table of Figures

List of Tables

TRENDS IN STREAMFLOW FROM OLD GROWTH FORESTED WATERSHEDS IN THE WESTERN CASCADES

Increasing temperatures in western North America are expected to result in a decline in winter snowpacks, earlier snowmelt, and a shift in the timing of streamflows, with an increasing fraction of streamflows occurring earlier in the water year and drier conditions during the summer. However, few streamflow datasets have associated climate and vegetation records adequate to interpret changes in climate, forest processes, and their consequences for streamflows. This study examined long-term streamflow records from three headwater watersheds in old growth forest at the H. J. Andrews Experimental Forest, Oregon, to seek evidence of trends and investigate possible explanations for these changes. The three small (8.5-60 ha) watersheds (WS2, WS8, and WS9) range in elevation from 432-1182 m and have streamflow records dating back to 1953, 1964, and 1969 respectively. Spring and summer average minimum temperatures have increased over the study period, while April 1st SWE at Santiam Junction has declined significantly. Although precipitation has remained unchanged over the period of study, runoff ratios have declined in spring (March through May) at rates ranging from 25.4% (WS2) to 41.2% (WS8) over the 40- to 50-year periods of streamflow record. Total declines in spring runoff equate to 1.13, 2.13, and 1.23 mm day-1 at WS2, WS8, and WS9, respectively. However, neither winter nor summer runoff ratios have changed significantly, nor has there been a significant shift in the date of water year median flow over the period of record. Winter and spring runoff ratios are negatively related to vapor pressure deficit and/or temperature in the corresponding season, while summer runoff

ratios are positively related to vapor pressure deficit and/or temperature. Overall, the findings of this study most strongly support the hypothesis that warming temperatures have resulted in a reduction in spring snowpacks, with an earlier onset of evapotranspiration in the spring and a reduction in evapotranspiration during the summer, due to stomatal closure when VPD becomes sufficiently large or soil moisture becomes limited.

1. Introduction

In the Pacific Northwest, where the majority of precipitation falls during the winter, mountain snowpacks provide an important source of streamflow during the dry summer months when water demands are frequently highest. Snowmelt-derived streamflow constitutes 50-80% of annual streamflows in snowmelt-dominated watersheds across Washington, Oregon, and California (Stewart et al., 2005). Increasing temperatures associated with climate change are expected to result in a decline in winter snowpacks in western North America, earlier snowmelt, and subsequently a shift in the timing of streamflows, with an increasing fraction of streamflows occurring earlier in the water year and drier conditions during the summer (Figure 1.1, Barnett et al 2008).

Winter and spring air temperatures have increased across western North America over the last half century (Figure 1.1a, Mote 2005 et al., Knowles et al. 2006, Hamlet et al. 2007). November-March air temperatures have increased at a rate of 1.6°C per century over the period 1950-1997 in western North America (Mote et al., 2005). Air temperature over the entire western U.S. increased by approximately 1°C per century for the period from 1916-2003 and approximately 2°C for the period from 1947-2003 (Hamlet et al. 2007). The greatest temperature increases occurred in January-March, and minimum temperatures have risen faster than maximum temperatures (Hamlet et al. 2007).

Long-term trends in precipitation have been more variable and less robust than those in air temperature (Figure 1.1b, Mote et al. 2005, Hamlet et al. 2007). Precipitation generally increased across western North America from 1916-2003, but precipitation declined in the Pacific Northwest from 1947-2003 (Hamlet et al. 2007). Mote et al.

(2005) also found that precipitation has mostly declined in the western parts of Oregon, Washington, and British Columbia over the past half century. Interannual precipitation variability has however increased across the western U.S. since 1973 (Hamlet et al, 2007).

Peak (April 1st) snow water equivalent (SWE) has declined sharply across the western U.S. over the past half century (Figure 1.1c, Mote 2003, Mote et al. 2005, Mote 2006). Increasing winter and spring air temperatures reduce spring SWE both by increasing the frequency of winter daily melt events (Mote et al. 2005) and increasing the ratio of precipitation falling as rain: snow in winter (Knowles et al. 2006). Three-quarters of cooperative weather station sites in the western United States show a decline in the fraction of precipitation falling as snow over the period from 1949-2004, and the greatest declines have occurred in relatively warm, low to moderate elevations (Knowles et al. 2006). SWE has declined most in March in western North America and in January near the West Coast, corresponding to warming during those months. This highlights the particular vulnerability of regions where snow accumulates close to the melting point (Regonda et al. 2005, Nolin and Daly, 2006).

These changes in air temperature, precipitation, and snowpacks have led to, or are expected to lead to, changes in streamflow hydrographs (Figure 1.1d). As spring snowpacks have declined, the timing of snowmelt-derived streamflow has shifted to earlier in the water year (Dettinger and Cayan 1995, Cayan et al. 2001, Regonda et al. 2005, Steward et al. 2005, Hamlet et al. 2007, Barnett et al. 2008, Jefferson et al, 2008). Across western North America streamflow timing is earlier in the water year by 1-4 weeks over the period from 1948-2002 (Stewart et al. 2005). Specific to the Pacific

Northwest, there have been large increases in March streamflows, and decreases in May and June (Regonda et al. 2005). Within the McKenzie river drainage, summer recessions are lasting 17days longer due to a shift in the hydrograph (Jefferson et al. 2008). The shift toward earlier snowmelt derived streamflow in the western United States occurred as a step change during the mid-1980's, which is related to a step increase in April-July temperatures over the same period (McCabe et al. 2005). While there has been an emphasis on the shift in timing of snowmelt derived streamflow, there has also evidence of increased variability in annual streamflows. Over the period from 1948-2006, streamflows in the Pacific Northwest during the driest (lowest streamflow) 25% of years show significant declines over time (Luce and Holden 2009).

Although precipitation and snow storage are major controls on streamflow, evapotranspiration also is a key factor in the water balance:

$$Q = P - ET - \Delta S \qquad (1)$$

where Q = streamflow, P = precipitation, ET = evapotranspiration, and ΔS is the change storage (which includes groundwater, soil moisture, snow and vegetation canopy). Few studies have investigated changes in evapotranspiration with climate warming and the subsequent effects on streamflow. Streamflow from forests provides two-thirds of the clean water supply in the United States (National Research Council, 2008), and forests cover about one-third of the Earth's land area, accounting for over two-thirds of terrestrial plant leaf area (Bond et al, 2007). Paired watershed experiments have shown the influence of vegetation on streamflow (Post and Jones, 2004), and in temperate regions evapotranspiration constitutes a large portion of the water budget in forested watersheds (Hewlett, 1982).

Transpiration is driven principally by photosynthetically active radiation, because stomata open in response to radiation incident upon a leaf surface up to a saturation level (Taiz and Zeiger, 1991, Bond et al, 2007). When radiation is not limited, vapor pressure deficit (VDP) is expected to be the most important atmospheric variable influencing transpiration (Unsworth et al, 2004, Chen et al, 2004). Transpiration can be expressed as:

$$E = g_{(leaf)} * VPD * LAI \qquad (2)$$

where, E is whole tree transpiration, $g_{(leaf)}$ is leaf-averaged stomatal conductance of water vapor, and LAI is the leaf area index for the forest stand (Whitehead, 1998, B. Bond, unpublished). This equation expresses transpiration as a function of water demand via VPD. Transpiration can also be expressed as a function of water supply or water flux from the soil to the leaves:

$$E = K * (\Psi_{(soil)} - \Psi_{(leaf)} - hpg) \quad (3)$$

where, K is average conductance from the soil to the leaves, $\Psi_{(soil)} - \Psi_{(leaf)}$ is the difference in average water potential from the soil to the leaves, and hpg is the average gravitational pull on the water column at a height h and a density p (Whitehead, 1998). By combining equations 2 and 3 and dividing by leaf area it can be shown that stomatal conductance is inversely related to VPD:

$$g_{(leaf)} = [K_L * (\Psi_{(soil)} - \Psi_{(leaf)} - hpg)] / VDP \qquad (4)$$

where, K_L is the average conductance for the whole tree from the soil to the leaves per unit leaf area. Isohydric species, such as Douglas-fir, further control stomata to prevent leaf water potential from dropping below a species-specific minimum. Thus transpiration levels off or even declines as stomata close with increasing VPD once leaf water potential

reaches its minimum (Tyree and Sperry, 1988, Bond and Kavanagh 1999, Bond et al, 2007). Transpiration in Douglas-fir forests is also controlled by soil moisture availability. As soil moisture becomes limited, transpiration is reduced (Unsworth et al 2004, Barnard, 2009).

In a warming climate with a shift towards earlier snowmelt and soil moisture recharge, it is anticipated that there will be a corresponding shift in the seasonal timing of evapotranspiration, with increases in the spring and decreases in the summer (Hamlet et al. 2007, Tague et al. 2009). Earlier water availability in the spring, and increased stomatal closure during the summer caused by rising vapor pressure deficits and decreased soil moisture, will contribute to this shift in timing of evapotranspiration (Law et al. 2000, Royce and Barbour 2001, Hamlet et al. 2007, Tague et al. 2009). Forests may be experiencing increased moisture stress: warming temperatures may be responsible for observed changes in tree mortality and growth in the western United States. Mantgem et al. (2009) found that mortality rates in old growth forests across the region have increased in recent decades without corresponding increases in recruitment, and attributed the finding to increased water deficits with climate warming. In general, trees growing in areas previously limited by moisture availability during the growing season are expected to decrease in productivity with climate warming, whereas trees in areas previously limited by low temperatures may have increased productivity (Nakawatase et al. 2006, Littell et al. 2008, Black et al. 2009,). This implies that overall evapotranspiration will decrease for lower elevations (where summer soil moisture availability is more likely to be limiting), but increase for higher elevations (where

growing season temperature is more likely to be the limiting factor) with climate warming (e.g. Tague et al 2009).

The purpose of this study is to examine trends in climate and streamflow at three old-growth watersheds in the western Cascades over the last half-century, to determine (1) how observed trends in these small watersheds compare to increased temperatures, declines in winter snowpacks, earlier snowmelt, and a shift in the timing of streamflows predicted for the Pacific Northwest region, and (2) the extent to which forest ecosystems appear to be responding to climate trends via changes in evapotranspiration. This study tests for trends in precipitation but examines two alternative hypotheses that both assume no change in precipitation. The first hypothesis predicts that the hydrologic response to climate change will be dominated by physical processes (i.e. there will be no changes in evapotranspiration).

(H1) Increased winter temperatures will lead to:

- (a) an increase in the winter runoff ratio resulting from an increase in winter snow melt events and an increase in the amount of winter precipitation falling as rain rather than snow.
- (b) a decrease in the winter runoff ratio resulting from higher evaporation due to longer dry intervals, increased variability in winter precipitation, and/or increased wind speeds.
- (c) a decline in April 1st SWE resulting from an increase in winter snow melt events and/or a decrease in the ratio of snow to rain winter precipitation.
- (d) a decrease in both the spring and summer runoff ratio resulting from a decline in April 1st SWE.

However, forest ecosystems may respond to climate trends by altering evapotranspiration.

(H2) Increased vapor pressure deficits will lead to:

- (a) a decrease in the winter runoff ratio as a result of increased evapotranspiration in the winter.
- (b) a decrease in the spring runoff ratio as a result of increased evapotranspiration in the spring.
- (c) an increase in the summer runoff ratio as a result of decreased evapotranspiration in the summer due to stomatal closure.

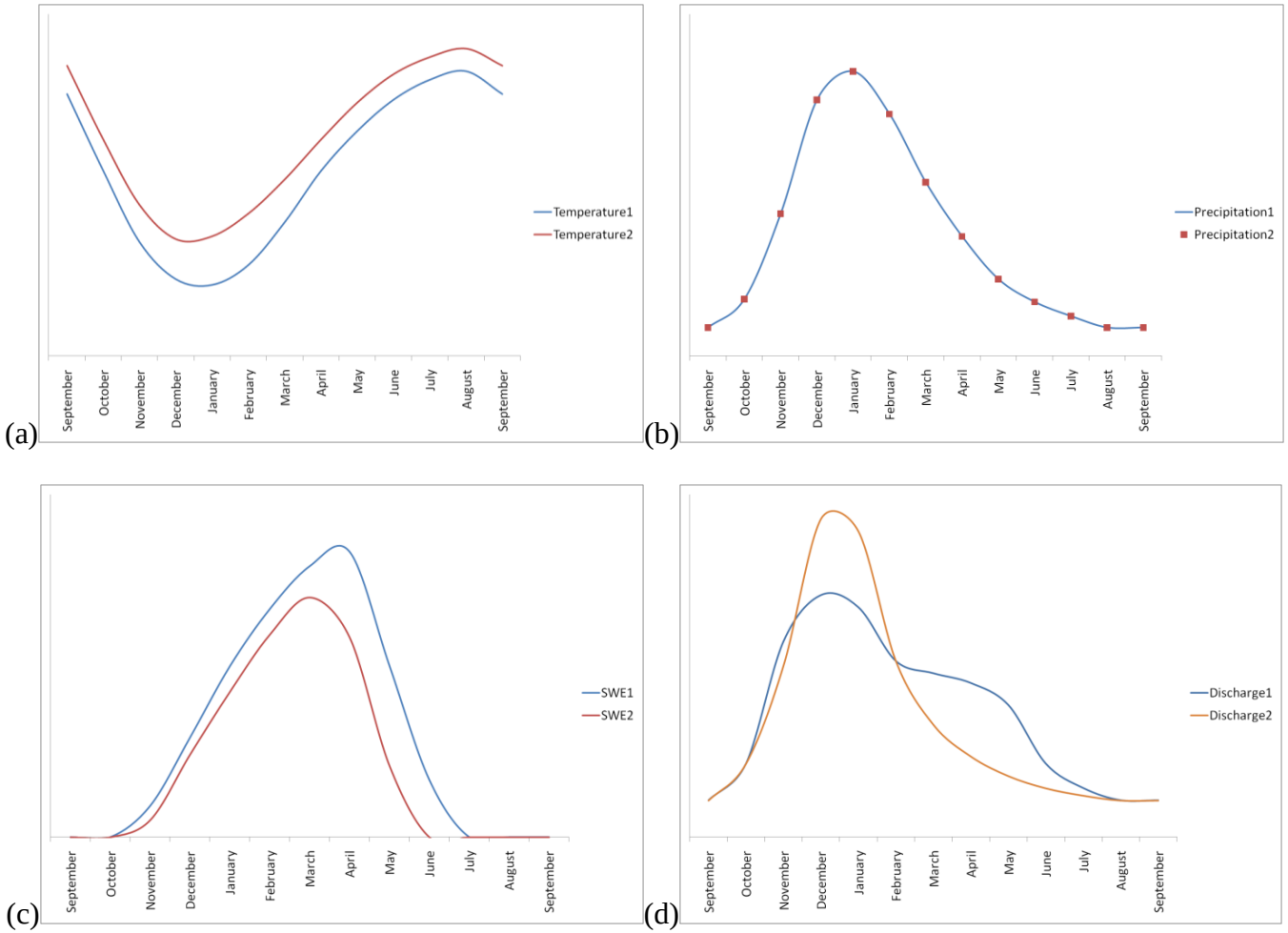

Figure 1.1: Conceptual models of widely anticipated climatic and hydrologic changes. Panels (a)-(d) respectively show the anticipated changes in temperature, precipitation, snow water equivalent, and streamflow.

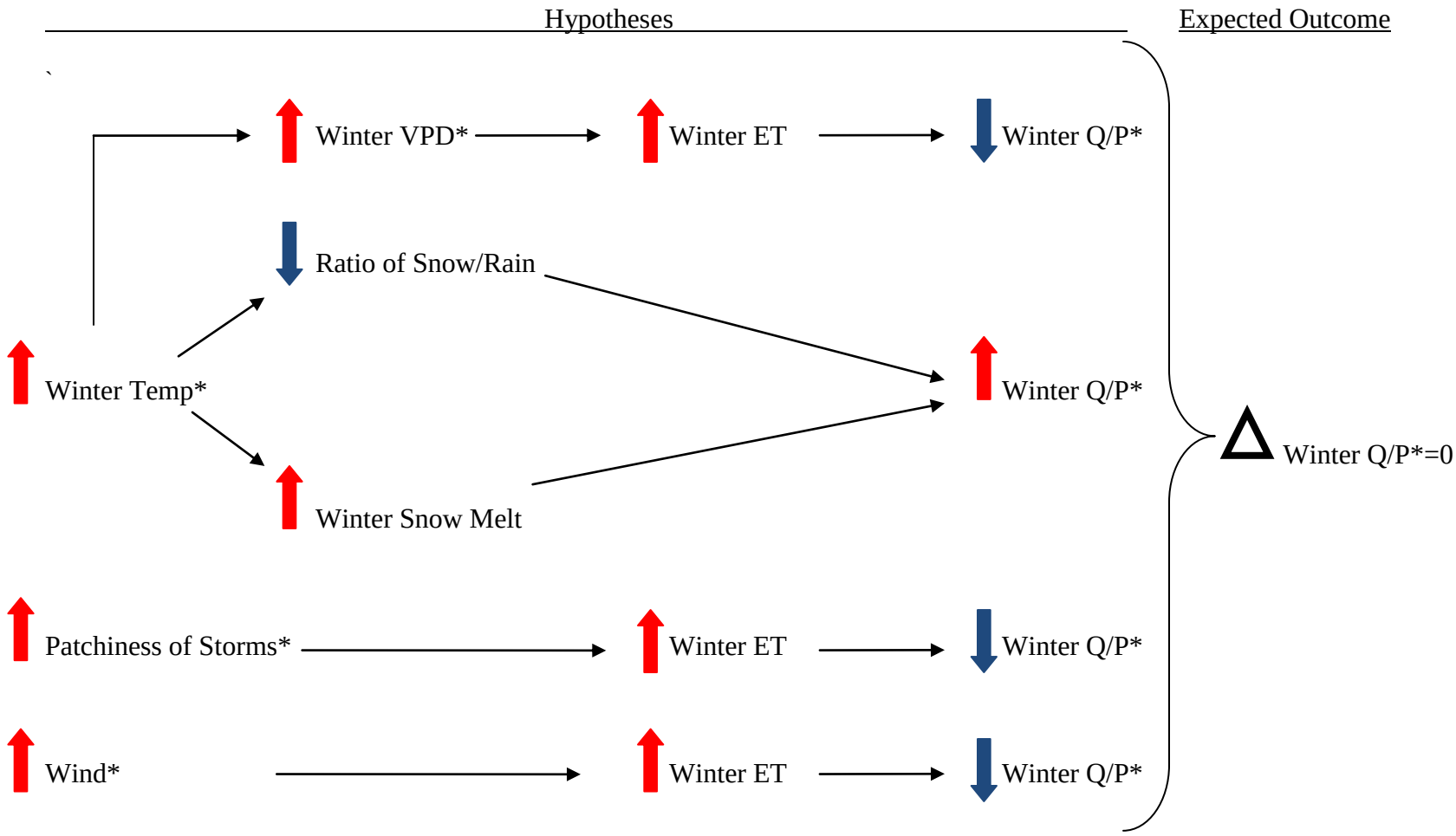

Figure 1.2: Conceptual models for changes in the winter runoff ratio and the determined result. * indicates a measured variable.

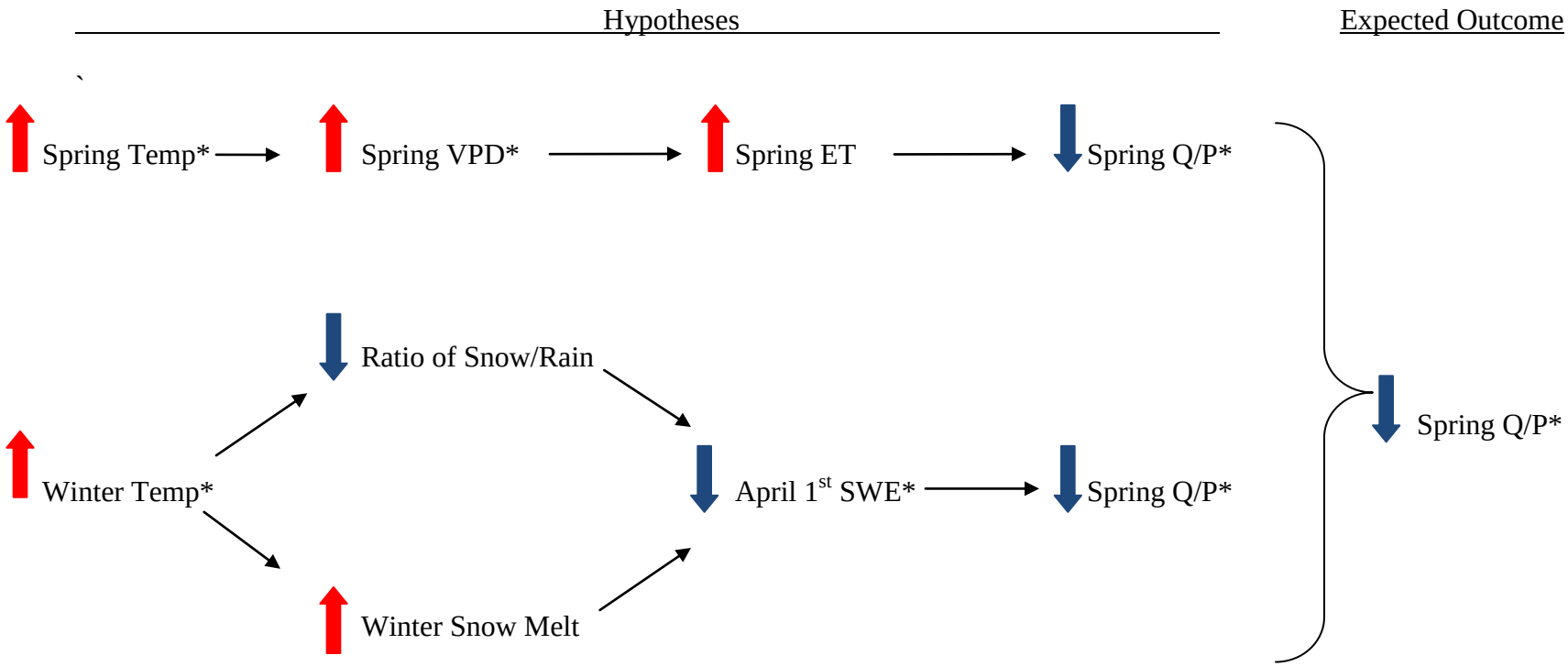

Figure 1.3: Conceptual models for changes in the spring runoff ratio and the determined result. * indicates a measured variable.

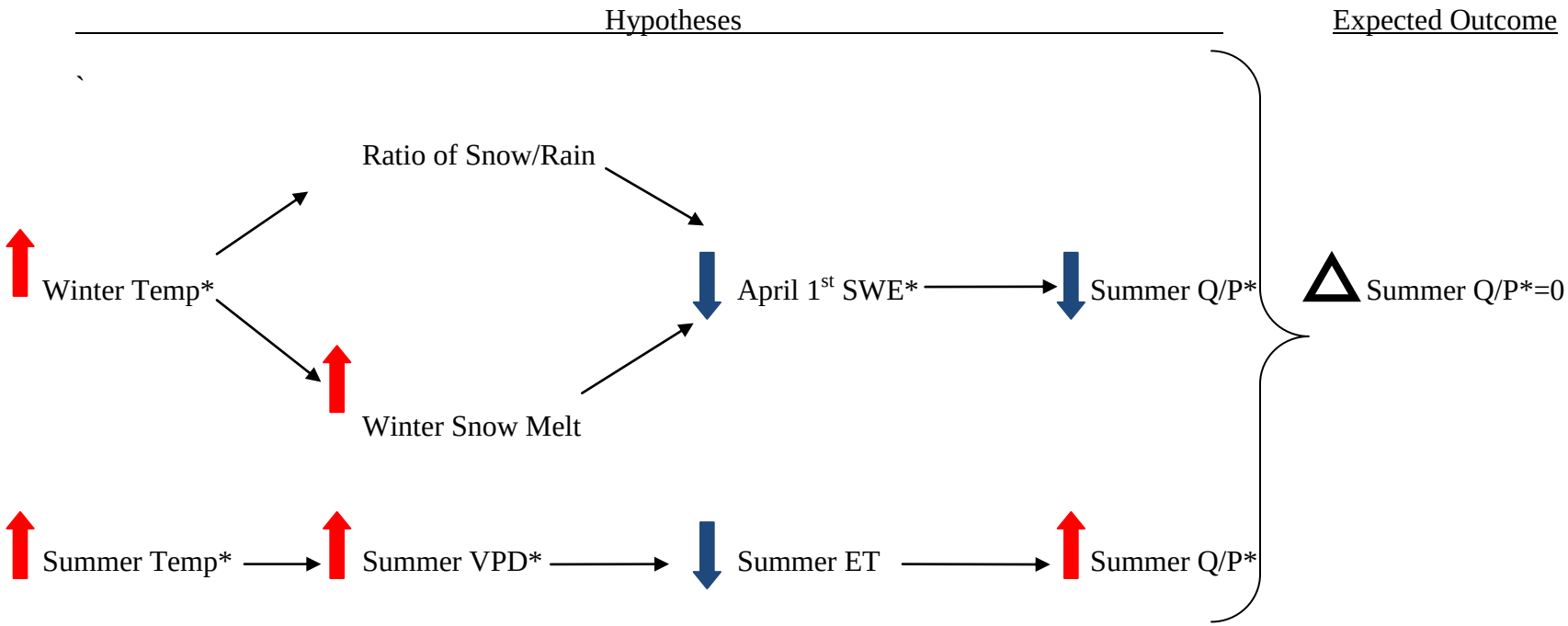

Figure 1.4 Conceptual models for changes in the summer runoff ratio and the determined result. * indicates a measured variable.

2. Site Description and Methodology

2.1. Site description

The HJ Andrews Experimental Forest (hereafter referred to as the HJ Andrews) is located in the western Cascade Mountains of Oregon, in the northwestern United States (44.2°N, 122.2°W) (Figure 2.1). The HJ Andrews encompasses the 6400 ha drainage basin of Lookout Creek. Elevation in the watershed ranges from 410 m to 1630 m. Figure 2.2 provides an oblique aerial photograph of the HJ Andrews and its surrounding landscape.

The HJ Andrews was established in 1948 and the US Forest Service has supported hydro-climatic monitoring since then, resulting in a continuous record of streamflow and meteorological data starting in the 1950s. Paired watershed experiments began in 1952 (WS 1, 2, 3), 1963 (WS 6, 7, 8) and 1968 (WS 9, 10). The experimental watersheds have been a focus for continued research during the 1970s (the HJ Andrews became part of the International Biosphere Program in 1970) and subsequent decades (the HJ Andrews has been a Long Term Ecological Research site since 1980). This study examined trends in long-term streamflow records from three headwater watersheds in old growth forest at the HJ Andrews (Fig. 2.3, Table 2.1). The three small (8.5-60.3 ha) watersheds (WS2, WS8, and WS9) range in elevation from 432-1182 m and have streamflow records dating back to 1953, 1964, and 1969 respectively.

Vegetation in the watersheds is forest dominated by conifers with an overstory of Douglas fir and western hemlock in WS2 and WS9, while WS8 marks the transition between western hemlock and silver fir (Dyrness and Hawk 1972, HJ Andrews Metadata Report).

The HJ Andrews has a maritime climate with wet, mild winters and cool, dry summers. Mean monthly temperatures range from about 1°C in January to about 18°C in July. Average annual rainfall ranges from about 2200 mm at low elevations to 2600 mm at high elevations. Precipitation follows the inverse seasonal trend to temperature, with about 80% of precipitation falling between November and April. Figure 2.4 shows climographs for the PRIMET, CS2MET and HI-15 meteorological stations at the HJ Andrews, which are in closest proximity to the gauging stations for WS9, WS2, and WS8 respectively. Figure 2.4 also shows climographs for PRISM data corresponding to WS2, WS8, and WS9. All the climographs are calculated for the period 1995-2006, which is the period of overlapping data from meteorological stations at the HJ Andrews.

The HJ Andrews spans the transition zone between a transient and seasonal snow pack (Figure 2.5). Snowpacks begin to accumulate in November with snow water equivalent (SWE) reaching a peak between February and April (Figure 2.6). Rain predominates at lower elevations with about 25% of precipitation falling as snow (HJ Andrews Metadata Report), while a seasonal snowpack develops at higher elevations whose mean annual maximum SWE frequently exceeds 1000 mm.

Streamflow is strongly seasonal; average monthly streamflow in the study watersheds reaches a maximum in December or January and a minimum in August or September (Figure 2.7). Average annual streamflow is 1319 mm for WS2 (1953-2007), 1163 mm for WS8 (1964-2007), and 1253 mm for WS9 (1969-2007).

2.2. Data and Methods

Data were obtained from three sources: the Forest Science Data Bank, the PRISM Climate Group, and the NRCS SNOTEL network. Meteorological and

streamflow data from the HJ Andrews were obtained from the Forest Science Data Bank, which hosts data provided by the HJ Andrews research program, funded by the National Science Foundation's Long-Term Ecological Research Program (DEB 08-23380), US Forest Service Pacific Northwest Research Station, and Oregon State University. Gridded temperature and precipitation data were also obtained from the PRISM climate group for the grid cells corresponding to WS2, WS8, and WS9 (Table 2.2). PRISM is an analytical model that uses point data and a digital elevation model (DEM) to generate gridded estimates of monthly and annual climatic variables (PRISM Climate Group, Oregon State University, http://www.prismclimate.org, 5/28/09). The data obtained has a resolution of 4km. Snow data were obtained from the Forest Science Data Bank for the VANMET meteorological station (the meteorological station with the longest snow record at the HJ Andrews), and from the NRCS SNOTEL network ftp://ftp-fc.sc.egov.usda.gov/OR/snow/snowcourse/or_data) for five SNOTEL sites – Santiam Junction, Three Creeks Meadow, McKenzie, Hogg Pass, and Jump Off Joe, which are located in the vicinity of the HJ Andrews (Table 2.3, Figure 2.8).

In all analyses seasons were defined as follows: December-February (winter), March-May (spring), June-August (summer), and September-November (fall). Annual analyses are conducted on a water year basis defined as October 1st-September 30th. The temporal extent of the analysis is from water year 1953-2007.

2.2.1. Precipitation analyses

Monthly precipitation data were obtained from PRISM, for the period 1925-2007 because only one precipitation record at the HJ Andrews, CS2MET at 485 m, has data extending back to 1958 and the longest precipitation record at high elevations within the

HJ Andrews begins in 1963 at Hi-15. Therefore PRISM data were used to match the record length of the streamflow data, which began in 1952. These data were summed by season and by water year. Daily precipitation data were obtained from the CS2MET meteorological station, which is located at the base of WS2, for the period of record starting on 10/1/1957. These data were summed by month, season and water year.

Simple linear regression analysis was used to assess trends in precipitation at CS2MET and the three PRISM grid cells corresponding to WS2, WS8, and WS9, for four seasons and annual (water year) data. Two time periods were analyzed for each dataset: (1) the periods of overlapping precipitation and streamflow records (1953-2007 for WS2, 1958-2007 for CS2MET, 1963-2007 for WS8 and 1969-2007 for WS9), and (2) the period of overlapping streamflow records (1969-2007).

The coefficient of variation (CV) was calculated by season for the daily precipitation record at CS2MET in order to assess whether there has been any change in the patchiness of precipitation events. The CV is calculated as average precipitation/standard deviation of precipitation. Simple linear regression analysis was used to assess any trends in CV over the period of record by season (Appendix A).

2.2.2. Temperature analyses

Monthly average minimum and maximum temperature data were obtained from PRISM for the period 1925-2007 because only one temperature station at the HJ Andrews, CS2MET at 485 m, has data extending back to 1958 and the longest temperature record at high elevations within the HJ Andrews begins in 1987. These data were averaged by season and by water year. Daily average minimum and maximum temperature data were obtained from the CS2MET meteorological station for the period

of record from 2/3/1958-2/19/2007. During this period there have been two temperature sensors located at CS2MET: the AIRCS201 sensor was available until 2/22/1999 and the AIRCS202 sensor started on 4/14/1998. This analysis makes use of AIRCS201 until the end of water year 1998 and switches to AIRCS202 on 10/1/1998. Daily air temperature data were averaged by month, season, and water year. There are periods of missing temperature data from CS2MET; months with fewer than 10 days of data were omitted from the analysis.

Simple linear regression analysis was used to assess trends in average minimum and maximum temperatures at CS2MET and the three PRISM grid cells corresponding to WS2, WS8, and WS9, on a monthly, seasonal, and water year basis. On the seasonal and water year basis, two time periods were analyzed for each dataset: (1) the periods of available record (1925-2007 for PRISM, 1958-2007 for CS2MET) and (2) the period of overlapping temperature and streamflow records. On the monthly basis only the periods of overlapping temperature and streamflow records were analyzed (Appendix B).

2.2.3. Snow analyses

April 1st SWE was obtained from the VANMET meteorological station for the period of available record, which began in 1988. April 1st SWE was also obtained from five SNOTEL sites – Santiam Junction, Three Creeks Meadow, McKenzie, Hogg Pass, and Jump Off Joe, for their respective periods of record (Table 2.3, Figure 2.8). SWE at VANMET was cross-correlated with SWE at each of the five snow course sites for the period of overlapping record from 1988-2004. Simple linear regression analysis was used to assess trends in April 1st SWE at the Santiam Junction site (which had the highest

correlation with VANMET), both for its period of record from 1941-2007 and for the periods of record corresponding to streamflows (Appendix C).

2.2.4. Vapor pressure deficit analyses

VPD was obtained from the PRIMET meteorological station at the HJ Andrews, which has the longest record of VPD spanning from 7/6/1988-1/24/2007. During this period two temperature sensors have operated at PRIMET. The VPDPRI05 sensor was available until 5/29/2000, and the VPDPRI04 sensor began on 6/4/1998. This analysis makes use of VPDPRI05 until the end of water year 1999 and switches to VPDPRI04 on 10/1/1999. The daily maximum VPD data were averaged by season. There are periods of missing VPD data from PRIMET; months with fewer than 10 days of data were omitted from the analysis. Simple linear regression analysis was used to assess trends in the seasonal average maximum VPD over the period of record.

VPD was also modeled using daily minimum and maximum temperatures from CS2MET, because CS2MET has the longest record of temperature at the HJ Andrews. VPD is the difference between ambient (E_a) and saturated vapor pressure (E_s):

$$VPD = E_s - E_a \qquad (5)$$

Saturated vapor pressure was modeled using the maximum daily temperature as:

$$0.6108 * \exp((17.27 * T_{\max}) / (T_{\max} + 237.3)) \qquad (6)$$

Ambient vapor pressure was modeled using the minimum daily temperature as:

$$0.6108 * \exp((17.27 * T_{\min}) / (T_{\min} + 237.3)) \quad (7)$$

Equations (5-7) assume that condensation occurs every day at the time of minimum temperature, and that the moisture content of the air remains unchanged. Pearson's R was calculated to assess the correlation between modeled VPD and VPD measured at

CS2MET for the measured period of record. The daily modeled VPD was averaged by season and simple linear regression analysis was used to assess trends both over the period of record (temperature record at CS2MET 1958-2007) and over the period corresponding to measured VPD at PRIMET (1988-2007) (Appendix D).

2.2.5. Wind analyses

Daily average wind speed was obtained from the PRIMET meteorological station at the HJ Andrews, which has the longest record of wind speeds spanning from 5/22/1973- 1/24/2007. The daily data were averaged by season. There are periods of missing wind data from PRIMET; months with fewer than 10 days of data were omitted from the analysis. Simple linear regression analysis was used to assess trends in seasonal average wind speed over the period of record. Since there is a substantial period of missing data prior to 1980, simple linear regression analysis was also used to assess trends in seasonal average wind speed since 1980 (Appendix E).

2.2.6. Discharge analyses

Monthly discharge data were obtained from the HJ Andrews for WS2, WS8 and WS9, for their respective periods of record. These data were summed seasonally and by water year. Simple linear regression analysis was used to assess trends in discharge on both a seasonal and annual basis for the period of record for each watershed as well as for the period of overlapping streamflow records from 1969-2007. Trends in WS9 summer discharge were also investigated excluding the period from 1980-1996, because a v-notch gauge was not installed in the summers of these years, and streamflow measurements are noticeably elevated.

Trends in daily discharge were also examined that had been smoothed using a low-pass wavelet filter to reduce high frequency variability in the streamflow record, following procedures outlined by C. Thomas (unpublished). Daily discharge data were obtained from the HJ Andrews for WS2, WS8 and WS9, for their respective periods of record through water year 2007. Daily discharge anomalies (defined as the difference of each daily flow from the mean flow on that day for the period of record) were calculated using average daily discharge for each watershed. The daily discharge anomalies were filtered using a low-pass wavelet (biorthogonal wavelet 5.5), at four dyadic decomposition scales equivalent to 6.28 days, 12.57 days, 25.13 days, and 50.27 days. The 12.57 day filter was of greatest interest as it corresponds most closely to the length of streamflow response to a precipitation event at the HJ Andrews (Post and Jones, 2001). Appendix F (section 4) provides a sample of the program used to conduct the wavelet analysis (Program developed by Chris Thomas). The low-pass wavelet filter smoothes the data by removing variation that is above a given frequency determined by the wavelet scale (Figure. 2.9). Removal of this high frequency 'noise' improves identification of trends in the low frequency signal. A simple linear regression analysis was conducted on the low-pass filtered daily discharge to assess trends in the filtered data by day of the water year. Trend significance was tested at the 5% level using a single factor ANOVA F-test (Appendix F).

Changes in the annual timing of discharge for each watershed were investigated using a simple linear regression to test 1) whether there has been any trend in the day of the water year at which 50% of the annual discharge has passed, and 2) whether there has been any trend in the proportion of annual discharge that has passed by March 1st (which

marks the break point between winter and spring seasons defined in this study) (Appendix F).

2.2.7. Runoff ratio analyses

Simple linear regression analysis was used to assess trends in the runoff ratios on both a seasonal and annual (water year) basis for up to three time periods for each watershed: (1) the period of streamflow record for each watershed (2) the period of overlapping streamflow records among watersheds (1969-2007), and (3) for summer runoff ratios from WS9, the period of record excluding 1980-1996, when V-notch weirs were not installed. In addition least squares regressions were fit to both spring discharge versus spring precipitation from PRISM and water year discharge versus water year precipitation from PRISM for each watershed for two periods (the period prior to 1980, and 2000 to 2007). Changes in the relationship between precipitation and discharge were assessed by a t-test for significant differences between the runoff ratios between the two periods (Appendix G).

2.2.8. Baseflow analyses

Baseflows were estimated to investigate changes in streamflows, unobscured by variability introduced by peak storm flows. Following Post and Jones (2001), the minimum streamflow for all 5-day periods was calculated from the daily streamflow record for all three watersheds, and the subset of 5-day minima that were less than 90% of adjacent 5-day minima were connected to create baseflow, using a program to calculate baseflow developed by David Post (Appendix H). In the event that the estimated baseflow exceeded total flow, baseflow was set equal to total flow.

Simple linear regression analysis was used to assess trends in baseflow on both a seasonal and annual basis for the period of record for each watershed. Trends in WS9 summer baseflow was also investigated without the period from 1980-1996, as with discharge and runoff ratio (Appendix H).

2.2.9. Linear cross regressions

Linear regression analysis was used to test the hypothesized relationships between the following variables:

1) Winter CV for precipitation as the explanatory variable for winter runoff ratios.
2) Winter average wind speeds as the explanatory variable for winter runoff ratios.
3) Winter average minimum and maximum temperatures as the explanatory variables for winter VPD, April 1st SWE at Santiam Junction, winter runoff ratios, spring runoff ratios, summer runoff ratios, spring baseflows, and summer baseflows.
4) April 1st SWE at Santiam Junction as the explanatory variable for spring and summer runoff ratios and baseflows.
5) Spring runoff ratios as the explanatory variable for summer runoff ratios.
6) Spring average minimum and maximum temperatures as the explanatory variables for spring VPD, spring runoff ratios and spring baseflows.
7) Summer average minimum and maximum temperatures as the explanatory variables for summer VPD, summer runoff ratios and summer baseflows.

8) Seasonal VPD as the explanatory variable for the corresponding seasonal runoff ratios and baseflows.

Although, trends in runoff ratios over time were calculated using both a measured precipitation record (CS2MET) as well as PRISM precipitation, in all linear cross-regressions involving a runoff ratio, the runoff ratio was calculated only using precipitation data from PRISM.

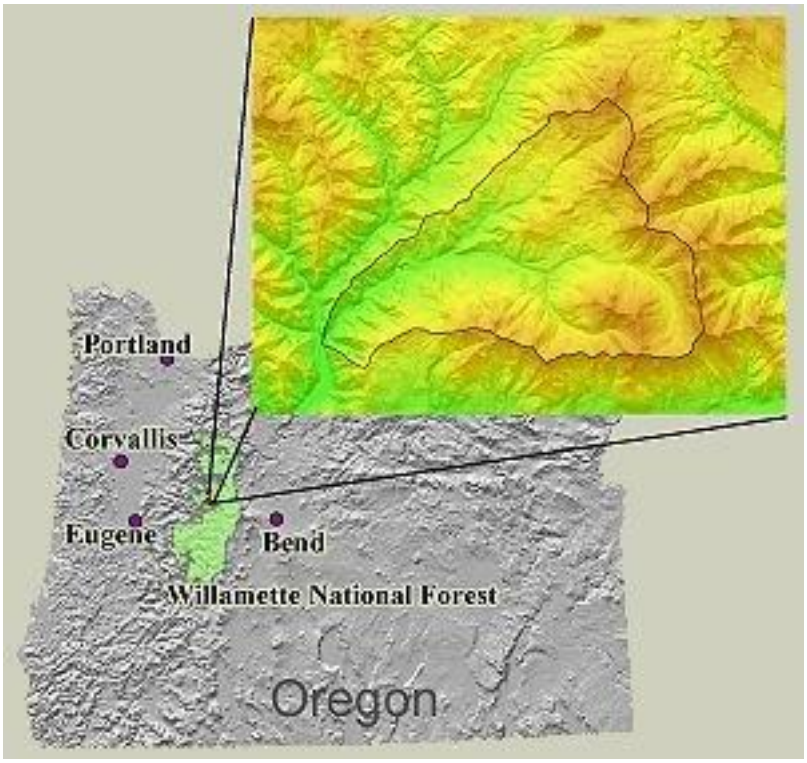

Figure 2.1: Location of the HJ Andrews Experimental Forest (Source: http://andrewsforest.oregonstate.edu/)

Figure 2.2: Oblique aerial photography of the HJ Andrews Experimental Forest (Photo credit: Al Levno, 7/1991)

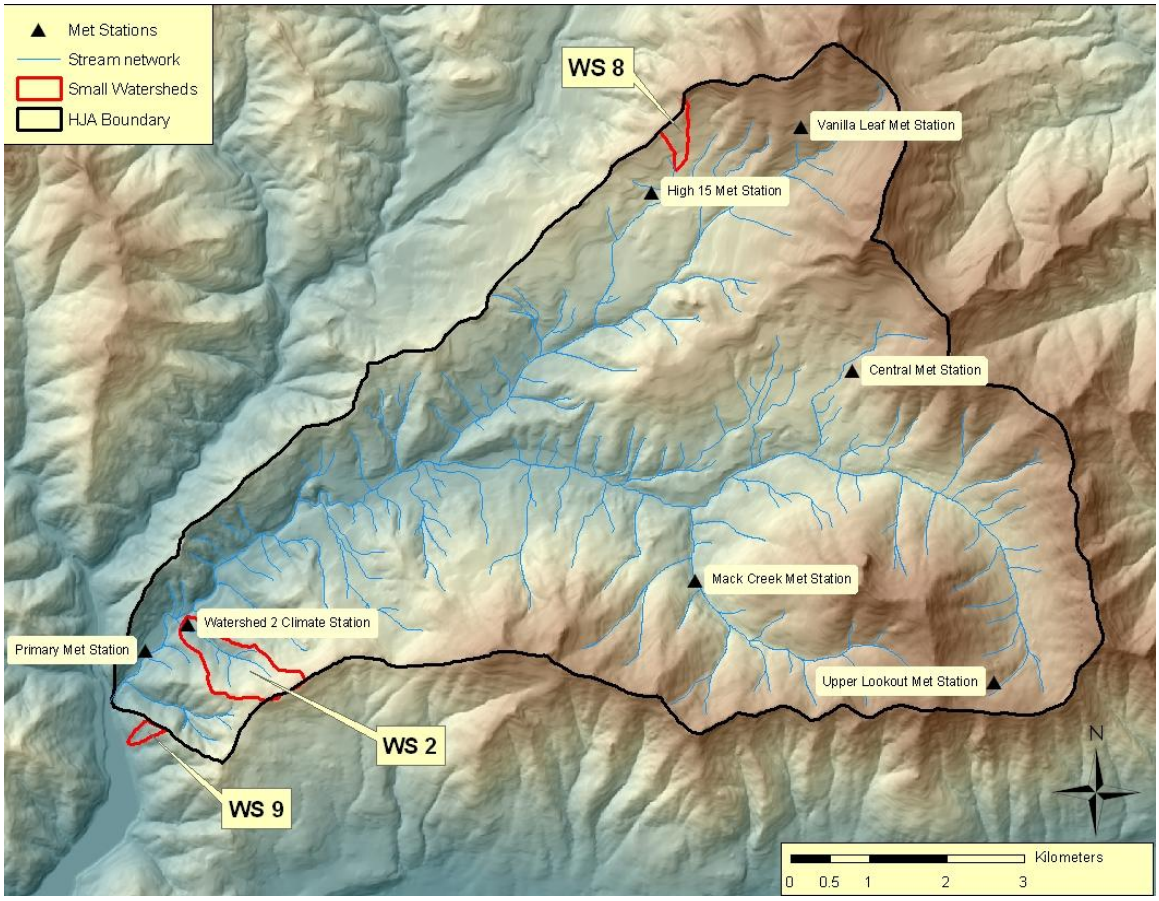

Figure 2.3. Locations of benchmark meteorological stations and WS2, WS8 and WS9 within the HJ Andrews Experimental Forest (Data source: Forest Science Data Bank)

Table 2.1: Small watershed characteristics (Source: HJ Andrews Metadata Report, F. Swanson personal communication)

Watershed	Area (ha)	Elevation Range (m)	Start of Record	Forest Age (Years)
2	60.3	548-1078	1953	500
8	21.4	993-1182	1964	150-500
9	8.5	432-731	1969	150-500

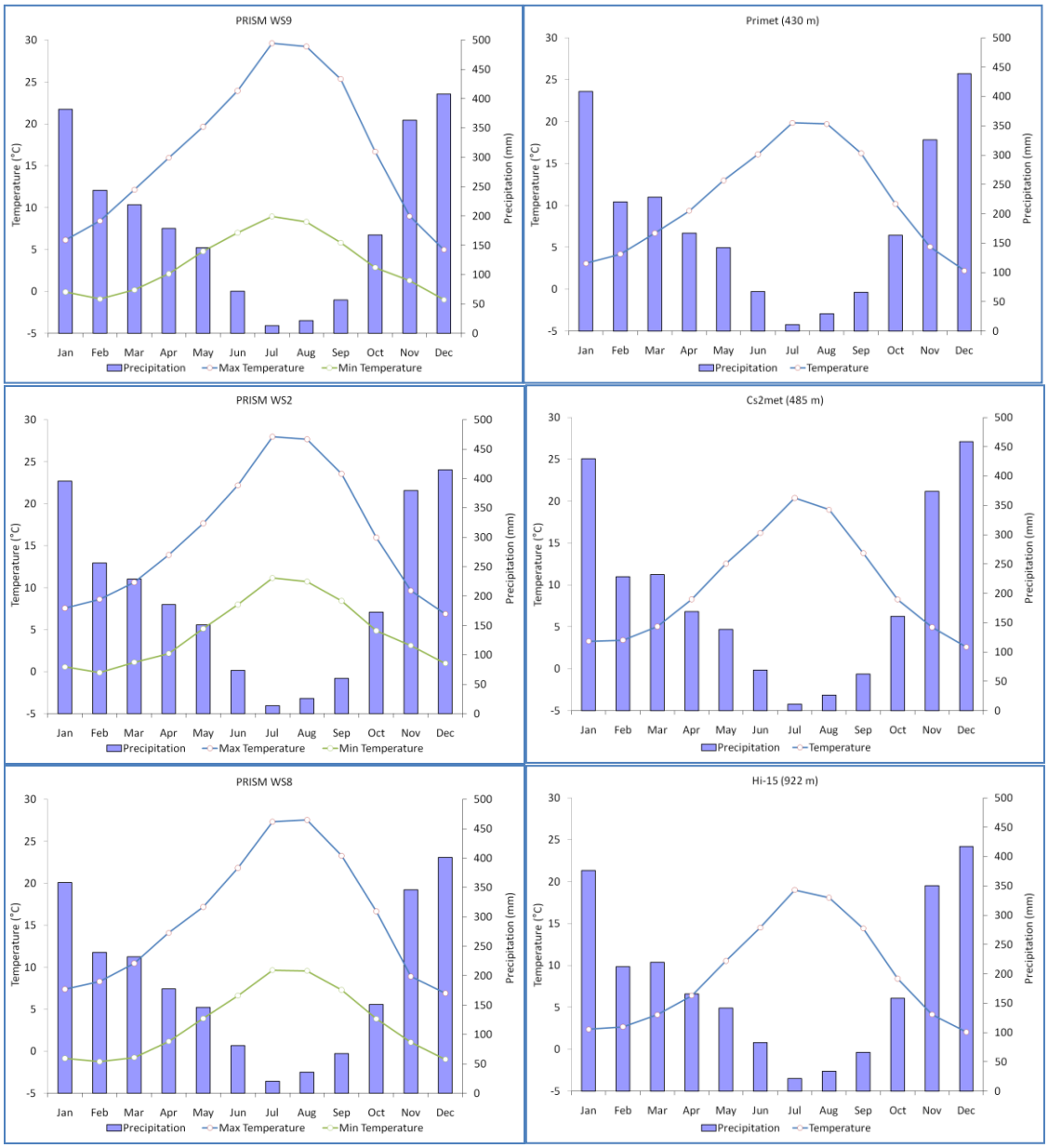

Figure 2.4: Climographs for (clockwise from top left) PRISM WS9, PRIMET, CS2MET, HI-15, PRISM WS8, and PRISM WS2 (J. Jones, unpublished data for HJ Andrews meteorological stations).

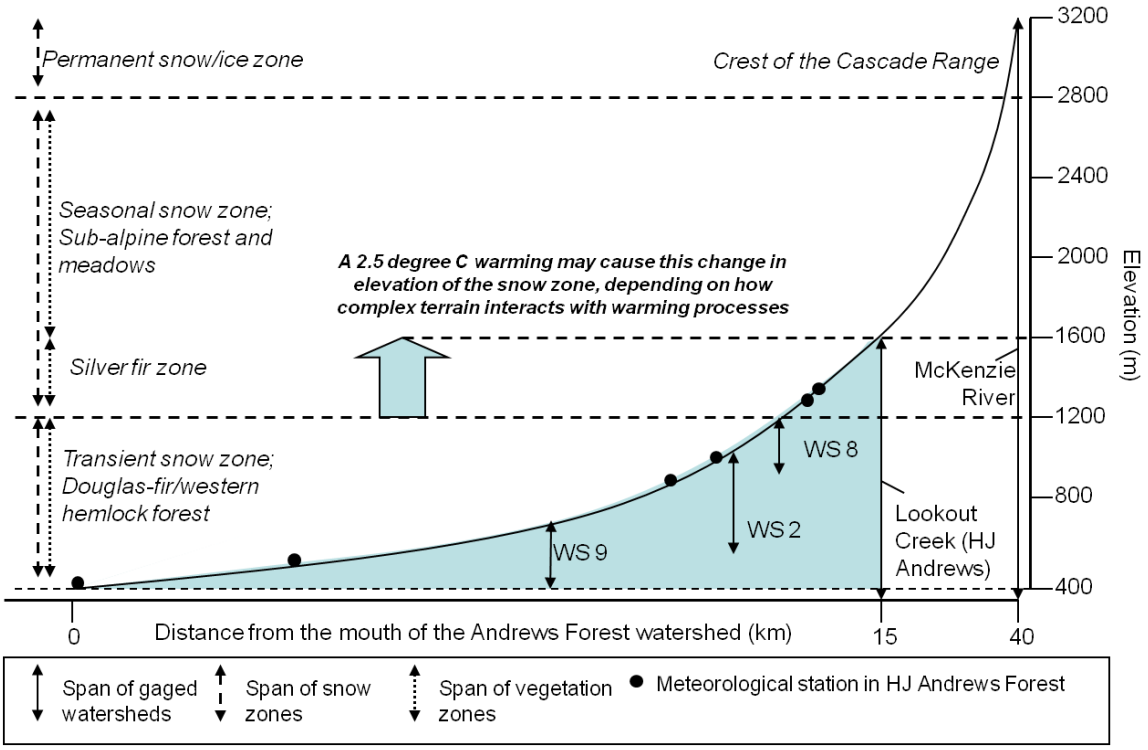

Figure 2.5: Climate and vegetation zones of the HJ Andrews (adapted from J. Jones, unpublished data)

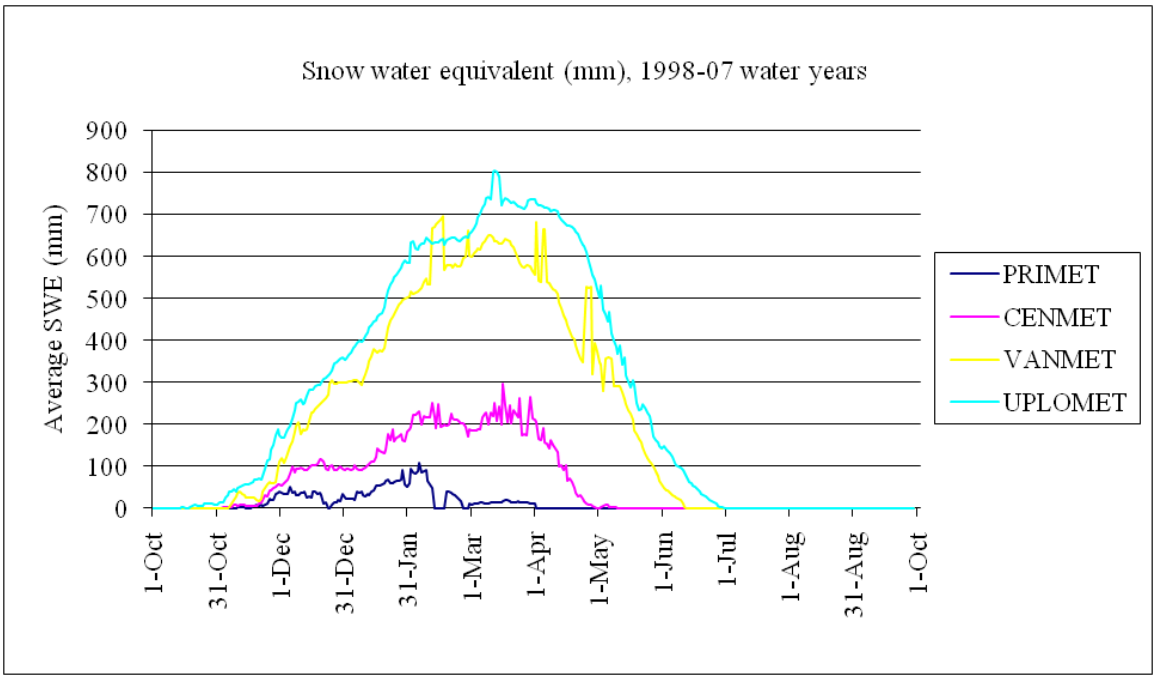

Figure 2.6: Average snowpack (SWE in millimeters) at HJ Andrews meteorological stations, for water years 1998 to 2007 (J. Jones, unpublished data)

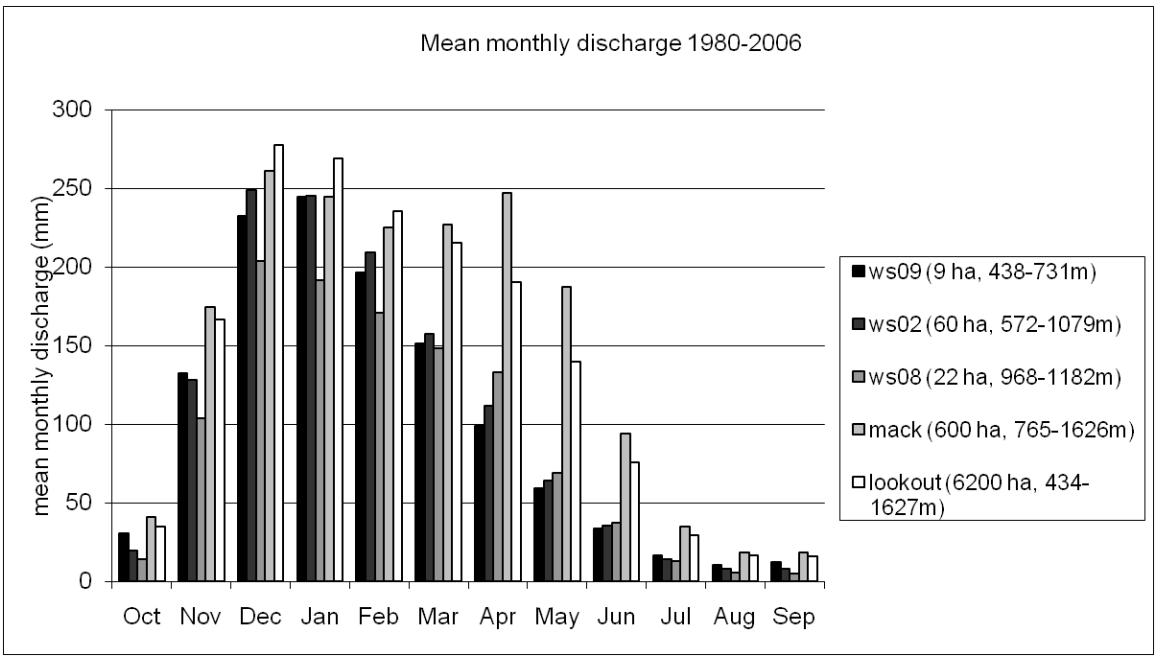

Figure 2.7: Mean monthly dischage at gauging stations with the HJ Andrews, for water years 1980 to 2006 (J. Jones, unpublished data)

Table 2.2: Geographic information for PRISM grids cells corresponding to WS2, WS8, and WS9.

ID	Name	Station Elevation	Grid Cell Elevation	Latitude	Longitude
GSWS02	WS#2 GS	548	764	44.2119	-122.2450
GSWS08	WS#8 GS	993	1030	44.2661	-122.1708
GSWS09	WS#9 GS	432	499	44.2014	-122.2577

Table 2.3: Characteristics of the snow sites.

Station Name	Elevation (m)	Latitude	Longitude
VANMET	1273	44.27	-122.15
Santiam Junction	1140	44.43	-121.94
McKenzie	1454	44.21	-121.87
Three Creeks Meadow	1734	44.14	-121.64
Hogg Pass	1460	44.42	-121.85
Jump Off Joe	1073	44.38	-122.16

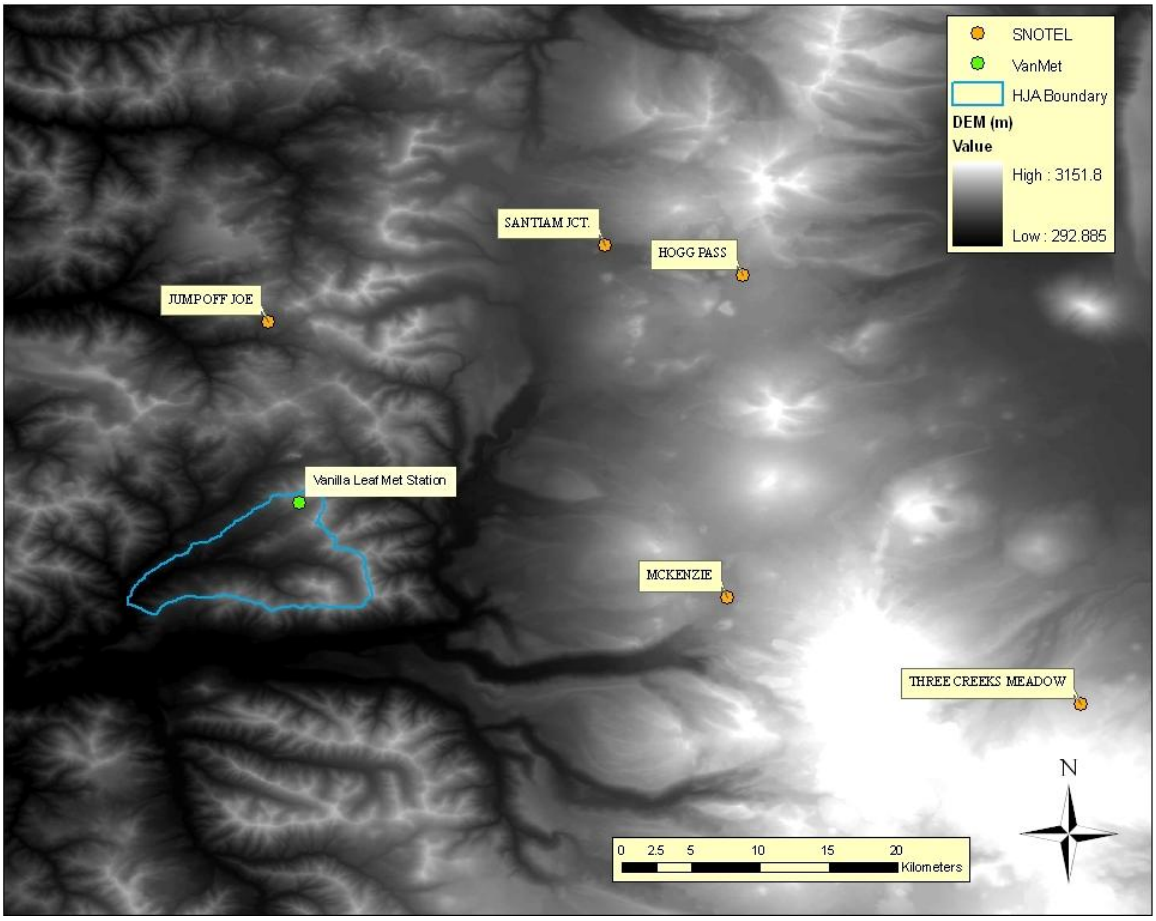

Figure 2.8: Relative location of the VANMET meteorological to nearby SNOTEL stations

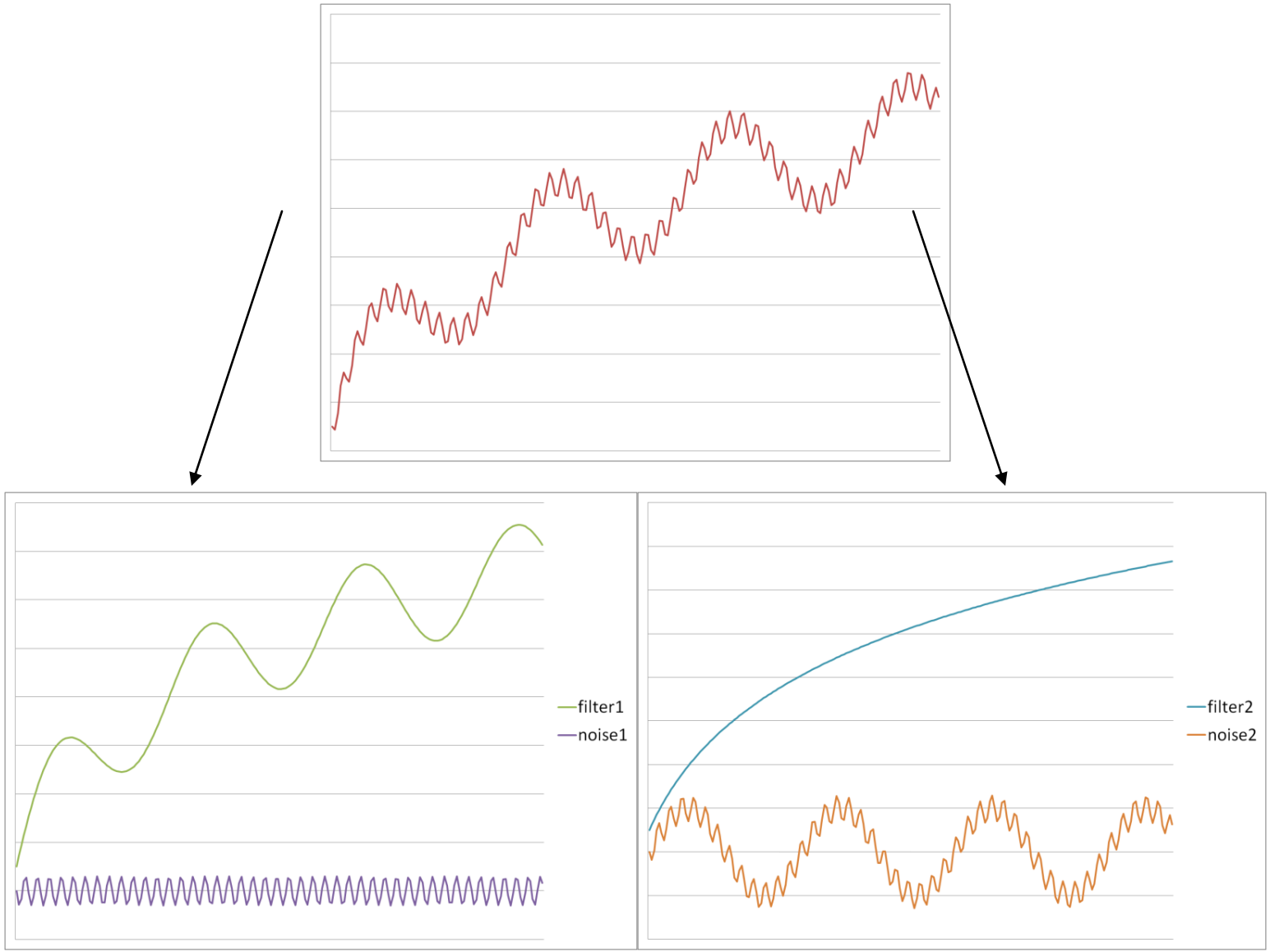

Figure 2.9. Conceptual diagram of a low-pass wavelet filter analysis at two scales.

3. Results

3.1. Precipitation

There has been no change in the amount of precipitation received over the study periods corresponding to streamflow for any of the PRISM datasets or for the period of record (1958-2007) for CS2MET, either seasonally or annually (Appendix A, Table A1, A2). Annual precipitation has ranged from 1264 mm (WS9 PRISM) to 3309 mm (CS2MET). Spring precipitation has ranged from 337 mm (WS8 PRISM) to 1039 mm (WS2 PRISM). Summer precipitation has ranged from 7 mm (CS2MET) to 289 mm (WS8 PRISM). Fall precipitation has ranged from 153 mm (CS2MET) to 1075 mm (WS2 PRISM). Winter precipitation has ranged from 264 mm (WS8 PRISM) to 1744 mm (WS2 PRISM). There has also been no change in the CV for precipitation measured at CS2MET for the period of record during any season (Appendix A, Table A3). The winter CV has ranged from 1.2 to 2.2.

3.2. Temperature

Annual and seasonal trends in temperature are consistently positive over the study period, with minimum temperatures exhibiting a more increases than maximum temperatures (Appendix B, Tables B3-B6). Maximum temperatures show some significant trends in the spring (WS2 PRISM) and summer (WS2 PRISM), while minimum temperatures show significant trends annually and during the spring (all three PRISM datasets and CS2MET), and some significant trends during the fall (WS9 PRISM) and summer (all three PRISM datasets). Most sites and record types exhibit increases in spring average minimum temperatures in all three months: March (WS2 PRISM, WS8 PRISM, and CS2MET), April (all three PRISM datasets and CS2MET),

and May (WS8 PRISM, WS9 PRISM, and CS2MET). All sites and record types exhibit increases in summer average minimum temperatures in July (all three PRISM datasets and CS2MET). The increase in WS9 PRISM fall average minimum temperature is due to an increase in October average minimum temperature. Monthly average maximum temperatures only show significant trends (which are positive) at WS2 PRISM and CS2MET in March.

The rate of increase in annual and seasonal temperature ranges from 0.012°C per year ($p<0.05$) (WS2 PRISM, annual average minimum) to 0.039°C per year ($p<0.01$) (WS8 PRISM, spring average minimum). Overall, the greatest rates of increase for each watershed have occurred during the spring. The rates of increase in spring temperatures range from 0.026°C per year ($p<0.01$) at WS2 (PRISM spring average minimum), equating to a net change of 1.4°C over the 55 year period corresponding to streamflow, to 0.039°C ($p<0.01$) per year at WS8 (PRISM spring average minimum), equating to a net change of 1.7°C over the 44 year period of record corresponding to streamflow (Figure 3.1). Analyses of temperature change using PRISM records produced essentially the same result as analyses using CS2MET (Figure 3.2).

3.3. Snow

April 1st SWE at Santiam Junction has declined significantly over the study period (Appendix C, Table C2). Over the periods of record relating to streamflows, Santiam Junction experienced annual declines of -11 mm ($p<0.01$) from 1953-2007 (-80% over the period), -13 mm ($p<0.01$) from 1964-2007 (-82%), and -13 mm ($p<0.01$) from 1969-2007 (- 82%) (Figure 3.3).

3.4. Vapor pressure deficit

Modeled VPD at C2MET shows no significant trends over the period of record from 1958-2007 (Appendix D, Table D2). Measured average maximum VPD at PRIMET in winter and summer increased significantly over the period of record from 1989-2006 (Appendix D, Table D1). Winter average maximum VPD increased by 0.072 mbar per year ($p<0.01$) (total increase of 1.3 mbar from 1989-2006), while summer average maximum VPD increased 0.57 mbar per year ($p<0.01$) (total increase of 10.3 mbar from 1989-2006). Modeled summer VPD at CS2MET increased significantly (0.46 mbar per year, $p<0.01$) from 1989-2006 (the period corresponding to VDP measured at PRIMET), but modeled winter VPD did not increase (Figure 3.4) (Appendix D, Table D3).

3.5. Wind

Average wind speeds show no significant trends over the period of record at PRIMET from 1974-2006/07 (Appendix E, Table E1). However, for the period of continuous record starting in 1980, average wind speeds show significant declines in all seasons (Appendix E, Table E2). Average annual wind speeds declined by -0.016 m/s per year ($p<0.01$) for a net change of -0.40 m/s from 1981 to 2006. Rates of decline in seasonal average wind speeds since 1980 range from -0.012 m/s per year (winter) ($p<0.01$) to -0.021 m/s per year (summer) ($p<0.01$) (Figure 3.5).

3.6. Discharge

Seasonal discharge has not changed significantly or consistently at most sites or seasons over the periods of streamflow record, but WS2 and WS8 have experienced some declining trends in spring discharge, and analyses of filtered daily records reveal periods

of spring days at WS2 and WS 8 that have experienced declining discharge. On a seasonal basis discharge has changed significantly over the full periods of streamflow record only in the case of WS2 spring flows (Appendix F, Table F1). Spring discharge for WS2 exhibits a decline of -2.54 mm per year ($p<0.05$) for a net change of 139.95 mm over the 55 year period of record. However, over the period of overlapping streamflows from 1969-2007, only WS8 spring discharge exhibits a significant trend (Appendix F, Table F2). Over this 39 year period WS8 spring discharge exhibits a decline of -4.86mm per year ($p<0.05$) for a net change of 189.61mm. There is no evidence of streamflow changes during the winter, summer or fall. There is also no indication that there has been a change in the timing of streamflow, as there has been no significant change either in the date at which 50% of the water year discharge has passed, or the proportion of water year discharge that has passed by March 1st (Appendix F, Table F3).

Daily discharges at WS2 and WS8, filtered with a 12.57 day filter, declined during the spring (Appendix F, Tables F4-F6). WS9 exhibits no significant daily discharge trends using the 12.57 wavelet filter (Figure. 3.6). Discharge declined significantly on 20 days in March and April at WS2 at rates ranging from -0.042 to -0.092 mm/year, and on ten days in October at rates ranging from -0.011 to -0.013 mm/year (Figure. 3.7). Discharge declined significantly on 24 days in April and May at WS8 at rates ranging from -0.049 to -0.092 mm/year (Figure. 3.8).

3.7. Runoff Ratio

Runoff ratios declined significantly during the spring at all three watersheds, but not during fall, winter, or summer. Analyses of runoff ratios using PRISM records produced essentially the same result as analyses using CS2MET (Appendix G, Tables

G1-G4, Figure 3.9). Over the periods of streamflow record, annual rates of decline in spring runoff ratios using PRISM records range from -0.003 (WS2) ($p<0.05$) to -0.009 (WS8) ($p<0.01$), while annual rates of decline in spring runoff ratios using CS2MET range from 0.004 (WS2) ($p<0.05$) to -0.009 (WS8) ($p<0.01$). Using the PRISM records, spring runoff ratios declined over the period of record by 25.4% at WS2 (55 years), 41.2% at WS8 (44 years), and 31.5% at WS9 (39 years). Using CS2MET, spring runoff ratios declined over the period of record by 23.4% at WS2 (50 years), 42.9% at WS8 (44 years), and 28.8% at WS9 (39 years)

Controlling for precipitation (using PRISM records), spring runoff for the period 2000-2007 declined by 17% (WS2) ($p<0.05$) to 33.02% (WS8) ($p<0.05$) relative to the period prior to 1981 (Figure 3.10).Controlling for precipitation, the change in annual runoff was not statistically significant between these two periods.

3.8. Baseflow

Annual baseflows decreased significantly at annual rates of -4.6 mm (WS8) ($p<0.05$) to -4.8 mm (WS9) ($p<0.05$), and spring baseflows decreased significantly at annual rates of -1.8 mm per year (WS2) ($p<0.01$) to -2.7 mm per year (WS8) ($p<0.05$) (Figure 3.11) (Appendix H, Table H1).

3.9. Cross Regressions

3.9.1 Relationship of temperature to SWE and VPD

April 1st SWE at Santiam Junction was significantly negatively related to average minimum and maximum winter air temperatures (Appendix I, Tables I1-I2). VPD Because VPD (modeled at CS2MET) was modeled from temperature, it was significantly negatively related to average minimum and maximum winter and summer air

temperatures (except for PRISM summer average minimum temperatures at WS9), but modeled VPD was significantly positively related to average maximum spring air temperatures (Appendix I, Tables I1-I6).

3.9.2 Factors influencing winter runoff ratios

Low winter runoff ratios were associated with high winter maximum air temperatures and high variability in precipitation. Winter runoff ratios (except for WS8) were significantly negatively related to average maximum winter air temperatures, but (for all three watersheds) were not significantly related to average minimum winter air temperatures (Appendix I, Tables I1-I2). because modeled VPD was estimated from temperature data, both winter runoff ratios and winter baseflows (apart from WS8 winter runoff ratio) were significantly negatively related to modeled VPD at CS2MET (Appendix I, Tables I10-I11). However, this relationship is not apparent with VPD at PRIMET over its shorter period of record (Appendix I, Tables I8-I9). Winter runoff ratios also were significantly negatively related to the CV of precipitation at CS2MET (Appendix I, Table I12). Winter runoff ratios were not related to average wind speed at PRIMET (Appendix I, Tables I13-I14).

3.9.3 Factors influencing spring runoff ratios

Low spring runoff ratios and low spring baseflow were associated with small April snowpacks, high winter and spring air temperatures and high VPD. Spring runoff ratios and baseflows were significantly positively related to April 1st SWE at Santiam Junction (Appendix I, Table I7). Spring runoff ratios were significantly negatively related to minimum and maximum average temperatures during the winter, but were not significantly related to spring average minimum or maximum temperatures (except at

WS8, where runoff ratio was significantly negatively related to spring average minimum temperature) (Appendix I, Tables I1-I4). Spring baseflows, however, were significantly negatively related to average minimum and maximum winter and spring air temperatures (apart from WS9, which does not exhibit a significant relationship with spring average minimum temperatures) (Appendix I, Tables I1-I4). Although spring runoff ratios were not significantly related to modeled VPD at CS2MET, spring baseflows (apart from WS8) were significantly negatively related to modeled VPD at CS2MET (Appendix I, Tables I10-I11), and both spring runoff ratios and baseflows at WS2 and WS9 were significantly negatively related to VPD at PRIMET over its shorter period of record (Appendix I, Tables I8-I9).

3.9.4 Factors influencing summer runoff ratios

Summer runoff ratios and baseflows were not consistently related to temperature, snowpack, or VPD. Summer runoff ratios and baseflows were not significantly related to winter temperatures (average minimum or maximum), April 1st SWE at Santiam Junction, spring runoff ratios, or minimum summer temperatures (except at WS9 where baseflow was significantly negatively related to both average minimum and maximum summer temperatures) (Appendix I, Tables I1, I2, and I5-I7). Summer runoff ratios (apart from WS9) do exhibit a significant positive relationship with summer average maximum temperatures (Appendix I, Tables I5-I6). Similarly, summer runoff ratios (apart from WS9) have a significant positive relationship with modeled VPD at CS2MET.WS9 summer baseflow however has a significant negative relationship with modeled VPD (Appendix I, Tables I10-I11). These relationships remain valid with VPD

at PRIMET over its shorter period of record (apart from the relationship with WS8 runoff ratio, which becomes insignificant) (Appendix I, Tables I8-I9).

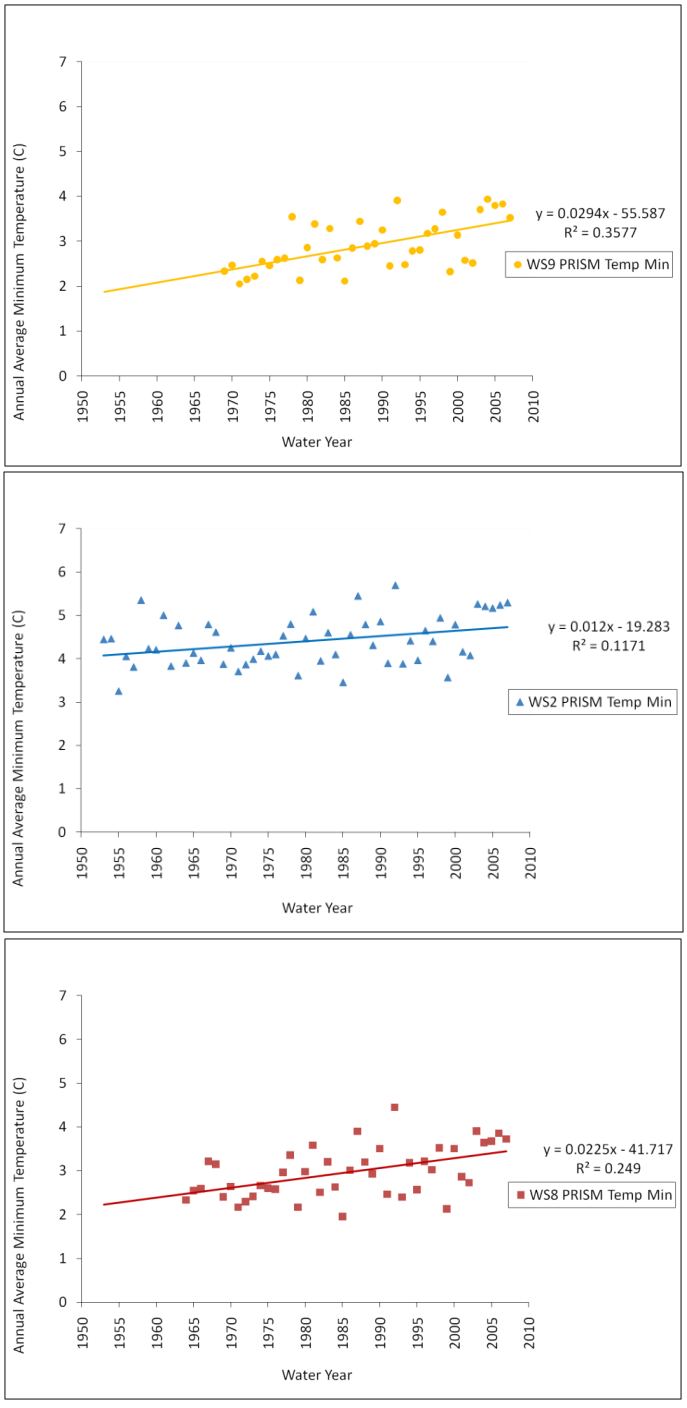

Figure 3.1: Significant trends in annual and seasonal average minimum and maximum temperature using PRISM data. Panels (a)-(c) show the trends in WS9, WS2, and WS8 annual average minimum temperature respectively. Panels (d)-(f) show the trends in WS9, WS2, and WS8 spring average minimum temperature respectively. Panels (g)-(i) show the trends in WS9, WS2, and WS8 summer average minimum temperature respectively. Panel (j) shows the trend in WS9 fall average minimum temperature. Panel (k) shows the trend in WS2 summer average maximum temperature. Panel (l) shows the trend in WS2 spring average maximum temperature.

(d)

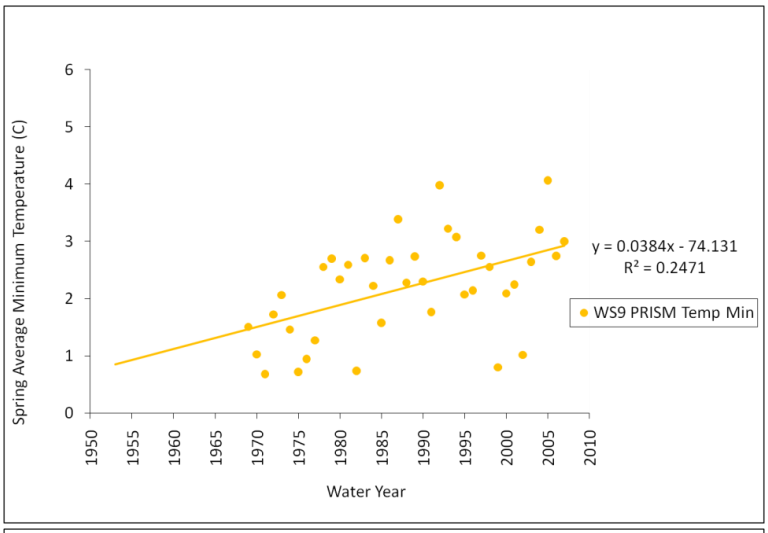

(e)

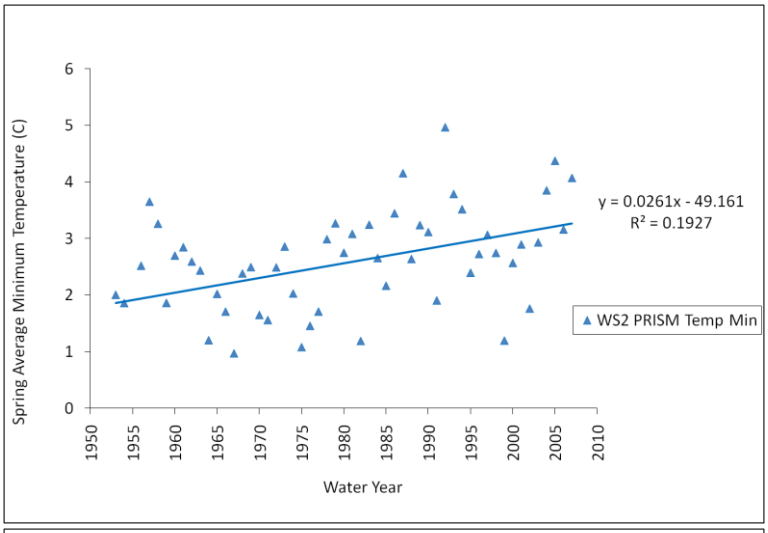

(f)

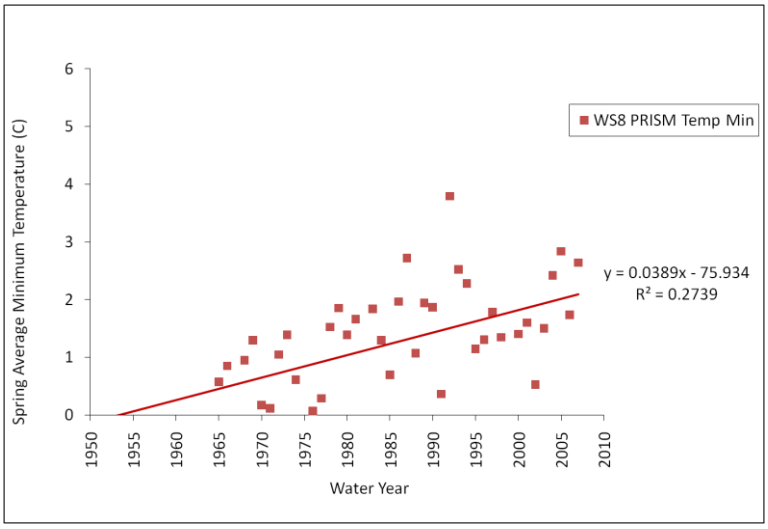

Figure 3.1: Continued.

(g)

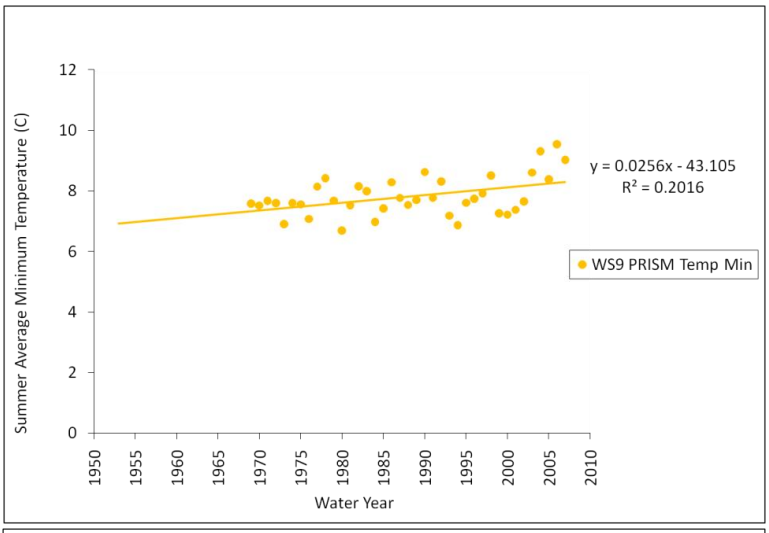

(h)

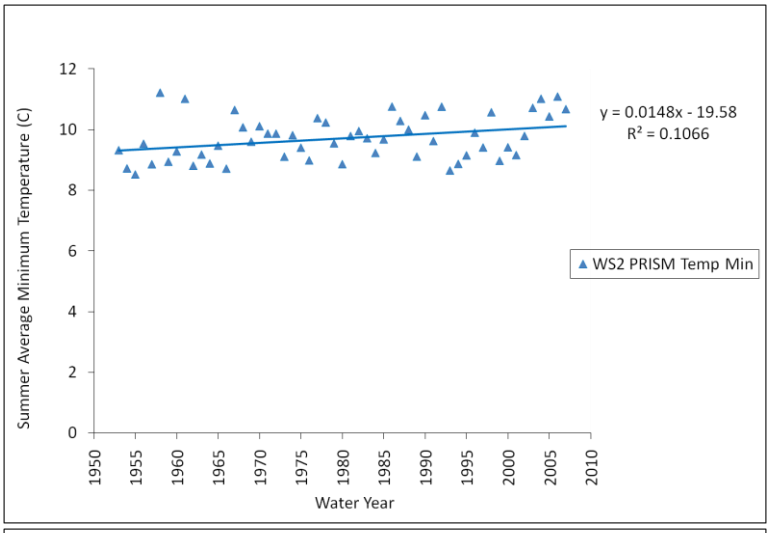

(i)

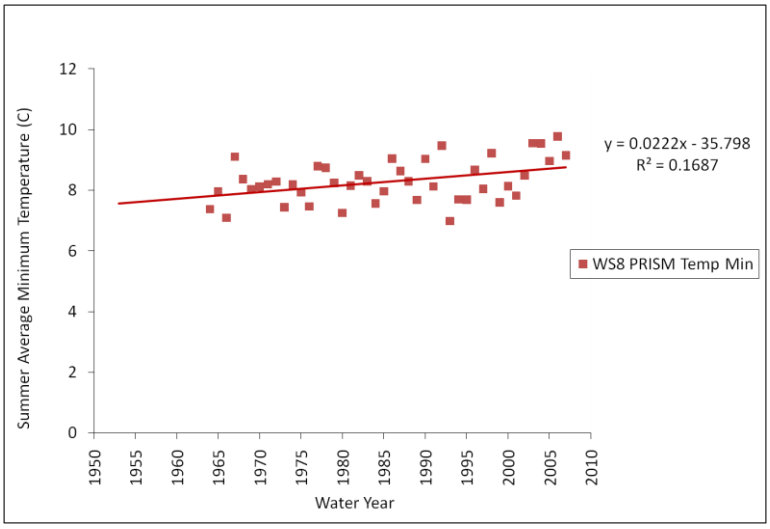

Figure 3.1: Continued.

(j)

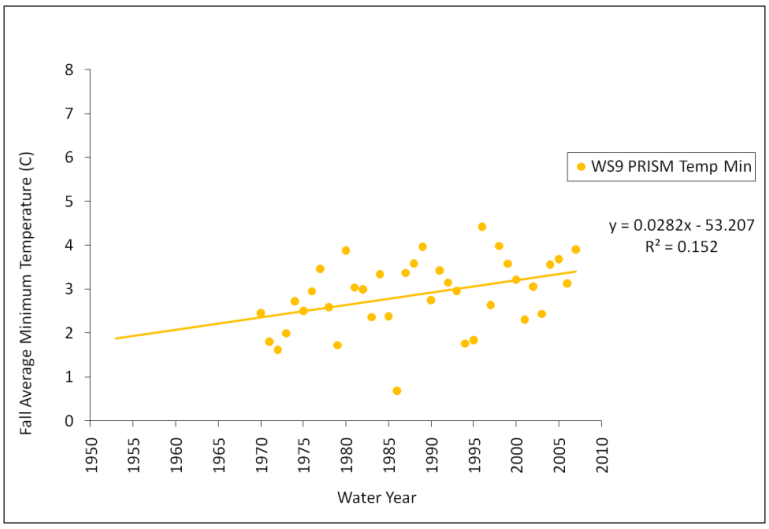

Figure 3.1: Continued.

(k) 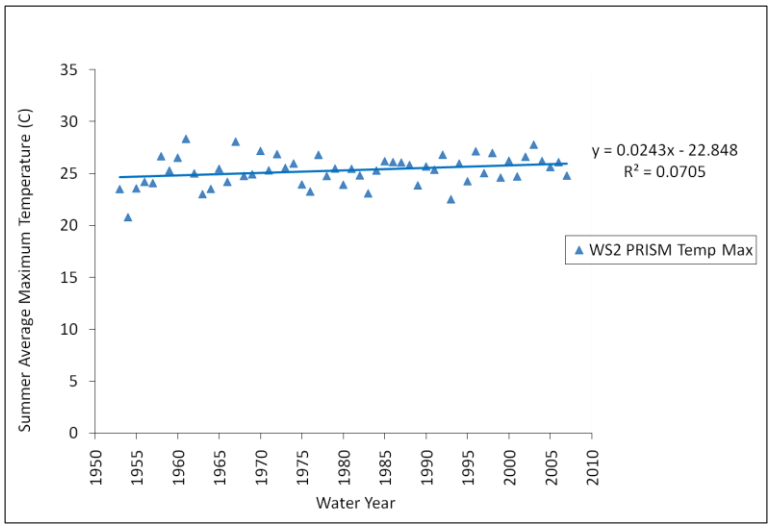

Figure 3.1: Continued.

(l)

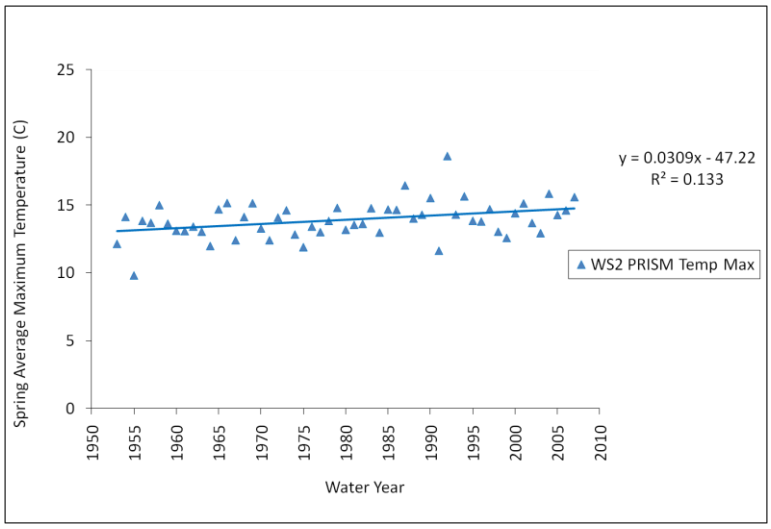

Figure 3.1: Continued.

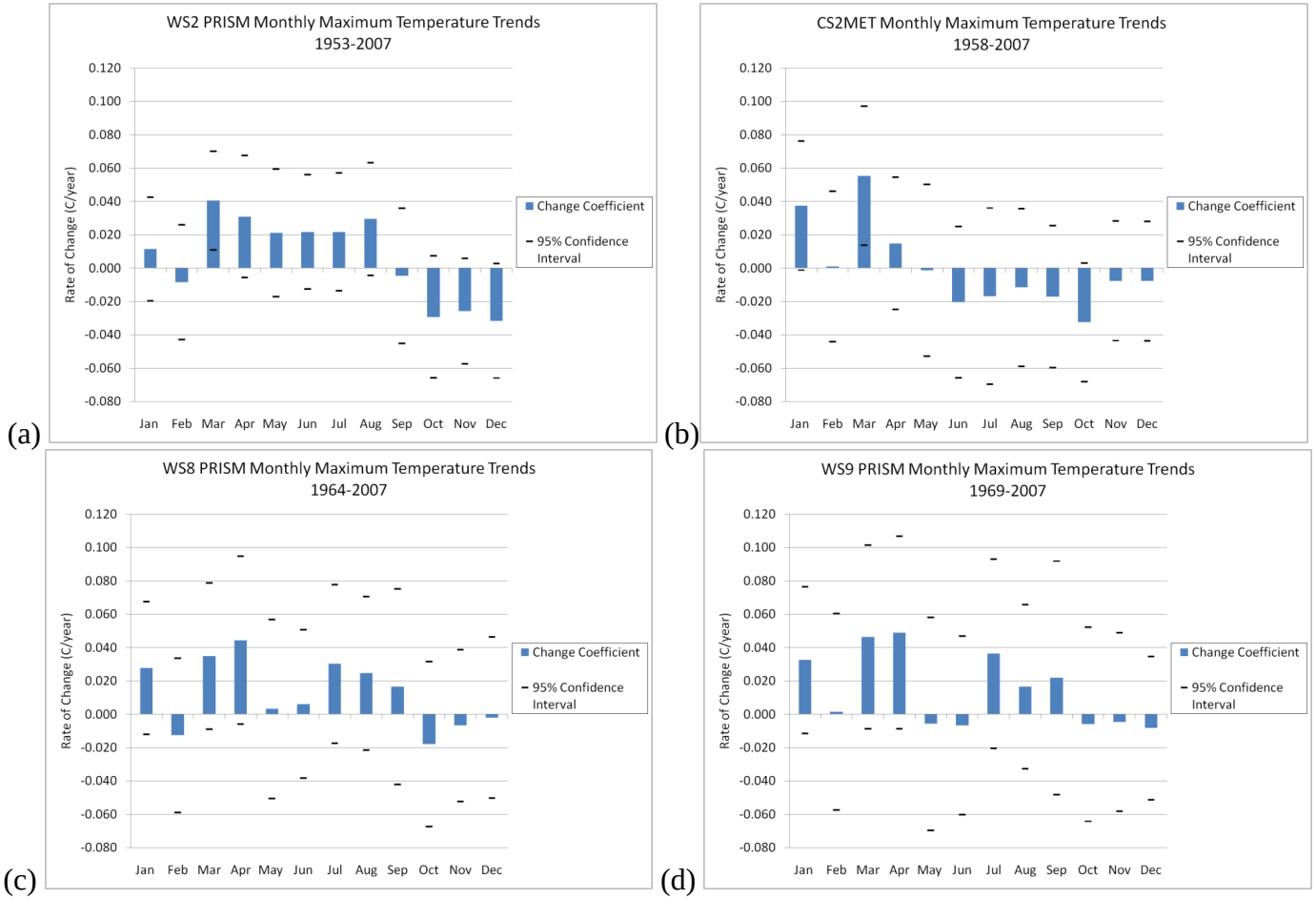

Figure 3.2: Trends in monthly average minimum and maximum temperatures for both CS2MET and PRISM data, shown with a 95% confidence interval. Panels (a)-(d) show the trend coefficients for WS2, CS2MET, WS8, and WS9 monthly average maximum temperatures respectively. Panels (e)-(f) show the trend coefficients for WS2, CS2MET, WS8, and WS9 monthly average minimum temperatures respectively.

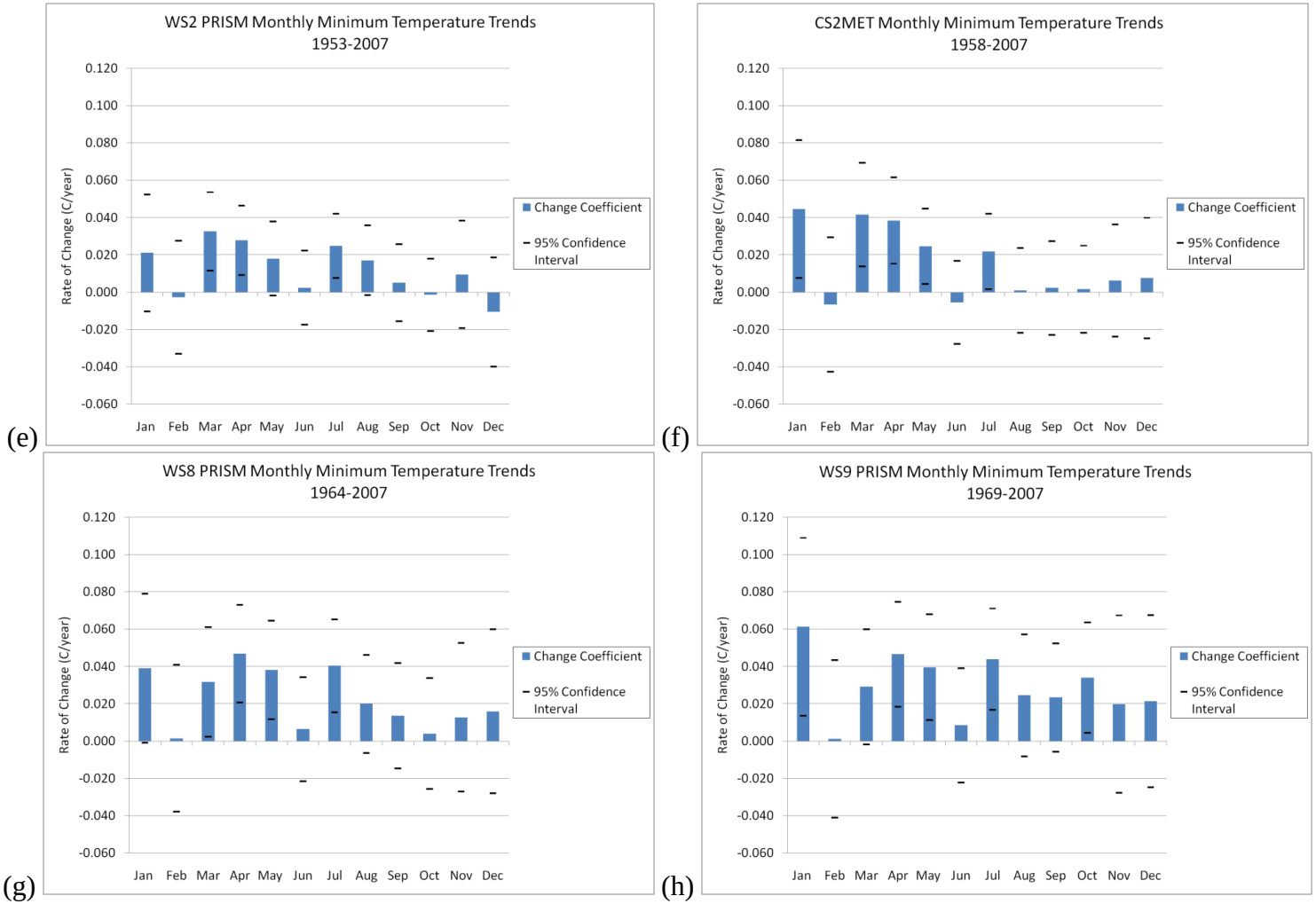

Figure 3.2: Continued.

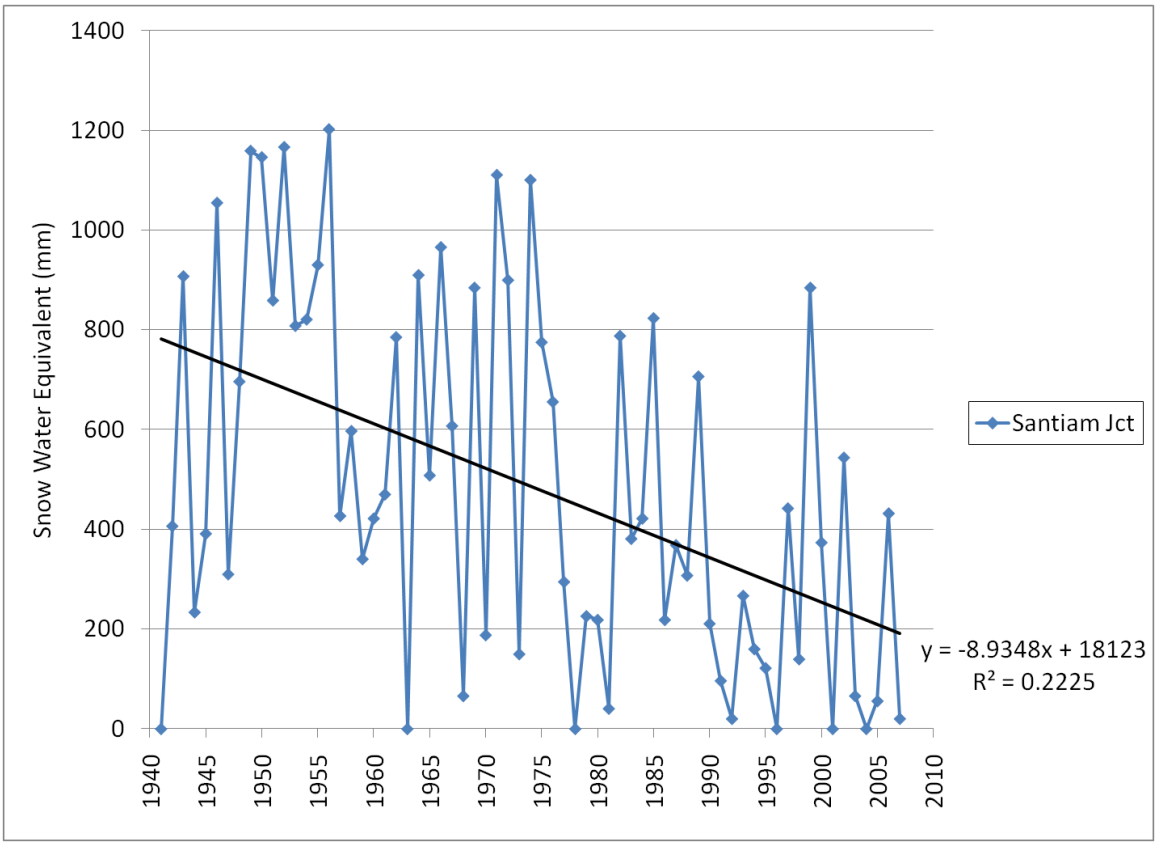

Figure 3.3. Trend in Santiam Junction April 1st Snow Water Equivalent for its period of record from 1941-2007

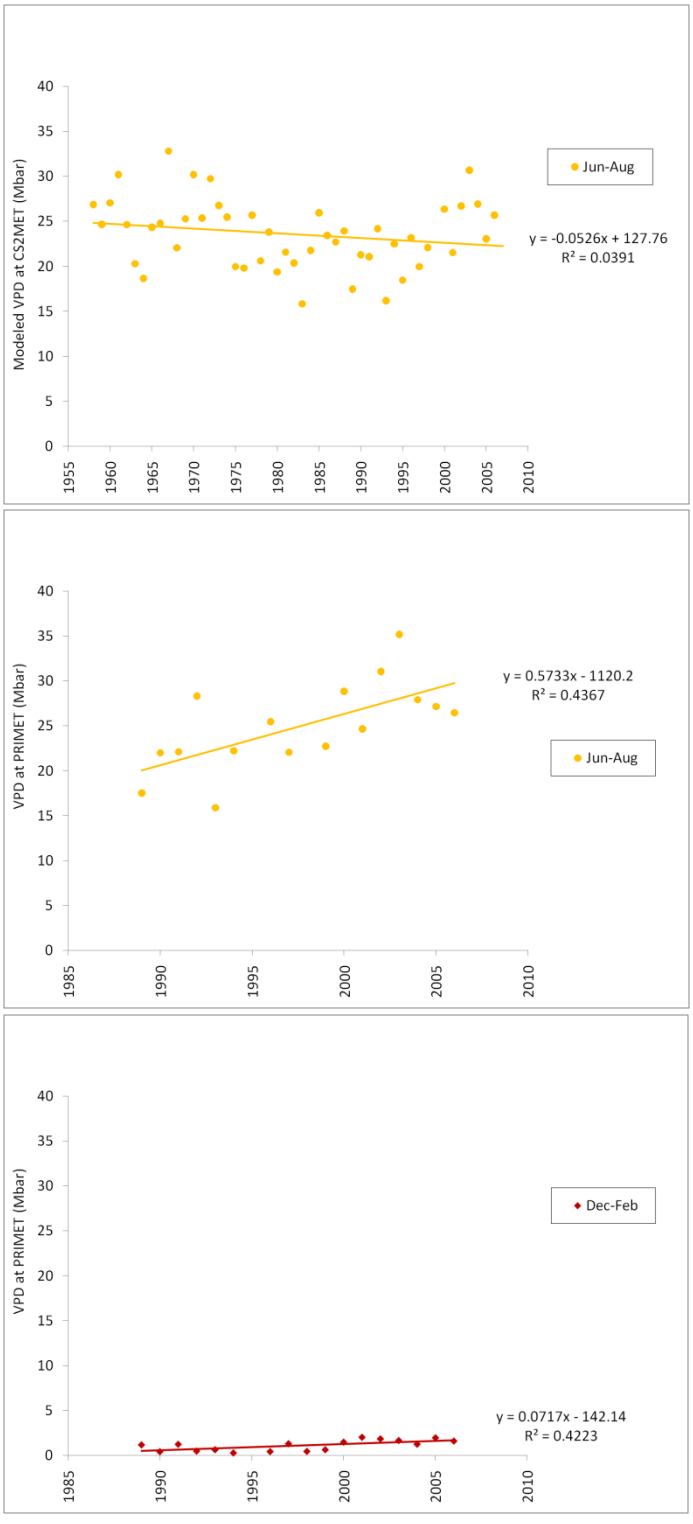

Figure 3.4: Panel (a) shows modeled summer VDP at CS2MET from 1958-2007, panel (b) shows the trend in summer average maximum VPD at PRIMET from 1989-2006, and panel (c) shows the trend in winter average maximum VPD at PRIMET from 1989-2006.

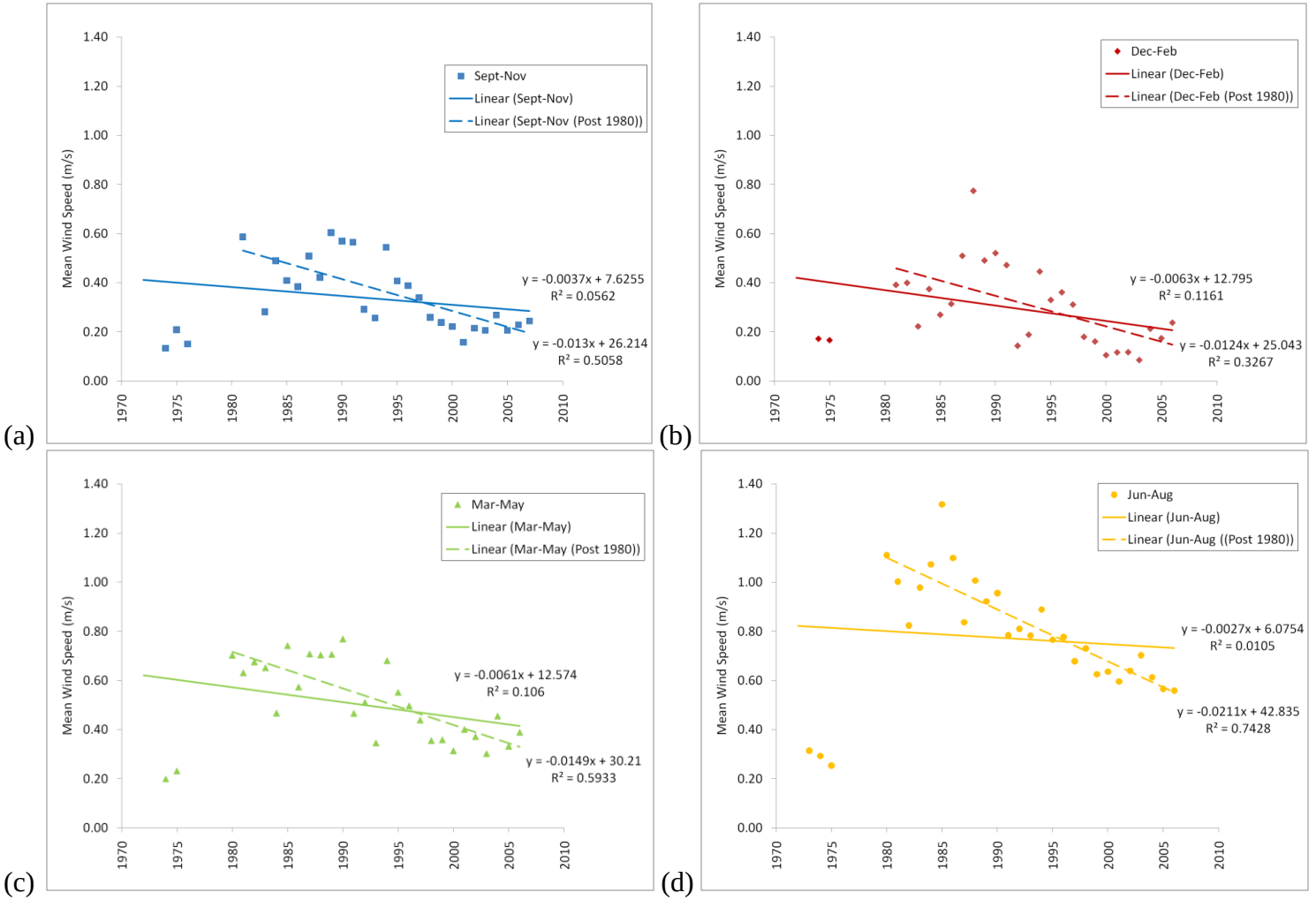

Figure 3.5: Daily Average Wind Speed at PRIMET for the period of record from 1974-2006/07. Panels (a)-(d) show the trends in fall, winter, spring, and summer daily average wind speeds respectively

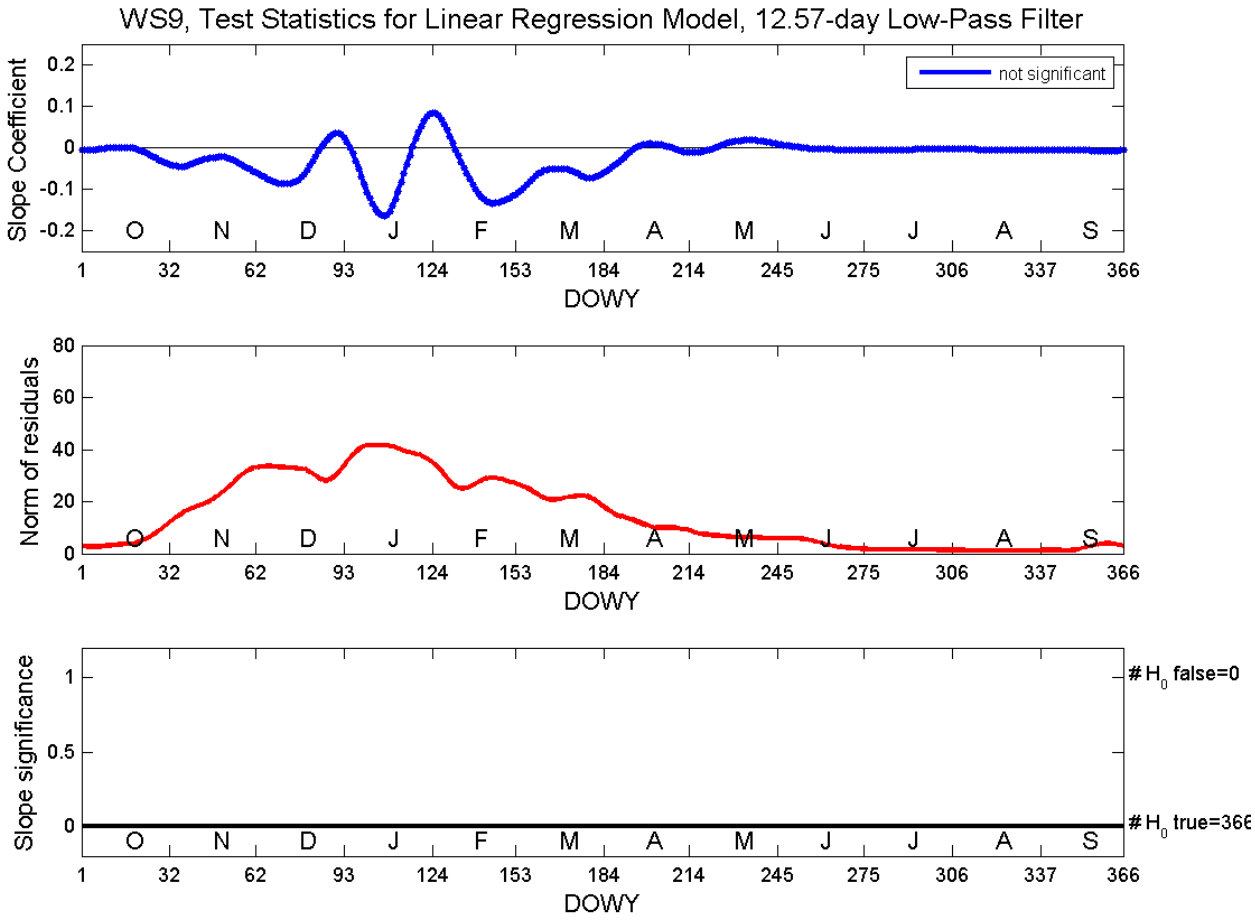

Figure 3.6. Trends in daily discharge at WS9 using a 12.57 day low-pass wavelet filter

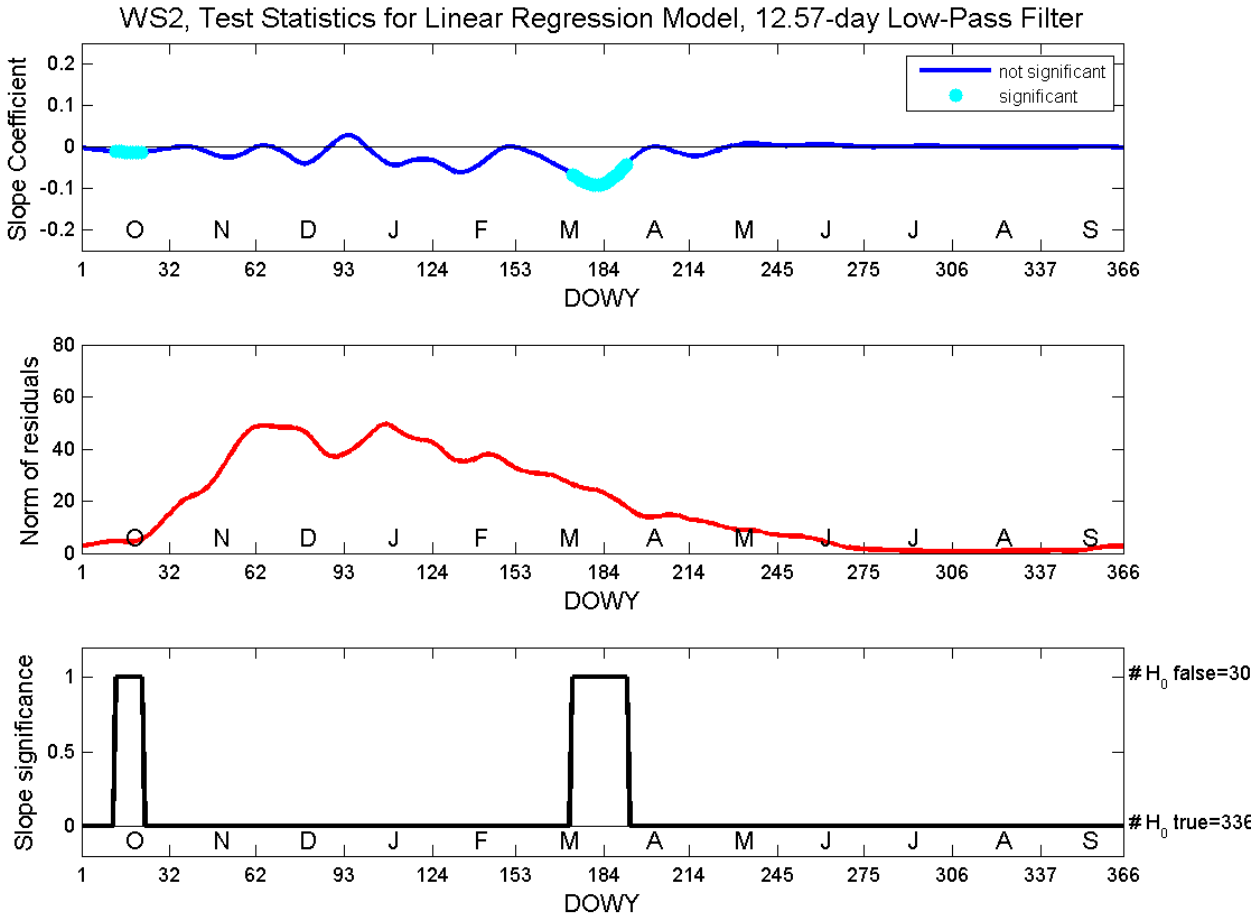

Figure 3.7: Trends in daily discharge at WS2 using a 12.57 day low-pass wavelet filter.

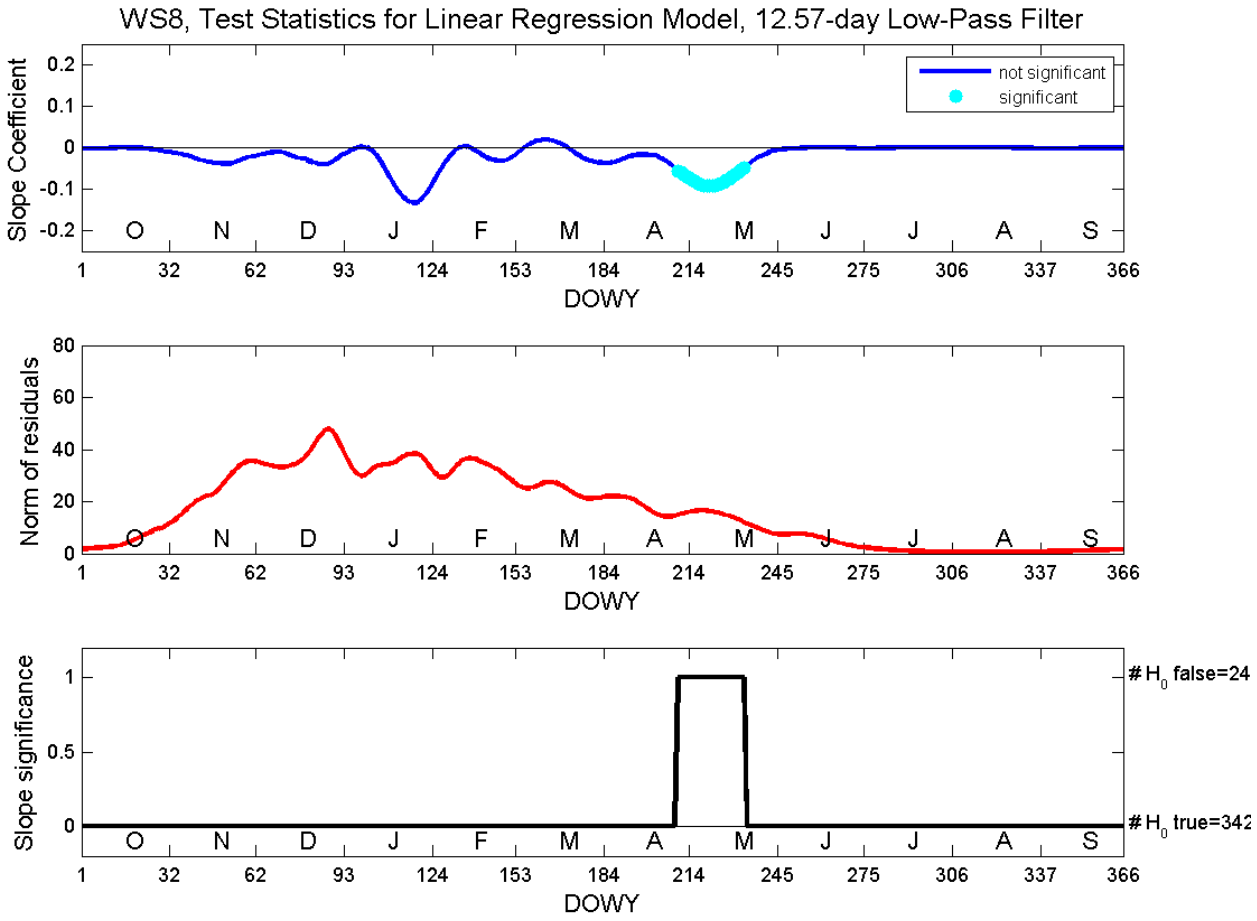

Figure 3.8: Trends in daily discharge at WS8 using a 12.57 day low-pass wavelet filter.

a)

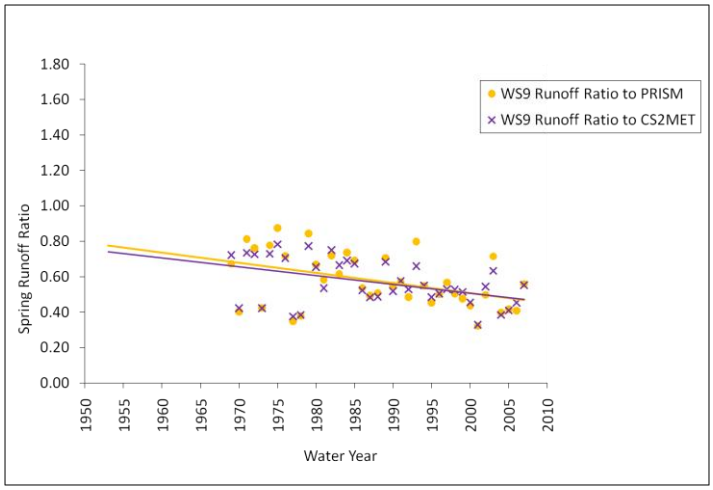

b)

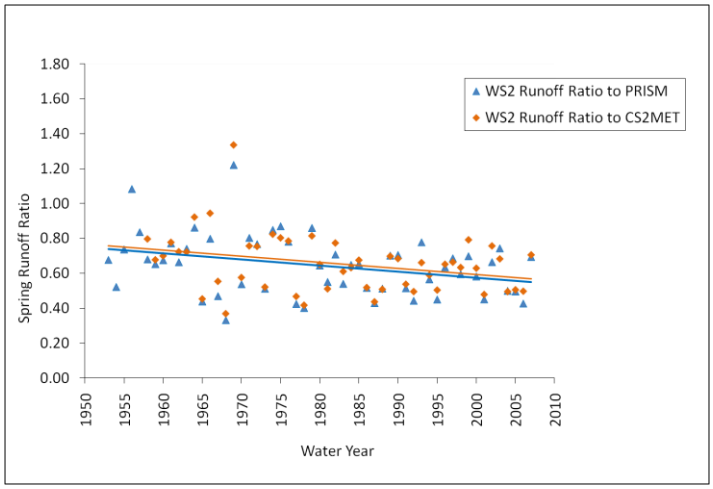

c)

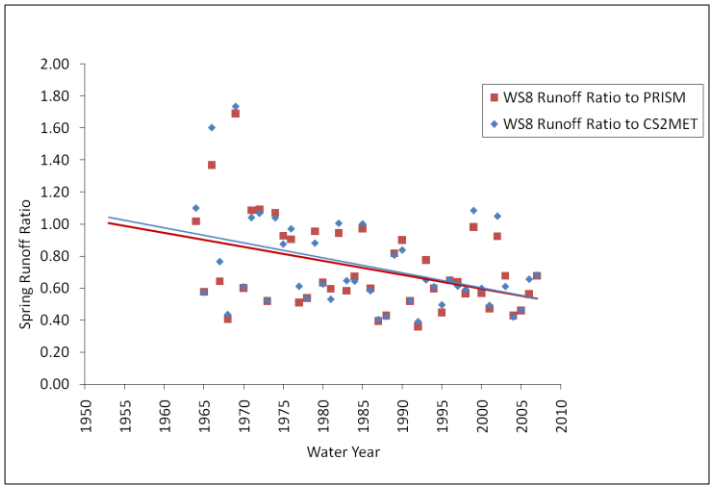

Figure 3.9: Trends in spring runoff ratios calculated using both PRISM records and CS2MET. Panels (a)-(c) show WS9, WS2, and WS8 respectively

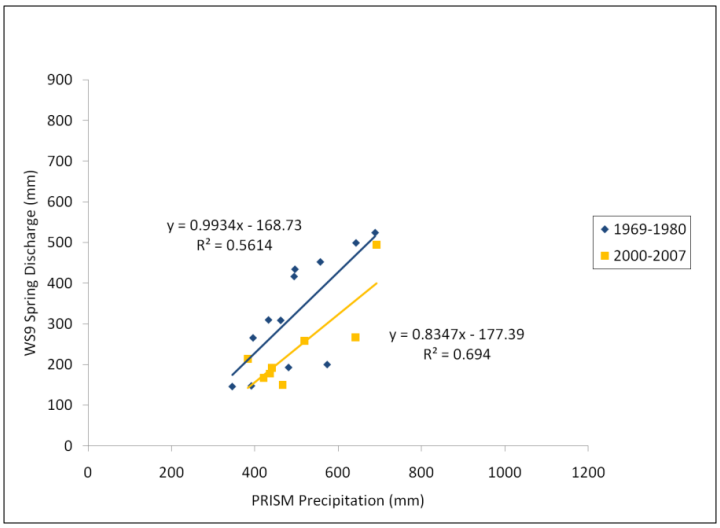

(a)

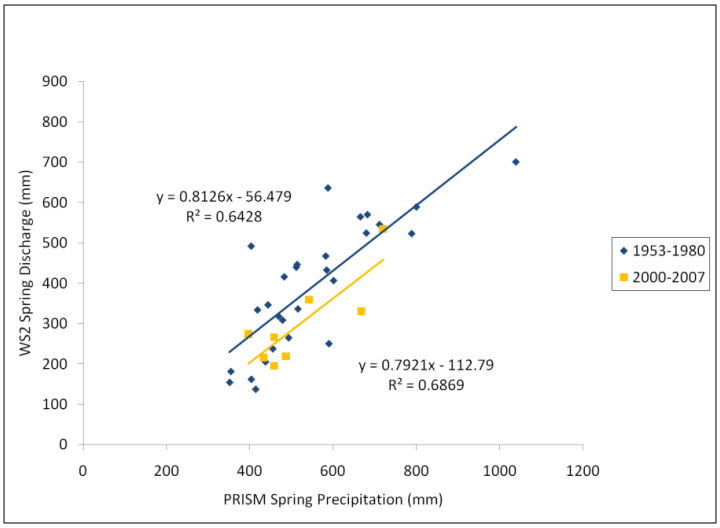

(b)

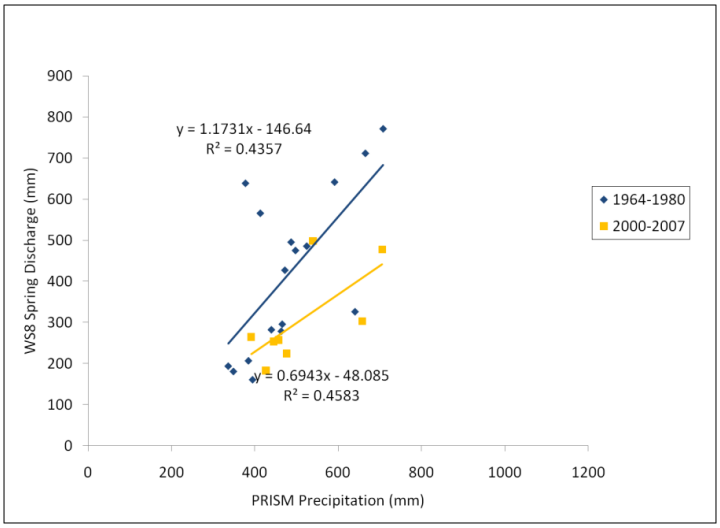

(c)

Figure 3.10: Spring discharge vs. precipitation for the period of record prior to 1981 and the period of record from 2000-2007. Panels (a)-(c) show WS9, WS2, and WS8 respectively.

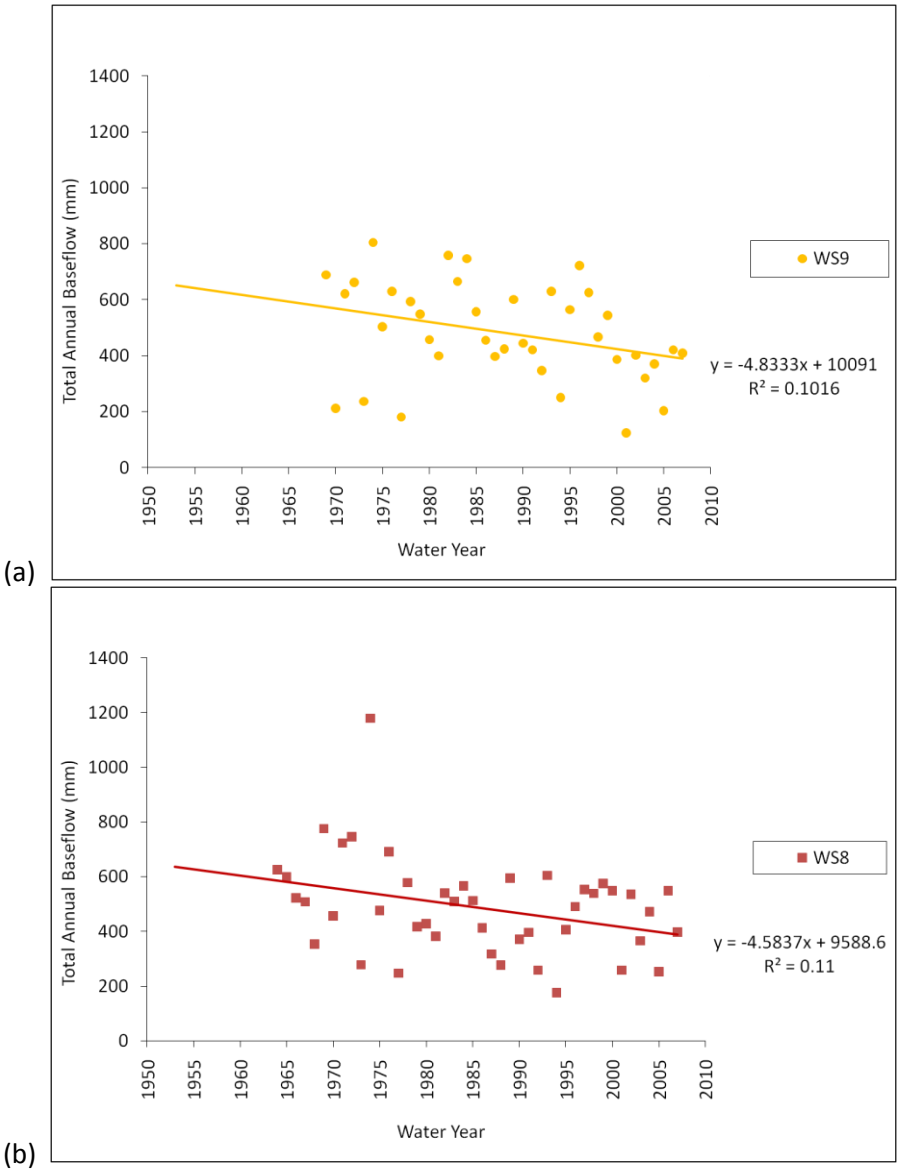

Figure 3.11: Significant trends in baseflow. Panels (a)-(b) show the trends in annual baseflow for WS9 and WS8 respectively. Panels (c)-(d) show the trends in spring baseflow for WS2 and WS8 respectively

(c)

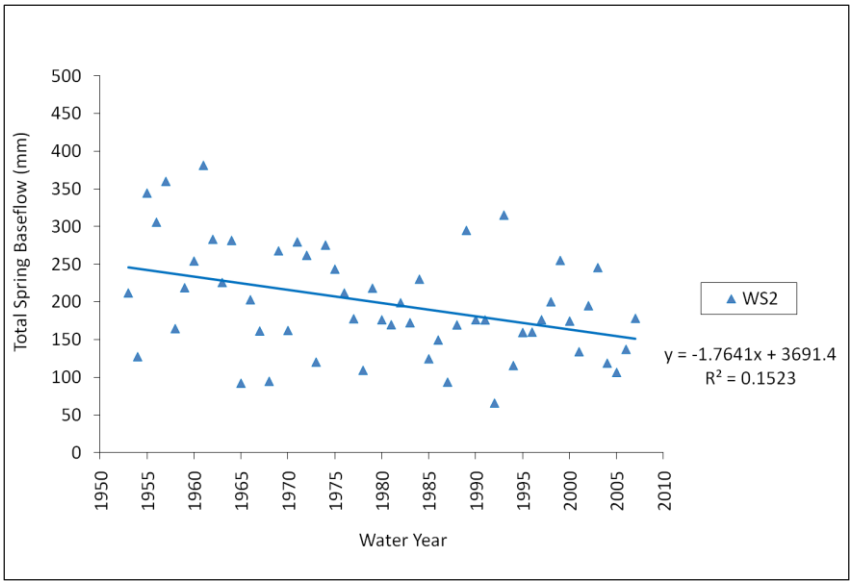

(d)

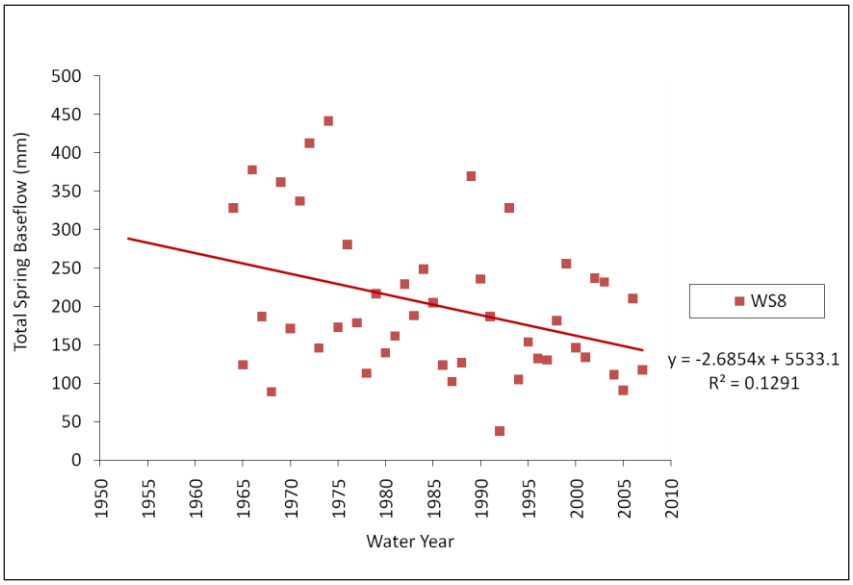

Figure 3.11: Continued.

4. Discussion

Precipitation (amount, timing and variability) has not changed significantly at the HJ Andrews over the last half decade (H1b, Appendix A, Tables A1-A3), and wind speeds have not changed consistently (H1b, Appendix E, Tables E1, E2). The observed changes in streamflow (Figures 3.7-3.10) must either be driven by changes in storage or evapotranspiration (Eq. 1)

Spring and summer air temperatures increased significantly at the HJ Andrews from the 1950s to 2007, based both on measured and modeled (PRISM) temperature records, but winter air temperatures did not change consistently. Measured records at the HJ Andrews are limited because only CS2MET at 485 m has data extending back to 1958, but the sensor was changed in 1999, and the longest temperature record at high elevations within the HJ Andrews only begins in 1987. PRISM data are based on stations that are active during particular years and are thereby limited by the availability of measured data. Nevertheless, trends in spring air temperatures at the HJ Andrews are consistent with warming trends noted elsewhere in the literature for the Pacific Northwest (Mote 2005 et al., Hamlet et al. 2007).

4.1. H1: Physically mediated climate change effects

Many studies (e.g. Regonda et al. 2005, Steward et al. 2005, Barnett et al. 2008) have focused on the anticipated hydrologic consequences of spring warming and earlier snowmelt, without considering how vegetation water use might respond to such changes. Warming spring air temperatures would be expected to have produced an increase in winter/early spring snow melt events and/or an increase in the amount of winter/early spring precipitation falling as rain rather than snow (Knowles et al. 2006, H1a, H1c,

Figures 1.2-1.4). If these changes occurred without any change in evapotranspiration, they should have produced a decline in April 1st SWE, an increase in winter/early spring discharges, a decrease in later spring and summer discharges, and a shift in the date of water year median flow (Dettinger and Cayan 1995, Cayan et al. 2001, Mote et al. 2005, Regonda et al. 2005, Steward et al. 2005, Hamlet et al. 2007, Barnett et al. 2008, Jefferson et al, 2008, H1a, H1c, H1d, Figures 1.1-1.4). In turn, warming temperatures are expected to have exacerbated the summer hydrologic drought (Barnett et al 2008). If this occurred without any changes in evapotranspiration, summer discharges should have declined, summer runoff ratios should be negatively related to April 1st SWE, and summer runoff ratios should be positively related to spring runoff ratios (H1d, Figure 1.1d, Figure 1.4).

Hypotheses H1a, H1c, and H1d are partially supported by the results presented here: April 1st SWE at Santiam Junction declined significantly over the periods of record corresponding to streamflow spanning from 1953-2007, while total precipitation remained unchanged. Given the lack of consistent increases in winter air temperature, it appears that increased air temperatures in March caused an increase in early spring snow melt events and/or an increase in the amount of early spring precipitation falling as rain rather than snow, leading to the decline in April 1st SWE. Spring runoff ratios and baseflows from all three watersheds were significantly positively related to April 1st SWE at Santiam Junction: larger snowpack produced higher runoff ratios and baseflow. Although spring discharges were too variable to reveal trends over time, spring runoff ratios from all three watersheds declined for their respective periods of record. Baseflows and low-pass filtered daily discharge at WS2 (548-1078 m) and WS8 (993-

1182 m) also declined during the spring. The declines in low-pass filtered daily discharge correspond with the expected timing of snowmelt which occurs in late March and early April for WS2, and in late April and May for WS8 (Figure. 4.1). The lack of trend in WS9 spring baseflow and low-pass filtered daily discharge may be due to the smaller influence of snow given its lower elevation (432-731 m). At the HJ Andrews, magnitudes of snowmelt increase with elevation and the timing of melt is delayed (Perkins, 1997).

4.2. H2: Biologically mediated effects

Despite this evidence, some aspects of hydrologic response in small watersheds at the HJ Andrews suggest that forest ecosystem water use (evapotranspiration) has changed, mitigating expected effects of climate change on hydrology. Paired watershed experiments in the Andrews Forest and elsewhere in the Pacific Northwest indicate that evergreen forest ecosystems in the marine west-coast climate experience peak evapotranspiration rates in the fall and spring, when soils are moist and temperatures are moderate (Figure 4.2, Jones and Post 2004). If forest ecosystems have responded to spring warming by an earlier onset of spring evapotranspiration, we would expect that April 1st SWE has declined, winter/early spring discharges have not changed, late spring discharges have declined, and winter/spring runoff ratios should be negatively related to winter/spring temperatures or VDP (H1c, H2a, H2b, Figures 1.2-1.3). If water use by dominant tree species at the HJ Andrews is regulated by vapor pressure deficit, warming summer temperatures could reduce summer transpiration, compensating for declining summer water availability (H2c). If this has occurred, then summer discharges should

have been unchanged over time, and summer runoff ratios should be positively related to summer temperatures or VPD (Figure 1.4).

Results of this study are consistent with these expectations: neither winter nor summer discharge/runoff ratios/baseflows have changed over the periods of streamflow record, nor has the date of water year median flow shifted earlier, in contrast to the results found by Regonda et al. (2005), Steward et al. (2005), and Jefferson et al, (2008) as examples (H1a, H1d). Moreover, summer runoff ratios/baseflows are independent of April 1st SWE at Santiam Junction and winter air temperatures, and summer runoff ratios are independent of spring runoff ratios. Thus, forest ecosystem water use in small watersheds at the Andrews Forest appears to be insensitive to the timing of spring snowmelt.

Additional evidence from this study supports the assertion that forest evapotranspiration has adapted to changes in winter and summer temperatures, so as to mitigate climate warming effects on streamflow in winter and summer. For example, winter runoff ratios for WS2 and WS9 were significantly negatively related to winter average maximum temperatures and to modeled VPD at CS2MET; indicating that photosynthesis and transpiration can occur in winter in these watersheds, which are at relatively low elevations with comparatively low snowpacks and near-zero winter air temperatures (Figure 2.4, Figure 2.6, Emmingham and Waring 1977, Emmingham 1982, Perkins and Jones 2008). Winter baseflows for all three watersheds were also significantly negatively related to modeled VPD at CS2MET, indicating that transpiration occurs during periods of warmer dry weather. There is also some evidence that summer runoff ratios are significantly positively related to summer temperatures and to summer

evapotranspiration as proxied by VPD, indicating that transpiration is suppressed during periods of warm dry weather during the summer, as indicated by the fact that WS2 and WS8 summer runoff ratios are significantly positively related to both summer average maximum temperatures as well as modeled VPD at CS2MET. Summer runoff ratios at WS2 are also significantly positively related with VPD at PRIMET over its shorter period of record.

Summer runoff ratios at WS9 are not related to average maximum summer air temperatures or modeled VPD, probably because summer discharges at WS9 are confounded by two different streamflow measurement techniques (see methods). Unlike WS2 and WS8, at WS 9 summer baseflows are significantly negatively related to summer temperatures and VDP (both measured at PRIMET and modeled VPD at CS2MET), meaning that runoff is lower (and evapotranspiration higher) during periods of warm dry weather. These results are probably driven by precipitation, because temperature and VPD are likely to be negatively correlated with precipitation, which is accounted for to a greater extent in runoff ratios than in baseflows.

These findings are consistent with the principle that dominant Douglas-fir trees limit transpiration through stomatal closure when VPD becomes sufficiently large or soil moisture becomes limited (Unsworth et al 2004, Barnard 2009). Douglas-fir trees are sensitive to summer water deficits, and increases in summer temperatures without compensatory increases in summer precipitation or moisture reserves are likely to cause decreases in growth (Littell et al. 2008). However, Brooks et al. (2009) assert that water used by trees during dry summers is physically separated from water entering streams, which is inconsistent with the finding that WS2 and WS8 summer runoff ratios are

related to summer VPD and/or summer average maximum temperatures. This disparity can be resolved by considering the scales of the analyses: Brooks et al (2009) sampled water from trees on a steep hillslope, which likely was not contributing water to summer streamflow, but water used by trees in other portions of the watershed is connected to summer streamflow. For example, transpiration within only 0.1 to 0.3% of the watershed area accounted for diel fluctuations in summer streamflows in WS1 at the HJ Andrews, and the vegetated area influencing streamflow became smaller as the summer progressed (Bond et al. 2002). Similarly, Wondzell et al. (2010) suggests that a large portion of the stream network in WS1 does not have substantial lateral inputs of hillslope water during baseflow, which could be intercepted and transpired by trees; Brooks et al (2009) apparently sampled trees in a similarly "unconnected" hillslope segment.

Although we infer that winter and summer transpiration rates may have responded to climate warming, this study found no trend in average maximum winter air temperatures or VPD from 1958-2007 (although winter VPD at PRIMET shows a significant increase over its shorter period of record from 1989-2006). Summer average maximum temperatures also did not increase consistently (only WS2 summer average maximum temperatures show a significant increase over time, and this trend is only evident for the period from 1953-2007, and not from 1926-2007). Furthermore, trends in VPD over time are inconclusive because measured records are too short to detect a trend and modeled VPD depends on the air temperature record.

The relationships between spring air temperature warming, VPD, transpiration, and streamflow depend upon location in the landscape: in places where soil moisture is limiting, transpiration may be negatively related to VPD, but in places where soil

moisture is not limiting, transpiration may be positively related to VPD up to then point when leaf water potential reaches its minimum. Although spring temperatures have increased significantly, neither measured spring VPD at PRIMET (1989-2006) nor modeled VPD at CS2MET (1958-2006) have increased. Forest water use appears to be higher in spring when air temperatures are high and humidity low (spring baseflows are significantly negatively related to both spring average minimum and maximum temperatures, except at WS9, and to modeled VPD) However, a relationship between spring runoff ratios and air temperatures is evident only at WS8. As already noted, the relationship between whole-watershed transpiration (as inferred from runoff) and temperature/VPD is confounded by precipitation. The negative relationship between WS8 spring runoff ratio and spring average minimum temperature may indicate an increase in tree growth and subsequent water use with increasing temperature. Littell et al. (2008) found that Douglas-fir trees at high elevations, which were previously limited by low growing season temperatures, may exhibit increases in growth in a warming climate.

The estimated changes in spring runoff over the half-century of this study can be explained by changes in transpiration rates that are within the range of measured rates of transpiration in these watersheds. The inverse relationship between spring runoff ratios and VPD at PRIMET from 1989-2006 indicates that transpiration increases, and spring runoff ratios decline during conditions of higher temperature and low humidity. The estimated total declines in spring runoff ratios over the periods of record at WS2, WS9, and WS8 equate to declines in daily streamflow of 1.13 mm, 1.23 mm, and 2.13 mm respectively, over the 50-year period of the analysis. These estimates fall within the

reported range of maximum daily transpiration for old-growth Douglas-fir dominated forests, which range from about 1mm day^{-1} to 2.3 mm day^{-1} (Chen et al, 2004, Moore et al, 2004, Unsworth et al, 2004). It is however unclear whether VPD at PRIMET is a better proxy for ET across the watersheds than modeled VPD at CS2MET. Barnard (2009) found that while transpiration of conifers within a steep, headwater watershed at the HJ Andrews (WS1, which is adjacent to WS2) is highly responsive to VPD, there is significant spatial variability in both VPD and transpiration across the watershed. Furthermore, Barnard (2009) found that spatial variability in micro-climatic variables alone (VPD and photosynthetically active radiation) were not able to fully predict variability in transpiration. Thus, climate change effects on VPD appear to be driving changes in watershed-wide transpiration, and only certain areas of forest within the watershed are likely to be responsible for the changes in discharge, but these areas are debated (Bond et al 2002, Barnard 2009, Brooks et al 2009, Wondzell et al 2010).

.

a)

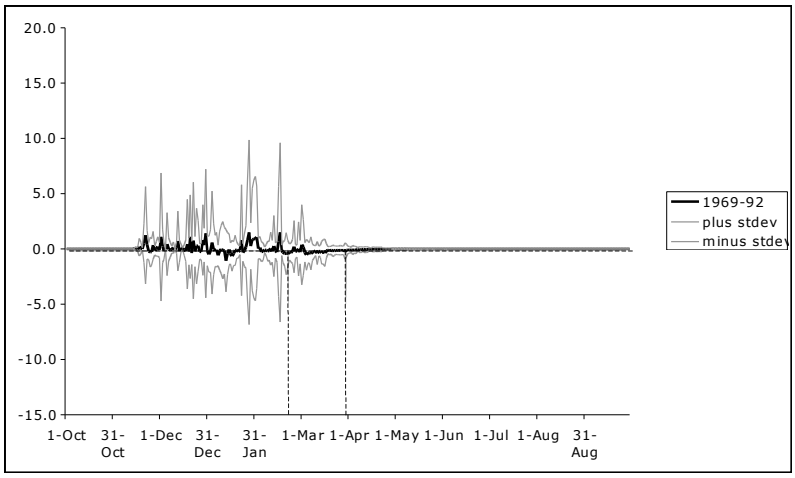

b)

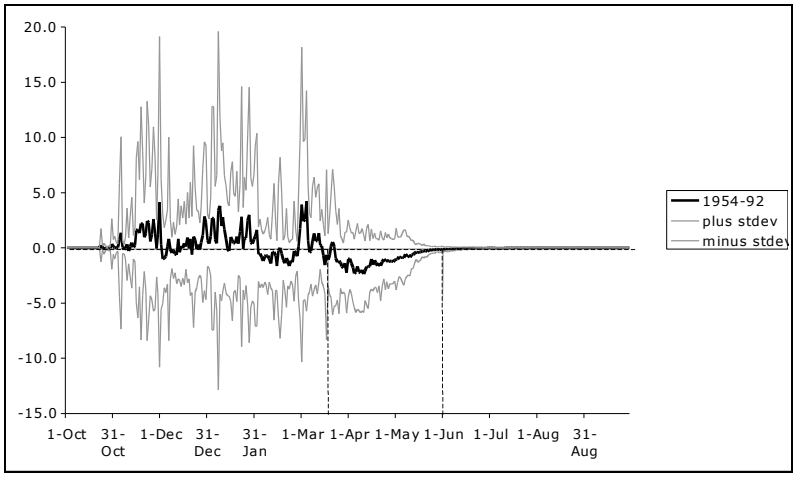

c)

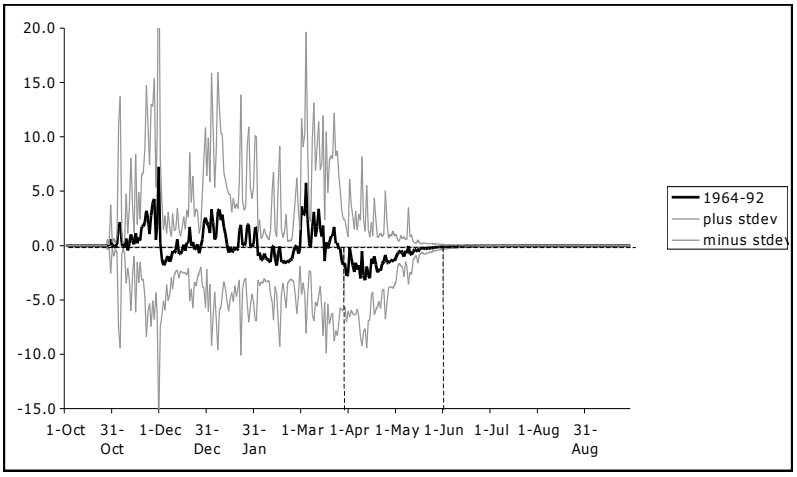

Figure 4.1 Average daily difference in modeled snow water equivalent (mm) at three small watersheds in the HJ Andrews Forest. (a) WS 9, 1969-92, (b) WS 2, 1954-92, and (c) WS 8, 1964-92. Positive values indicate snowpack accumulation; negative values indicate snowmelt relative to the day before. Vertical dashed lines show the period of prolonged spring snowmelt." Source: Perkins RM. 1997.

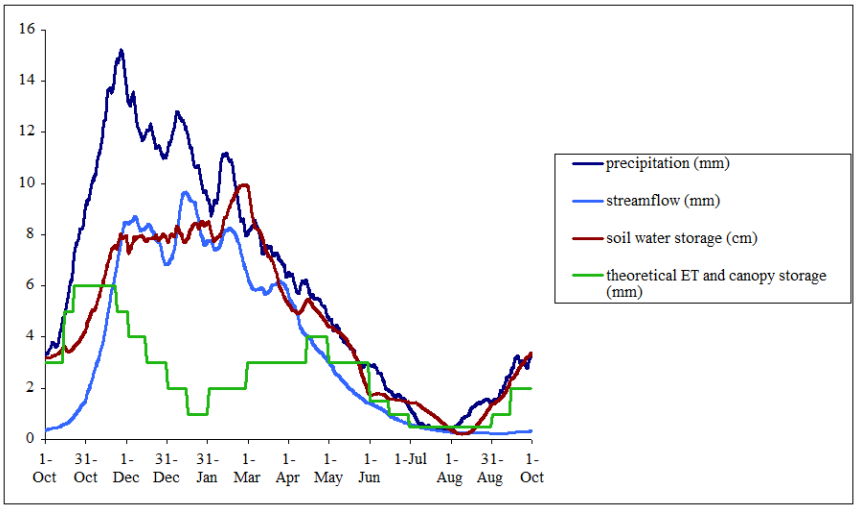

Figure 4.2 Annual hyetograph, hydrograph, soil water storage, and estimated ET + canopy water storage + groundwater recharge, by day of water year, based on data for Watershed 2, 1953-2002 (Source: J. Jones, personal communication. Created from a soil moisture balance using average daily values of P and Q, and estimated ET values from analysis of post-harvest changes in Q (Jones and Post 2004).

5. Conclusion

The findings of this study most strongly support the hypothesis that warming temperatures have resulted in a reduction in spring snowpacks, leading to a decrease in spring runoff, but to some extent these changes have been mitigated by forest transpiration responses to climate, including an earlier onset of evapotranspiration in the spring and reduced evapotranspiration during the summer. These responses are attributable to the dominant trees' capacity for stomatal closure when VPD becomes sufficiently large or soil moisture becomes limited and their potential for opportunistic photosynthesis when conditions are favorable (Emmingham and Waring, 1977, Emmingham 1982). Spring and summer average minimum temperatures increased by 1 to 2°C, while April 1st SWE at Santiam Junction declined by 80% over the half-century of the study. The decline in April 1st SWE is likely due to increases in March temperatures. Although spring runoff ratios from all three watersheds declined over 40 to 50-year periods of record, neither winter nor summer runoff ratios changed, nor was there a shift in the date of water year median flow. Despite limitations in some records, it appears that forest ecosystems at the Andrews Forest have mitigated expected effects of climate warming on hydrology by adjusting water use. The concept that forest ecosystems may mitigate climate change effects on hydrology has not been considered in most climate change-hydrology studies (e.g. Regonda et al. 2005, Steward et al. 2005, Barnett et al. 2008) but it deserves further study, both within the Andrews Forest and more generally throughout the western United States. Further inquiry should also be given to the role of forest succession and changes in leaf area, which were not addressed in this current study.

Appendix A: Precipitation

Precipitation exhibits no significant trends in the three PRISM datasets or CS2MET, either annually or by season for both the periods of record corresponding to streamflow or the period of overlapping streamflow from 1969-2007 (Tables A1, A2). Figures A1-A5 show the trends in precipitation by season for the periods of record corresponding to streamflow for the three PRISM datasets, and for the full period of record for CS2MET. Trend lines and equations are shown on the figures along with an R^2 goodness of fit estimate.

The coefficient of variation for precipitation at CS2MET exhibits no significant trends by season for the period of record (Table A3). Figure A6 shows the coefficient of variation for precipitation at CS2MET by season for the period of record. Trend lines and equations are shown on the figures along with an R^2 goodness of fit estimate.

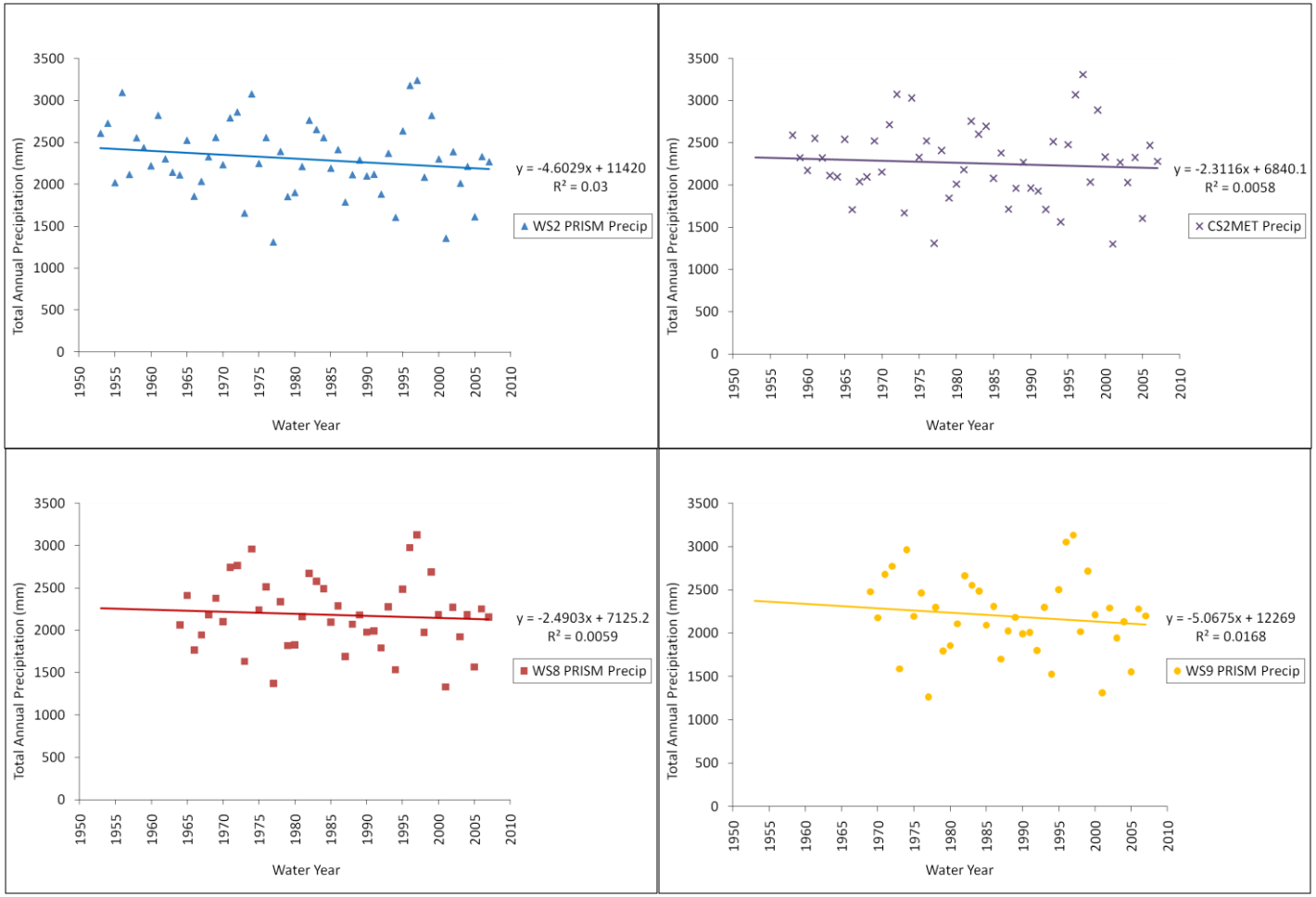

Figure A1. Trends in annual precipitation at (clockwise from top left) WS2 PRISM, CS2MET, WS9 PRISM, and WS8 PRISM.

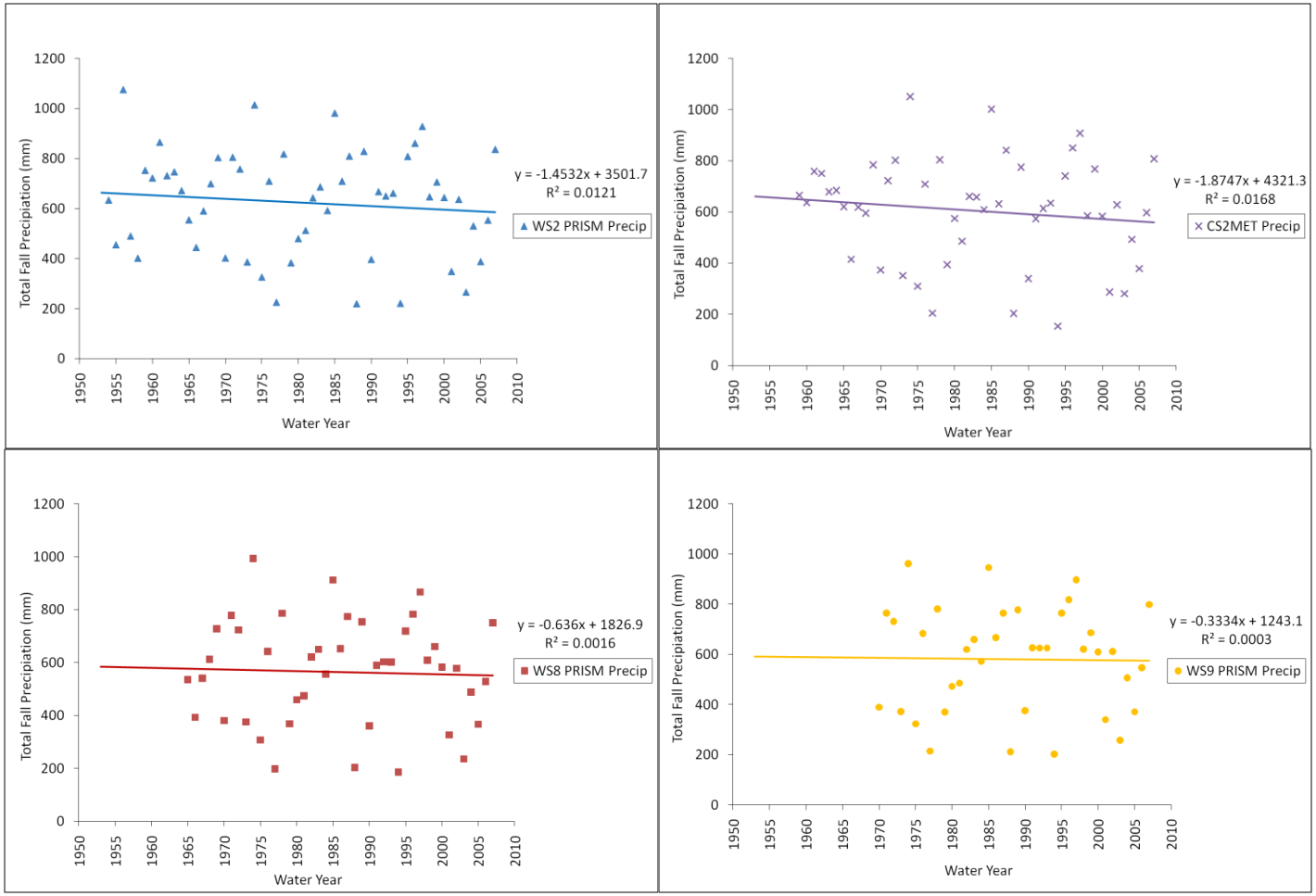

Figure A2. Trends in fall precipitation at (clockwise from top left) WS2 PRISM, CS2MET, WS9 PRISM, and WS8 PRISM.

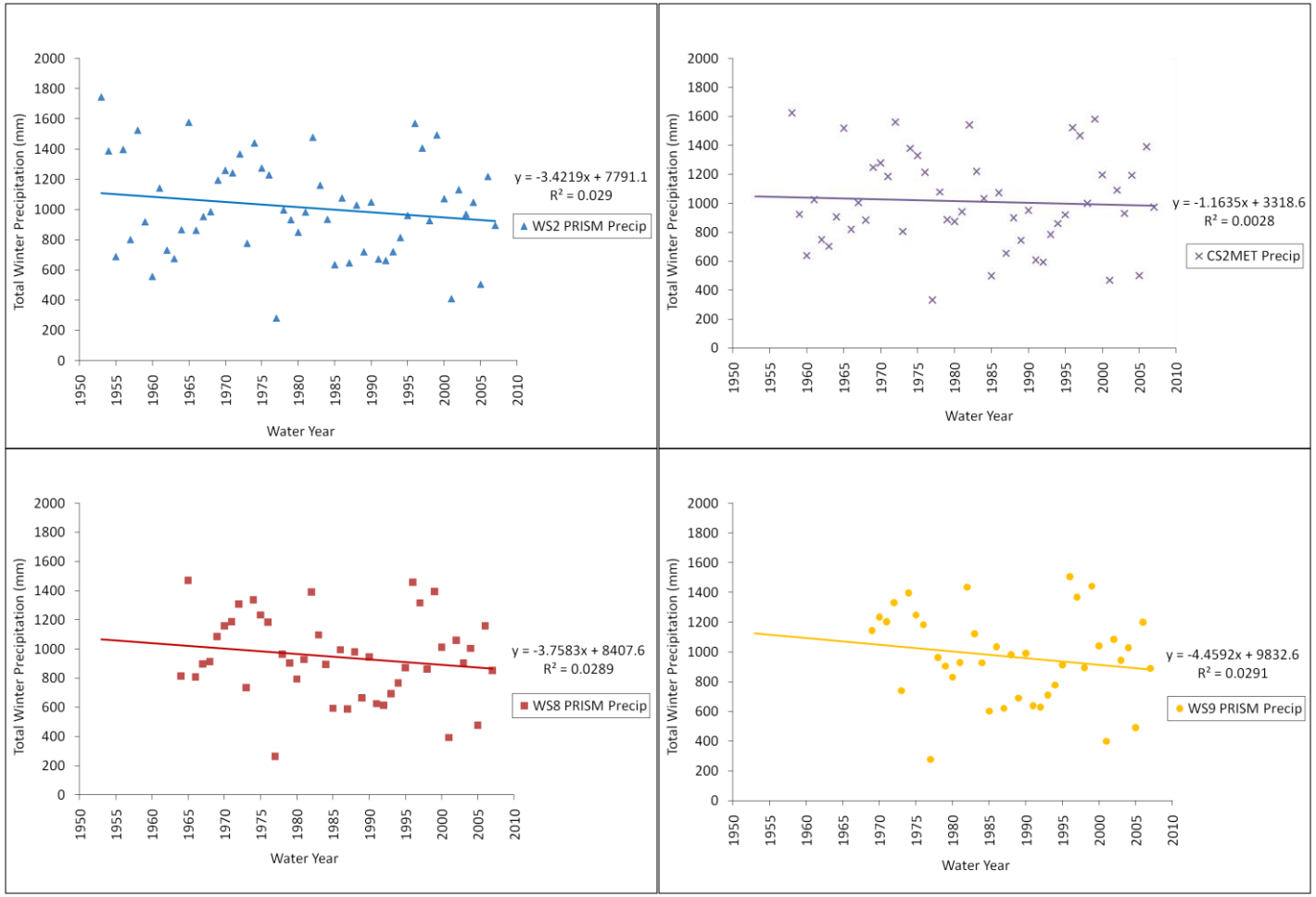

Figure A3. Trends in winter precipitation at (clockwise from top left) WS2 PRISM, CS2MET, WS9 PRISM, and WS8 PRISM.

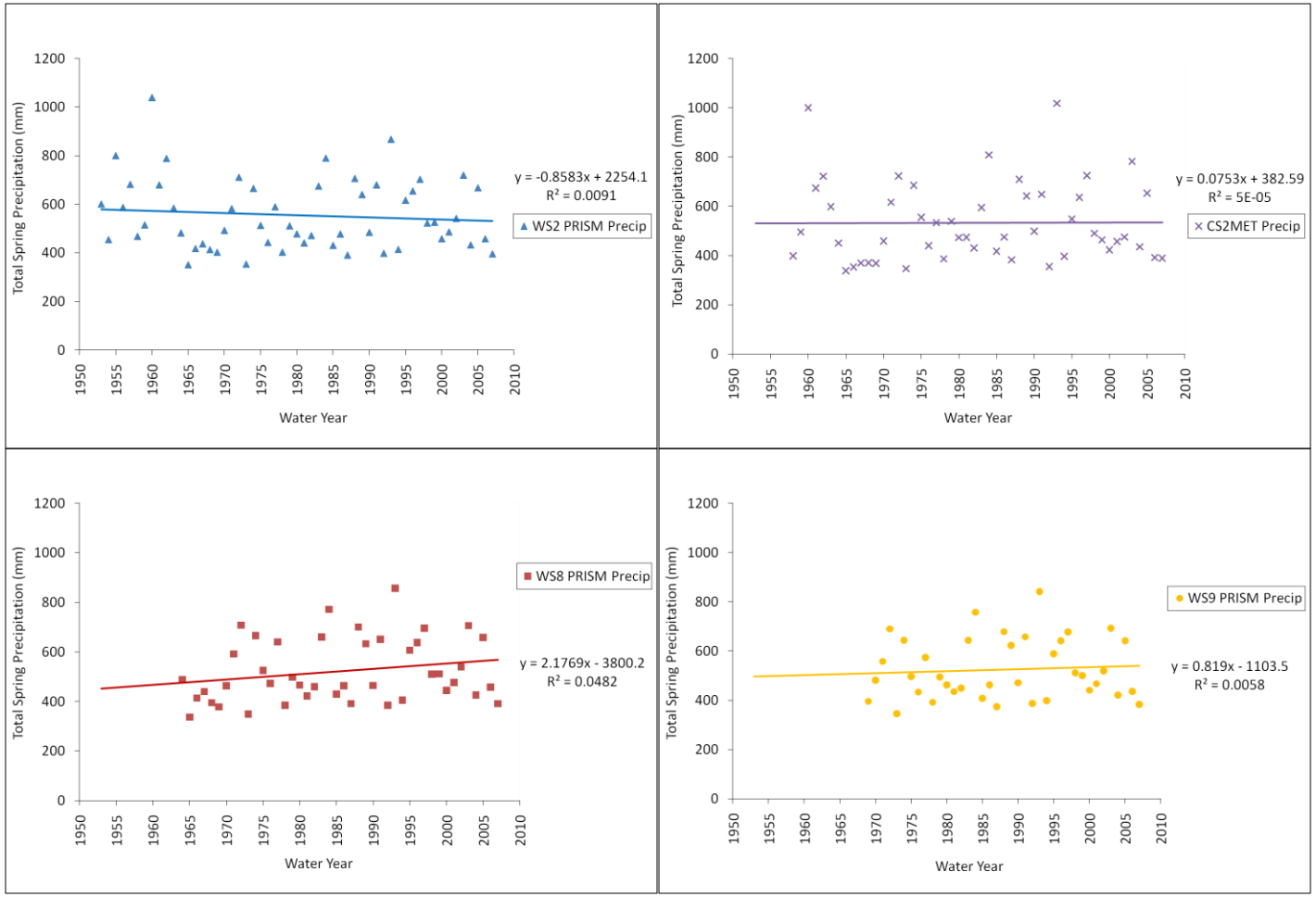

Figure A4. Trends in spring precipitation at (clockwise from top left) WS2 PRISM, CS2MET, WS9 PRISM, and WS8 PRISM.

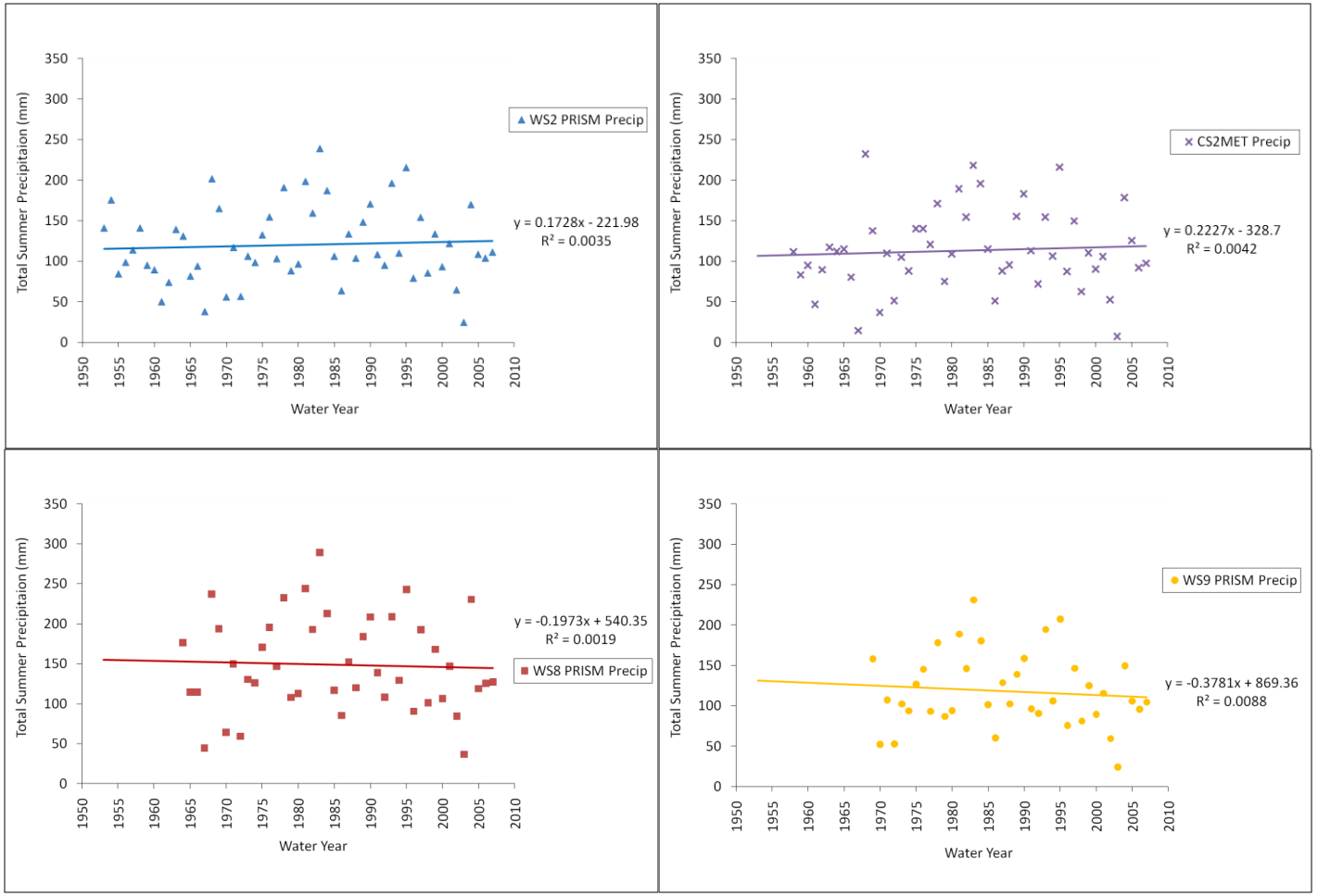

Figure A5. Trends in summer precipitation at (clockwise from top left) WS2 PRISM, CS2MET, WS9 PRISM, and WS8 PRISM.

Table A1. Summary regression table of trends in precipitation at CS2MET for the period of record, and at WS2 PRISM, WS8 PRISM, and WS9 PRISM for the periods corresponding to streamflows.

Simple Linear Regression Models of Precipitation over Time

	Explanatory Variable Coefficients			
Dependent Variable	**Intercept**	**Year**	**P-value**	**R^2**	**N**
CS2MET Annual Precipitation	6840.12	-2.312	0.599	0.006	50
WS2 Annual PRISM Precipitation	11419.6	-4.603	0.206	0.030	55
WS8 Annual PRISM Precipitation	7125.19	-2.490	0.620	0.006	44
WS9 Annual PRISM Precipitation	12269.5	-5.068	0.431	0.017	39
CS2MET Fall Precipitation	4321.35	-1.875	0.375	0.017	49
WS2 Fall PRISM Precipitation	3501.67	-1.453	0.428	0.012	54
WS8 Fall PRISM Precipitation	1826.93	-0.636	0.798	0.002	43
WS9 Fall PRISM Precipitation	1243.14	-0.333	0.916	0.000	38
CS2MET Winter Precipitation	3318.55	-1.164	0.717	0.003	50
WS2 Winter PRISM Precipitation	7791.12	-3.422	0.214	0.029	55
WS8 Winter PRISM Precipitation	8407.6	-3.758	0.270	0.029	44
WS9 Winter PRISM Precipitation	9832.64	-4.459	0.299	0.029	39
CS2MET Spring Precipitation	382.592	0.075	0.963	0.000	50
WS2 Spring PRISM Precipitation	2254.12	-0.858	0.489	0.009	55
WS8 Spring PRISM Precipitation	-3800.23	2.177	0.152	0.048	44
WS9 Spring PRISM Precipitation	-1103.47	0.819	0.645	0.006	39
CS2MET Summer Precipitation	-328.697	0.223	0.657	0.004	50
WS2 Summer PRISM Precipitation	-221.983	0.173	0.668	0.003	55
WS8 Summer PRISM Precipitation	540.349	-0.197	0.780	0.002	44
WS9 Summer PRISM Precipitation	869.364	-0.378	0.570	0.009	39

Table A2. Summary regression table of trends in precipitation at CS2MET, WS2 PRISM, WS8 PRISM, and WS9 PRISM for period of overlapping streamflows from 1969-2007.

Simple Linear Regression Models of Precipitation over Time, 1969-2007

	Explanatory Variable Coefficients			
Dependent Variable	**Intercept**	**Year**	**P-value**	**R^2**	**N**
CS2MET Annual Precipitation	12578.1	-5.188	0.458	0.015	39
WS2 Annual PRISM Precipitation	12476.7	-5.129	0.440	0.016	39
WS8 Annual PRISM Precipitation	13984.8	-5.931	0.344	0.024	39
WS9 Annual PRISM Precipitation	12269.5	-5.068	0.431	0.017	39
CS2MET Fall Precipitation	3620.24	-1.522	0.643	0.006	39
WS2 Fall PRISM Precipitation	2753.49	-1.078	0.734	0.003	39
WS8 Fall PRISM Precipitation	3859.29	-1.655	0.580	0.008	39
WS9 Fall PRISM Precipitation	1243.14	-0.333	0.916	0.000	38
CS2MET Winter Precipitation	8615.33	-3.820	0.420	0.018	39
WS2 Winter PRISM Precipitation	10352.8	-4.704	0.286	0.031	39
WS8 Winter PRISM Precipitation	9972.86	-4.543	0.274	0.032	39
WS9 Winter PRISM Precipitation	9832.64	-4.459	0.299	0.029	39
CS2MET Spring Precipitation	-341.45	0.440	0.839	0.001	39
WS2 Spring PRISM Precipitation	-1374.99	0.965	0.601	0.007	39
WS8 Spring PRISM Precipitation	-951.289	0.748	0.686	0.004	39
WS9 Spring PRISM Precipitation	-1103.47	0.819	0.645	0.006	39
CS2MET Summer Precipitation	826.637	-0.357	0.618	0.007	39
WS2 Summer PRISM Precipitation	868.373	-0.374	0.591	0.008	39
WS8 Summer PRISM Precipitation	1228.27	-0.542	0.515	0.012	39
WS9 Summer PRISM Precipitation	869.364	-0.378	0.570	0.009	39

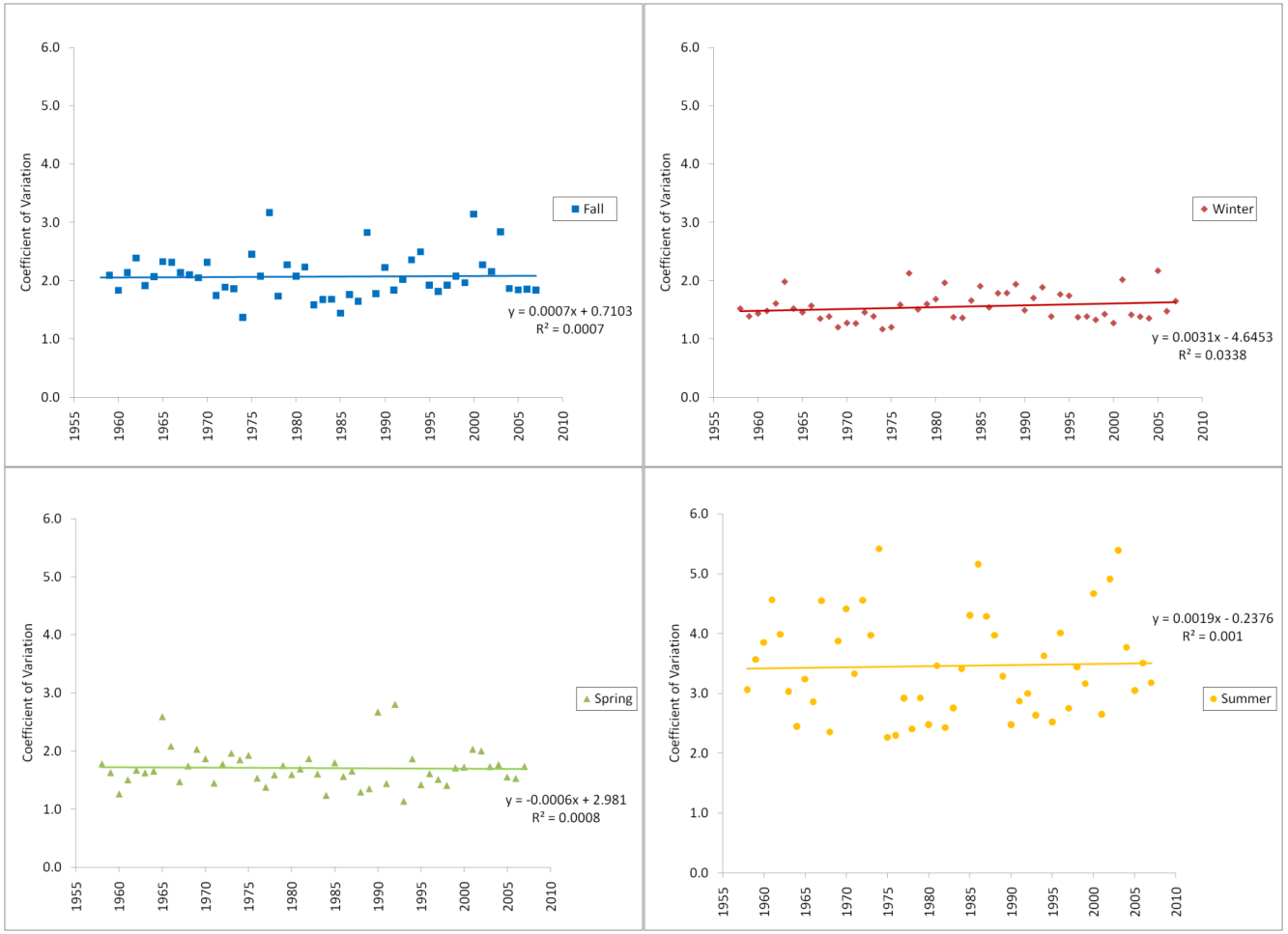

Figure A6. Trends in the coefficient of variation for precipitation at CS2MET for the period of record from 1958-2007 in the (clockwise from top left) fall, winter, summer, and spring.

Table A3. Summary regression table of trends in the coefficient of variation for precipitation at CS2MET by season for the period of record from 1958-2007.

Simple Linear Regression Model of the Coefficient of Variation for Precipitation at CS2MET											
		Explanatory Variable Coefficients									
Dependent Variable		**Intercept**		**Year**		**P-value**		**R^2**		**Period**	**N**
Fall		0.71		0.001		0.860		0.001		1959-2007	49
Winter		-4.65		0.003		0.201		0.034		1958-2007	50
Spring		2.98		-0.001		0.845		0.001		1958-2007	50
Summer		-0.24		0.002		0.827		0.001		1958-2007	50

Appendix B: Temperature

1 Trends in annual and seasonal average maximum and minimum temperatures

Figures B1-B10 plot the average minimum and maximum temperature data by season for the periods of record corresponding to streamflow for the three PRISM datasets, and for the full period of record for CS2MET. Trend lines and equations are shown on the figures along with an R^2 goodness of fit estimate.

Annual average maximum temperatures show no significant trends over time, either at CS2MET or for the three PRISM datasets (either over the 82 year period from 1926-2007 or for the periods of record corresponding to streamflow) (Table B1, B3). Annual average minimum temperatures have increased significantly over the 82 year period from 1926-2007 for WS8 PRISM and WS9 PRISM (Table B2). WS8 PRISM exhibits a rate of increase of 0.007°C per year ($p<0.05$) for a net change of 0.56°C over the 82 year period. WS9 PRISM exhibits a rate of increase of 0.012°C per year ($p<0.01$) for a net change of 0.95°C over the 82 year period. Annual average minimum temperatures have also increased significantly over the periods of record corresponding to streamflow data for all three PRISM datasets, and for CS2MET over its period of record (Table B4). WS2 PRISM exhibits a rate of increase of 0.012°C per year ($p<0.05$) for a net change of 0.66°C over the 55 year period corresponding to streamflow. WS8 PRISM exhibits a rate of increase of 0.023°C per year ($p<0.01$) for a net change of 0.99°C over the 44 year period of record corresponding to streamflow. WS9 PRISM exhibits a rate of increase of 0.029°C per year ($p<0.01$) for a net change of 1.15°C over the 39 year period corresponding to streamflow. CS2MET exhibits a rate of increase of 0.019°C per year ($p<0.01$) for a net change of 0.92°C over its 48 year period of record.

Fall average maximum temperatures show no significant trends over time, either at CS2MET or for the three PRISM datasets (either over the 81 year period from 1927-2007 or for the periods of record corresponding to streamflow) (Table B1, B3). Fall average minimum temperatures have increased significantly only in the case of WS9 PRISM. WS9 PRISM exhibits a rate of increase of 0.009°C per year ($p<0.05$) for a net change of 0.71°C over the 81 year period from 1927-2007, and a rate of increase of 0.028°C per year ($p<0.05$) for a net change of 1.07°C over the 38 year period of record corresponding to streamflow (Table B2, B4).

Winter average maximum temperatures show no significant trends over time, either at CS2MET or for the three PRISM datasets (either over the 82 year period from 1926-2007 or for the periods of record corresponding to streamflow) (Table B1, B3). Winter average minimum temperatures have increased significantly only in the case of WS9 PRISM for the period from 1926-2007. WS9 PRISM exhibits a rate of increase of 0.014°C per year ($p<0.05$) for a net change of 1.12°C over the 82 year period. (Table B2, B4).

Spring average maximum temperatures show no significant trends over the period from 1926-2007 (Table B1). Over the periods of record corresponding to streamflow data, spring average maximum temperatures have increased significantly only for the WS2 PRISM dataset (Table B3). WS2 PRISM exhibits a rate of increase of 0.031°C per year ($p<0.01$) for a net change of 1.70°C over the 55 year period corresponding to streamflow. Spring average minimum temperatures show no significant trends over the period from 1926-2007 (Table B2). However, spring average minimum temperatures have increased significantly over the periods of record corresponding to streamflow data

for all three PRISM datasets, and for CS2MET over its period of record (Table B4). WS2 PRISM exhibits a rate of increase of 0.026°C per year ($p<0.01$) for a net change of 1.44°C over the 55 year period corresponding to streamflow. WS8 PRISM exhibits a rate of increase of 0.039°C per year ($p<0.01$) for a net change of 1.71°C over the 44 year period of record corresponding to streamflow. WS9 PRISM exhibits a rate of increase of 0.038°C per year ($p<0.01$) for a net change of 1.50°C over the 39 year period corresponding to streamflow. CS2MET exhibits a rate of increase of 0.034°C per year ($p<0.01$) for a net change of 1.68°C over its 49 year period of record.

Summer average maximum temperatures have increased significantly only in the case of WS2 PRISM for the 55 year period of record corresponding to streamflow. WS2 PRISM exhibits a rate of increase of 0.024°C per year ($p=0.05$) for a net change of 1.34°C (Table B1, B3). Summer average minimum temperatures have increased significantly over the period from 1926-2007 for all three PRISM datasets (Table B2). WS2 PRISM exhibits a rate of increase of 0.008°C per year ($p<0.05$) for a net change of 0.67°C over its 82 year period of record. WS8 PRISM exhibits a rate of increase of 0.010°C per year ($p<0.01$) for a net change of 0.83°C over its 82 year period of record. WS9 PRISM exhibits a rate of increase of 0.016°C per year ($p<0.01$) for a net change of 1.31°C over its 82 year period of record. Summer average minimum temperatures have also increased significantly over the periods of record corresponding to streamflow data for all three PRISM datasets (Table B4). WS2 PRISM exhibits a rate of increase of 0.015°C per year ($p<0.05$) for a net change of 0.81°C over the 55 year period corresponding to streamflow. WS8 PRISM exhibits a rate of increase of 0.022°C per year ($p<0.01$) for a net change of 0.98°C over the 44 year period of record corresponding

to streamflow. WS9 PRISM exhibits a rate of increase of 0.026°C per year ($p<0.01$) for a net change of 1.00°C over the 39 year period corresponding to streamflow. However, CS2MET shows no significant trend over its 48 year period of record.

2 Trends in monthly average maximum and minimum temperatures

Trends in monthly average maximum and minimum temperatures for the periods of record corresponding to streamflow are shown in Tables B5, B6 and Figures B11, B12. October average maximum temperatures show no significant trends. October average minimum temperatures have changed significantly only in the case of WS9 PRISM. WS9 PRISM exhibits a rate of increase of 0.034°C per year ($p<0.05$) for a net change of 1.33°C over the 39 year period corresponding to streamflow. November average maximum and minimum temperatures exhibit no significant trends. December average maximum and minimum temperatures exhibit no significant trends. January average maximum temperatures show no significant trends. January average minimum temperatures have increased significantly for WS9 PRISM, and CS2MET. WS9 PRISM exhibits a rate of increase of 0.061°C per year ($p<0.05$) for a net change of 2.39°C over the 39 year period corresponding to streamflow. CS2MET exhibits a rate of increase of 0.045°C per year ($p<0.05$) for a net change of 2.19°C over its 49 year period of record. February average maximum and minimum temperatures exhibit no significant trends. March average maximum temperatures have increased significantly for WS2 PRISM and CS2MET. WS2 PRISM exhibits a rate of increase of 0.041°C per year ($p<0.01$) for a net change of 2.23°C over the 55 year period corresponding to streamflow. CS2MET exhibits a rate of increase of 0.055°C per year ($p<0.05$) for a net change of 2.71°C over its 49 year period of record. March average minimum temperatures have increased

significantly for the WS2 PRISM and WS8 PRISM datasets and for CS2MET. WS2 PRISM exhibits a rate of increase of 0.033°C per year ($p<0.01$) for a net change of 1.79°C over the 55 year period corresponding to streamflow. WS8 PRISM exhibits a rate of increase of 0.032°C per year ($p<0.05$) for a net change of 1.39°C over the 44 year period of record corresponding to streamflow. CS2MET exhibits a rate of increase of 0.042°C per year ($p<0.01$) for a net change of 2.04°C over its 49 year period of record. April average maximum temperatures show no significant trends. April average minimum temperatures have increased significantly for all three PRISM datasets and CS2MET. WS2 PRISM exhibits a rate of increase of 0.028°C per year ($p<0.01$) for a net change of 1.53°C over the 55 year period corresponding to streamflow. WS8 PRISM exhibits a rate of increase of 0.047°C per year ($p<0.01$) for a net change of 2.06°C over the 44 year period of record corresponding to streamflow. WS9 PRISM exhibits a rate of increase of 0.047°C per year ($p<0.01$) for a net change of 1.81°C over the 39 year period corresponding to streamflow. CS2MET exhibits a rate of increase of 0.038°C per year ($p<0.01$) for a net change of 1.88°C over its 49 year period of record. May average maximum temperatures exhibit no significant trends. May average minimum temperatures have increased significantly for the WS8 PRISM and WS9 PRISM datasets and for CS2MET. WS8 PRISM exhibits a rate of increase of 0.038°C per year ($p<0.01$) for a net change of 1.68°C over the 44 year period of record corresponding to streamflow. WS9 PRISM exhibits a rate of increase of 0.040°C per year ($p<0.01$) for a net change of 1.54°C over the 39 year period corresponding to streamflow. CS2MET exhibits a rate of increase of 0.025°C per year ($p<0.05$) for a net change of 1.20°C over its 49 year period of record. June average maximum and minimum temperatures exhibit no significant

trends. July average maximum temperatures exhibit no significant trends. July average minimum temperatures have increased significantly for all three PRISM datasets and CS2MET. WS2 PRISM exhibits a rate of increase of 0.025°C per year ($p<0.01$) for a net change of 1.37°C over the 55 year period corresponding to streamflow. WS8 PRISM exhibits a rate of increase of 0.040°C per year ($p<0.01$) for a net change of 1.77°C over the 44 year period of record corresponding to streamflow. WS9 PRISM exhibits a rate of increase of 0.044°C per year ($p<0.01$) for a net change of 1.71°C over the 39 year period corresponding to streamflow. CS2MET exhibits a rate of increase of 0.022°C per year ($p<0.05$) for a net change of 1.07°C over its 49 year period of record. August average maximum and minimum temperatures exhibit no significant trends. September average maximum and minimum temperatures exhibit no significant trends.

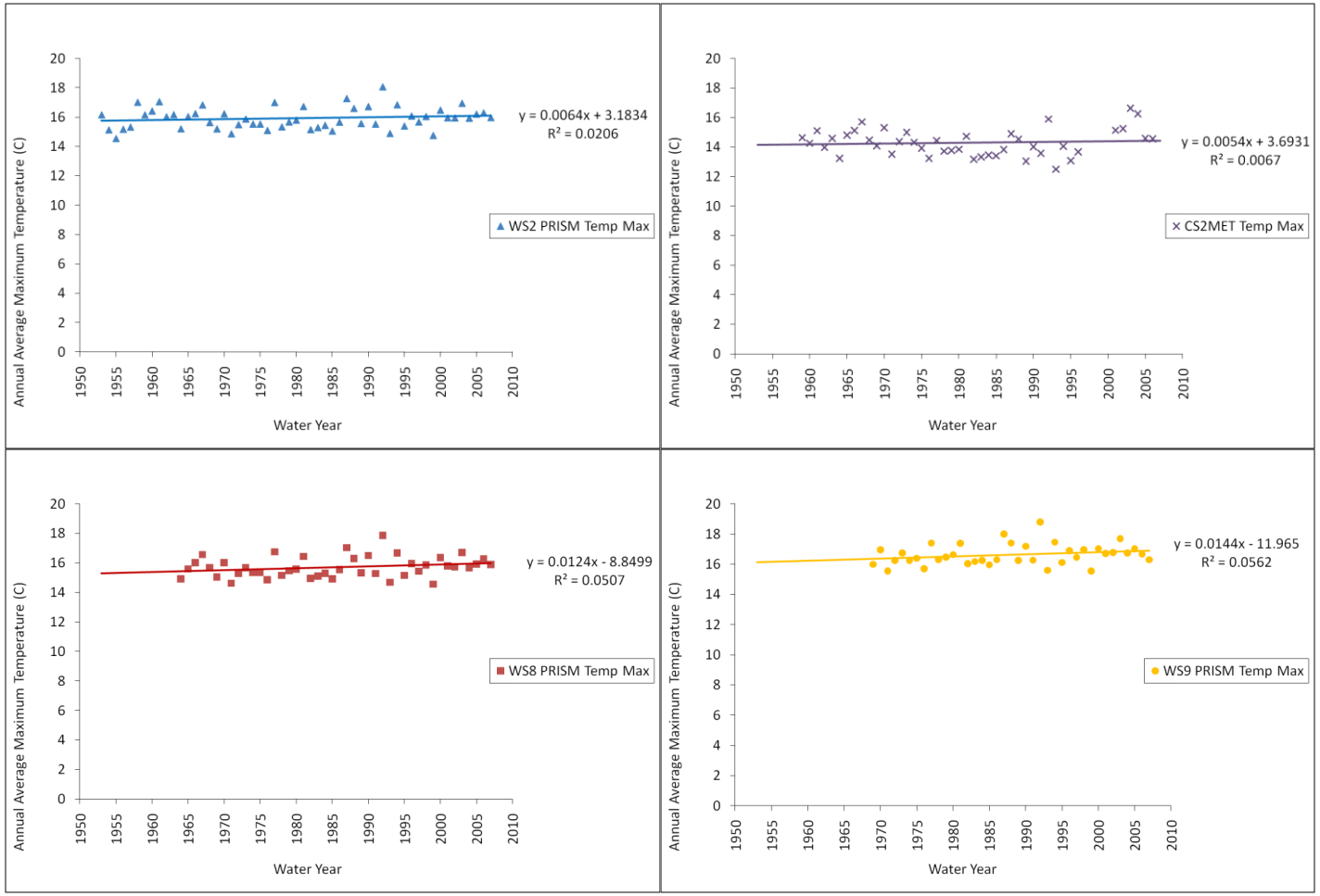

Figure B1. Trends in annual average maximum temperature at (clockwise from top left) WS2 PRISM, CS2MET, WS9 PRISM, and WS8 PRISM

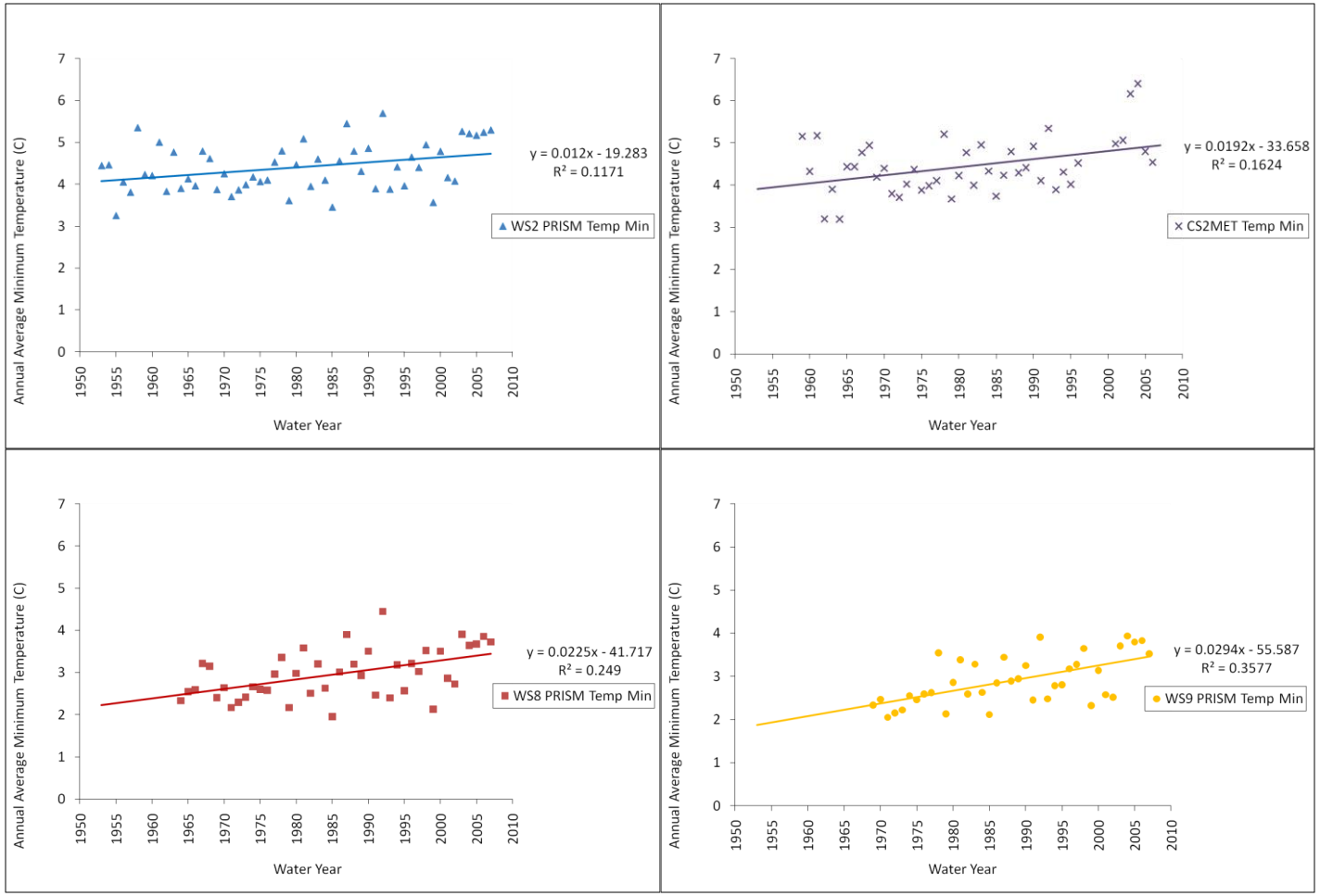

Figure B2. Trends in annual average minimum temperature at (clockwise from top left) WS2 PRISM, CS2MET, WS9 PRISM, and WS8 PRISM

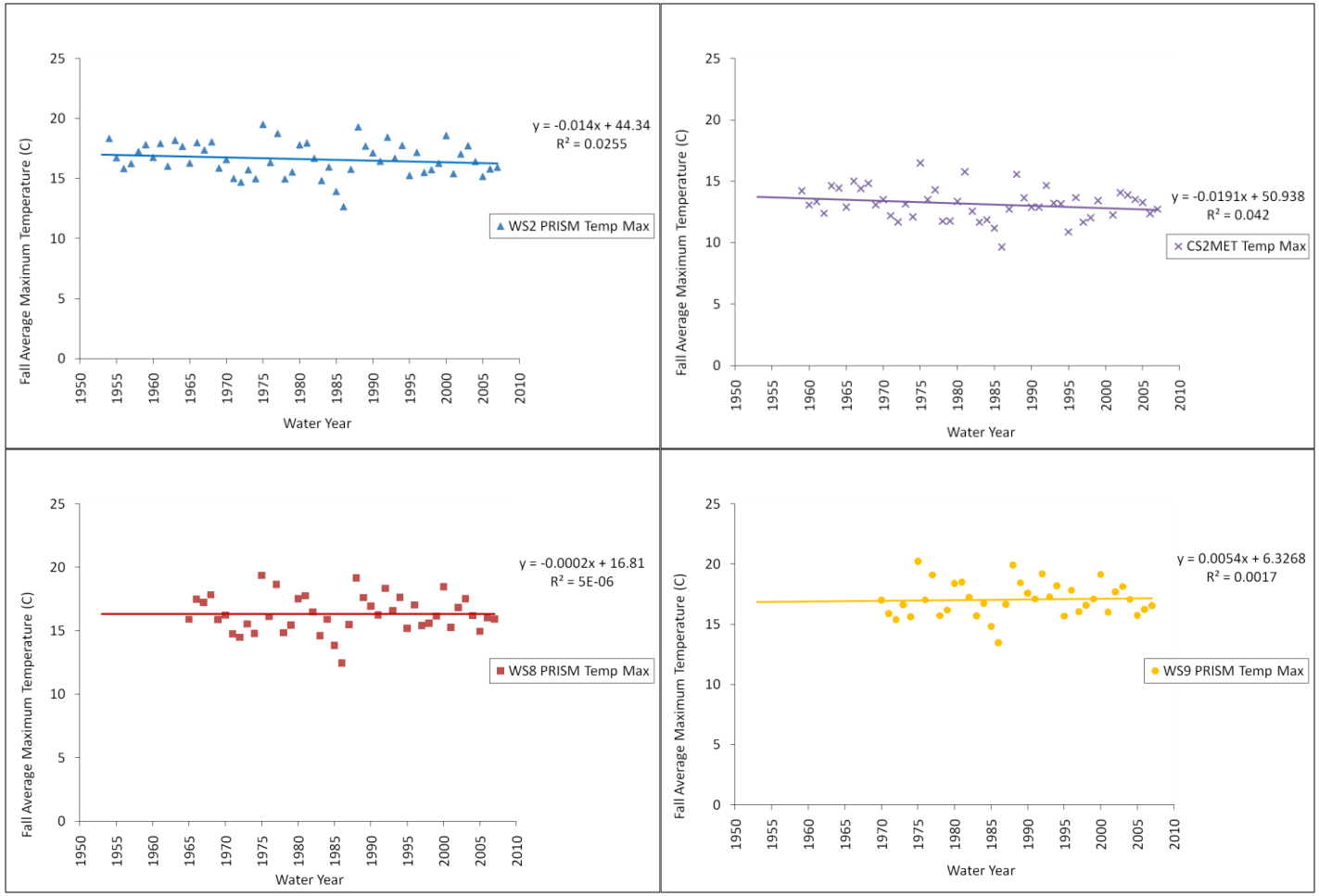

Figure B3. Trends in fall average maximum temperature at (clockwise from top left) WS2 PRISM, CS2MET, WS9 PRISM, and WS8 PRISM

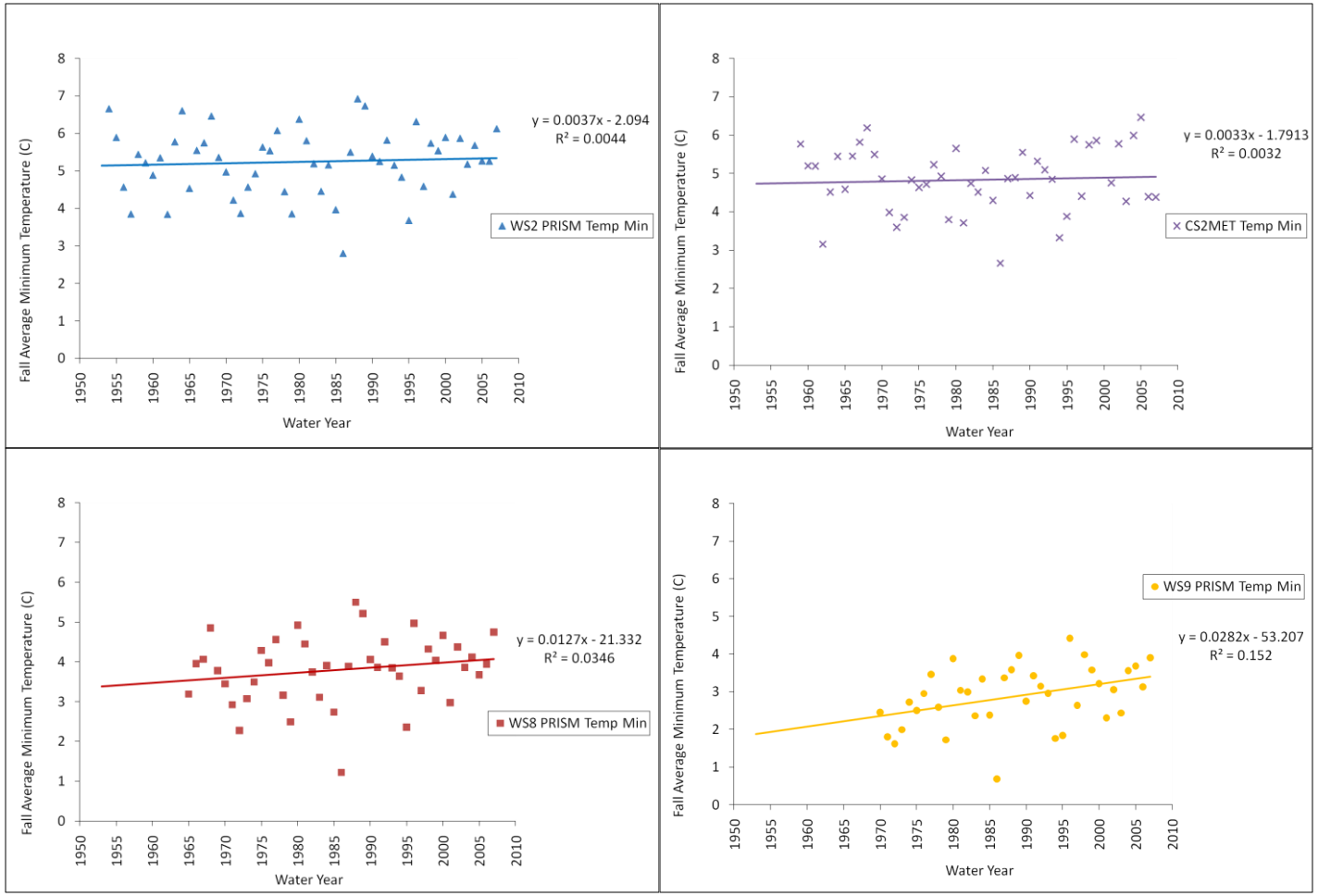

Figure B4. Trends in fall average minimum temperature at (clockwise from top left) WS2 PRISM, CS2MET, WS9 PRISM, and WS8 PRISM

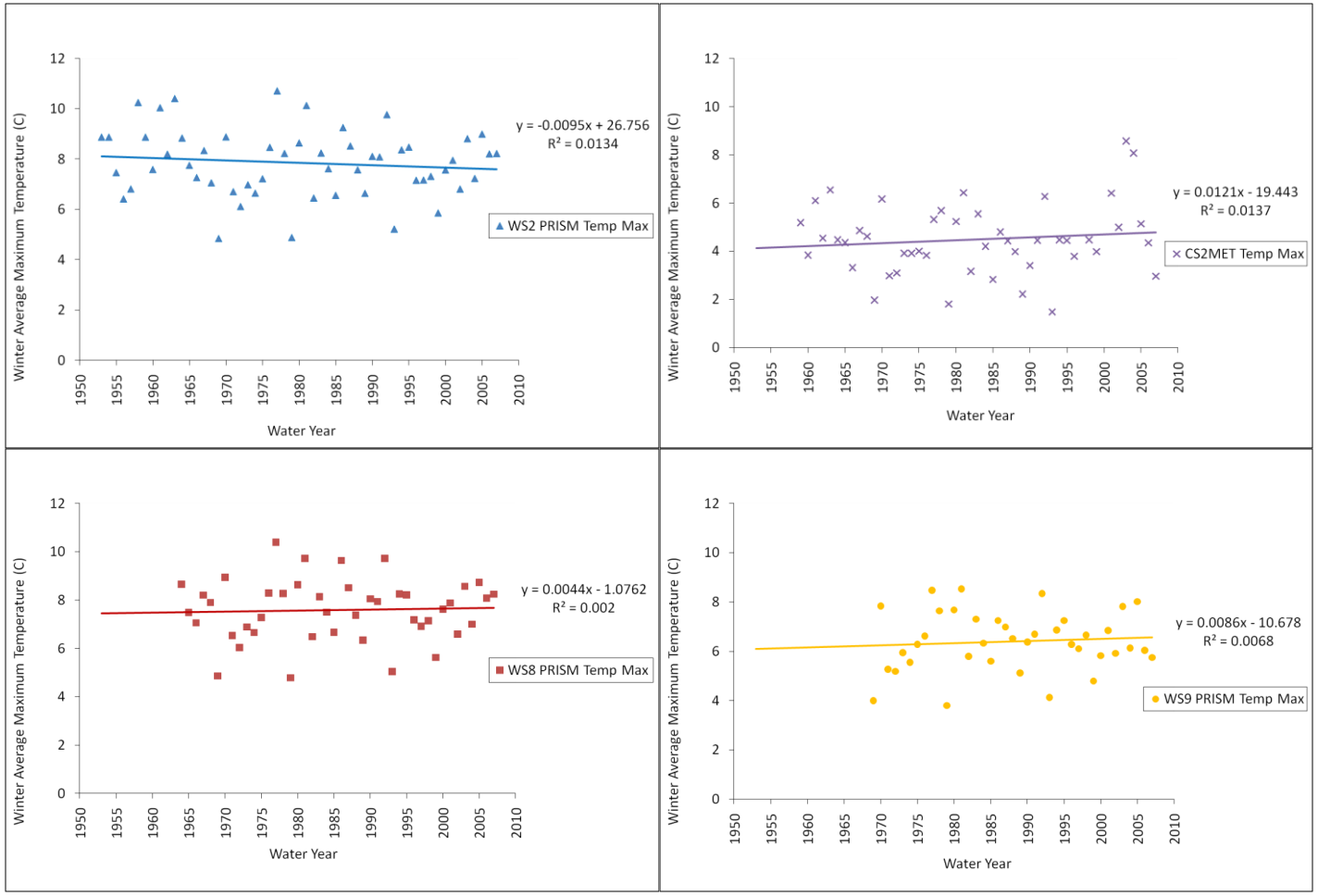

Figure B5. Trends in winter average maximum temperature at (clockwise from top left) WS2 PRISM, CS2MET, WS9 PRISM, and WS8 PRISM

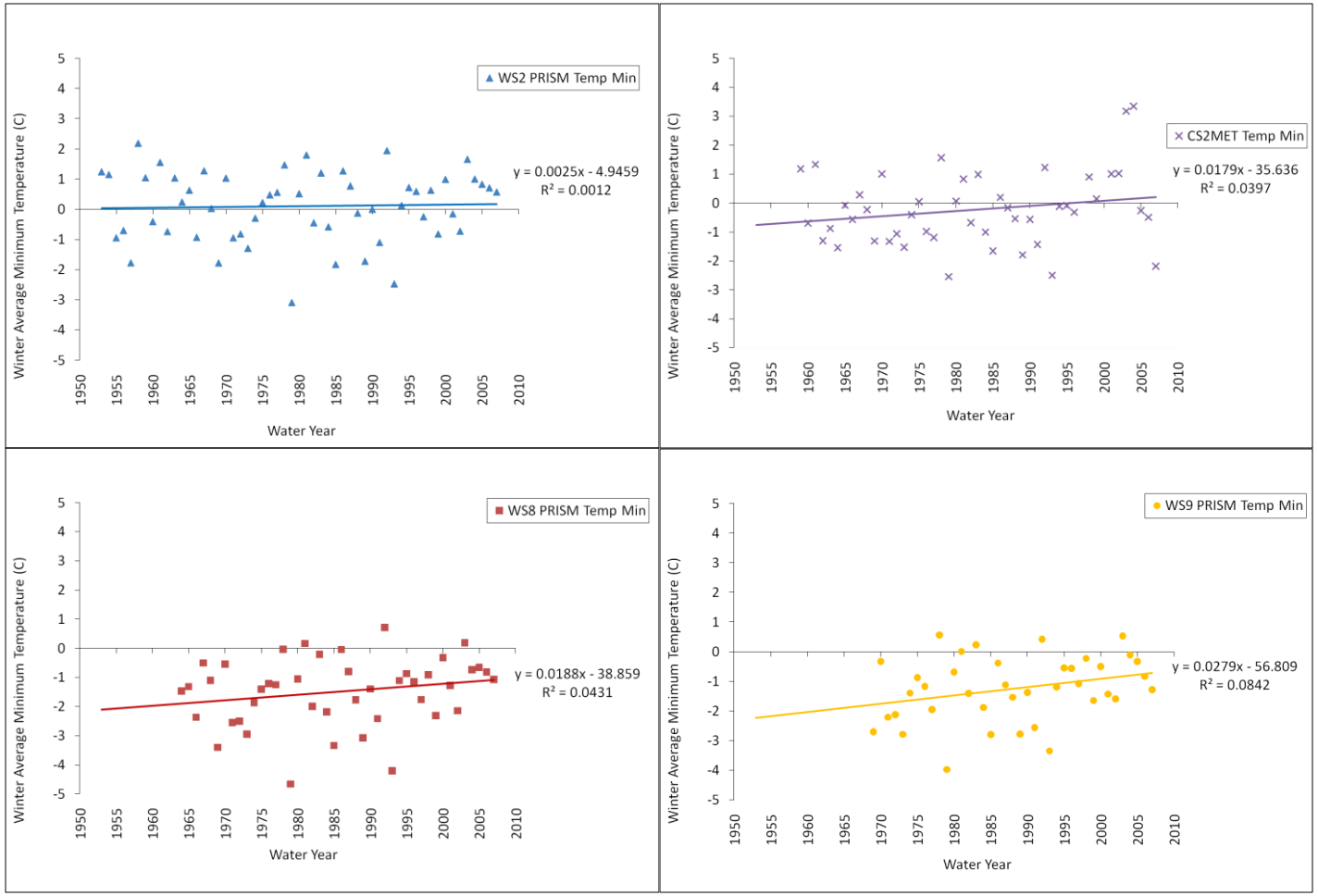

Figure B6. Trends in winter average minimum temperature at (clockwise from top left) WS2 PRISM, CS2MET, WS9 PRISM, and WS8 PRISM

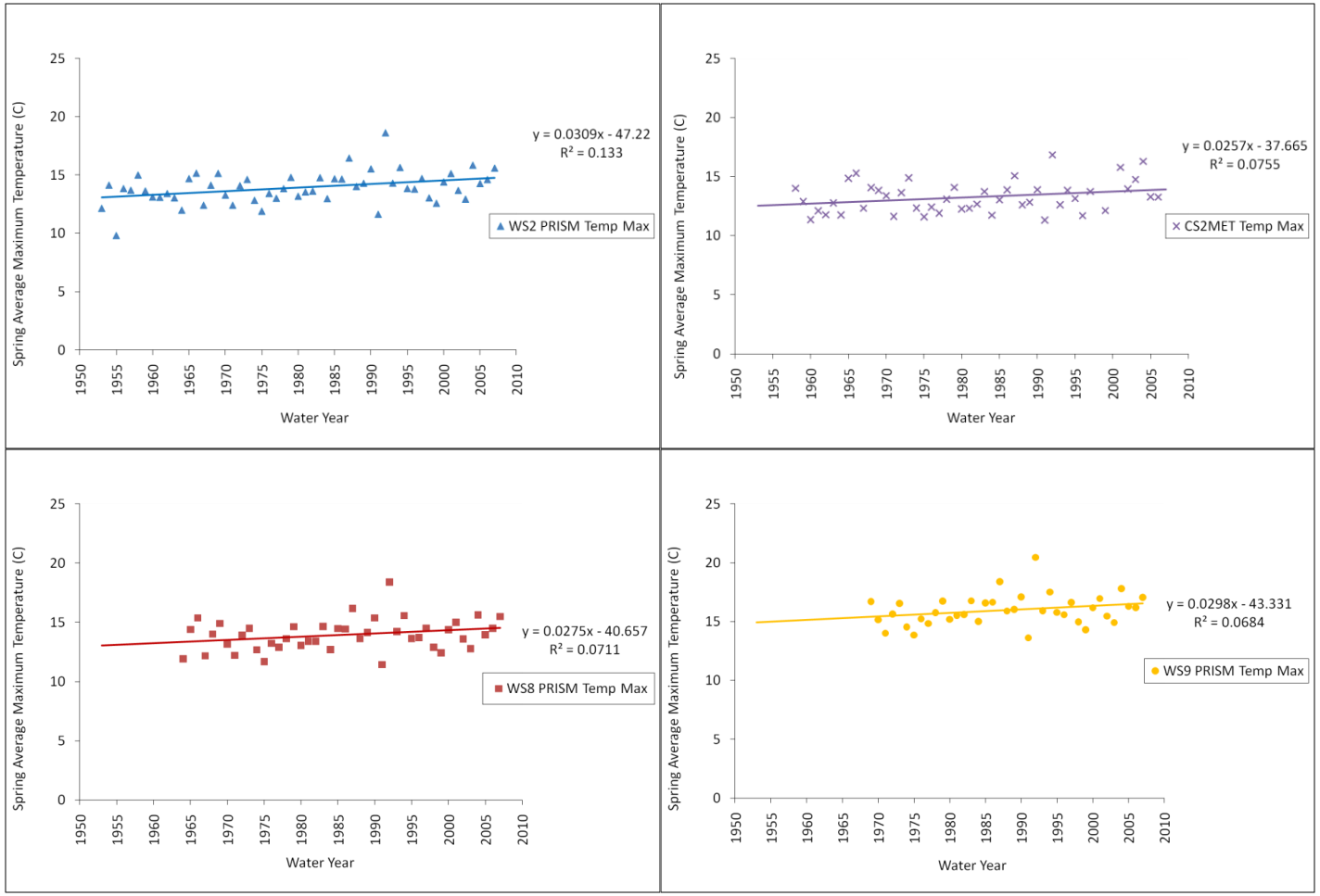

Figure B7. Trends in spring average maximum temperature at (clockwise from top left) WS2 PRISM, CS2MET, WS9 PRISM, and WS8 PRISM

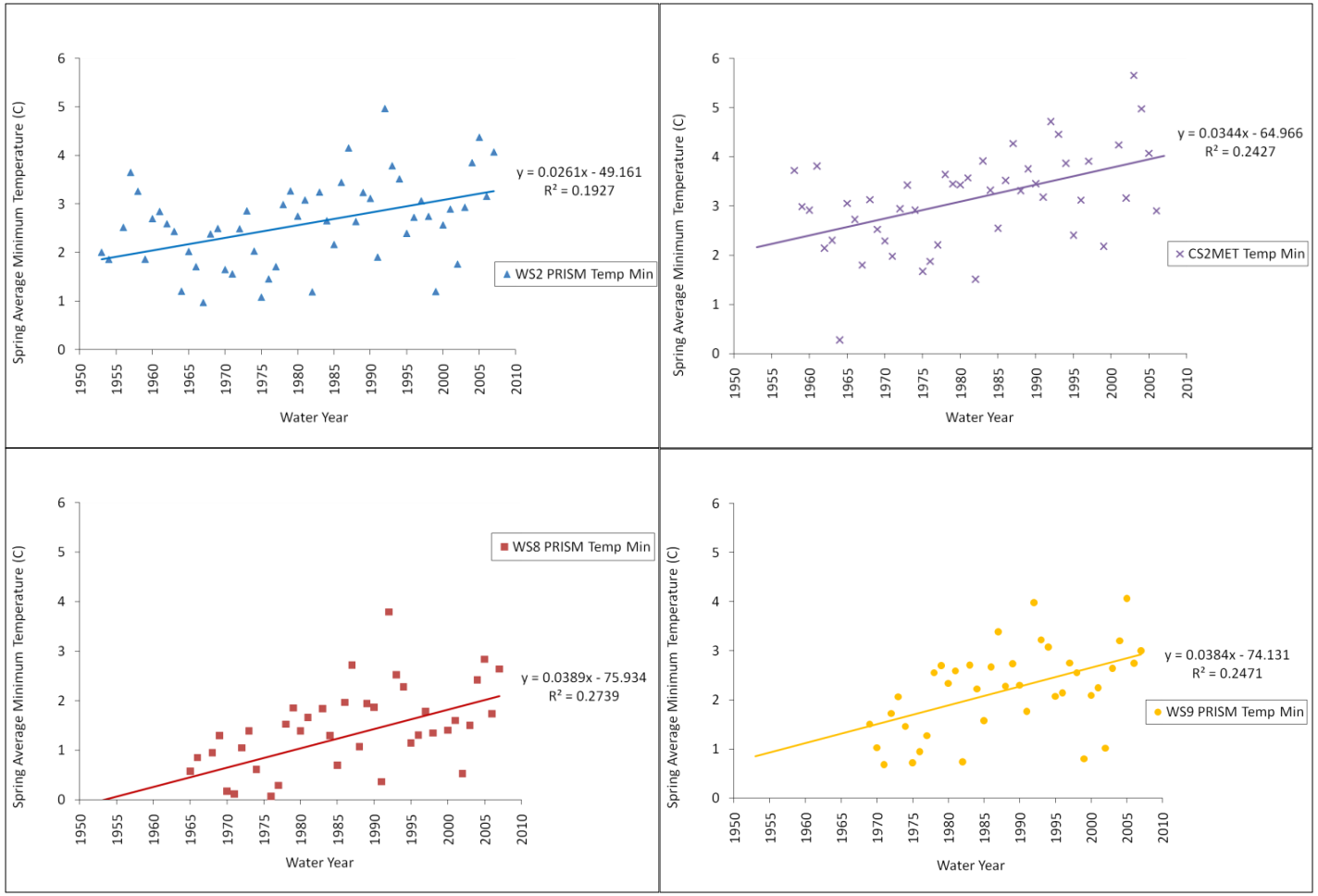

Figure B8. Trends in spring average minimum temperature at (clockwise from top left) WS2 PRISM, CS2MET, WS9 PRISM, and WS8 PRISM

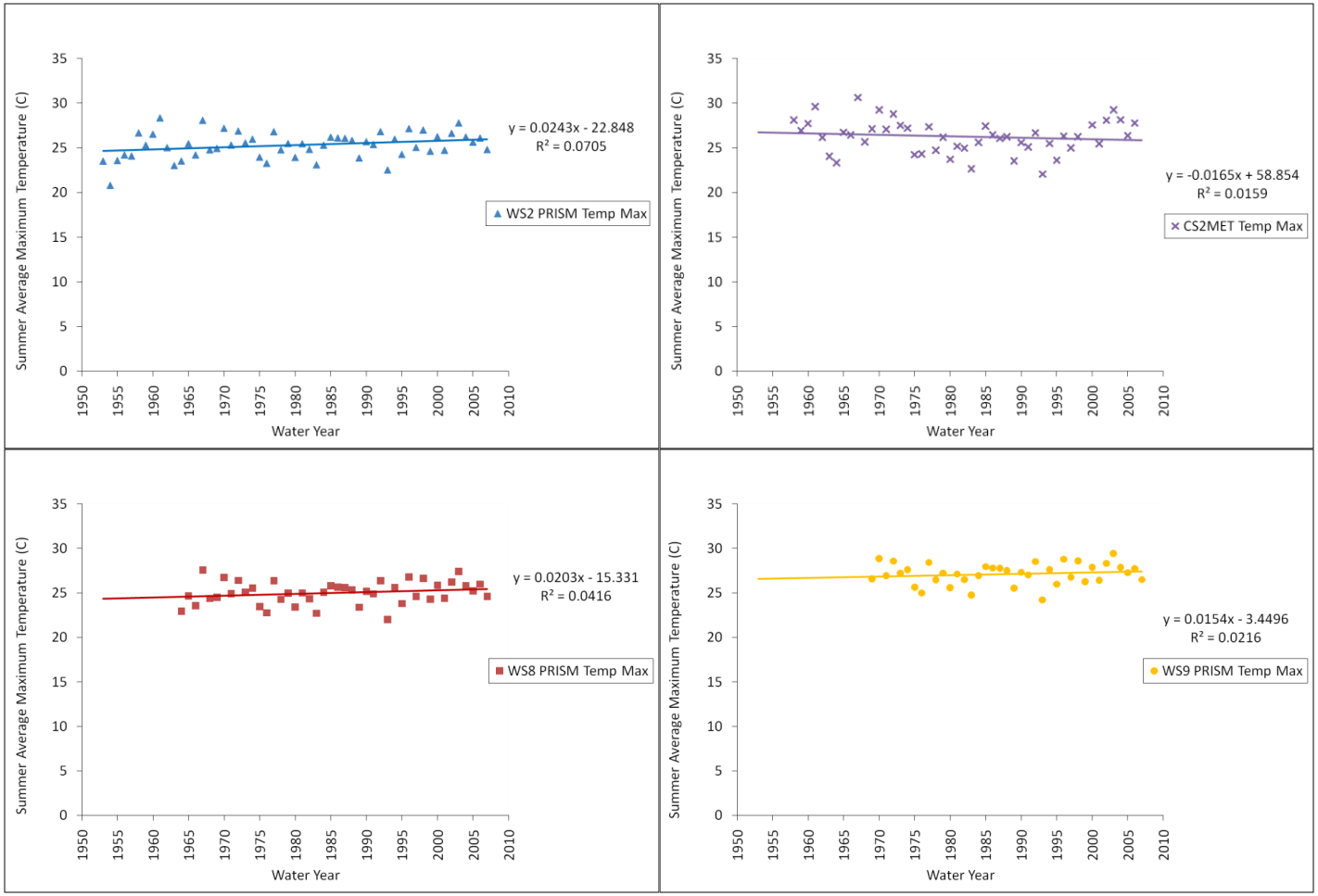

Figure B9. Trends in summer average maximum temperature at (clockwise from top left) WS2 PRISM, CS2MET, WS9 PRISM, and WS8 PRISM

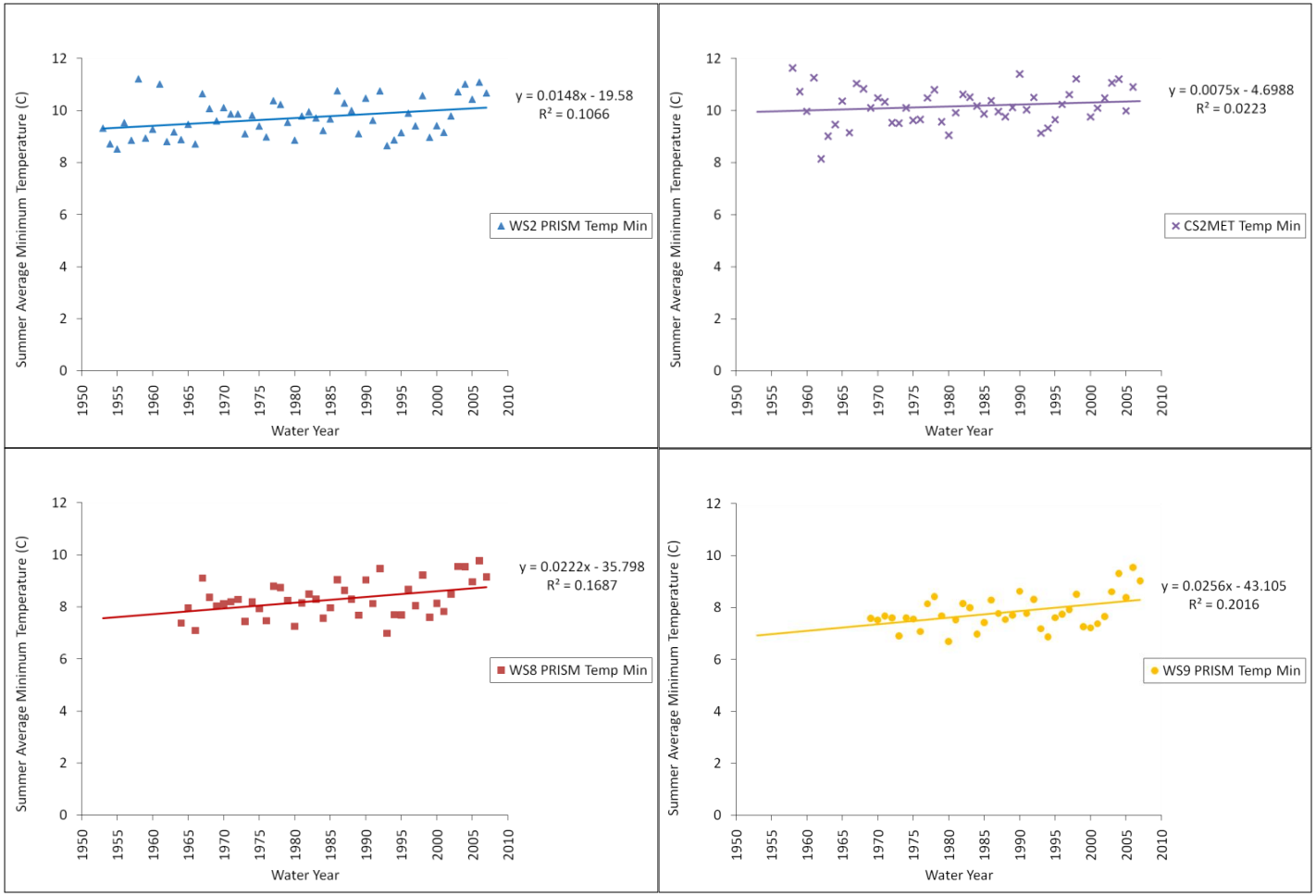

Figure B10. Trends in summer average minimum temperature at (clockwise from top left) WS2 PRISM, CS2MET, WS9 PRISM, and WS8 PRISM

Table B1. Summary regression table of trends in average maximum temperature at WS2 PRISM, WS8 PRISM, and WS9 PRISM for the period from 1926-2007.

Simple Linear Regression Model of Maximum Temperature over Time for the Period from 1926-2007					
	Explanatory Variable Coefficients				
Dependent Variable	**Intercept**	**Year**	**P-value**	**R^2**	**Period of Record**	**N**
WS2 PRISM Annual	20.521	-0.002	0.535	0.005	1926-2007	82
WS8 PRISM Annual	20.743	-0.003	0.492	0.006	1926-2007	82
WS9 PRISM Annual	19.766	-0.002	0.665	0.002	1926-2007	82
WS2 PRISM Fall	32.802	-0.008	0.224	0.019	1927-2007	81
WS8 PRISM Fall	32.414	-0.008	0.226	0.019	1927-2007	81
WS9 PRISM Fall	32.249	-0.008	0.240	0.017	1927-2007	81
WS2 PRISM Winter	5.176	0.001	0.852	0.000	1926-2007	82
WS8 PRISM Winter	5.764	0.001	0.890	0.000	1926-2007	82
WS9 PRISM Winter	-4.461	0.006	0.378	0.010	1926-2007	82
WS2 PRISM Spring	22.987	-0.004	0.532	0.005	1926-2007	82
WS8 PRISM Spring	23.907	-0.005	0.480	0.006	1926-2007	82
WS9 PRISM Spring	24.729	-0.004	0.536	0.005	1926-2007	82
WS2 PRISM Summer	20.361	0.003	0.683	0.002	1926-2007	82
WS8 PRISM Summer	20.184	0.002	0.697	0.002	1926-2007	82
WS9 PRISM Summer	25.687	0.001	0.909	0.000	1926-2007	82

Table B2. Summary regression table of trends in average minimum temperature at WS2 PRISM, WS8 PRISM, and WS9 PRISM for the period from 1926-2007.

Simple Linear Regression Model of Minimum Temperature over Time for the Period from 1926-2007											
		Explanatory Variable Coefficients									
Dependent Variable		**Intercept**		**Year**		**P-value**		**R^2**		**Period of Record**	**N**
WS2 PRISM Annual		-5.998		0.005		0.073		0.040		1926-2007	82
WS8 PRISM Annual		-10.687		0.007		0.024	*	0.062		1926-2007	82
WS9 PRISM Annual		-20.158		0.012		0.000	**	0.205		1926-2007	82
WS2 PRISM Fall		2.259		0.002		0.717		0.002		1927-2007	81
WS8 PRISM Fall		-1.703		0.003		0.497		0.006		1927-2007	81
WS9 PRISM Fall		-14.412		0.009		0.029	*	0.059		1927-2007	81
WS2 PRISM Winter		-12.511		0.006		0.326		0.012		1926-2007	82
WS8 PRISM Winter		-19.975		0.009		0.157		0.025		1926-2007	82
WS9 PRISM Winter		-28.265		0.014		0.025	*	0.061		1926-2007	82
WS2 PRISM Spring		-6.606		0.005		0.312		0.013		1926-2007	82
WS8 PRISM Spring		-8.858		0.005		0.279		0.015		1926-2007	82
WS9 PRISM Spring		-14.050		0.008		0.055		0.045		1926-2007	82
WS2 PRISM Summer		-6.355		0.008		0.012	*	0.077		1926-2007	82
WS8 PRISM Summer		-11.816		0.010		0.002	**	0.112		1926-2007	82
WS9 PRISM Summer		-23.882		0.016		0.000	**	0.256		1926-2007	82

Table B3. Summary regression table of trends in average maximum temperature at CS2MET for the period of record, and at WS2 PRISM, WS8 PRISM, and WS9 PRISM for the periods corresponding to streamflow record.

Simple Linear Regression Model of Maximum Temperature over Time for the Periods Corresponding to Streamflow and the Period of Record at CS2MET										
		Explanatory Variable Coefficients								
Dependent Variable		**Intercept**		**Year**		**P-value**		**R^2**	**Period**	**N**
WS2 PRISM Annual		3.183		0.006		0.296		0.021	1953-2007	55
WS8 PRISM Annual		-8.850		0.012		0.142		0.051	1964-2007	44
WS9 PRISM Annual		-11.965		0.014		0.146		0.056	1969-2007	39
CS2MET Annual		3.693		0.005		0.598		0.007	1959-2006	44
WS2 PRISM Fall		44.340		-0.014		0.249		0.025	1954-2007	54
WS8 PRISM Fall		16.810		0.000		0.989		0.000	1965-2007	43
WS9 PRISM Fall		6.327		0.005		0.804		0.002	1970-2007	38
CS2MET Fall		50.938		-0.019		0.163		0.042	1959-2007	48
WS2 PRISM Winter		26.756		-0.010		0.401		0.013	1953-2007	55
WS8 PRISM Winter		-1.076		0.004		0.775		0.002	1964-2007	44
WS9 PRISM Winter		-10.678		0.009		0.618		0.007	1969-2007	39
CS2MET Winter		-19.443		0.012		0.434		0.014	1959-2007	47
WS2 PRISM Spring		-47.220		0.031		0.006	**	0.133	1953-2007	55
WS8 PRISM Spring		-40.657		0.027		0.080		0.071	1964-2007	44
WS9 PRISM Spring		-43.331		0.030		0.108		0.068	1969-2007	39
CS2MET Spring		-37.665		0.026		0.062		0.076	1958-2006	47
WS2 PRISM Summer		-22.848		0.024		0.050	*	0.070	1953-2007	55
WS8 PRISM Summer		-15.331		0.020		0.184		0.042	1964-2007	44
WS9 PRISM Summer		-3.450		0.015		0.372		0.022	1969-2007	39
CS2MET Summer		58.854		-0.016		0.393		0.016	1958-2006	48

Table B4. Summary regression table of trends in average minimum temperature at CS2MET for the period of record, and at WS2 PRISM, WS8 PRISM, and WS9 PRISM for the periods corresponding to streamflow record.

Simple Linear Regression Model of Minimum Temperature over Time for the Periods Corresponding to Streamflow and the Period of Record at CS2MET										
		Explanatory Variable Coefficients								
Dependent Variable		**Intercept**		**Year**		**P-value**		**R^2**	**Period**	**N**
WS2 PRISM Annual		-19.283		0.012		0.011	*	0.117	1953-2007	55
WS8 PRISM Annual		-41.717		0.023		0.001	**	0.249	1964-2007	44
WS9 PRISM Annual		-55.587		0.029		0.000	**	0.358	1969-2007	39
CS2MET Annual		-33.658		0.019		0.007	**	0.162	1959-2006	44
WS2 PRISM Fall		-2.094		0.004		0.634		0.004	1954-2007	54
WS8 PRISM Fall		-21.332		0.013		0.232		0.035	1965-2007	43
WS9 PRISM Fall		-53.207		0.028		0.016	*	0.152	1970-2007	38
CS2MET Fall		-1.791		0.003		0.701		0.003	1959-2007	48
WS2 PRISM Winter		-4.946		0.003		0.800		0.001	1953-2007	55
WS8 PRISM Winter		-38.859		0.019		0.177		0.043	1964-2007	44
WS9 PRISM Winter		-56.809		0.028		0.073		0.084	1969-2007	39
CS2MET Winter		-35.636		0.018		0.179		0.040	1959-2007	47
WS2 PRISM Spring		-49.161		0.026		0.001	**	0.193	1953-2007	55
WS8 PRISM Spring		-75.934		0.039		0.000	**	0.274	1964-2007	44
WS9 PRISM Spring		-74.131		0.038		0.001	**	0.247	1969-2007	39
CS2MET Spring		-64.966		0.034		0.000	**	0.243	1958-2006	47
WS2 PRISM Summer		-19.580		0.015		0.015	*	0.107	1953-2007	55
WS8 PRISM Summer		-35.798		0.022		0.006	**	0.169	1964-2007	44
WS9 PRISM Summer		-43.105		0.026		0.004	**	0.202	1969-2007	39
CS2MET Summer		-4.699		0.007		0.311		0.022	1958-2006	48

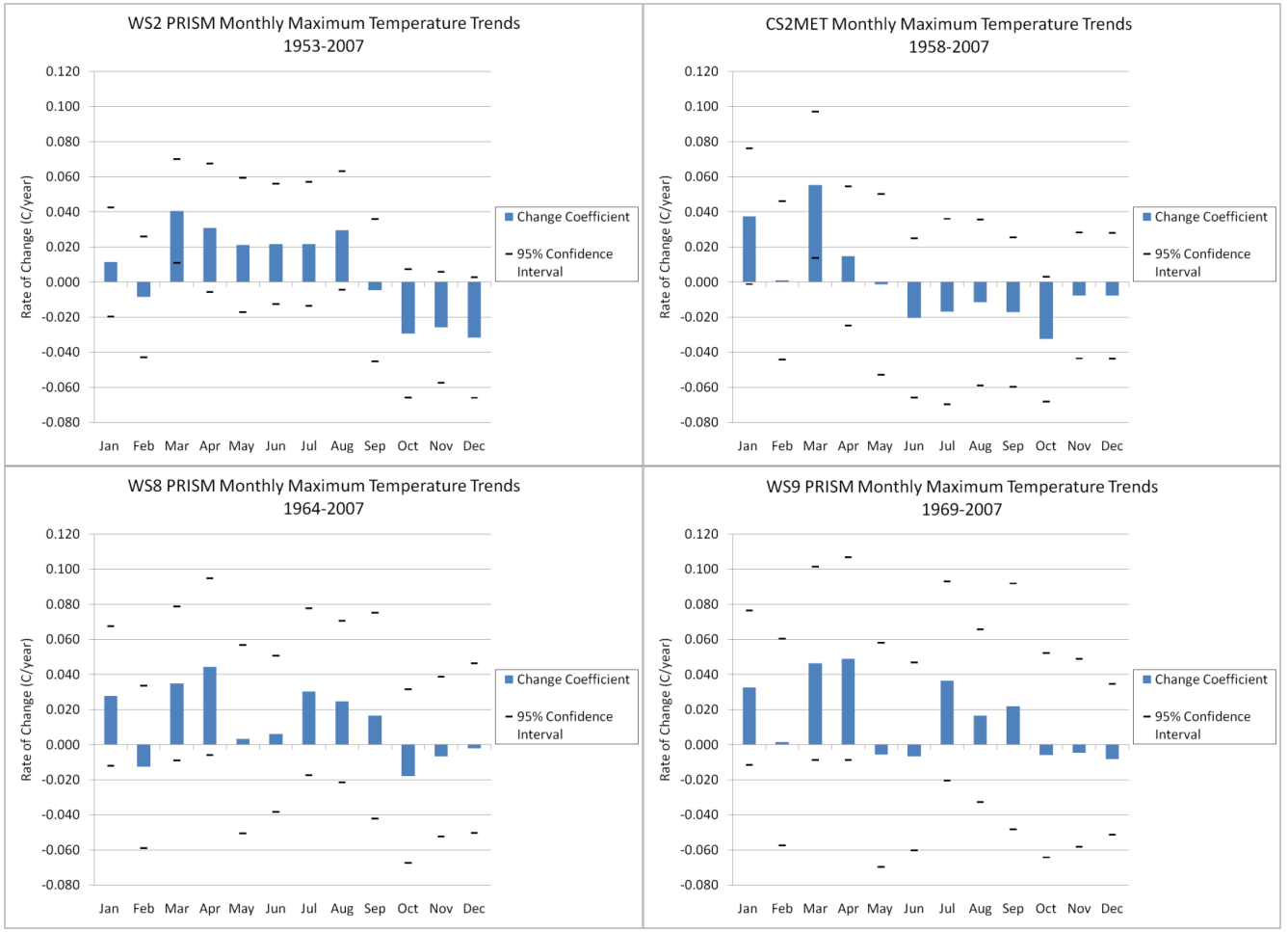

Figure B11. Trends in monthly average maximum temperature at (clockwise from top left) WS2 PRISM, CS2MET, WS9 PRISM, and WS8 PRISM

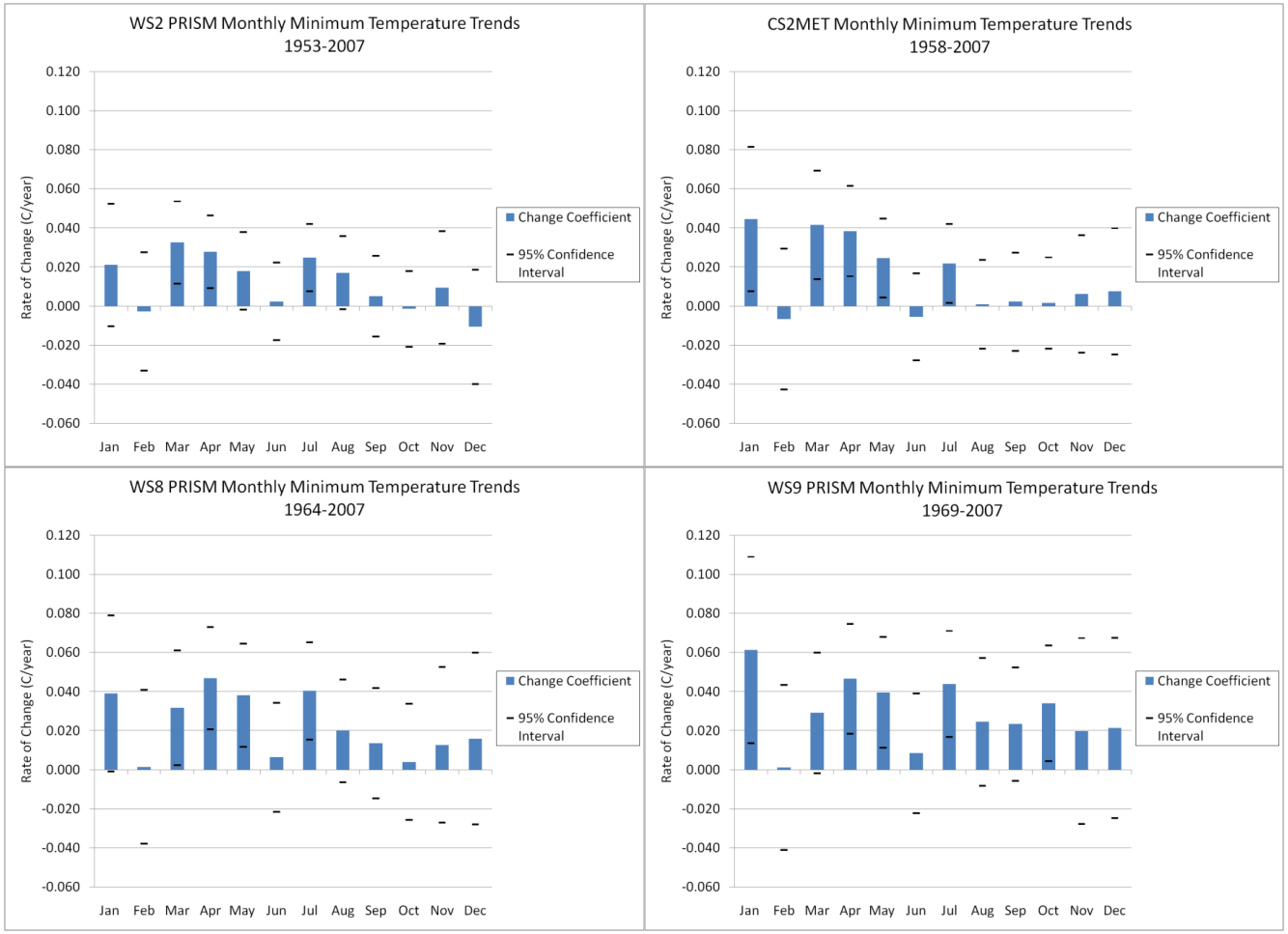

Figure B12. Trends in monthly average minimum temperature at (clockwise from top left) WS2 PRISM, CS2MET, WS9 PRISM, and WS8 PRISM.

Table B5: Trends in monthly average maximum temperature at CS2MET for the period of record, and at WS2 PRISM, WS8 PRISM, and WS9 PRISM for the periods corresponding to streamflow record.

Simple Linear Regression Model of Monthly Maximum Temperature over Time for Period Corresponding to Streamflow									
		Explanatory Variable Coefficients							
Dependent Variable		**Intercept**	**Year**	**P-value**		**R^2**		**Period**	**N**
WS2 PRISM October		74.950	-0.029	0.115		0.046		1953-2007	55
WS8 PRISM October		53.079	-0.018	0.468		0.013		1964-2007	44
WS9 PRISM October		29.292	-0.006	0.835		0.001		1969-2007	39
CS2MET October		77.240	-0.033	0.072		0.069		1959-2007	48
WS2 PRISM November		60.482	-0.026	0.106		0.048		1953-2007	55
WS8 PRISM November		21.803	-0.007	0.766		0.002		1964-2007	44
WS9 PRISM November		17.765	-0.005	0.861		0.001		1969-2007	39
CS2MET November		22.005	-0.008	0.673		0.004		1959-2007	48
WS2 PRISM December		69.826	-0.032	0.071		0.060		1953-2007	55
WS8 PRISM December		10.897	-0.002	0.934		0.000		1964-2007	44
WS9 PRISM December		21.406	-0.008	0.699		0.004		1969-2007	39
CS2MET December		19.418	-0.008	0.662		0.004		1959-2007	48
WS2 PRISM January		-15.194	0.011	0.464		0.010		1953-2007	55
WS8 PRISM January		-47.766	0.028	0.166		0.045		1964-2007	44
WS9 PRISM January		-58.805	0.033	0.143		0.057		1969-2007	39
CS2MET January		-70.597	0.038	0.057		0.076		1959-2007	48
WS2 PRISM February		25.635	-0.008	0.623		0.005		1953-2007	55
WS8 PRISM February		33.640	-0.013	0.584		0.007		1964-2007	44
WS9 PRISM February		5.364	0.002	0.958		0.000		1969-2007	39
CS2MET February		3.864	0.001	0.966		0.000		1958-2007	48
WS2 PRISM March		-69.803	0.041	0.008	**	0.125		1953-2007	55
WS8 PRISM March		-58.798	0.035	0.116		0.058		1964-2007	44
WS9 PRISM March		-79.799	0.046	0.097		0.073		1969-2007	39
CS2MET March		-101.496	0.055	0.010	**	0.137		1958-2006	47
WS2 PRISM April		-47.670	0.031	0.097		0.051		1953-2007	55
WS8 PRISM April		-74.397	0.044	0.082		0.070		1964-2007	44
WS9 PRISM April		-81.646	0.049	0.094		0.074		1969-2007	39
CS2MET April		-16.609	0.015	0.455		0.012		1958-2006	49
WS2 PRISM May		-24.186	0.021	0.272		0.023		1953-2007	55
WS8 PRISM May		11.223	0.003	0.907		0.000		1964-2007	44
WS9 PRISM May		31.450	-0.006	0.856		0.001		1969-2007	39
CS2MET May		21.288	-0.001	0.960		0.000		1958-2006	49
WS2 PRISM June		-21.035	0.022	0.210		0.029		1953-2007	55
WS8 PRISM June		9.593	0.006	0.782		0.002		1964-2007	44
WS9 PRISM June		37.318	-0.007	0.801		0.002		1969-2007	39
CS2MET June		63.822	-0.020	0.369		0.017		1958-2006	49
WS2 PRISM July		-16.165	0.022	0.222		0.028		1953-2007	55
WS8 PRISM July		-33.635	0.030	0.207		0.038		1964-2007	44
WS9 PRISM July		-43.672	0.036	0.202		0.044		1969-2007	39
CS2MET July		61.734	-0.017	0.525		0.009		1958-2006	49
WS2 PRISM August		-31.345	0.029	0.086		0.054		1953-2007	55
WS8 PRISM August		-21.952	0.025	0.286		0.027		1964-2007	44
WS9 PRISM August		-3.995	0.016	0.502		0.012		1969-2007	39
CS2MET August		49.970	-0.012	0.625		0.005		1958-2006	48
WS2 PRISM September		32.704	-0.005	0.821		0.001		1953-2007	55
WS8 PRISM September		-9.887	0.017	0.572		0.008		1964-2007	44
WS9 PRISM September		-18.261	0.022	0.531		0.011		1969-2007	39
CS2MET September		53.554	-0.017	0.423		0.014		1958-2006	48

Table B6: Trends in monthly average minimum temperature at CS2MET for the period of record, and at WS2 PRISM, WS8 PRISM, and WS9 PRISM for the periods corresponding to streamflow record.

Simple Linear Regression Model of Monthly Minimum Temperature over Time for Period Corresponding to Streamflow									
	Explanatory Variable Coefficients								
Dependent Variable	**Intercept**	**Year**	**P-value**		**R^2**		**Period**		**N**
WS2 PRISM October	7.978	-0.001	0.881		0.000		1953-2007		55
WS8 PRISM October	-3.866	0.004	0.788		0.002		1964-2007		44
WS9 PRISM October	-65.061	0.034	0.026	*	0.128		1969-2007		39
CS2MET October	1.617	0.002	0.896		0.000		1959-2007		48
WS2 PRISM November	-16.625	0.010	0.510		0.008		1953-2007		55
WS8 PRISM November	-25.120	0.013	0.521		0.010		1964-2007		44
WS9 PRISM November	-38.777	0.020	0.404		0.019		1969-2007		39
CS2MET November	-10.560	0.006	0.678		0.004		1959-2007		48
WS2 PRISM December	21.685	-0.011	0.469		0.010		1953-2007		55
WS8 PRISM December	-33.130	0.016	0.469		0.013		1964-2007		44
WS9 PRISM December	-44.089	0.021	0.353		0.023		1969-2007		39
CS2MET December	-15.342	0.008	0.638		0.005		1959-2007		48
WS2 PRISM January	-42.010	0.021	0.183		0.033		1953-2007		55
WS8 PRISM January	-79.313	0.039	0.055		0.085		1964-2007		44
WS9 PRISM January	-122.942	0.061	0.013	*	0.155		1969-2007		39
CS2MET January	-88.990	0.045	0.019	*	0.114		1959-2007		48
WS2 PRISM February	5.488	-0.003	0.856		0.001		1953-2007		55
WS8 PRISM February	-4.133	0.001	0.940		0.000		1964-2007		44
WS9 PRISM February	-3.395	0.001	0.953		0.000		1969-2007		39
CS2MET February	13.235	-0.007	0.716		0.003		1958-2007		48
WS2 PRISM March	-63.385	0.033	0.003	**	0.153		1953-2007		55
WS8 PRISM March	-63.661	0.032	0.035	*	0.102		1964-2007		44
WS9 PRISM March	-57.638	0.029	0.063		0.090		1969-2007		39
CS2MET March	-81.288	0.042	0.004	**	0.168		1958-2006		47
WS2 PRISM April	-53.154	0.028	0.004	**	0.145		1953-2007		55
WS8 PRISM April	-91.920	0.047	0.001	**	0.236		1964-2007		44
WS9 PRISM April	-90.511	0.047	0.002	**	0.233		1969-2007		39
CS2MET April	-73.396	0.038	0.002	**	0.192		1958-2006		49
WS2 PRISM May	-30.945	0.018	0.075		0.058		1953-2007		55
WS8 PRISM May	-72.223	0.038	0.006	**	0.169		1964-2007		44
WS9 PRISM May	-74.243	0.040	0.008	**	0.178		1969-2007		39
CS2MET May	-42.964	0.025	0.018	*	0.114		1958-2006		49
WS2 PRISM June	3.209	0.002	0.806		0.001		1953-2007		55
WS8 PRISM June	-6.155	0.006	0.646		0.005		1964-2007		44
WS9 PRISM June	-9.867	0.008	0.579		0.008		1969-2007		39
CS2MET June	19.802	-0.006	0.621		0.005		1958-2006		49
WS2 PRISM July	-38.658	0.025	0.005	**	0.137		1953-2007		55
WS8 PRISM July	-71.068	0.040	0.002	**	0.203		1964-2007		44
WS9 PRISM July	-78.852	0.044	0.002	**	0.225		1969-2007		39
CS2MET July	-32.374	0.022	0.035	*	0.091		1958-2006		49
WS2 PRISM August	-23.291	0.017	0.072		0.060		1953-2007		55
WS8 PRISM August	-30.172	0.020	0.134		0.053		1964-2007		44
WS9 PRISM August	-40.596	0.024	0.139		0.058		1969-2007		39
CS2MET August	8.811	0.001	0.933		0.000		1958-2006		48
WS2 PRISM September	-1.692	0.005	0.625		0.005		1953-2007		55
WS8 PRISM September	-19.844	0.014	0.336		0.022		1964-2007		44
WS9 PRISM September	-41.080	0.023	0.111		0.067		1969-2007		39
CS2MET September	3.572	0.002	0.858		0.001		1958-2006		48

Appendix C: Snow

Figure C1 shows the relationship and trends in April 1st snow water equivalent from Vanmet, Santiam Junction, Three Creeks Meadow, McKenzie, Hogg Pass, and Jump Off Joe for their respective periods of record through 2007. The correlation between Vanmet and these SNOTEL sites ranges from 0.70-0.90 (Table C1), for the period of overlapping data from 1988-2004, the highest correlation being with Santiam Junction.

Figure C2 shows the trend in April 1st snow water equivalent for Santiam Junction from 1941-2007. Over this period of record, April 1st snow water equivalent exhibits a decline of 8.93mm per year ($p<0.01$) for a net decline of 76% (Table C2). Over the periods of record relating to streamflows, Santiam Junction exhibits a decline of 10.97mm per year ($p<0.01$) from 1953-2007 for a net decline of 83%, a decline of -12.85mm per year ($p<0.01$) from 1964-2007 for a net decline of 88%, and a decline of 13.36mm per year ($p<0.01$) from 1969-2007 for a net decline of 88% (Table C2).

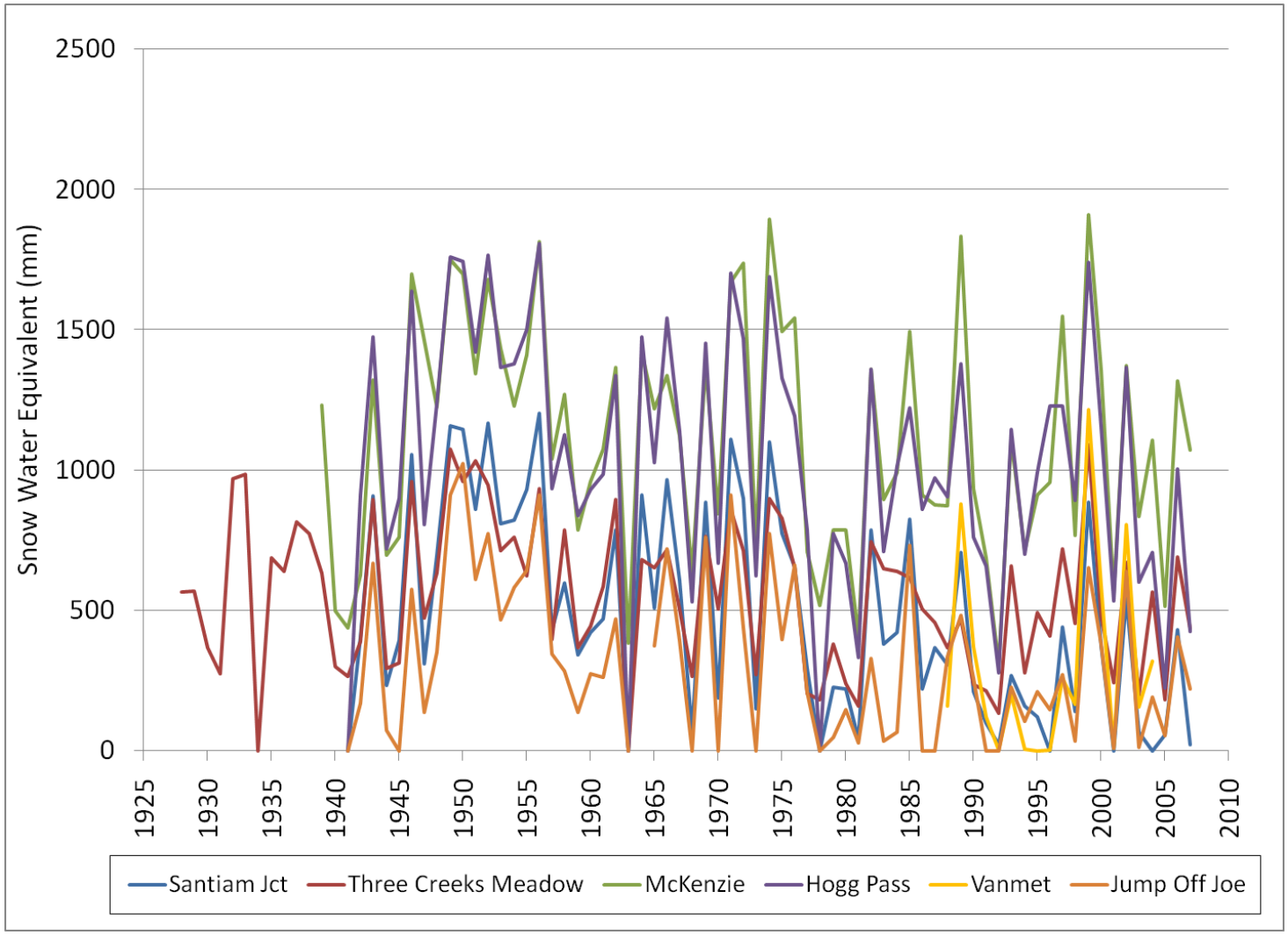

Figure C1. April 1st SWE at Vanmet and nearby SNOTEL sites for their respective periods of record starting in 1928

Table C1. Correlation coefficients between April 1st SWE at Vanmet and nearby SNOTEL sites for the period of overlapping record from 1988-2004

Correlation of April 1st Snowpack between Vanmet and nearby SNOTEL sites 1988-2004					
	Three Creeks Meadow	Santiam Jct	McKenzie	Hogg Pass	Jumpoff Joe
Correlation Coefficient	0.70	0.90	0.86	0.75	0.88

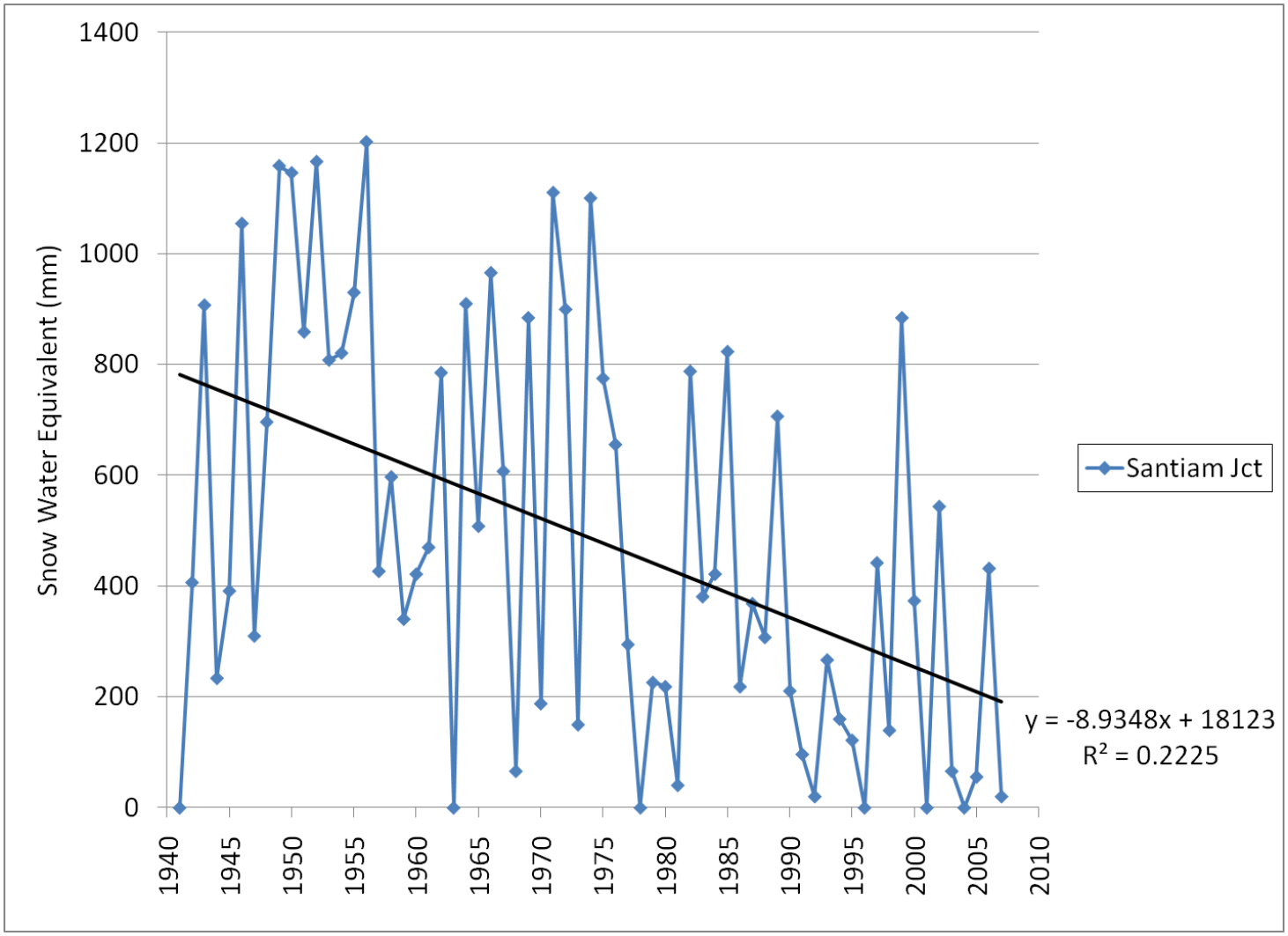

Figure C2. Trend in Santiam Junction April 1st SWE for the period of record from 1941-2007.

Table C2. Summary table of trends in Santiam Junction April 1st SWE for the period of record as well as the periods corresponding to streamflow record.

Simple Linear Regression Models of April 1st Snow Water Equivalent at Santiam Junction

		Explanatory Variable Coefficients									
Dependent Variable		**Intercept**		**Year**		**P-value**		**R^2**		**Period**	**N**
April 1st SWE		18123		-8.93		0.000	**	0.222		1941-2007	67
April 1st SWE		22162		-10.97		0.000	**	0.257		1953-2007	55
April 1st SWE		25914		-12.85		0.001	**	0.236		1964-2007	44
April 1st SWE		26921		-13.36		0.003	**	0.210		1969-2007	39

Appendix D: Vapor Pressure Deficit

Figure D1 shows daily maximum VPD at Primet for the five year period from 10/1/1996-9/30/2001. This period shows correspondence between sensors VPDPRI04 and VPDPRI05. Vapor pressure deficit follows a seasonal pattern, with highest vapor pressure deficits typically occurring during the summer and lowest vapor pressure deficits during the winter.

Average maximum vapor pressure deficit has changed significantly over the period of record from 1989-2006 at Primet during the winter and summer (Table D1). Winter average maximum vapor pressure deficit exhibits an increase of 0.072 mbar per year ($p<0.01$) for a net increase of 1.29 mbar. Summer average maximum vapor pressure deficit exhibits an increase of 0.573 mbar per year ($p<0.01$) for a net increase of 10.32 mbar.

Figure D2 shows the correspondence between daily maximum VPD at CS2MET and modeled VPD at CS2MET for the period of VPD record at CS2MET from 4/14/1998-2/19/2007. Modeled VPD has a correlation of 0.97 with measured max VPD at CS2MET during this period. The daily discrepancy between modeled VPD and actual maximum VPD at CS2MET is shown in Figure D3. The average discrepancy over the period is 1.68 mbar. Figure D4 shows the seasonal pattern in the modeled VPD for the five year period from 10/1/2001-9/30/2006. As with the measured VPD, the highest vapor pressure deficits typically occur during the summer and lowest vapor pressure deficits during the winter.

Modeled VPD shows no significant trends over the period of record (Table D2). During the period of record corresponding to VDP measured at PRIMET from 1989-

2006, modeled VPD at CS2MET exhibits a significant trend only during the summer (Table D3). During the summer modeled VPD exhibits an increase of 0.458 mbar per year ($p<0.01$) for a net increase of 8.25 mbar.

Figure D5 shows the modeled VPD data by season. Trend lines and equations are shown on the figures along with an R^2 goodness of fit estimate.

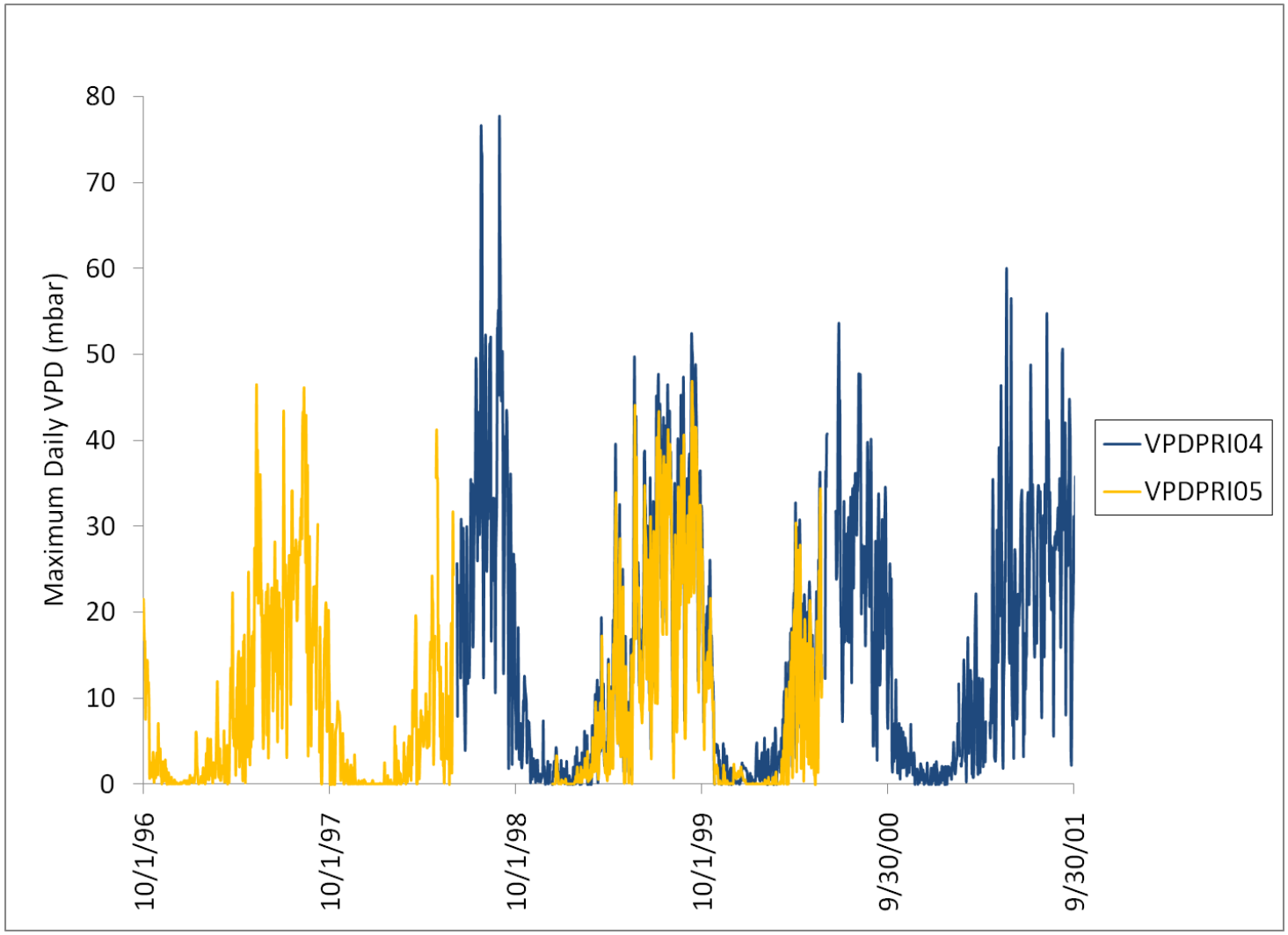

Figure D1. Maximum daily VPD at PRIMET for the period 10/1/1996-9/30/2001

Table D1. Summary regression table of trends in VPD at PRIMET by Season

Simple Linear Regression Model of Vapor Pressure Deficit at PRIMET over Time											
		Explanatory Variable Coefficients									
Dependent Variable		**Intercept**		**Year**		**P-value**		**R^2**		**Period**		**N**
Fall		48.9		-0.019		0.895		0.001		1989-2006		16
Winter		-142.1		0.072		0.005	**	0.422		1989-2006		17
Spring		-279.4		0.145		0.221		0.098		1989-2006		17
Summer		-1120.2		0.573		0.005	**	0.437		1989-2006		16

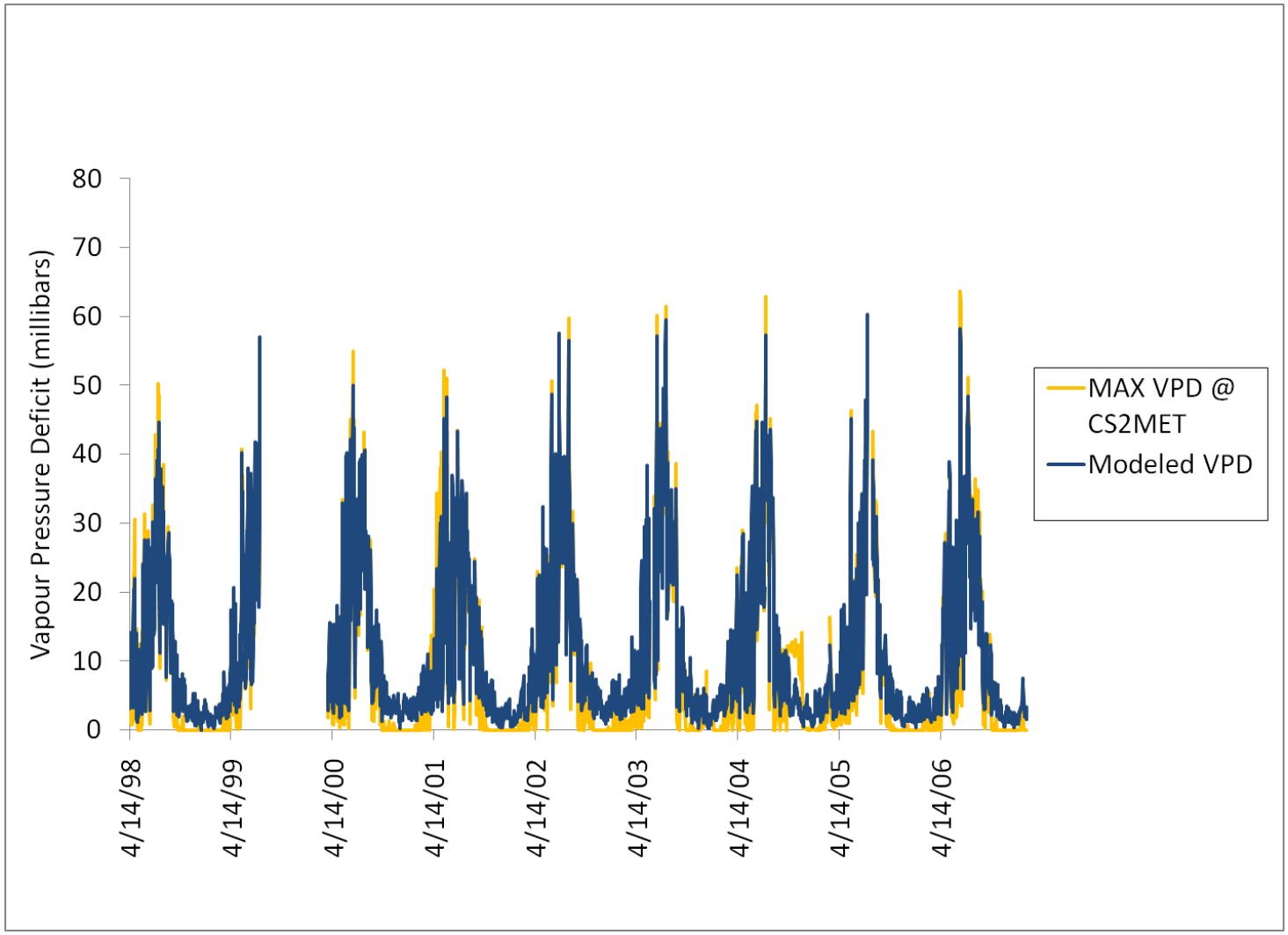

Figure D2. Modeled daily VPD versus actual maximum VPD at CS2MET, 4/14/1998-2/19/2007

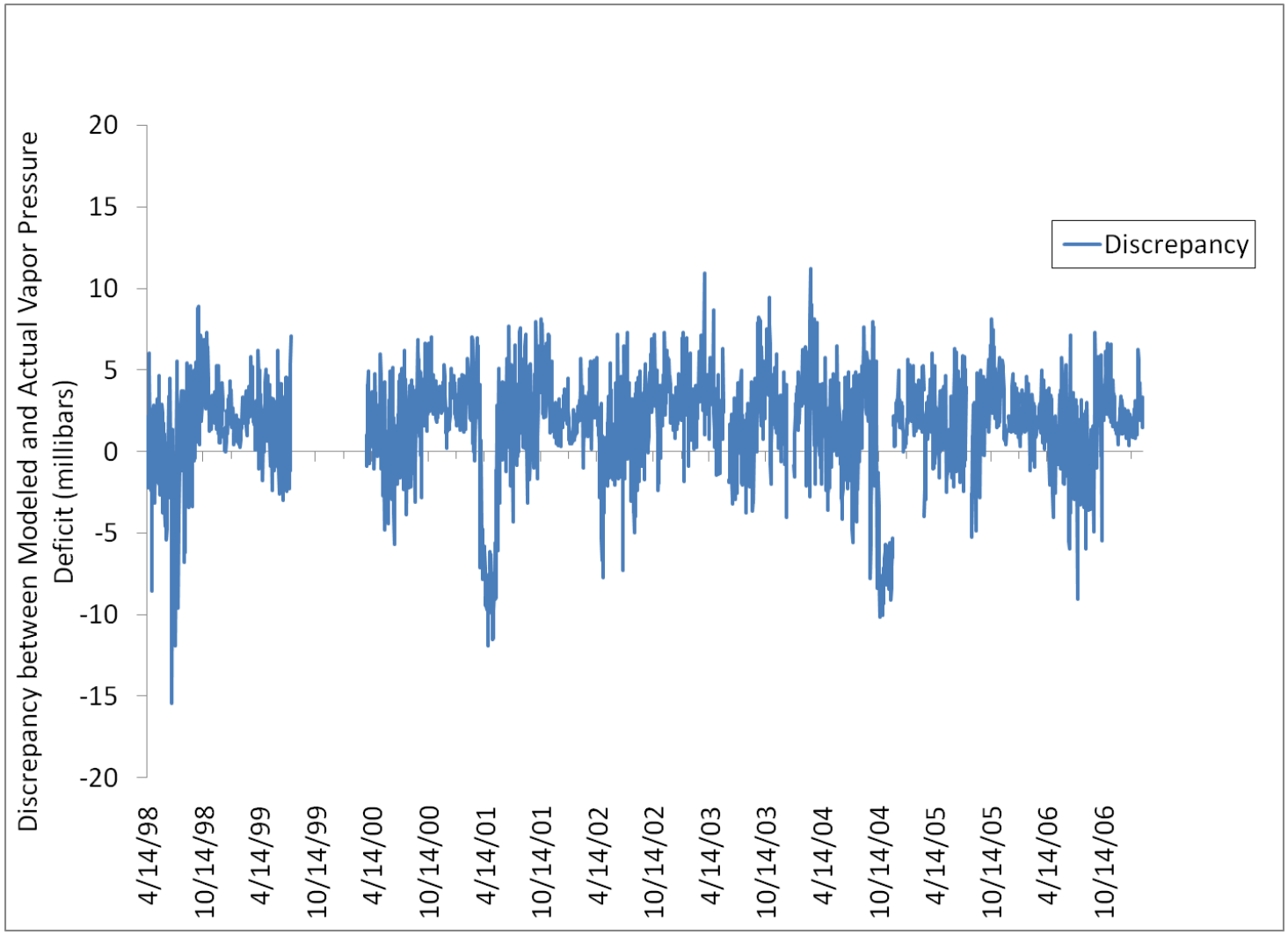

Figure D3. Discrepancy between Modeled daily VPD and actual maximum VPD at CS2MET, 4/14/1998-2/19/2007

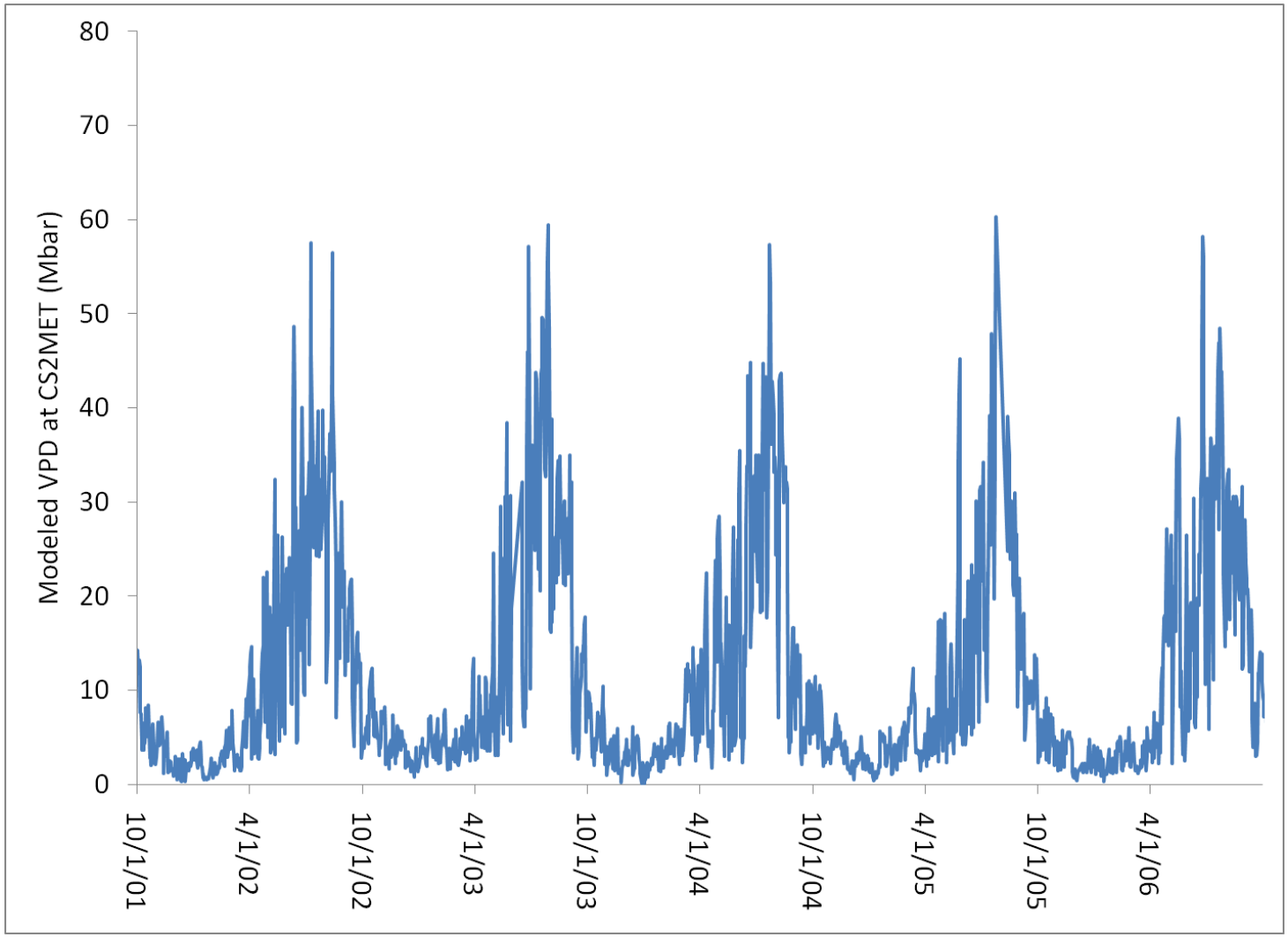

Figure D4. Modeled daily VPD at CS2MET for the period 10/1/01 to 9/30/2006

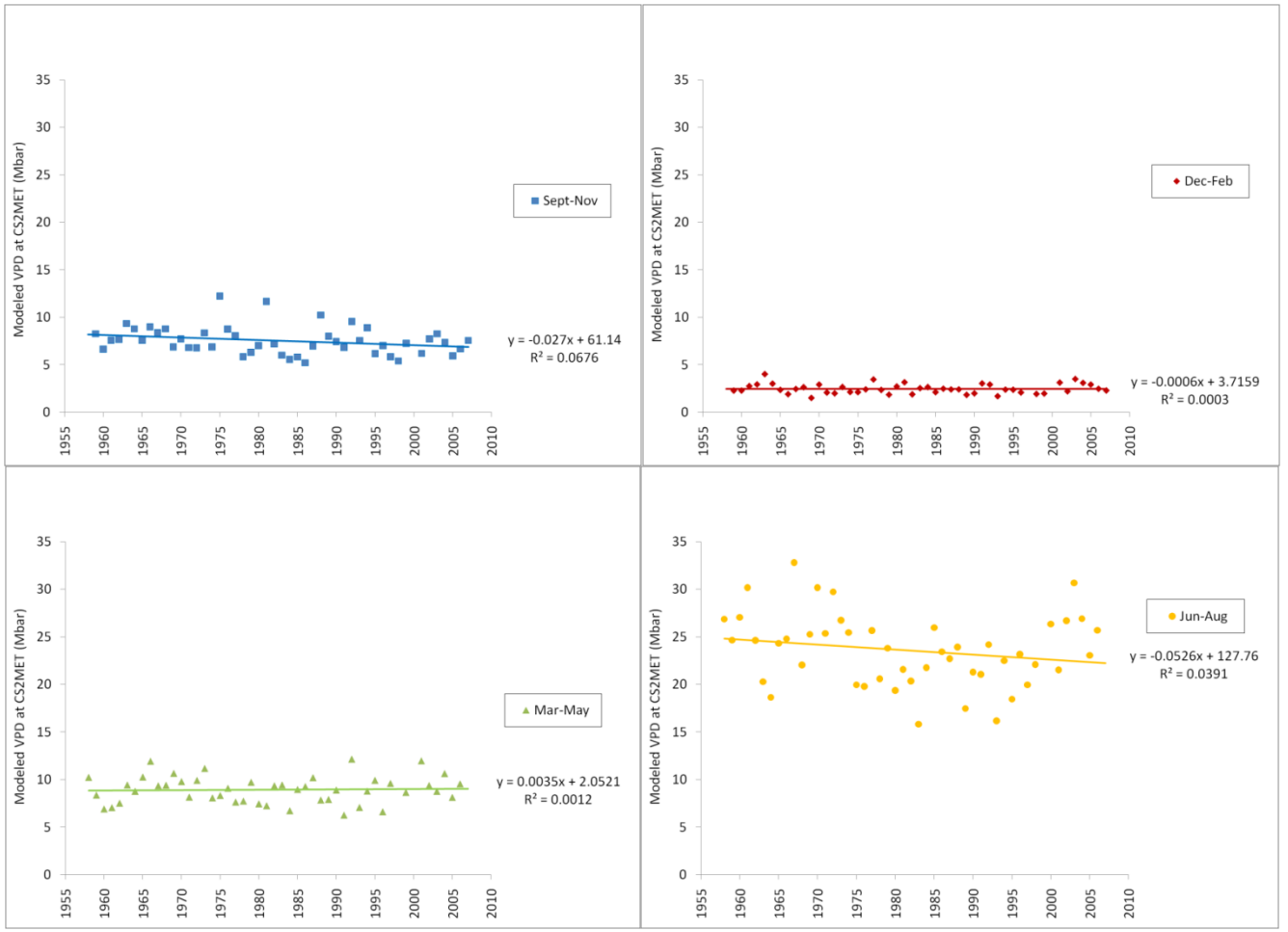

Figure D5. Trends in modeled daily VPD at CS2MET for the period of record from 2/3/1958-2/19/2007 in the (clockwise from top left) fall, winter, summer, and spring.

Table D2. Summary regression table of trends in modeled VPD at CS2MET by season for the full period of record from 2/3/1958-2/19/2007.

Simple Linear Regression Model of Modeled Vapor Pressure Deficit at CS2MET over Time											
		Explanatory Variable Coefficients									
Dependent Variable		**Intercept**		**Year**		**P-value**		**R^2**		**Period**		**N**
Fall		61.1		-0.027		0.074		0.068		1959-2007		48
Winter		3.7		-0.001		0.908		0.000		1959-2007		47
Spring		2.1		0.003		0.817		0.001		1958-2006		47
Summer		127.8		-0.053		0.178		0.039		1958-2006		48

Table D3. Summary regression table of trends in modeled VPD at CS2MET by season for the period of record corresponding to measured VPD at PRIMET from 1989-2006.

Simple Linear Regression Model of Modeled Vapor Pressure Deficit at CS2MET 1989-2006

		Explanatory Variable Coefficients										
Dependent Variable		**Intercept**		**Year**		**P-value**		**R^2**		**Period**		**N**
Fall		143.2		-0.068		0.191		0.111		1989-2006		17
Winter		-84.3		0.043		0.088		0.194		1989-2006		16
Spring		-158.1		0.084		0.288		0.080		1989-2006		16
Summer		-892.2		0.458		0.003	**	0.452		1989-2006		17

Appendix E: Wind

Figure E1 shows daily average wind speed at Primet for the five year period from 10/01/2001-9/30/2006. Average wind speed follows a seasonal pattern, with highest average daily wind speeds typically occurring during the summer and lowest average daily wind speeds during the winter. Average wind speeds show no significant trends over the period of record from 1974-2006/07 (Table E1). However, for the period of continuous record starting in 1980, average wind speeds show significant declines in all seasons (Table E2). On an annual basis, average wind speeds have declined by 0.016m/s per year ($p<0.01$) for a net change of -0.403m/s over the 26 year period. During the fall, average wind speeds have declined by 0.013m/s per year ($p<0.01$) for a net change of -0.337m/s over the 27 year period. During the winter, average wind speeds have declined by 0.012m/s per year ($p<0.01$) for a net change of -0.323m/s over the 26 year period. During the spring, average wind speeds have declined by 0.015m/s per year ($p<0.01$) for a net change of -0.402m/s over the 27 year period of record. During the summer, average wind speeds have declined by 0.021m/s per year ($p<0.01$) for a net change of -0.569m/s over the 27 year period of record. Figure E2 shows the average wind speed data by season. Trend lines and equations are shown on the figures along with an R^2 goodness of fit estimate.

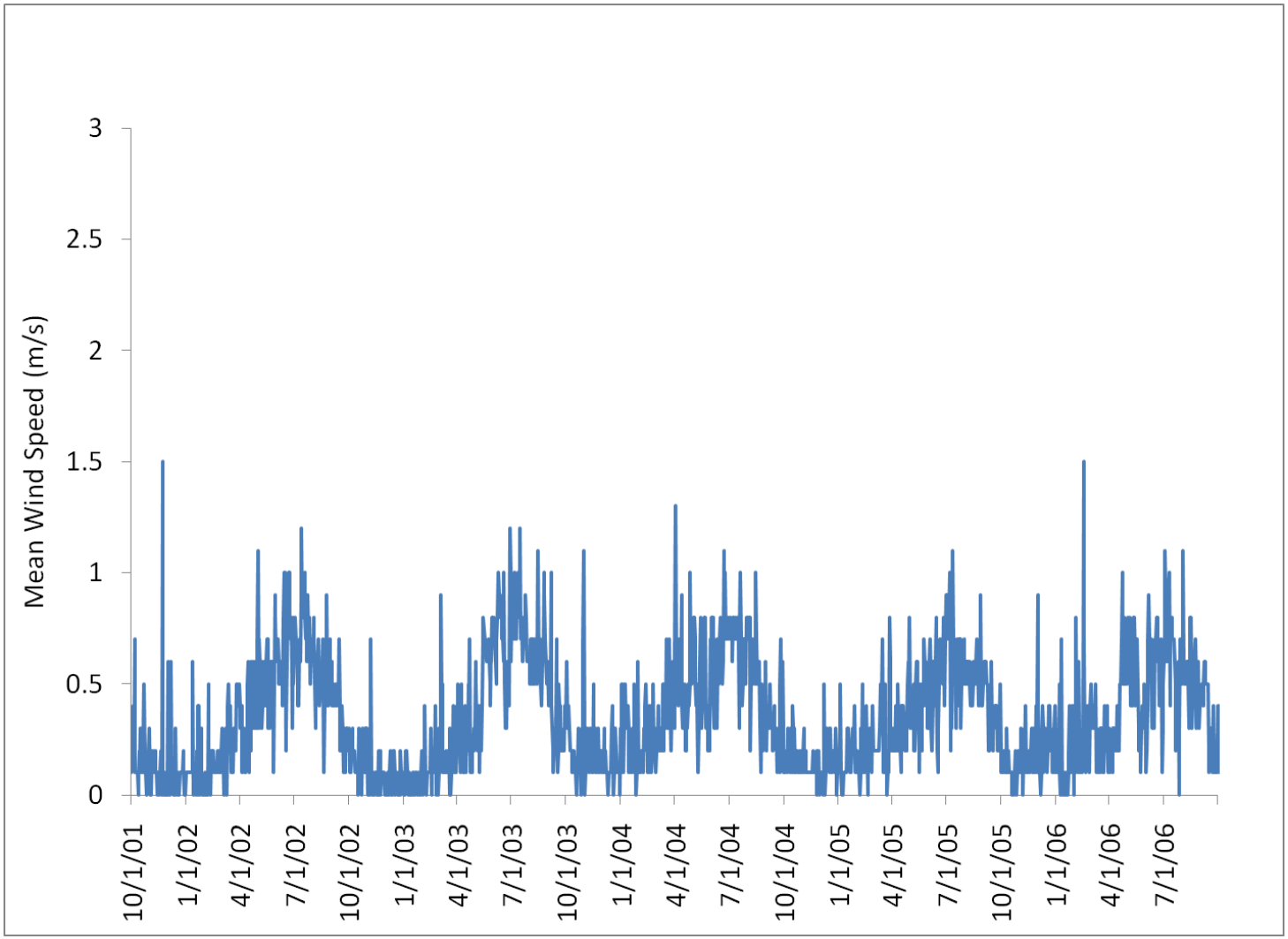

Figure E1. Daily average wind speed at PRIMET for the period 10/01/2001-9/30/2006

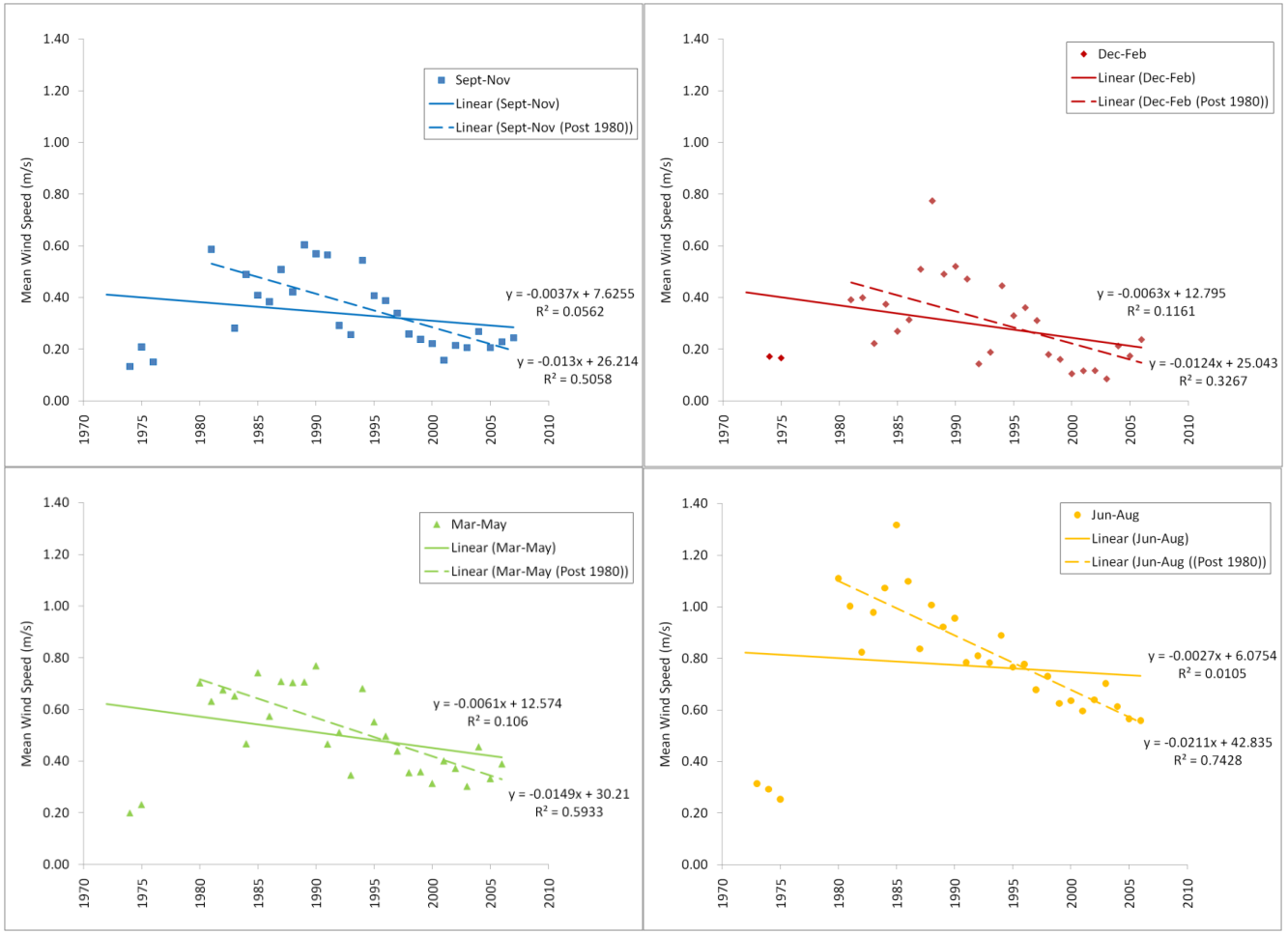

Figure E2. Trends in daily average wind speed at PRIMET during (clockwise from top left) fall, winter, summer, and spring for the period of record from 1974-2006/07.

Table E1. Summary regression table of trends in average wind speed at PRIMET by season for the period of record.

Simple Linear Regression Model of Average Wind Speed over Time at PRIMET											
		Explanatory Variable Coefficients									
Dependent Variable		**Intercept**		**Year**		**P-value**		**R^2**		**Period**	**N**
Annual		12.07		-0.006		0.085		0.109		1974-2006	28
Fall		7.63		-0.004		0.216		0.056		1974-2007	29
Winter		12.80		-0.006		0.076		0.116		1974-2006	28
Spring		12.57		-0.006		0.085		0.106		1974-2006	29
Summer		6.08		-0.003		0.590		0.011		1974-2006	30

Table E2. Summary regression table of trends in average wind speed at PRIMET by season for the period of record since 1980.

Simple Linear Regression Model of Average Wind Speed over Time at PRIMET since 1980										
		Explanatory Variable Coefficients								
Dependent Variable		**Intercept**		**Year**		**P-value**		**R^2**	**Period**	**N**
Annual		31.41		-0.016		0.000	**	0.700	1981-2006	26
Fall		26.21		-0.013		0.000	**	0.506	1981-2007	26
Winter		25.04		-0.012		0.002	**	0.327	1981-2006	26
Spring		30.21		-0.015		0.000	**	0.593	1980-2006	27
Summer		42.84		-0.021		0.000	**	0.743	1980-2006	27

Appendix F: Discharge

1 Discharge

Over the full periods of record, discharge has changed significantly only in the case of WS2 spring flows (Table F1). Spring discharge for WS2 exhibits a decline of -2.54mm per year ($p<0.05$) for a net change of 139.95mm over the 55 year period of record. Over the period of overlapping streamflows from 1969-2007, only WS8 spring discharge exhibits a significant trend (Table F2). WS8 spring discharge exhibits a decline of -4.86mm per year ($p<0.05$) for a net change of 189.61mm over the 39 year period. Figures F1-F5 show the discharge data by season for the WS2, WS8, and WS9. Trend lines and equations are shown on the figures along with an R^2 goodness of fit estimate.

2 Date of median flow analysis

There has been no significant change either in the date at which 50% of the water year discharge has passed, or the proportion of water year discharge that has passed by March 1st (Table F3). Figure F6 shows the date of 50% water year discharge over time for each of the three watersheds, and Figure F7 shows the proportion of water year discharge by March 1st over time for each of the three watersheds. Trend lines and equations are shown on the figures along with an R^2 goodness of fit estimate.

3 Wavelet analysis of daily discharge

Figures F8-F11 show the results of the daily linear regression analysis using low-pass filters of 6.28 days, 12.57 days, 25.13 days, and 50.27 days respectively for WS2 discharge. In each of the figures, the top panel shows the estimated slope coefficient by day of water year, the middle panel shows the norm of residuals by day of water year, and the bottom panel indicates whether the slope coefficient is significant ($p<0.05$). Using the 6.28 day filter, WS2 has 25 days

that have trended significantly. There are 5 days in October with significant negative coefficients ranging from -0.014 to -0.016, and there are 20 days in March and April with significant negative coefficients ranging from -0.045 to -0.090. Using the 12.57 day filter, WS2 has 30 days that have trended significantly. There are 10 days in October with significant negative coefficients ranging from -0.011 to -0.013, and there are 20 days in March and April with significant negative coefficients ranging from -0.042 to -0.092. Using the 25.13 day filter, WS2 has 31 days that have trended significantly. There is 1 day in September with a significant negative coefficient of -0.006, and there are 30 days in March and April with significant negative coefficients ranging from -0.031 to -0.054. Using the 50.27 day filter, WS2 has 32 days that have trended significantly. These days fall in March and April and have significant negative coefficients ranging from -0.031 to -0.044.

Figures F12-15 show the results of the daily linear regression analysis using low-pass filters of 6.28 days, 12.57 days, 25.13 days, and 50.27 days respectively for WS8 discharge. Using the 6.28 day filter, WS8 has 25 days that have trended significantly. There are 7 days in January with significant negative coefficients ranging from -0.157 to -0.203, and there are 18 days in April and May with significant negative coefficients ranging from -0.062 to -0.103. Using the 12.57 day filter, WS8 has 24 days that have trended significantly. These days fall in April and May and have significant negative coefficients ranging from -0.049 to -0.092. Using the 25.13 day filter, WS8 has 36 days that have trended significantly. These days fall in April and May and have significant negative coefficients ranging from -0.041 to -0.068. Using the 50.27 day filter, WS8 has 15 days that have trended significantly. These days fall in June and have significant negative coefficients ranging from -0.019 to -0.062.

Figures 16-19 show the results of the daily linear regression analysis using low-pass filters of 6.28 days, 12.57 days, 25.13 days, and 50.27 days respectively for WS9 discharge. Using the 6.28 day filter, WS9 has 9 days that have trended significantly. There are 2 days in August with significant negative coefficients of -0.005 and -0.006, and there are 7 days in September with significant negative coefficients ranging from -0.006 to -0.008. Using the 12.57 day filter, WS9 has no days that have trended significantly. Using the 25.13 day filter, WS9 has 14 days that have trended significantly. These days are in March and have significant negative coefficients ranging from -0.092 to -0.105. Using the 50.27 day filter, WS8 has no days that have trended significantly.

Tables F4-F6 summarizes the significant results of the daily linear regression analysis using the low-pass filters for each of the watersheds respectively.

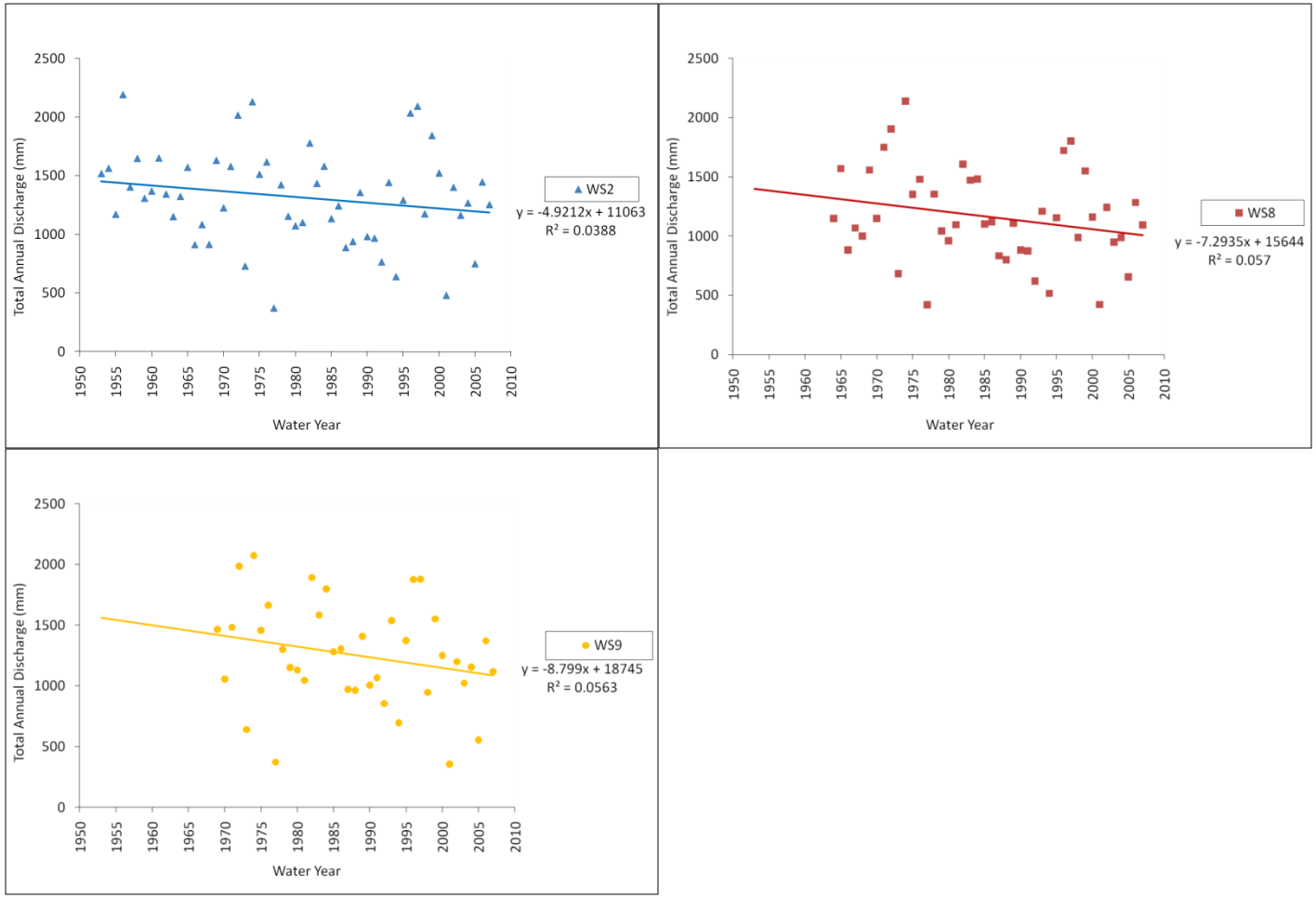

Figure F1. Annual discharge at (clockwise from bottom left) WS9, WS2, and WS8.

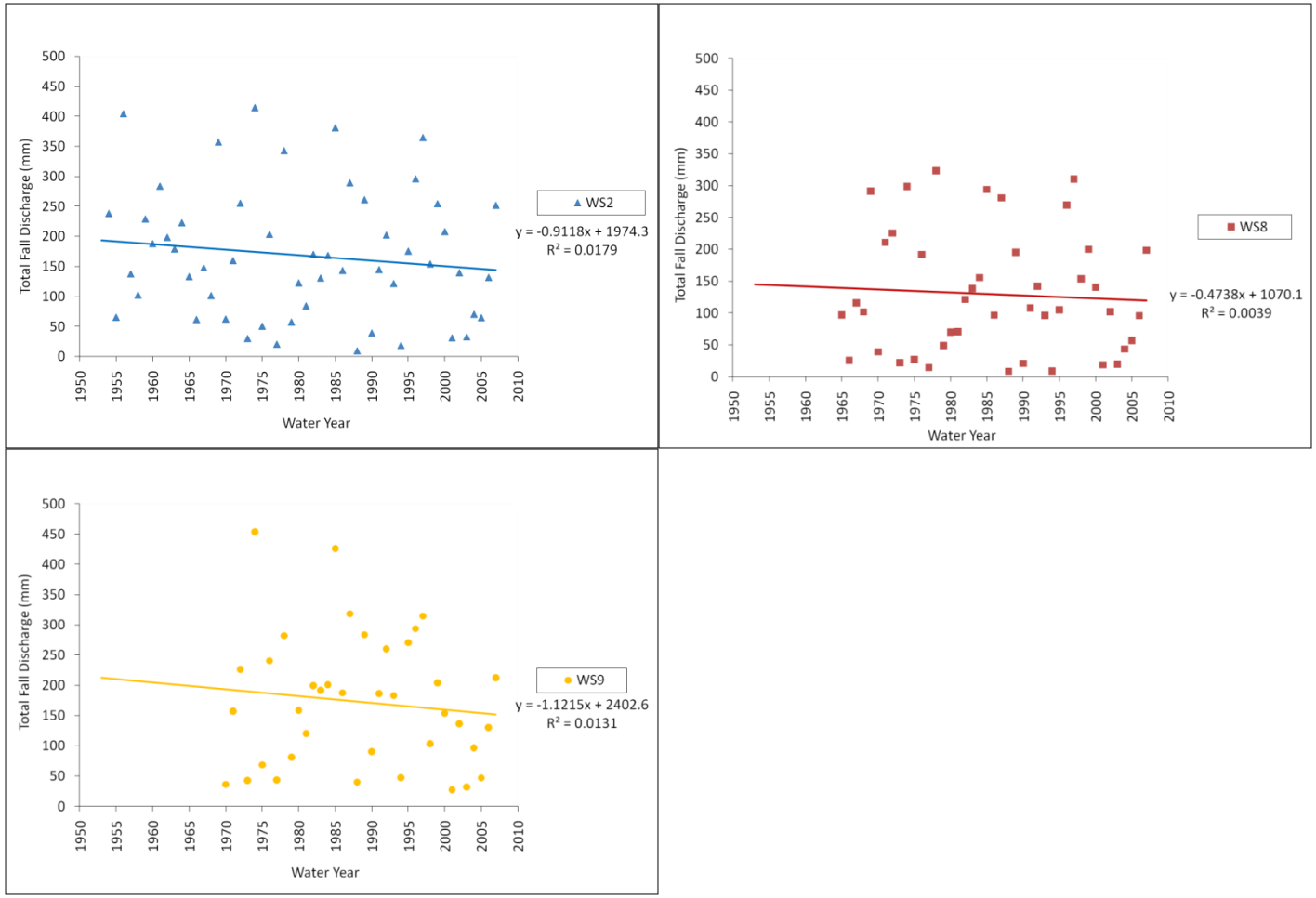

Figure F2. Fall discharge at (clockwise from bottom left) WS9, WS2, and WS8.

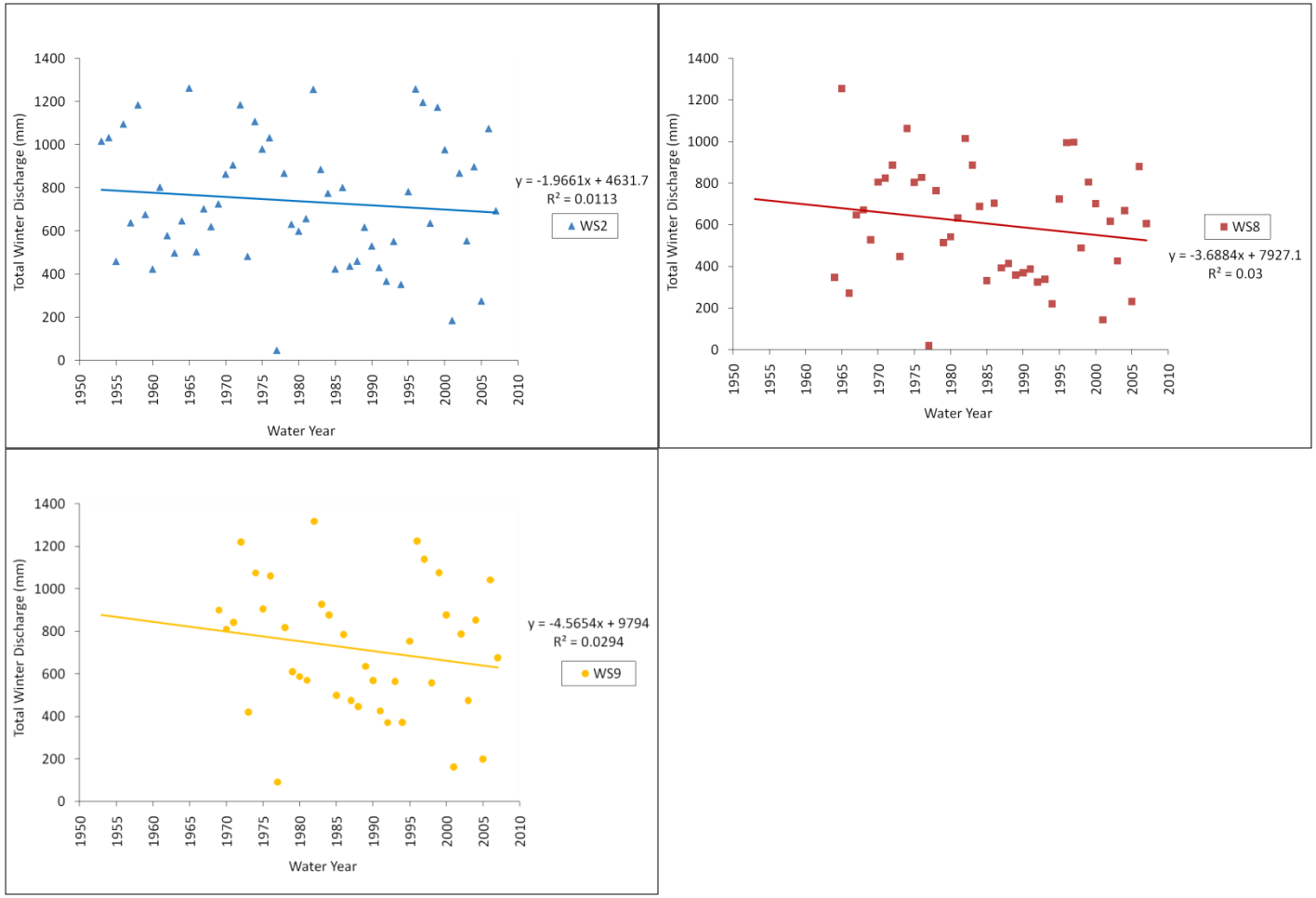

Figure F3. Winter discharge at (clockwise from bottom left) WS9, WS2, and WS8.

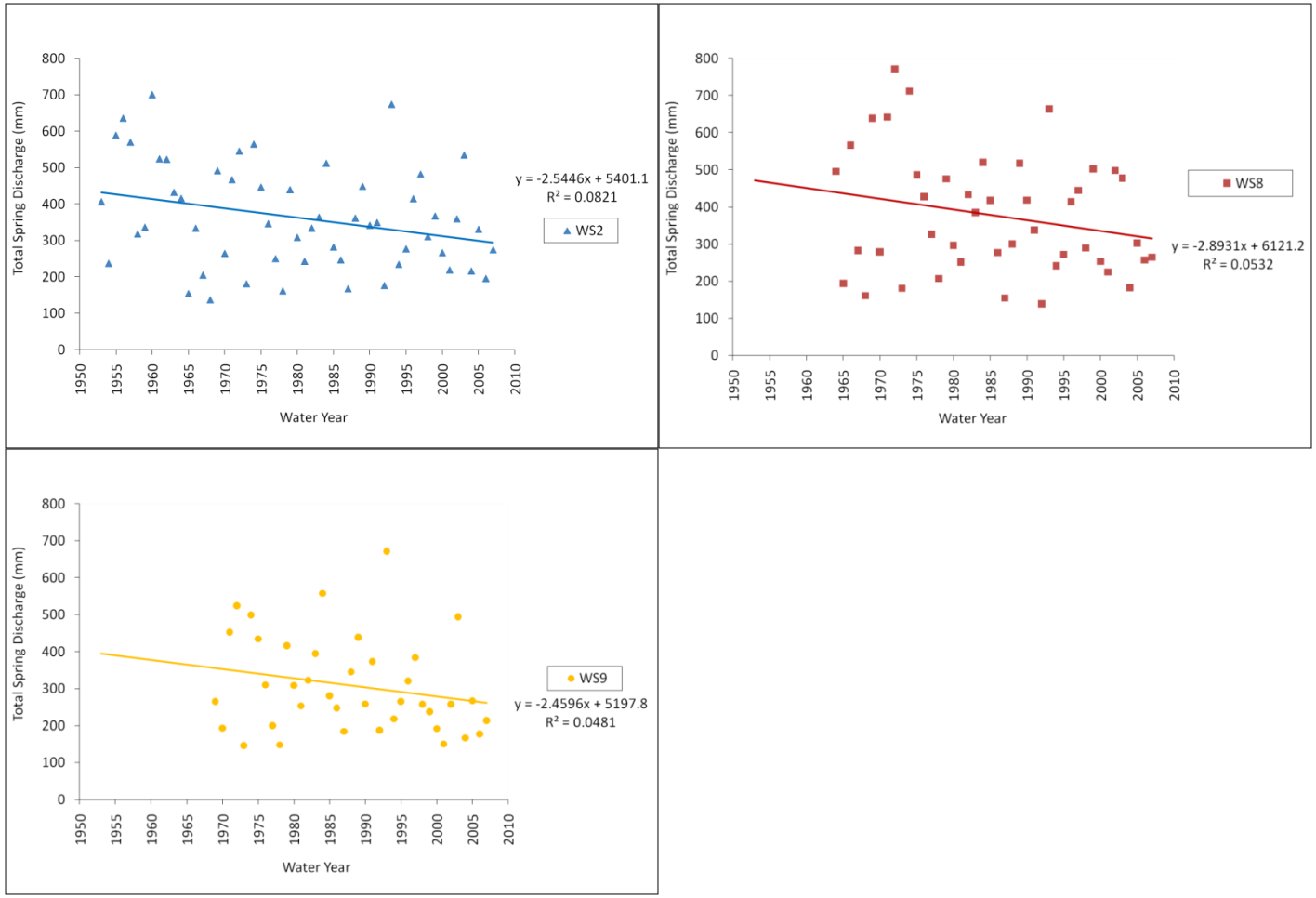

Figure F4. Spring discharge at (clockwise from bottom left) WS9, WS2, and WS8.

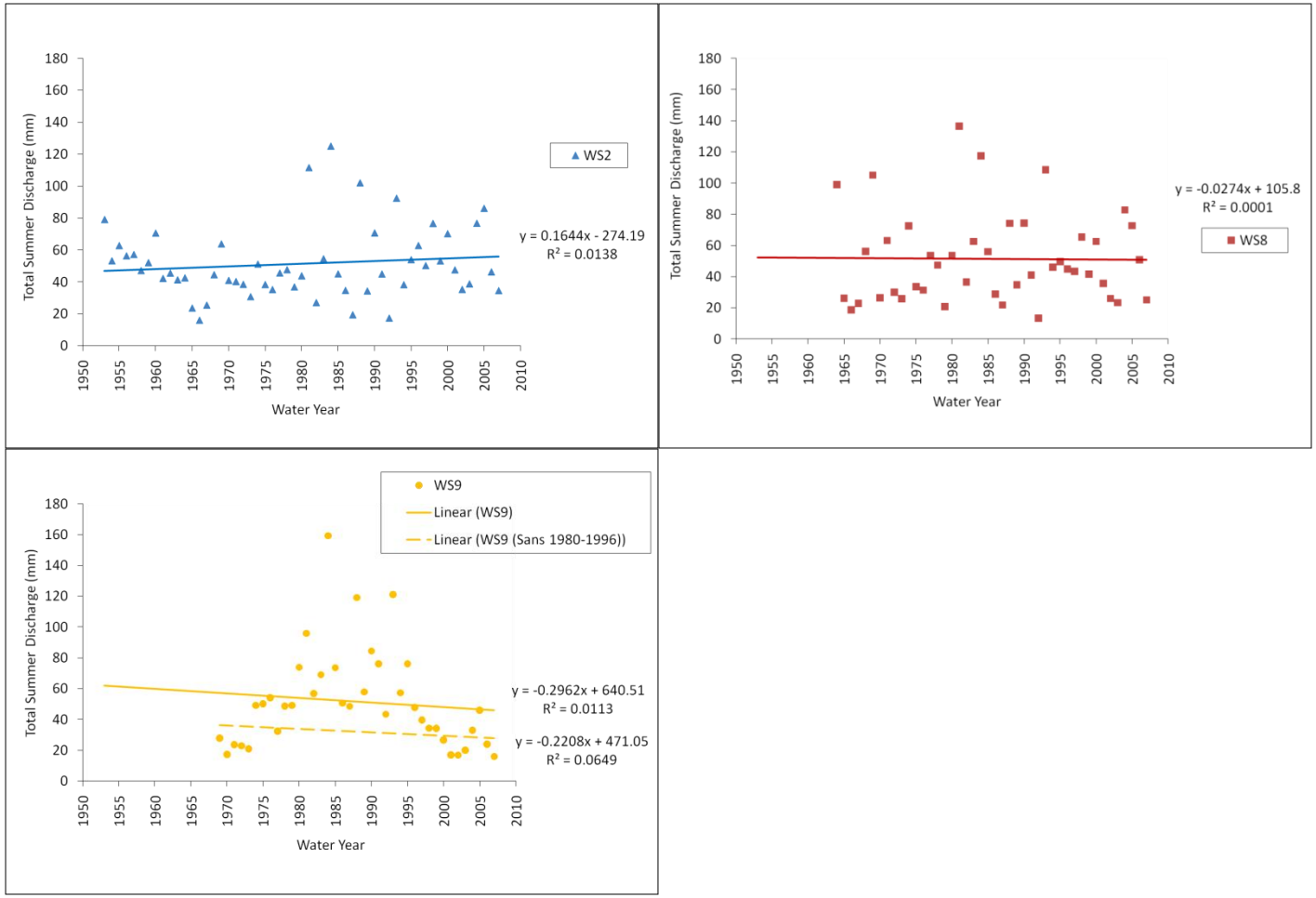

Figure F5. Summer discharge at (clockwise from bottom left) WS9, WS2, and WS8.

Table F1. Summary regression table of trends in discharge for WS2, WS8, and WS9 over their respective periods of record.

Simple Linear Regression Model of Discharge over Time									
		Explanatory Variable Coefficients							
Dependent Variable		**Intercept**		**Year**		**P-value**		**R^2**	**N**
WS2 Annual Discharge		11062.555		-4.921		0.149		0.039	55
WS8 Annual Discharge		15644.300		-7.294		0.119		0.057	44
WS9 Annual Discharge		18745.151		-8.799		0.146		0.056	39
WS2 Fall Discharge		1974.304		-0.912		0.335		0.018	54
WS8 Fall Discharge		1070.082		-0.474		0.692		0.004	43
WS9 Fall Discharge		2402.555		-1.122		0.493		0.013	38
WS2 Winter Discharge		4631.651		-1.966		0.439		0.011	55
WS8 Winter Discharge		7927.108		-3.688		0.260		0.030	44
WS9 Winter Discharge		9793.957		-4.565		0.297		0.029	39
WS2 Spring Discharge		5401.081		-2.545		0.034	*	0.082	55
WS8 Spring Discharge		6121.150		-2.893		0.132		0.053	44
WS9 Spring Discharge		5197.822		-2.460		0.180		0.048	39
WS2 Summer Discharge		-274.193		0.164		0.392		0.014	55
WS8 Summer Discharge		105.803		-0.027		0.937		0.000	44
WS9 Summer Discharge		640.508		-0.296		0.520		0.011	39

Table F2. Summary regression table of trends in discharge for WS2, WS8, and WS9 for the period of overlapping streamflow record from 1969-2007.

Simple Linear Regression Model of Discharge over Time 1969-2007									
		Explanatory Variable Coefficients							
Dependent Variable		**Intercept**		**Year**		**P-value**		**R^2**	**N**
WS2 Annual Discharge		12161.269		-5.467		0.379		0.021	39
WS8 Annual Discharge		22982.892		-10.974		0.058		0.094	39
WS9 Annual Discharge		18745.151		-8.799		0.146		0.056	39
WS2 Fall Discharge		972.723		-0.409		0.807		0.002	38
WS8 Fall Discharge		1831.694		-0.856		0.556		0.010	38
WS9 Fall Discharge		2402.555		-1.122		0.493		0.013	38
WS2 Winter Discharge		6012.005		-2.656		0.551		0.010	39
WS8 Winter Discharge		9617.529		-4.536		0.228		0.039	39
WS9 Winter Discharge		9793.957		-4.565		0.297		0.029	39
WS2 Spring Discharge		4323.699		-2.002		0.267		0.033	39
WS8 Spring Discharge		10046.840		-4.862		0.031	*	0.120	39
WS9 Spring Discharge		5197.822		-2.460		0.180		0.048	39
WS2 Summer Discharge		-560.034		0.308		0.381		0.021	39
WS8 Summer Discharge		396.847		-0.173		0.674		0.005	39
WS9 Summer Discharge		640.508		-0.296		0.520		0.011	39

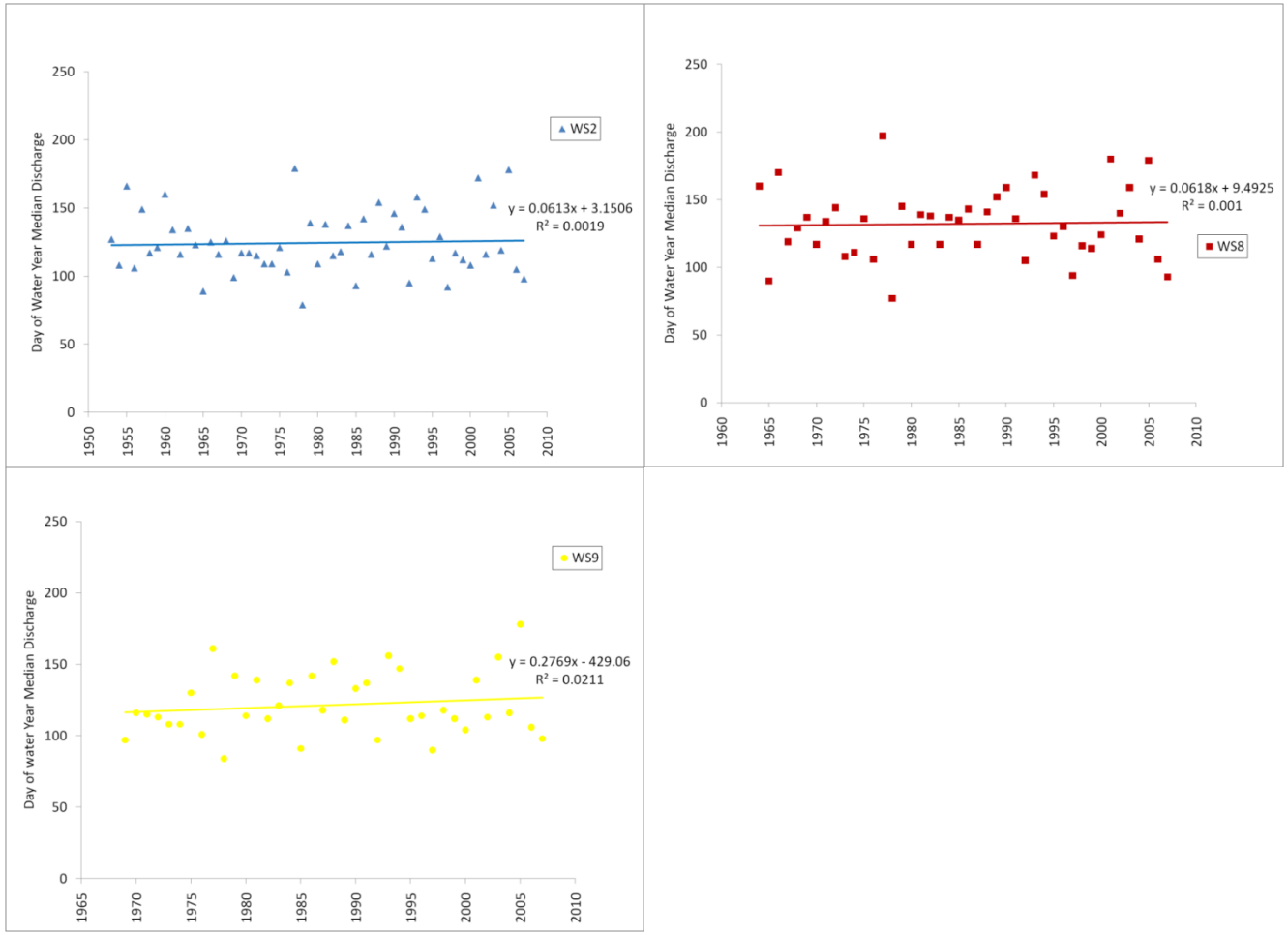

Figure F6. Median flow day at (clockwise from bottom left) WS9, WS2, and WS8.

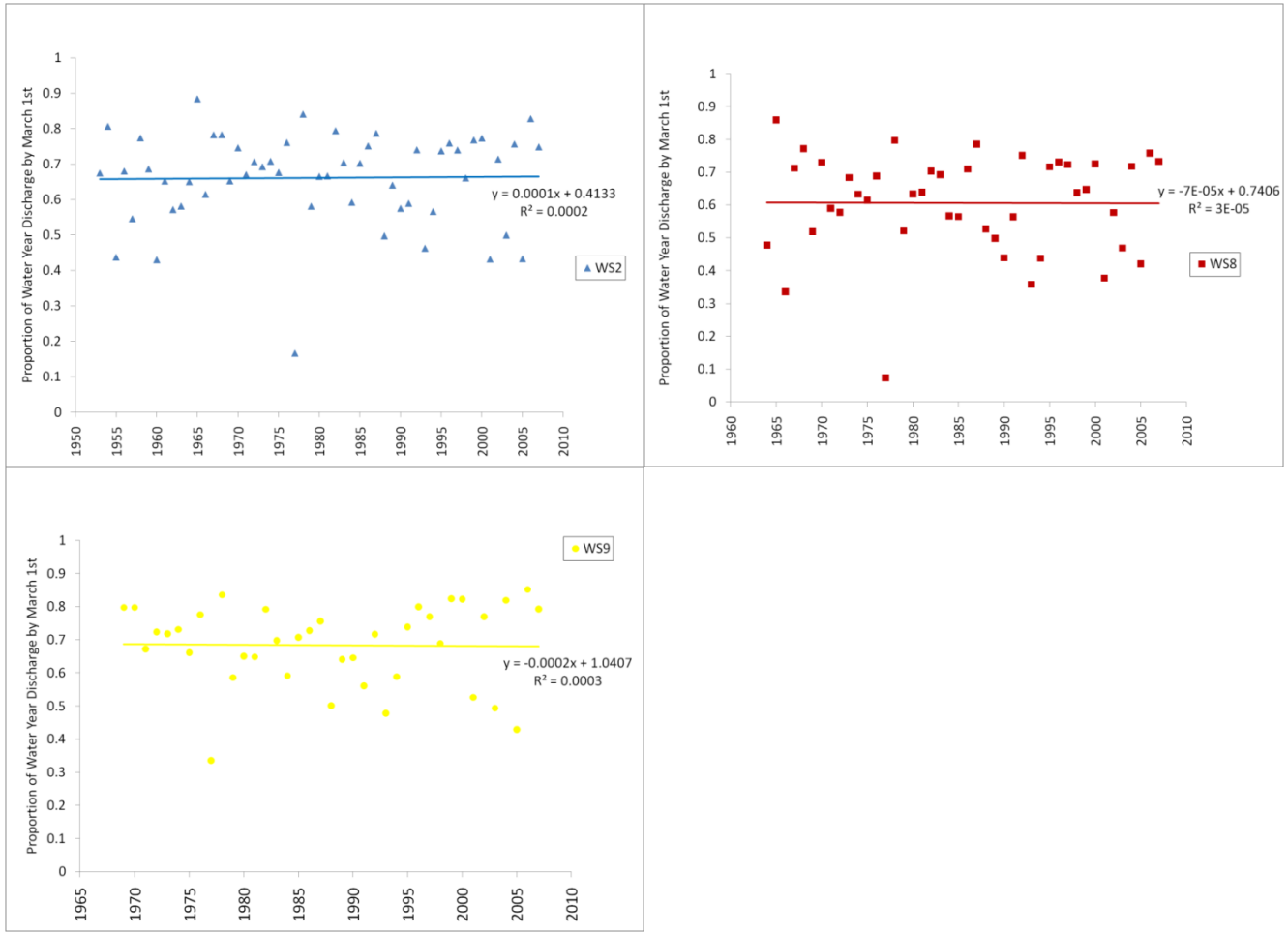

Figure F7. Proportion of Water Year Discharge by March 1st at (clockwise from bottom left) WS9, WS2, and WS8.

Table F3. Summary regression table of trends in discharge timing at WS2, WS8, and WS9 for their respective periods of record.

Simple Linear Regression Model of Water Year Flow Timing									
		Explanatory Variable Coefficients							
Dependent Variable		**Intercept**		**Year**		**P-value**		**R^2**	**N**
WS2 Water Year Day of Median Discharge		3.2		0.061		0.754		0.002	55
WS8 Water Year Day of Median Discharge		9.5		0.062		0.842		0.001	44
WS9 Water Year Day of Median Discharge		-429.1		0.277		0.378		0.021	39
WS2 Proportion of Water Year Discharge by March 1st		0.4		0.000		0.912		0.000	55
WS8 Proportion of Water Year Discharge by March 1st		0.7		0.000		0.971		0.000	44
WS9 Proportion of Water Year Discharge by March 1st		1.0		0.000		0.920		0.000	39

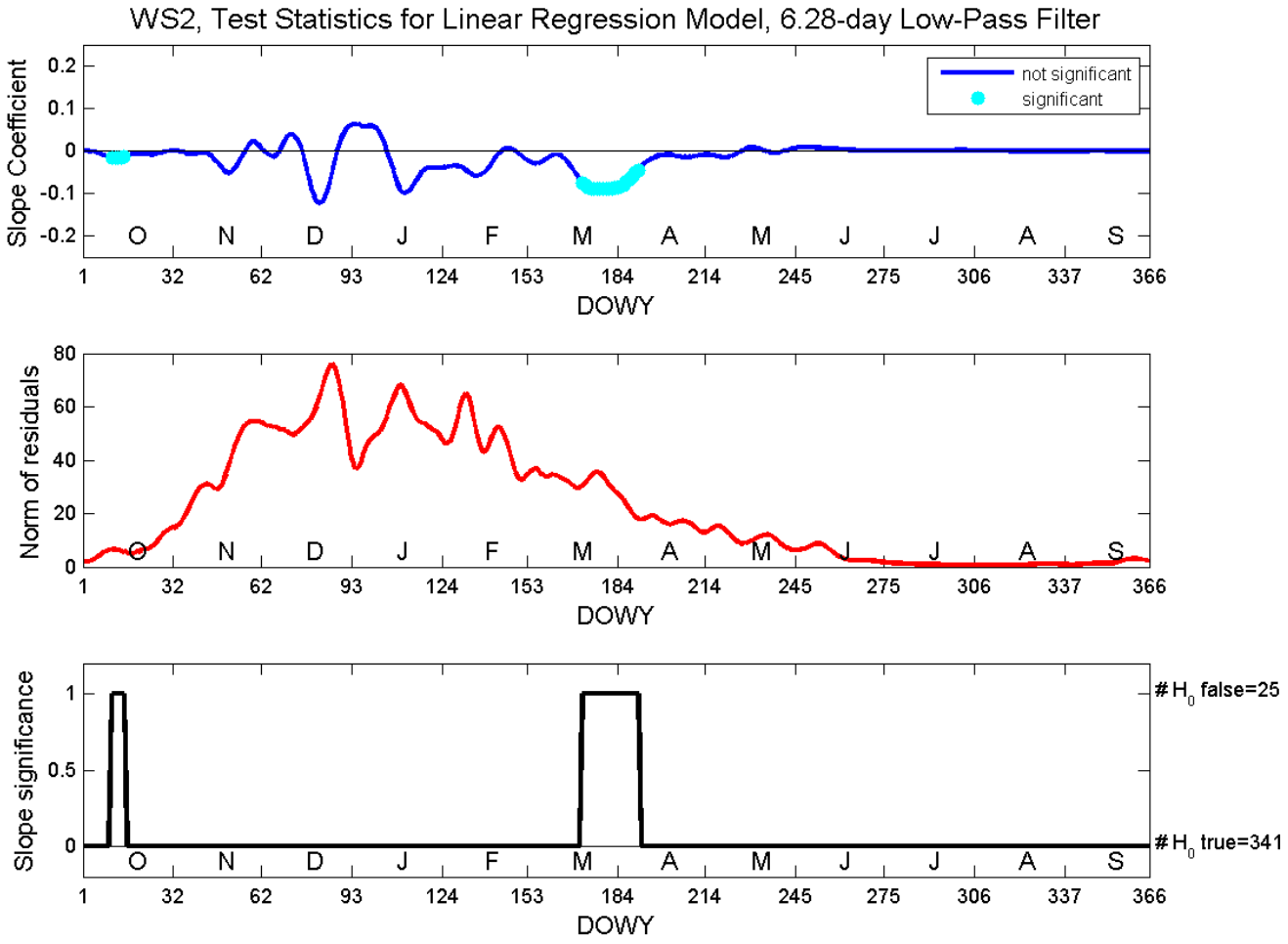

Figure F8. Daily linear regression model for WS2 using a 6.28 day low-pass filter wavelet.

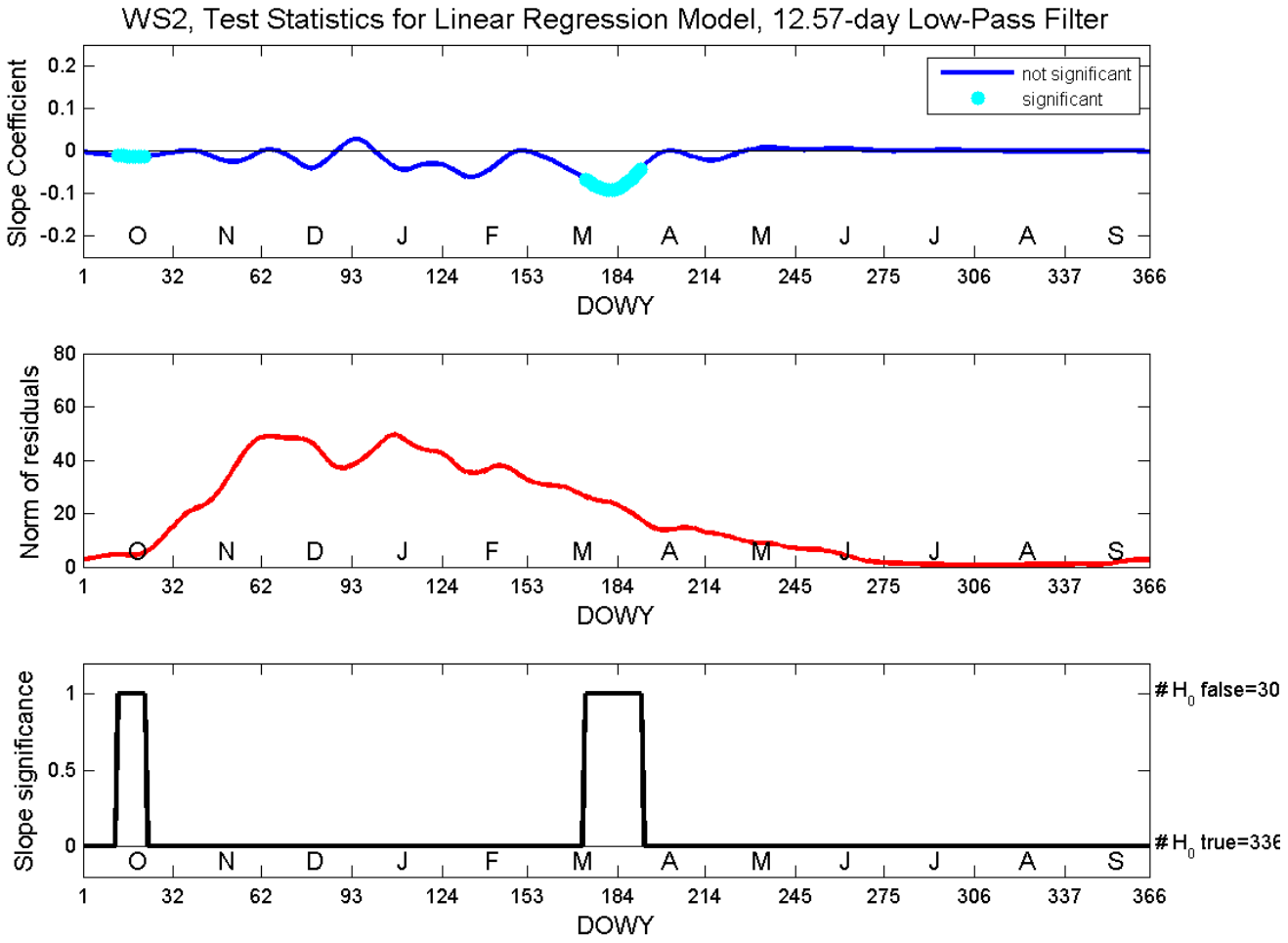

Figure F9. Daily linear regression model for WS2 using a 12.57 day low-pass filter wavelet.

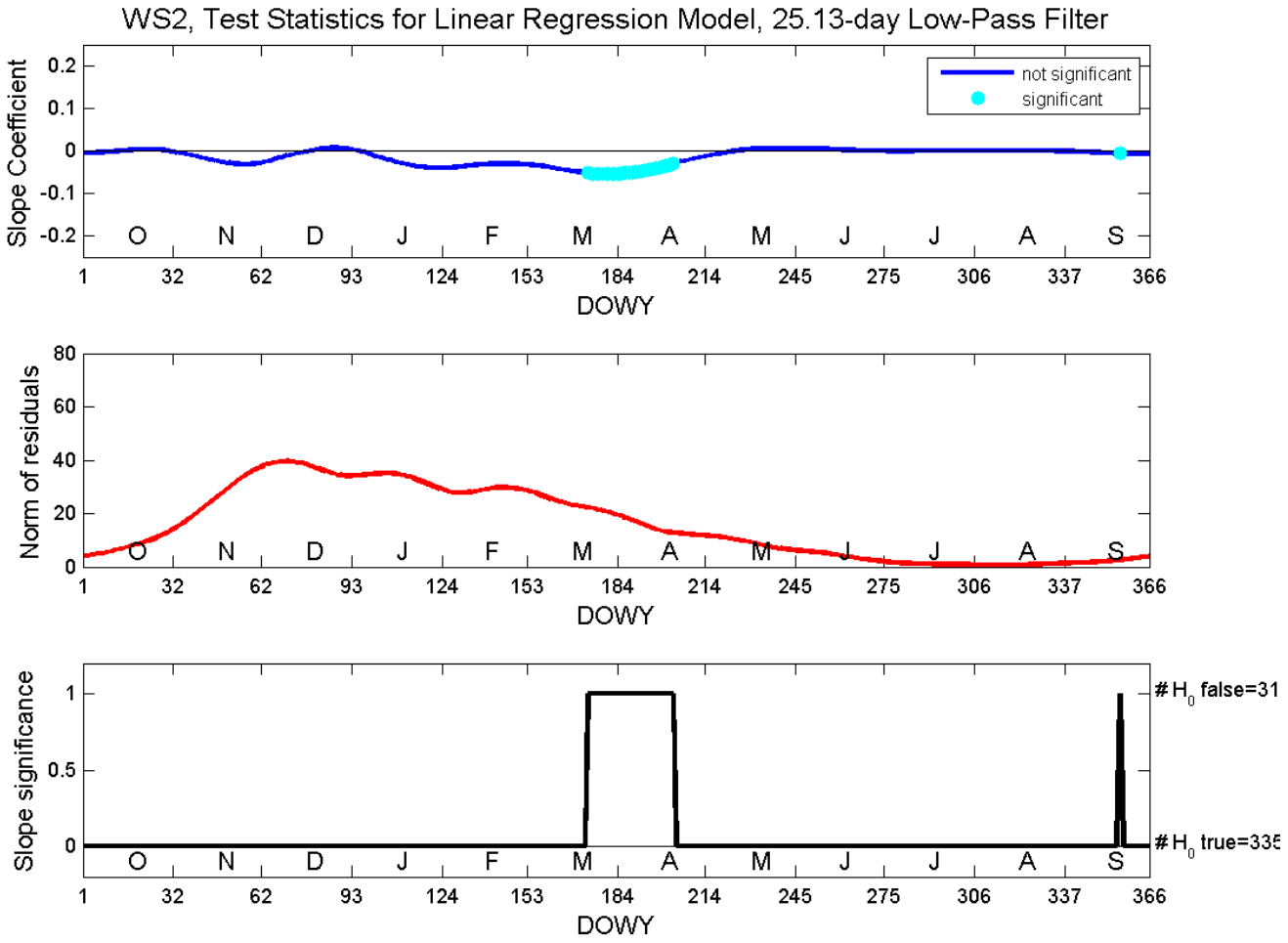

Figure F10. Daily linear regression model for WS2 using a 25.13 day low-pass filter wavelet.

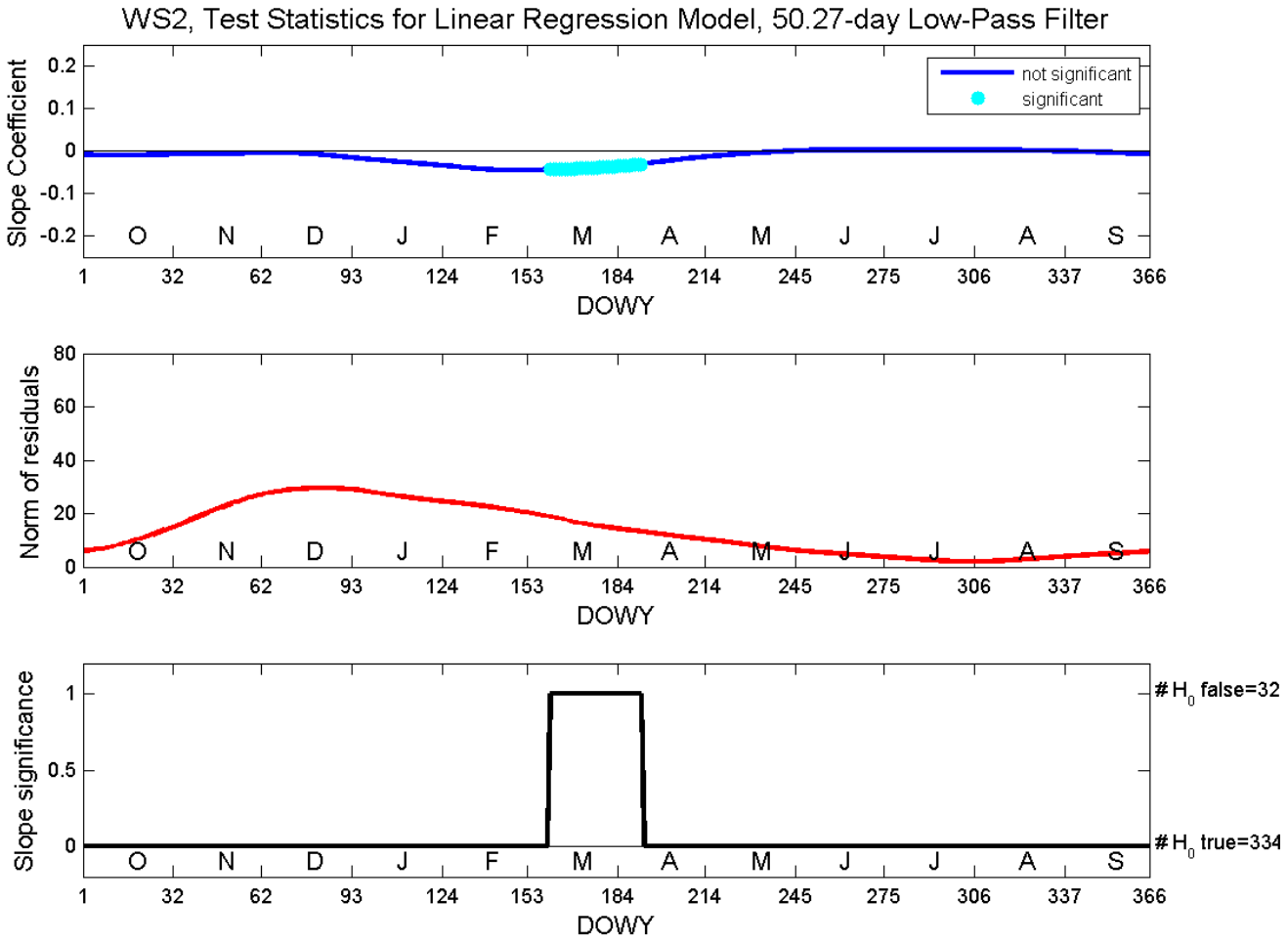

Figure F11. Daily linear regression model for WS2 using a 50.27 day low-pass filter wavelet.

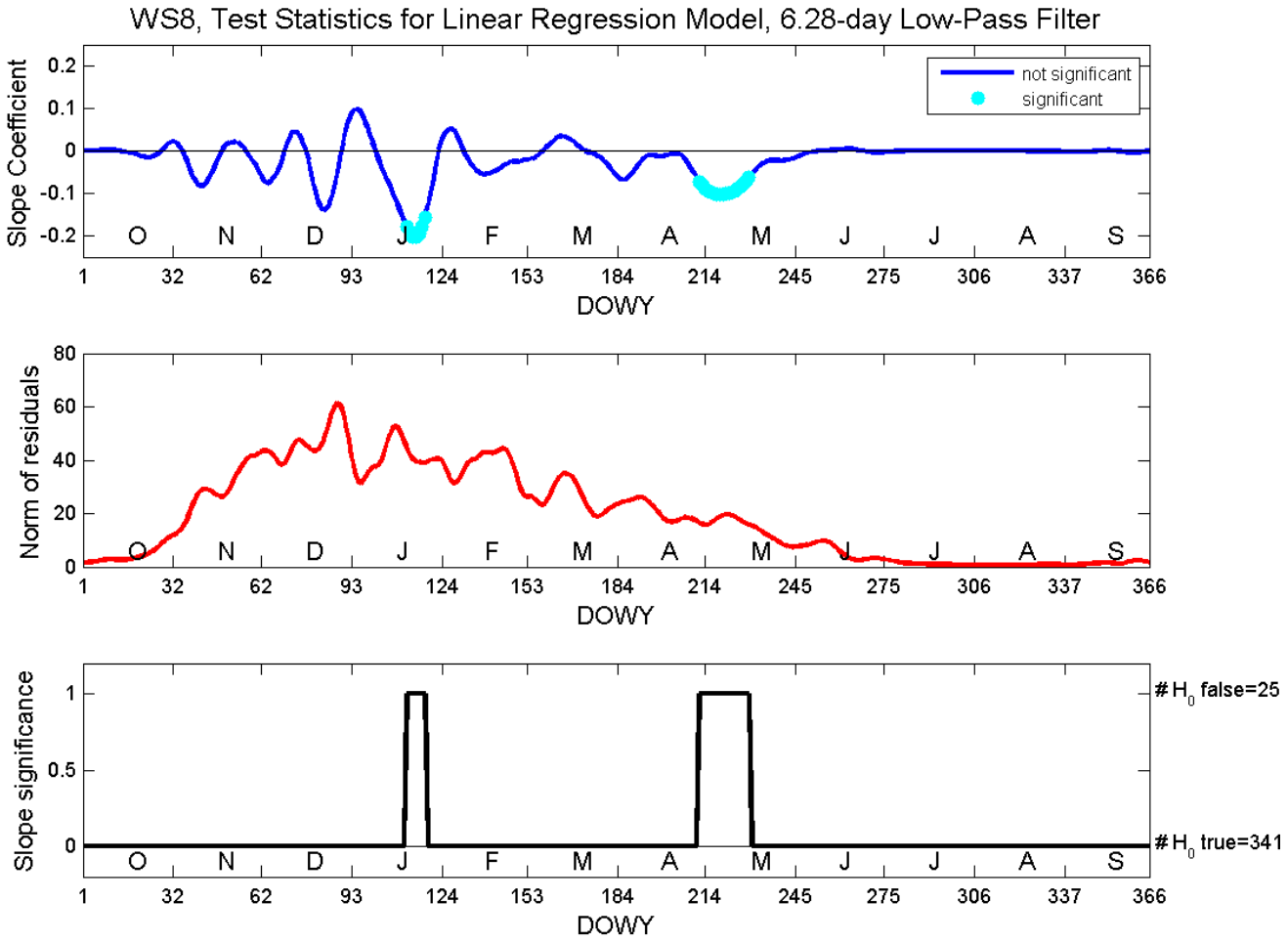

Figure F12. Daily linear regression model for WS8 using a 6.28 day low-pass filter wavelet.

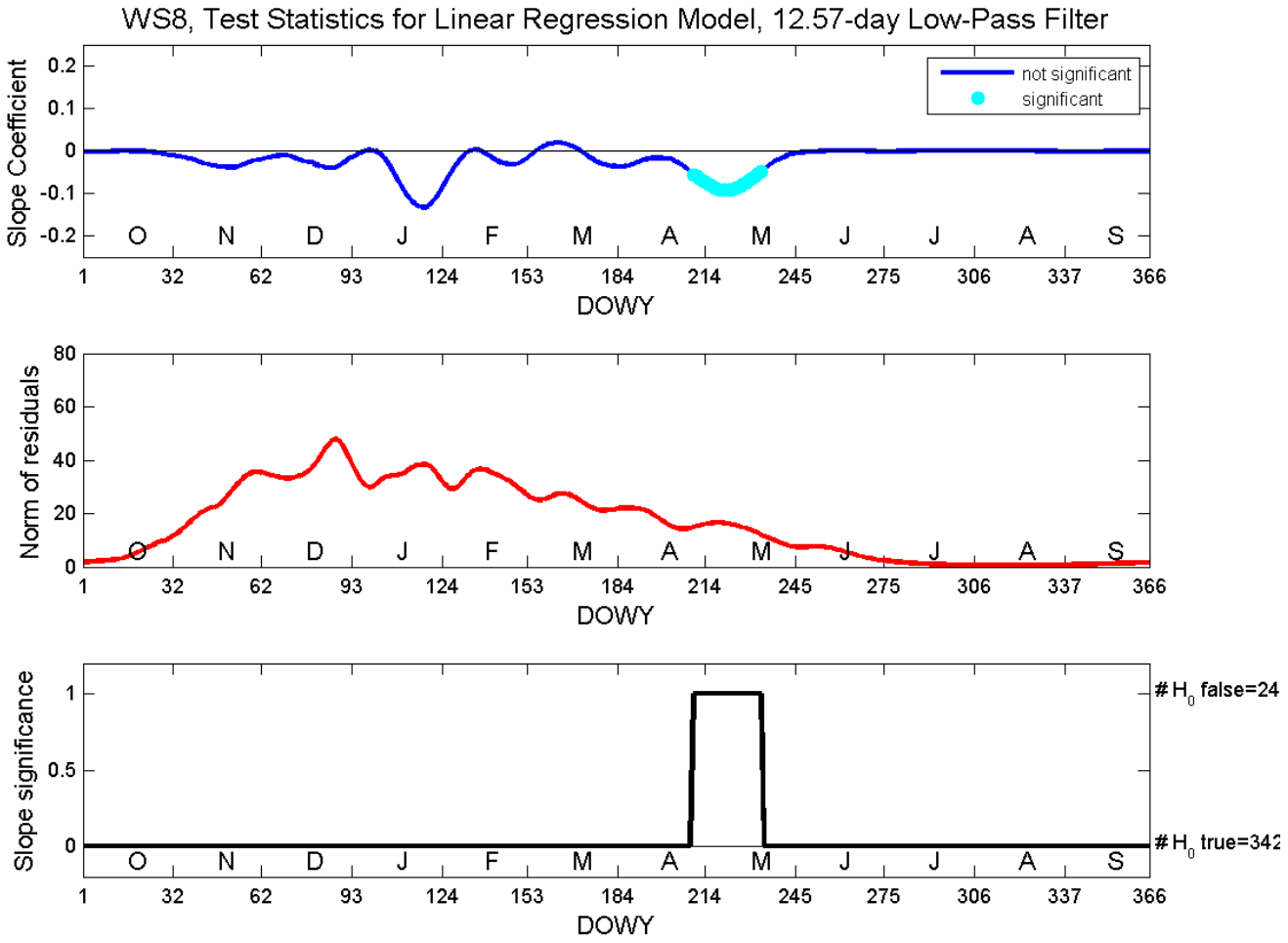

Figure F13. Daily linear regression model for WS8 using a 12.57 day low-pass filter wavelet.

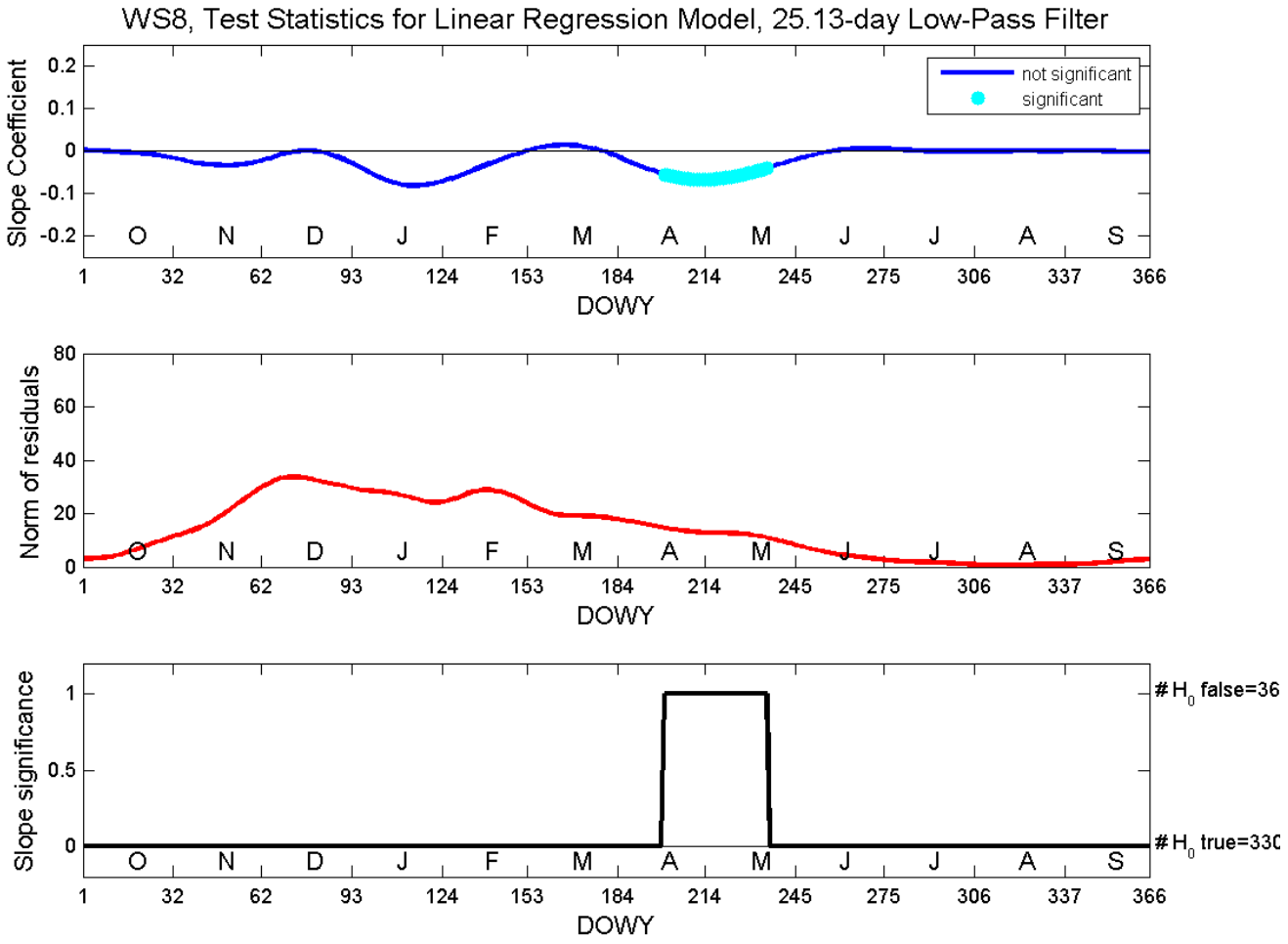

Figure F14. Daily linear regression model for WS8 using a 25.13 day low-pass filter wavelet.

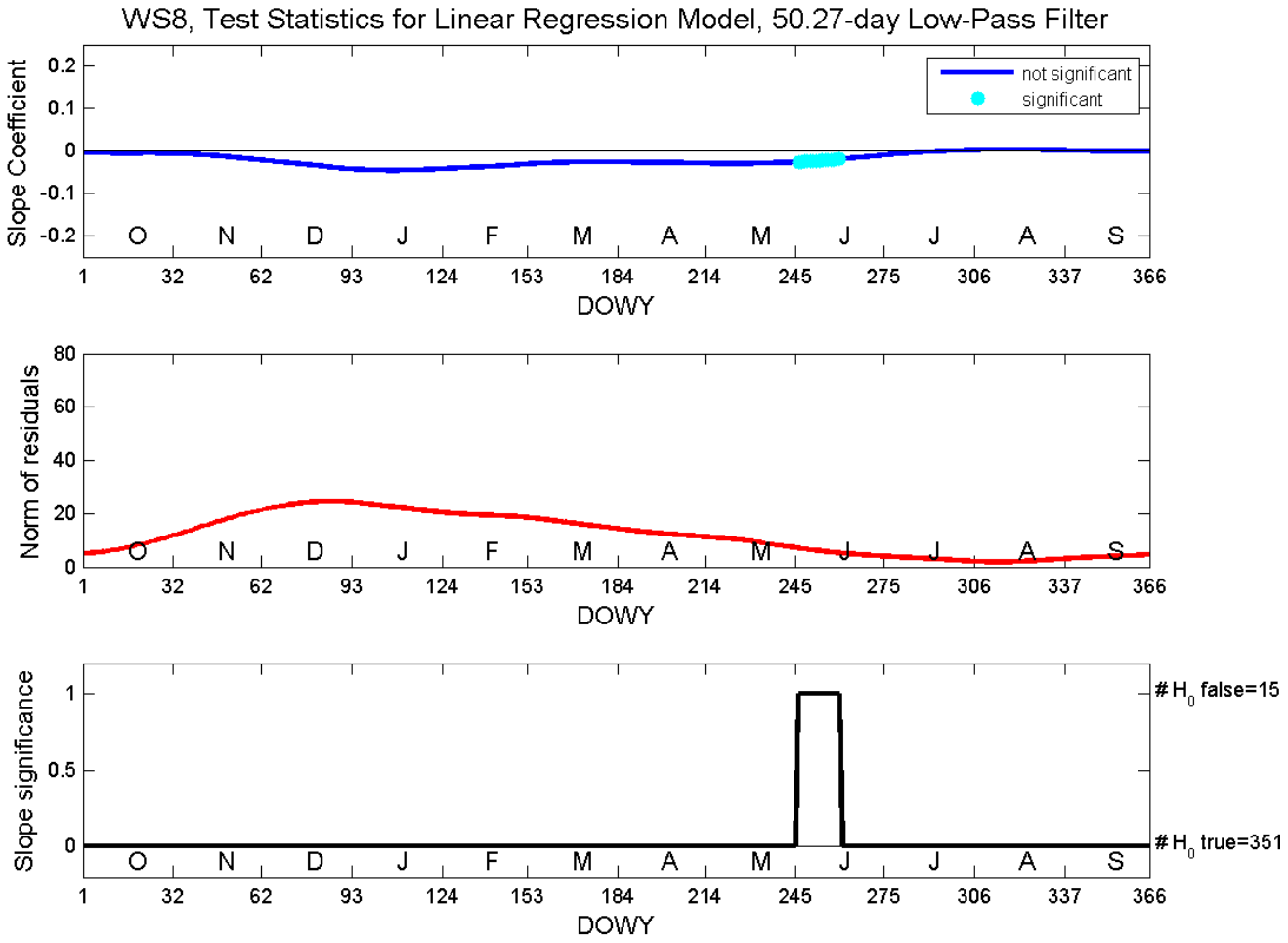

Figure F15. Daily linear regression model for WS8 using a 50.27 day low-pass filter wavelet.

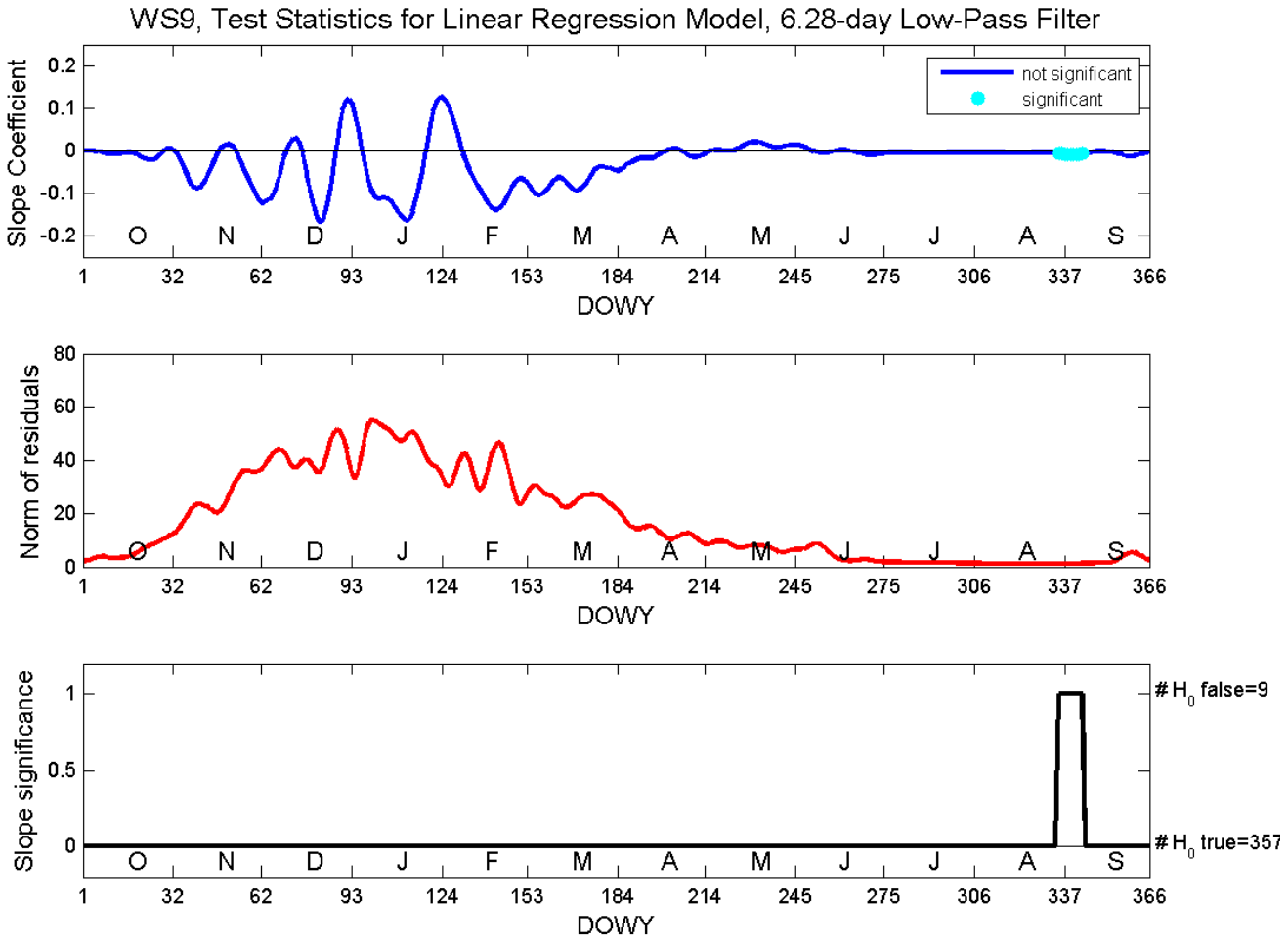

Figure F16. Daily linear regression model for WS9 using a 6.28 day low-pass filter wavelet.

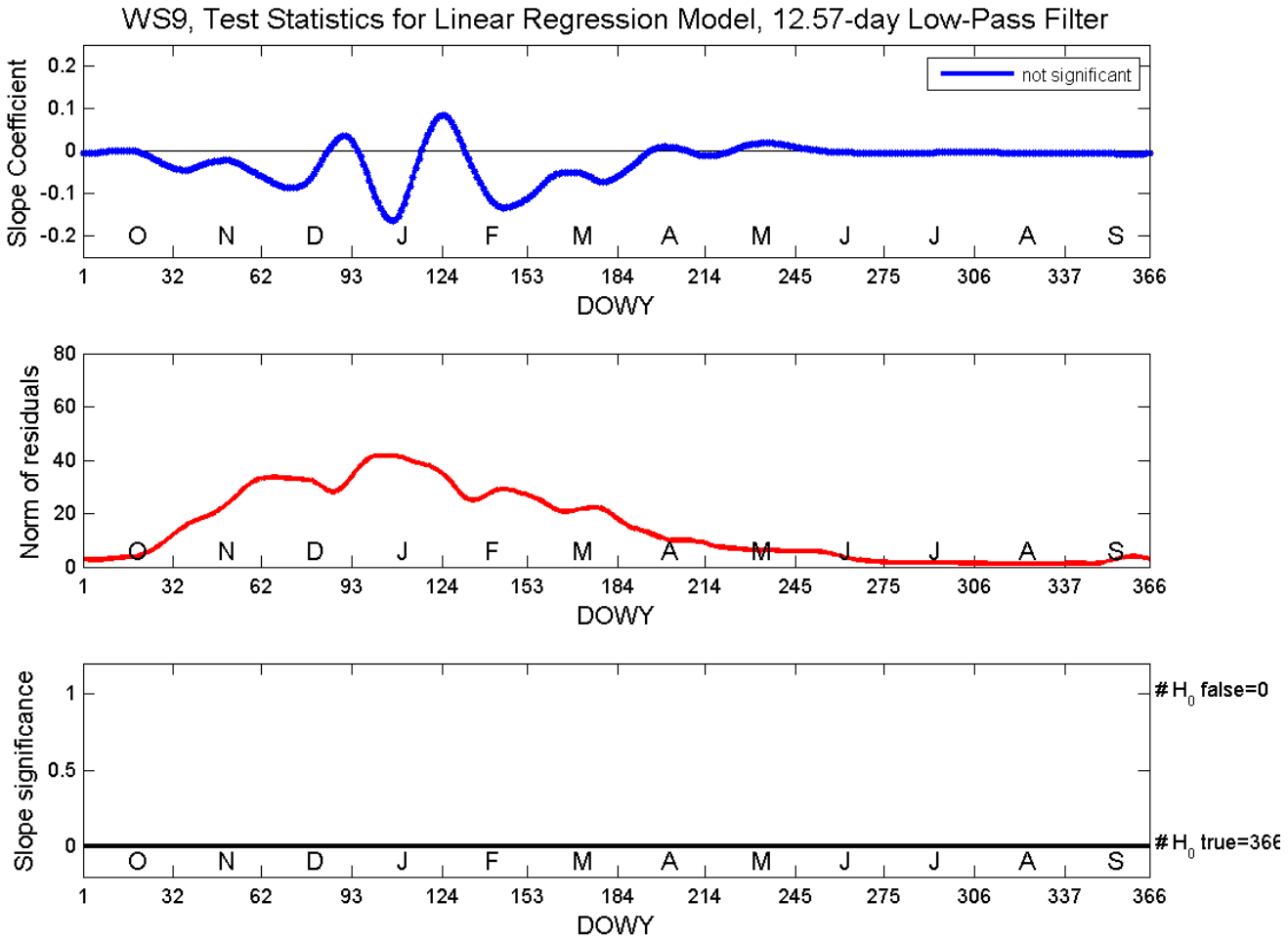

Figure F17. Daily linear regression model for WS9 using a 12.57 day low-pass filter wavelet.

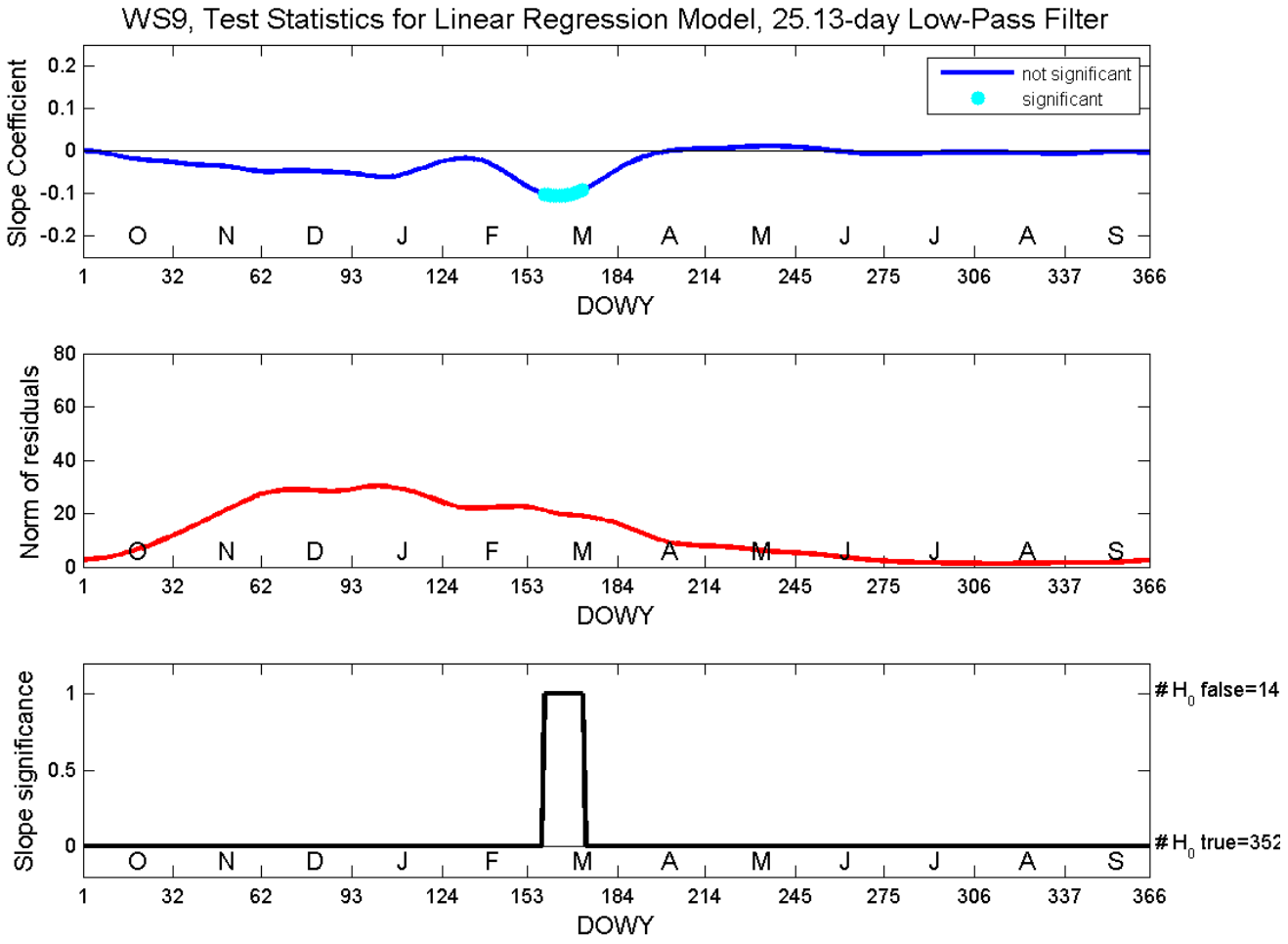

Figure F18. Daily linear regression model for WS9 using a 25.13 day low-pass filter wavelet.

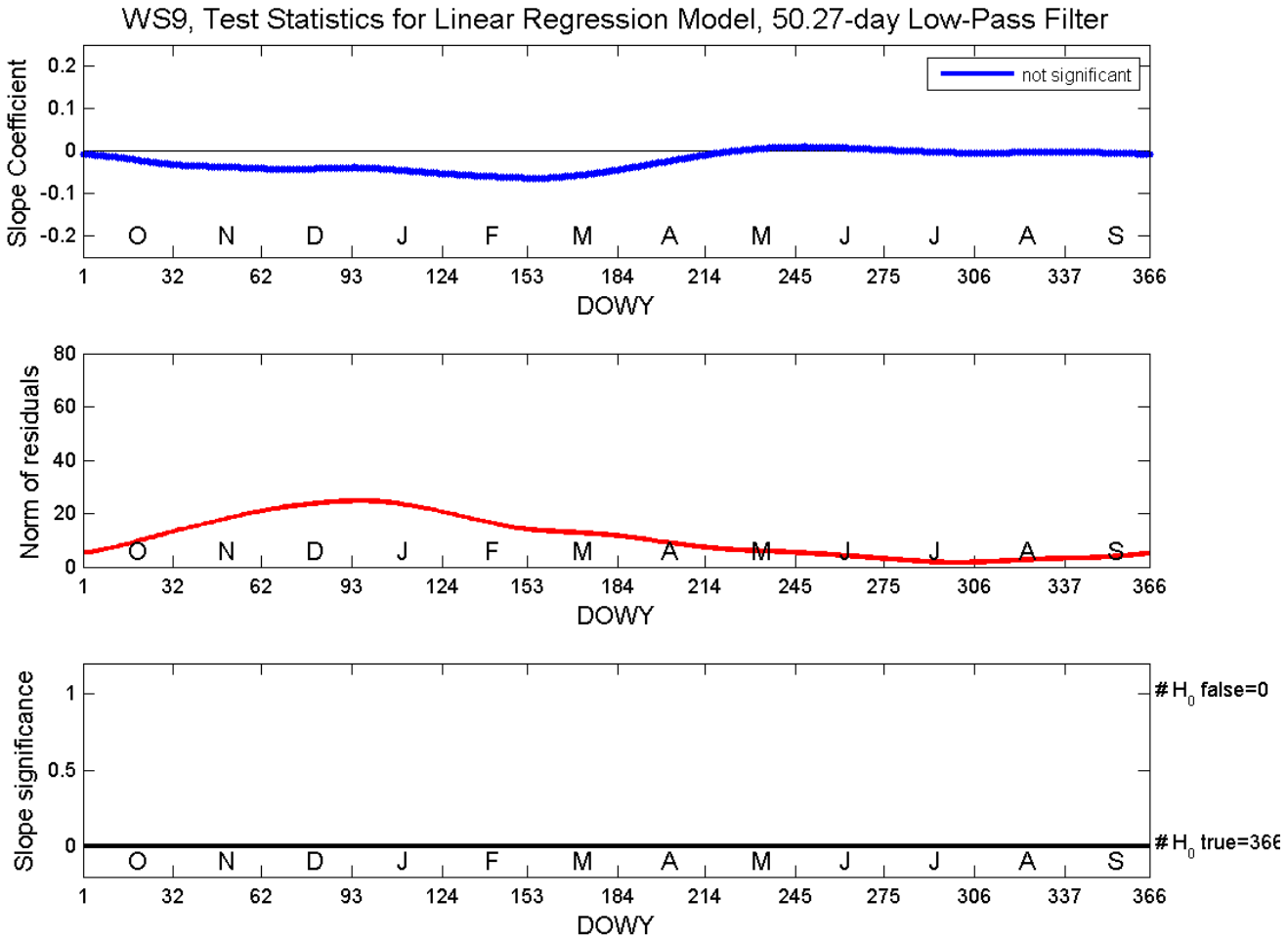

Figure F19. Daily linear regression model for WS9 using a 50.27 day low-pass filter wavelet.

Table F4. Summary table significant trends in WS2 daily discharge using low-pass filter wavelets.

WS2 Significant (p<0.05) Slope Coefficients for Daily Regressions using Low-Pass Filters									
6.28 day low-pass filtered			**12.57 day low-pass filtered**			**25.13 day low-pass filtered**			**50.27 day low-pass filtered**	
DOWY	Slope Coefficient		DOWY	Slope Coefficient		DOWY	Slope Coefficient		DOWY	Slope Coefficient
11-Oct	-0.016		13-Oct	-0.011		22-Mar	-0.052		9-Mar	-0.044
12-Oct	-0.017		14-Oct	-0.011		23-Mar	-0.053		10-Mar	-0.044
13-Oct	-0.017		15-Oct	-0.012		24-Mar	-0.053		11-Mar	-0.044
14-Oct	-0.016		16-Oct	-0.012		25-Mar	-0.054		12-Mar	-0.043
15-Oct	-0.014		17-Oct	-0.013		26-Mar	-0.054		13-Mar	-0.043
20-Mar	-0.075		18-Oct	-0.013		27-Mar	-0.054		14-Mar	-0.043
21-Mar	-0.081		19-Oct	-0.013		28-Mar	-0.054		15-Mar	-0.043
22-Mar	-0.085		20-Oct	-0.013		29-Mar	-0.054		16-Mar	-0.042
23-Mar	-0.088		21-Oct	-0.012		30-Mar	-0.054		17-Mar	-0.042
24-Mar	-0.089		22-Oct	-0.012		31-Mar	-0.054		18-Mar	-0.042
25-Mar	-0.090		21-Mar	-0.067		1-Apr	-0.053		19-Mar	-0.042
26-Mar	-0.090		22-Mar	-0.071		2-Apr	-0.053		20-Mar	-0.041
27-Mar	-0.090		23-Mar	-0.076		3-Apr	-0.053		21-Mar	-0.041
28-Mar	-0.090		24-Mar	-0.080		4-Apr	-0.052		22-Mar	-0.040
29-Mar	-0.089		25-Mar	-0.084		5-Apr	-0.051		23-Mar	-0.040
30-Mar	-0.088		26-Mar	-0.088		6-Apr	-0.051		24-Mar	-0.040
31-Mar	-0.087		27-Mar	-0.090		7-Apr	-0.050		25-Mar	-0.039
1-Apr	-0.086		28-Mar	-0.091		8-Apr	-0.049		26-Mar	-0.039
2-Apr	-0.084		29-Mar	-0.092		9-Apr	-0.048		27-Mar	-0.039
3-Apr	-0.080		30-Mar	-0.092		10-Apr	-0.046		28-Mar	-0.038
4-Apr	-0.074		31-Mar	-0.091		11-Apr	-0.045		29-Mar	-0.038
5-Apr	-0.067		1-Apr	-0.088		12-Apr	-0.044		30-Mar	-0.037
6-Apr	-0.060		2-Apr	-0.085		13-Apr	-0.042		31-Mar	-0.037
7-Apr	-0.052		3-Apr	-0.081		14-Apr	-0.041		1-Apr	-0.036
8-Apr	-0.045		4-Apr	-0.076		15-Apr	-0.039		2-Apr	-0.036
			5-Apr	-0.070		16-Apr	-0.038		3-Apr	-0.035
			6-Apr	-0.064		17-Apr	-0.036		4-Apr	-0.035
			7-Apr	-0.057		18-Apr	-0.034		5-Apr	-0.034
			8-Apr	-0.049		19-Apr	-0.033		6-Apr	-0.033
			9-Apr	-0.042		20-Apr	-0.031		7-Apr	-0.033
						20-Sep	-0.006		8-Apr	-0.032
									9-Apr	-0.031

Table F5. Summary table significant trends in WS8 daily discharge using low-pass filter wavelets.

WS8 Significant (p<0.05) Slope Coefficients for Daily Regressions using Low-Pass Filters									
6.28 day low-pass filtered			**12.57 day low-pass filtered**			**25.13 day low-pass filtered**			**50.27 day low-pass filtered**	
DOWY	Slope Coefficient		DOWY	Slope Coefficient		DOWY	Slope Coefficient		DOWY	Slope Coefficient
20-Jan	-0.179		27-Apr	-0.055		17-Apr	-0.056		2-Jun	-0.026
21-Jan	-0.193		28-Apr	-0.060		18-Apr	-0.057		3-Jun	-0.026
22-Jan	-0.202		29-Apr	-0.065		19-Apr	-0.059		4-Jun	-0.025
23-Jan	-0.203		30-Apr	-0.070		20-Apr	-0.061		5-Jun	-0.025
24-Jan	-0.196		1-May	-0.074		21-Apr	-0.062		6-Jun	-0.024
25-Jan	-0.179		2-May	-0.078		22-Apr	-0.063		7-Jun	-0.024
26-Jan	-0.157		3-May	-0.082		23-Apr	-0.064		8-Jun	-0.024
29-Apr	-0.073		4-May	-0.086		24-Apr	-0.065		9-Jun	-0.023
30-Apr	-0.082		5-May	-0.089		25-Apr	-0.066		10-Jun	-0.023
1-May	-0.090		6-May	-0.091		26-Apr	-0.066		11-Jun	-0.022
2-May	-0.094		7-May	-0.092		27-Apr	-0.067		12-Jun	-0.022
3-May	-0.097		8-May	-0.092		28-Apr	-0.067		13-Jun	-0.021
4-May	-0.100		9-May	-0.092		29-Apr	-0.067		14-Jun	-0.021
5-May	-0.102		10-May	-0.091		30-Apr	-0.068		15-Jun	-0.020
6-May	-0.103		11-May	-0.089		1-May	-0.068		16-Jun	-0.019
7-May	-0.103		12-May	-0.086		2-May	-0.067			
8-May	-0.101		13-May	-0.083		3-May	-0.067			
9-May	-0.099		14-May	-0.079		4-May	-0.066			
10-May	-0.097		15-May	-0.075		5-May	-0.066			
11-May	-0.095		16-May	-0.070		6-May	-0.065			
12-May	-0.090		17-May	-0.066		7-May	-0.064			
13-May	-0.084		18-May	-0.060		8-May	-0.063			
14-May	-0.077		19-May	-0.054		9-May	-0.062			
15-May	-0.070		20-May	-0.049		10-May	-0.061			
16-May	-0.062					11-May	-0.060			
						12-May	-0.059			
						13-May	-0.058			
						14-May	-0.056			
						15-May	-0.054			
						16-May	-0.053			
						17-May	-0.051			
						18-May	-0.049			
						19-May	-0.047			
						20-May	-0.045			
						21-May	-0.043			
						22-May	-0.041			

Table F6. Summary table significant trends in WS9 daily discharge using low-pass filter wavelets.

WS9 Significant (p<0.05) Slope Coefficients for Daily Regressions using Low-Pass Filters				
6.28 day low-pass filtered			**25.13 day low-pass filtered**	
DOWY	Slope Coefficient		DOWY	Slope Coefficient
30-Aug	-0.005		7-Mar	-0.101
31-Aug	-0.006		8-Mar	-0.103
1-Sep	-0.007		9-Mar	-0.104
2-Sep	-0.007		10-Mar	-0.105
3-Sep	-0.008		11-Mar	-0.105
4-Sep	-0.008		12-Mar	-0.105
5-Sep	-0.008		13-Mar	-0.105
6-Sep	-0.007		14-Mar	-0.105
7-Sep	-0.006		15-Mar	-0.103
			16-Mar	-0.102
			17-Mar	-0.100
			18-Mar	-0.098
			19-Mar	-0.095
			20-Mar	-0.092

4 Sample wavelet analysis program

```
%% LTER: WS2 record analysis
% Christoph Thomas, COAS, OSU
% Edited by Kathleen Moore, GEO, OSU

%% Set paths and variables

path.home   =   'C:/Users/Kathleen/Documents/School/LTER/WS2/';
ftsz        =   10;
ytick_vect  =   [1 32 62 93 124 153 184 214 245 275 306 337 366];
month_vect  =   ['O'; 'N'; 'D'; 'J'; 'F'; 'M'; 'A'; 'M'; 'J'; 'J'; 'A'; 'S'];
site_id     =   'WS2';
years_lim   =   [1953 2007];
date_today  =   datestr(fix(now),1);

%% Importing data
d.total =   csvread(fullfile(path.home,'terraformat','WS02.csv'),3,0);

% Create Serial datetime
dt.serial      =   terra_dt(d.total(:,1:7));

% Create DOY and year
doy     =   date2doy(d.total(:,1),d.total(:,2),d.total(:,3));

% Parse into matric with 1st line years, 1st col DOY, each year has 366 days
d.total_new   =   NaN(367,length([min(d.total(:,1)):1:max(d.total(:,1))]));
d.total_new(1,:)  =   [NaN min(d.total(:,1))+1:1:max(d.total(:,1))];
cc          =   2;
% Determine all leap year in the range
years       =   [min(d.total(:,1)):1:max(d.total(:,1))];
year_leap   =   years(find(eomday([min(d.total(:,1)):1:max(d.total(:,1))],2) == 29));

for ii = years(2):1:years(end)  % Exclude 1st calendar year due to WY definition
   index   =   find((dt.serial >= datenum([ii-1 10 1 0 0 0])) & (dt.serial < datenum([ii 10 1
0 0 0])));
   d.total_new(1,cc) =   ii;
   if isempty(find(ii == year_leap)) % Non-leap year
      d.total_new(2: 151 + 1,cc)    =   d.total(index(1:151),8);  % Period Oct 01 - Feb 28
      d.total_new(154:end,cc)       =   d.total(index(152:end),8);% Period Mar 01 - Sep 30

   else
      d.total_new(2:end,cc)         =   d.total(index,8);
   end
   cc  = cc + 1;
```

```
end
cc = 2;
for ii = 275:1:366
   d.total_new(cc,1) =   ii;
   cc            =   cc + 1;
end
for ii = 1:1:274
   d.total_new(cc,1) =   ii;
   cc            =   cc + 1;
end

% Rename fields
d.total_orig  =   d.total;
d.total       =   d.total_new;


%% Compute mean for period 1953-2007 and fill gaps with daily ensemble avgs
d.total_climavg   =   [];
i.curr  =   find(d.total(1,:) >= 1953 & d.total(1,:) <= 2007);
for ii = 2 : 1 : size(d.total,1)
   d.total_climavg(ii-1,1) =   nanmean(d.total(ii,i.curr));
   d.total_climstd(ii-1,1) =   nanstd(d.total(ii,i.curr));
   d.total_climmed(ii-1,1) =   nanmedian(d.total(ii,i.curr));
end

for ii = 2 : 1 : size(d.total,1)
   for iii = 2 : 1 : size(d.total,2)
      if isnan(d.total(ii,iii))
         d.total(ii,iii)   =   d.total_climavg(ii-1,1);
      end
   end
end

%% Substitute anomalies for daily values
d.total_anom = NaN(size(d.total));
for ii = 2 : 1 : size(d.total,1)
   d.total_anom(ii, i.curr) = (d.total(ii, i.curr)-d.total_climavg(ii-1,1));
   d.total(ii, i.curr) = d.total_anom(ii, i.curr);
end


%% Create numeric vect and reshaping matrices
dt.num  =   [1:1:55*366];
d.totalvec =   reshape(d.total(2:end,2:end),55*366,1);

%% Low-pass filtering the time series
```

```
for ii = 1 : 6
  [den.totalvec(ii,:),det.totalvec(ii,:)] = waldschrat_denoise(d.totalvec,ii,'bior5.5');
end

% Calculating the corresponding cut-off frequencies
Dc  =   (2.^([1:6])*(60*60*24)*pi/4)./(60*60*24);

%% Compute mean for period 1953-2007 for low-pass filtered time series
i.curr  =   find(d.total(1,2:end) >= 1953 & d.total(1,2:end) <= 2007);
iii     =   6;
den.total =   reshape(den.totalvec(iii,:),366,55);
for ii = 1 : 1 : 366
   den.total_climavg(ii,1) =   nanmean(den.total(ii,i.curr));
   den.total_climstd(ii,1) =   nanstd(den.total(ii,i.curr));
   den.total_climmed(ii,1) =   nanmedian(den.total(ii,i.curr));
end

%% Determine  anomalies

for ii = 1 : 1 : 55
   den.total_prime(:,ii) =   den.total(:,ii) - den.total_climavg;
end;

%% Calculate linear trends for each DOWY

for ii = 1 : 1 : 366
   index   =   find(~isnan(den.total_prime(ii,:)));
   x       =   d.total(1,2:end);
   [beta_total(ii,:),S.(genvarname(['total_',num2str(ii,'%i')]))] =
polyfit(x(index),den.total_prime(ii,index),1);
end

% Extract norm of residuals
for ii = 1 : 1 : 366
   normres.total(ii,1)   =   S.(genvarname(['total_',num2str(ii,'%i')])).normr;
end

% Test for slope significantly differen from zero
% H = 0 (null hypothesis, ie slope = 0)
% H = 1 (alternate hypothesism ie slope ~= 0)
% ANOVA, one factor (k=2,N=55, DF1 = 1, DF2 = 53); one-sided: F^{k-1}_{N-k}
F_tab   =   4.023017;
for ii = 1 : 1 : 366
   index   =   find(~isnan(den.total_prime(ii,:)));
   x       =   d.total(1,2:end);
```

```
    % Evaluate regression for Total Discharge
    y_reg   =   polyval(beta_total(ii,:),x(index));
    y_regmu =   mean(y_reg);
    y_obs   =   den.total_prime(ii,index);
    % Test if mean squared residuals between predicted values and mean prediction (y_reg
- y_regmu) is
    % different from mean squared residuals between predicted values and observations
    %regression
    mqa     =   sum((y_reg-y_regmu).^2)./1;
    %residual
    mqu     =   sum((y_reg-y_obs).^2)./53;
    if mqa/mqu > F_tab
        H.total(ii,1) = 1;
    else
        H.total(ii,1) = 0;
    end

end

%% Plot linear trends, norm residuals, and slope significance

h_f = figure;
subplot (3,1,1); box on;
x_vect  =   [1:366];
i.curr  =   find(H.total == 1);
h(1) = plot ([1:366],beta_total(:,1),'color','b','linewidth',2);
line ([1 366],[0 0],'linestyle','-','color','k');
h(2) = line
(x_vect(i.curr),beta_total(i.curr,1),'color','c','marker','.','markersize',20,'linestyle','none');
set (gca,'ylim',[-0.25 0.25],'xtick',ytick_vect,'fontsize',ftsz-2,'xlim',[1 366]);
for ii = 1 : 1 : 12
    text(mean(ytick_vect(ii:ii+1)),-0.20,month_vect(ii),'fontsize',ftsz);
end
xlabel ('DOWY','fontsize',ftsz);
ylabel ('Slope Coefficient','fontsize',ftsz);
title ([score2hyph(site_id),', Test Statistics for Linear Regression Model, 50.27-day Low-
Pass Filter'],'fontsize',ftsz+2);
h_l = legend(h,'not significant','significant','location','NE');
set (h_l,'fontsize',ftsz-3);
sig_tr_DOY = [x_vect(i.curr);beta_total(i.curr,1)'];
xlswrite(fullfile(path.home,'plots',[site_id,'_sig_tr_DOY_6']),[sig_tr_DOY]);

subplot (3,1,2); box on;
plot ([1:366],normres.total,'color','r','linewidth',2);
line ([1 366],[0 0],'linestyle','-','color','k');
set (gca,'ylim',[0 80],'xtick',ytick_vect,'fontsize',ftsz-2,'xlim',[1 366]);
```

```
for ii = 1 : 1 : 12
   text(mean(ytick_vect(ii:ii+1)),6,month_vect(ii),'fontsize',ftsz);
end
xlabel ('DOWY','fontsize',ftsz);
ylabel ('Norm of residuals','fontsize',ftsz);


subplot (3,1,3); box on;
plot ([1:366],H.total,'color','k','linewidth',2);
line ([1 366],[0 0],'linestyle','-','color','k');
set (gca,'ylim',[-0.2 1.2],'xtick',ytick_vect,'fontsize',ftsz-2,'xlim',[1 366]);
for ii = 1 : 1 : 12
   text(mean(ytick_vect(ii:ii+1)),-0.1,month_vect(ii),'fontsize',ftsz);
end
xlabel ('DOWY','fontsize',ftsz);
ylabel ('Slope significance','fontsize',ftsz);
text (368,0,['# H_0 true=',num2str(length(find(H.total==0)),'%i')],'fontsize',ftsz-2);
text (368,1,['# H_0 false=',num2str(length(find(H.total==1)),'%i')],'fontsize',ftsz-2);

saveas (h_f,fullfile(path.home,'plots',[site_id,'_slope_stat_6']),'png');
```

Appendix G: Runoff Ratio

1 Runoff ratio

Runoff ratios calculated both with PRISM and CS2MET data, and both for the period corresponding to streamflow record and for the overlapping period of streamflow from 1969-2007, exhibit significant declines both during the spring for all three watersheds and on an annual basis for WS8 (Tables G1-G4).

The WS8 annual runoff ratio to PRISM exhibits a decline of -0.003 per year ($p<0.05$) for a net decline of 20.2% or 0.7mm/day over the 44 year period of streamflows. For the period of overlapping streamflows, the annual runoff ratio for WS8 to PRISM also exhibits a decline of -0.003 per year ($p<0.05$). The annual runoff ratio for WS8 to CS2MET exhibits similar declines. Over the 44 year period of streamflows, the annual runoff ratio for WS8 to CS2MET exhibits a decline of -0.003 per year ($p<0.01$) for a net decline of 21.9% or 0.77mm/day. For the period of overlapping streamflows, the annual runoff ratio for WS8 to CS2MET also exhibits a decline of -0.003 per year ($p<0.01$).

The WS2 spring runoff ratio to PRISM exhibits a decline of -0.003 per year ($p<0.05$) for a net decline of 25.4% or 1.13mm/day over the 55 year period of streamflows. For the period of overlapping streamflows, the spring runoff ratio for WS2 to PRISM exhibits a slightly steeper decline of -0.005 per year ($p<0.05$) for a net decline of 27.6% or 1.19mm/day over the 39 year period. The spring runoff ratio for WS2 to CS2MET exhibits similar declines. Over the 50 year period relating to CS2MET, the spring runoff ratio for WS2 exhibits a decline of -0.004 per year ($p<0.05$) for a net decline of 23.4% or 1.00mm/day. For the period of overlapping streamflows, the spring runoff ratio for WS2 to CS2MET also exhibits a slightly steeper decline of -0.005 per year ($p<0.05$).

The WS8 spring runoff ratio to PRISM exhibits a decline of -0.009 per year ($p<0.01$) for a net decline of 41.2% or 2.13mm/day over the 44 year period of streamflows. For the period of overlapping streamflows, the spring runoff ratio for WS8 to PRISM exhibits a slightly steeper decline of -0.010 per year ($p<0.01$) for a net decline of 43.7% or 2.32mm/day over the 39 year period. The spring runoff ratio for WS8 to CS2MET exhibits similar declines. Over the 44 year period of streamflows, the spring runoff ratio for WS8 exhibits a decline of -0.009 per year ($p<0.01$) for a net decline of 42.9% or 2.26mm/day. For the period of overlapping streamflows, the spring runoff ratio for WS8 to CS2MET also exhibits a slightly steeper decline of -0.010 per year ($p<0.01$).

The WS9 spring runoff ratio to PRISM exhibits a decline of -0.006 per year ($p<0.01$) for a net decline of 31.5% or 1.23mm/day over the 39 year period of streamflows. The spring runoff ratio for WS9 to CS2MET exhibits a similar decline of -0.005 per year ($p<0.01$) for a net decline of 28.8% or 1.10mm/day.

Figures G1-G10 show the runoff ratios (both calculated with PRISM and CS2MET precipitation) by season for the WS2, WS8, and WS9. Trend lines and equations are shown on the figures along with an R^2 goodness of fit estimate.

2 Discharge vs. precipitation: Two-period analysis

Figure G11 shows the relationship between annual discharge and precipitation for all three watersheds over two separate periods – the respective period of record prior to 1981 and the period of record from 2000-2007. Figure G12 shows the same analysis for spring discharge and precipitation. Trend lines and equations are shown on the figures along with an R^2 goodness of fit estimate. T-tests indicate that on an annual basis there has been no change in the relationship between discharge and precipitation between the two separate time periods for any

of the watersheds. However, the relationship between spring discharge and precipitation has changed significantly. On average between the two time periods, WS2 shows a 17.06% reduction ($p<0.05$) in discharge for a given amount of precipitation, WS8 shows a 33.02% reduction ($p<0.05$) in discharge for a given amount of precipitation, and WS9 shows a 25.76% reduction ($p<0.05$) in discharge for a given amount of precipitation.

Figure G1. Trends in annual runoff ratio (using PRISM precipitation) at (clockwise from bottom left) WS9, WS2, and WS8.

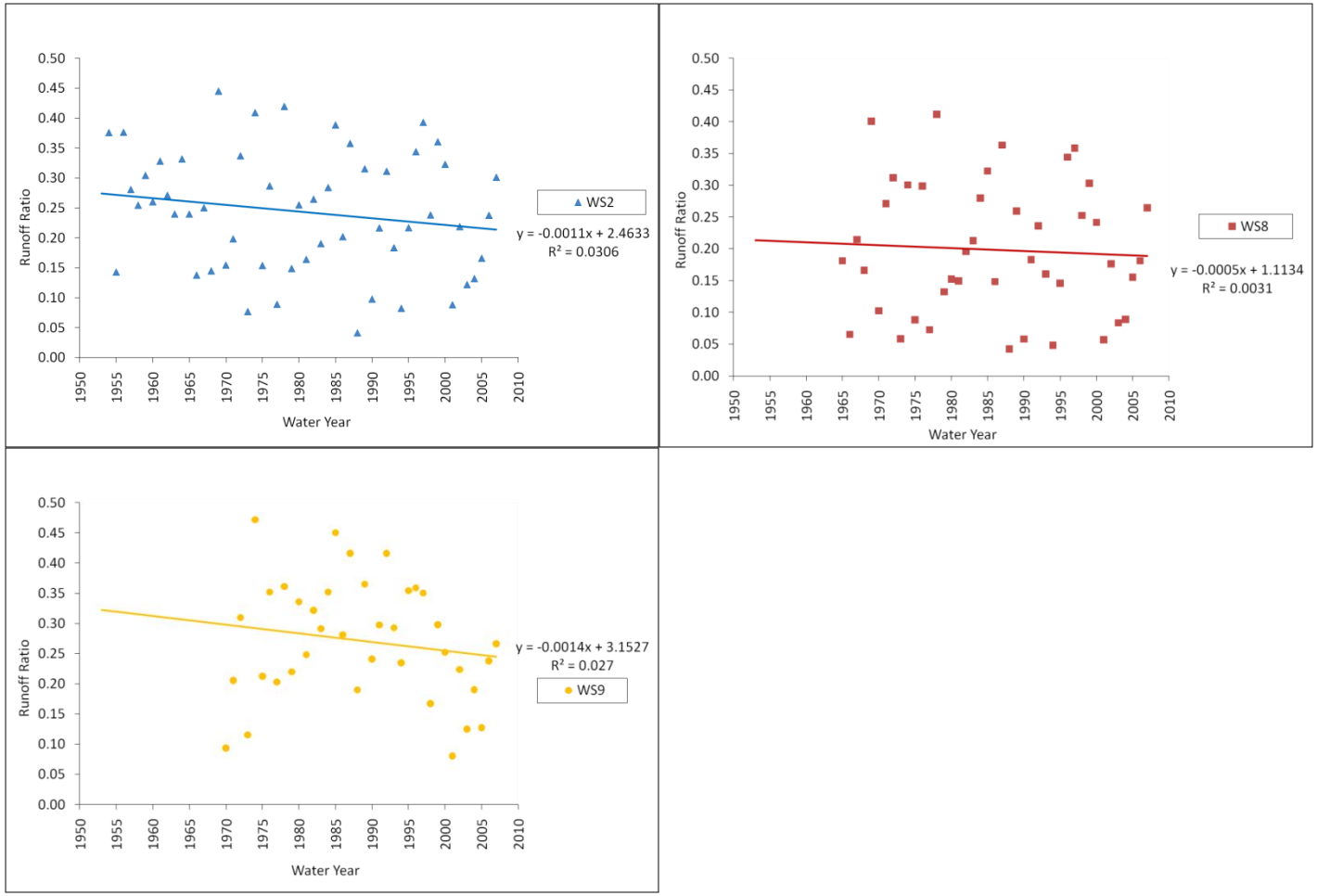

Figure G2. Trends in fall runoff ratio (using PRISM precipitation) at (clockwise from bottom left) WS9, WS2, and WS8.

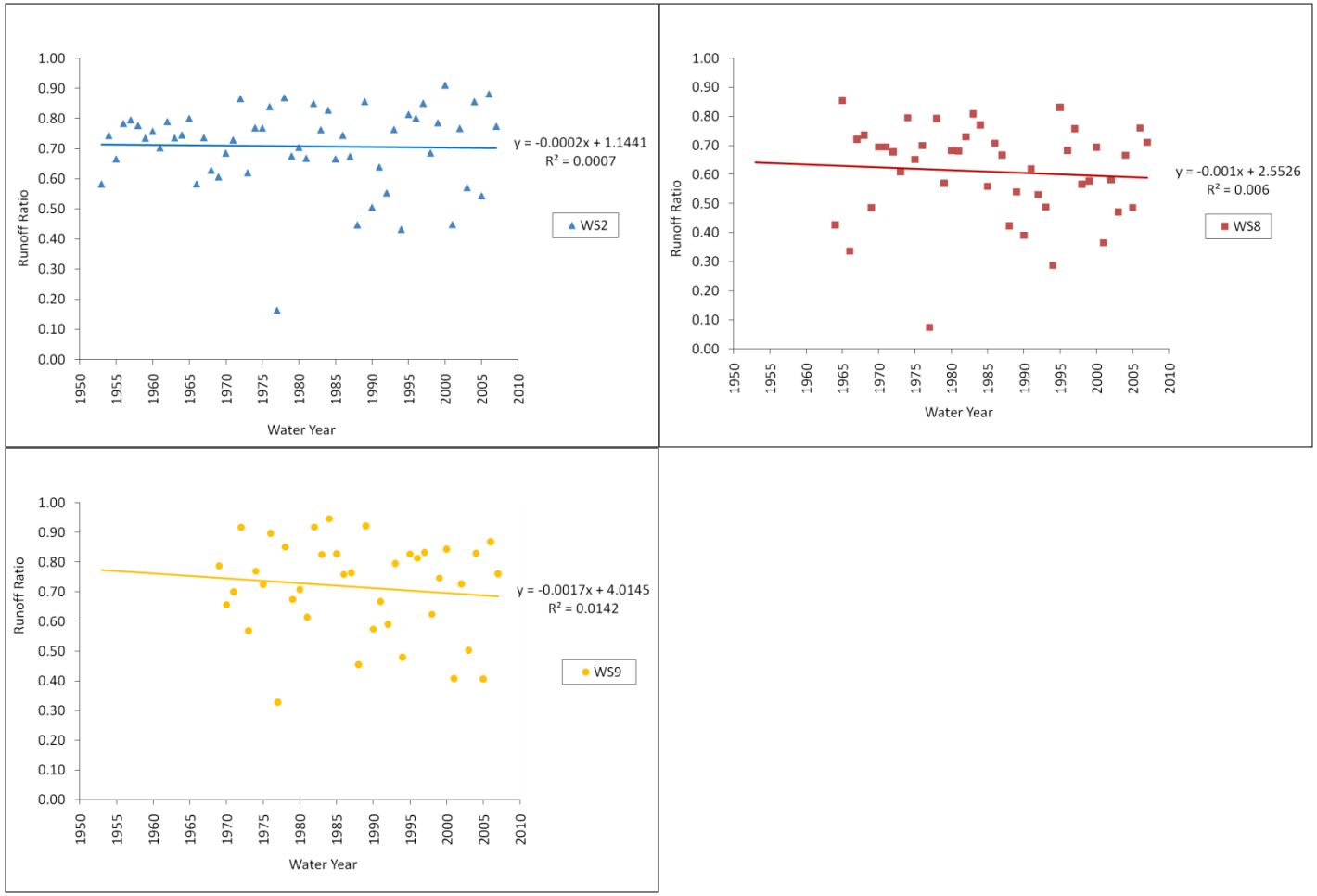

Figure G3. Trends in winter runoff ratio (using PRISM precipitation) at (clockwise from bottom left) WS9, WS2, and WS8.

Figure G4. Trends in spring runoff ratio (using PRISM precipitation) at (clockwise from bottom left) WS9, WS2, and WS8.

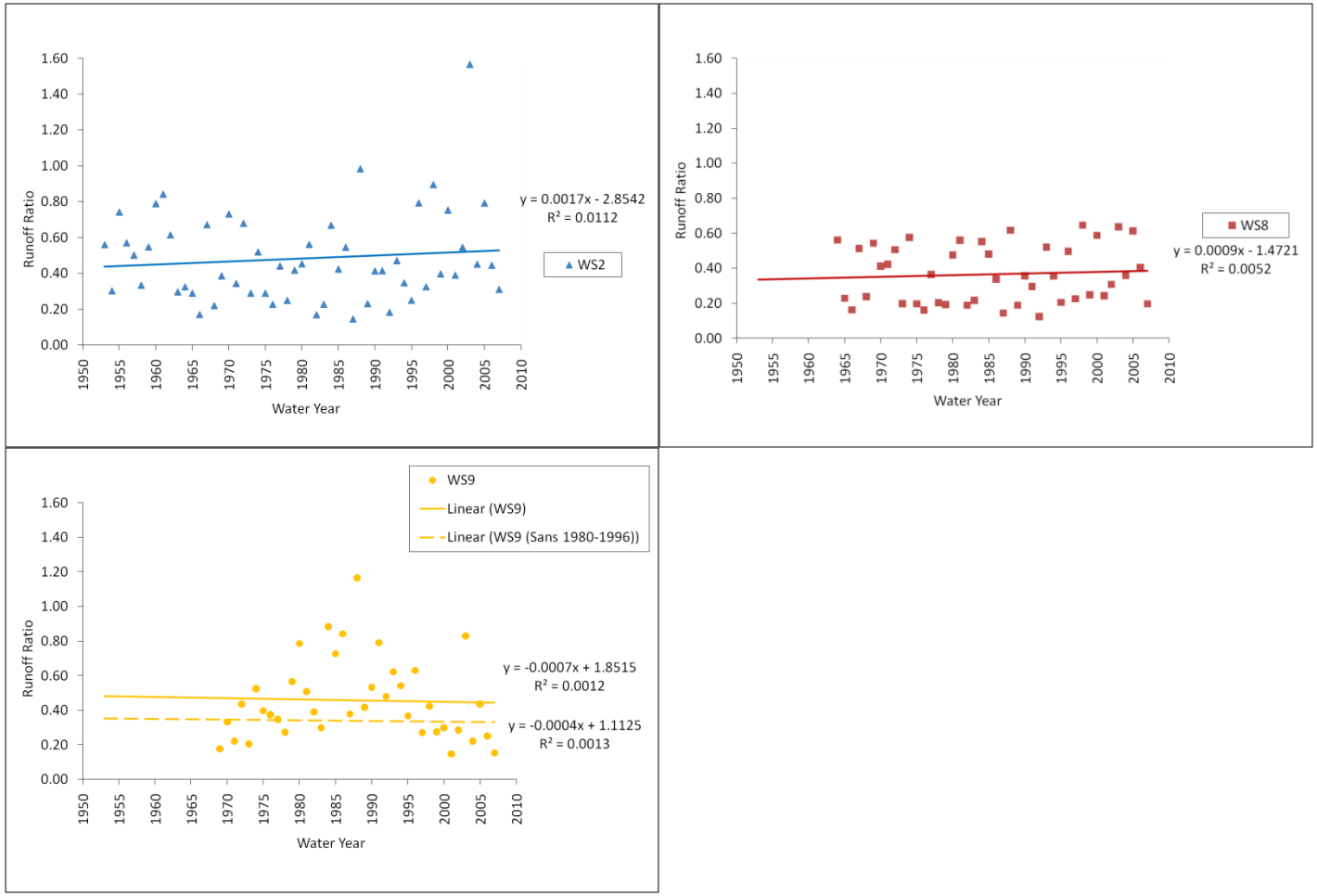

Figure G5. Trends in summer runoff ratio (using PRISM precipitation) at (clockwise from bottom left) WS9, WS2, and WS8.

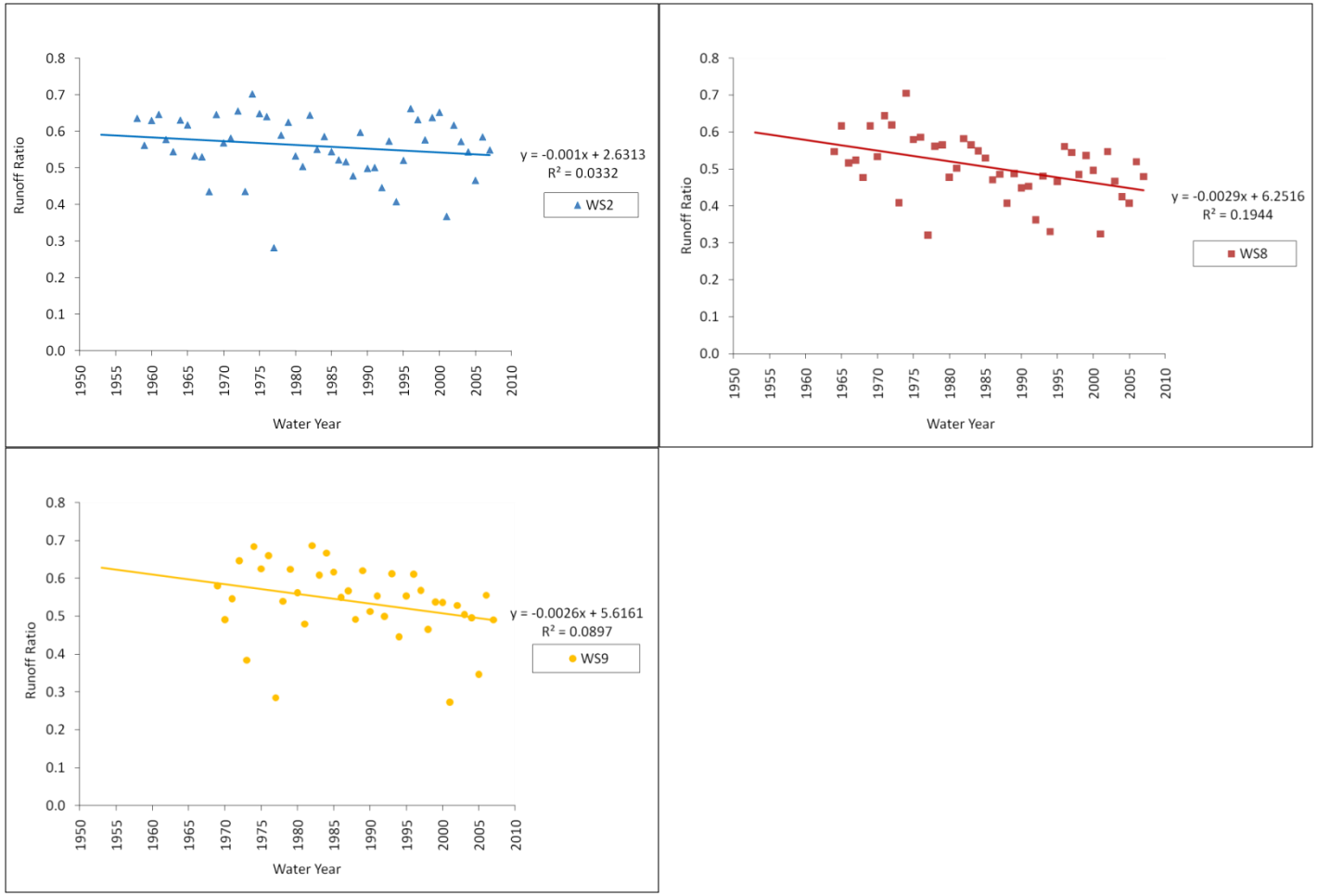

Figure G6. Trends in annual runoff ratio (using CS2MET precipitation) at (clockwise from bottom left) WS9, WS2, and WS8.

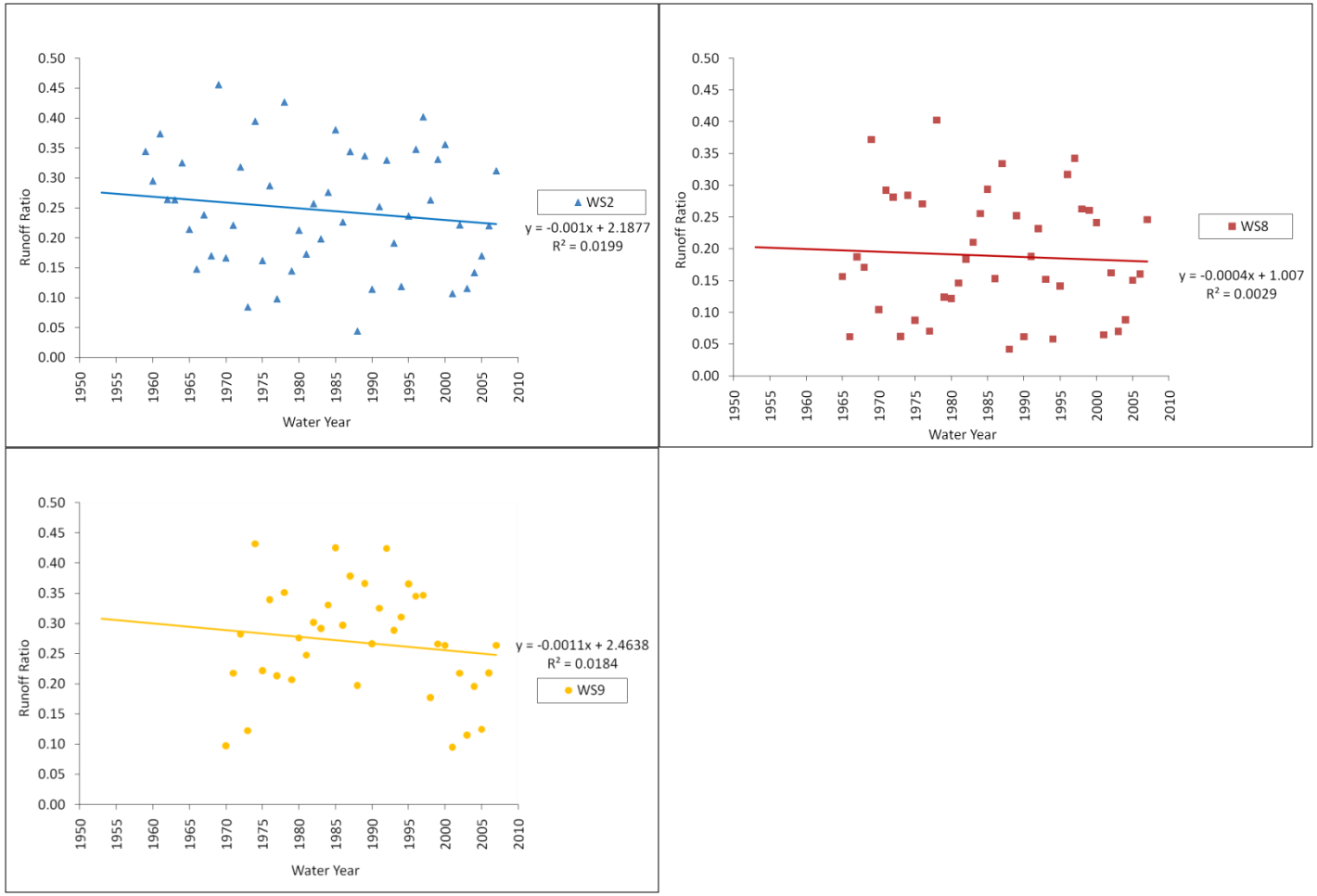

Figure G7. Trends in fall runoff ratio (using CS2MET precipitation) at (clockwise from bottom left) WS9, WS2, and WS8.

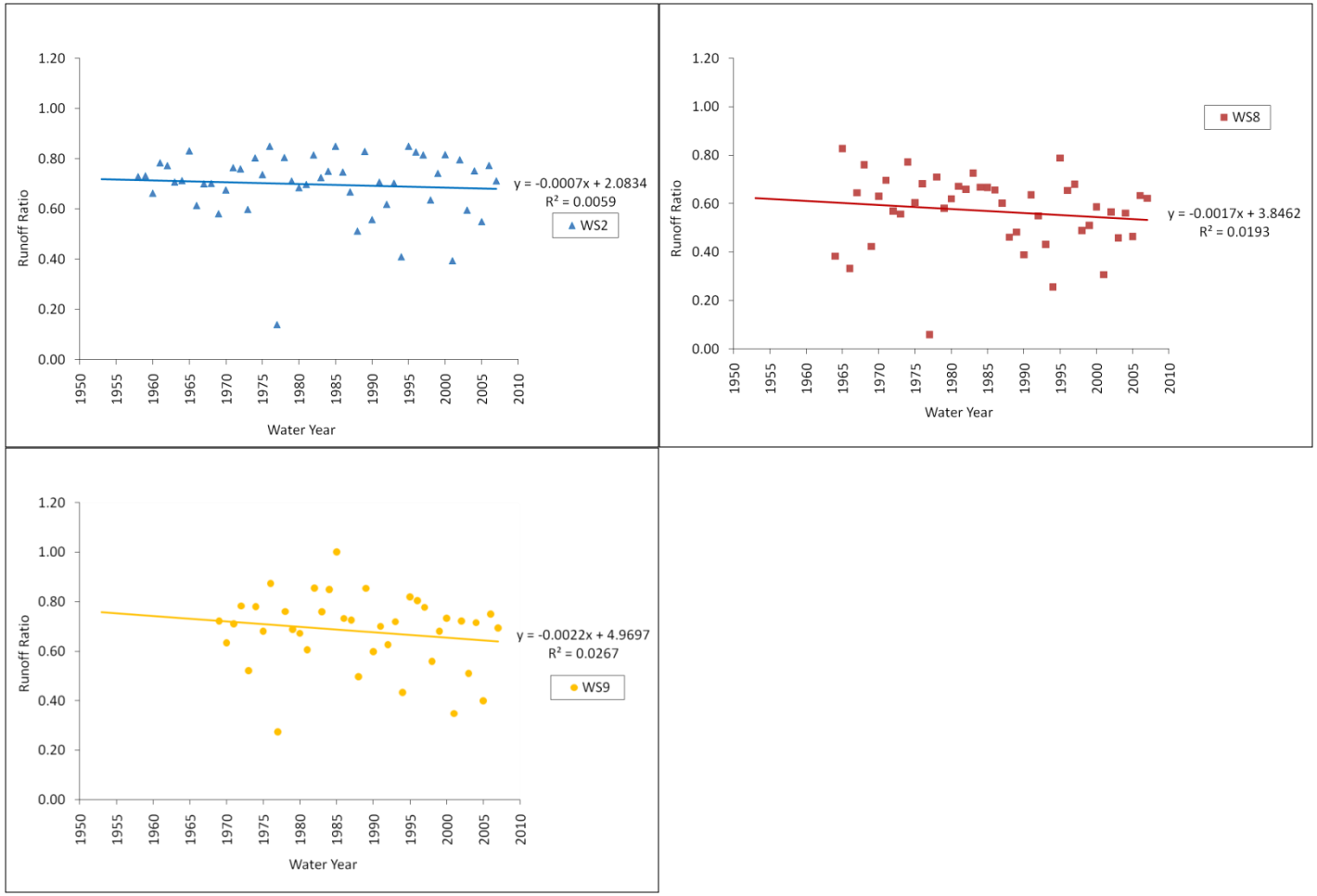

Figure G8. Trends in winter runoff ratio (using CS2MET precipitation) at (clockwise from bottom left) WS9, WS2, and WS8.

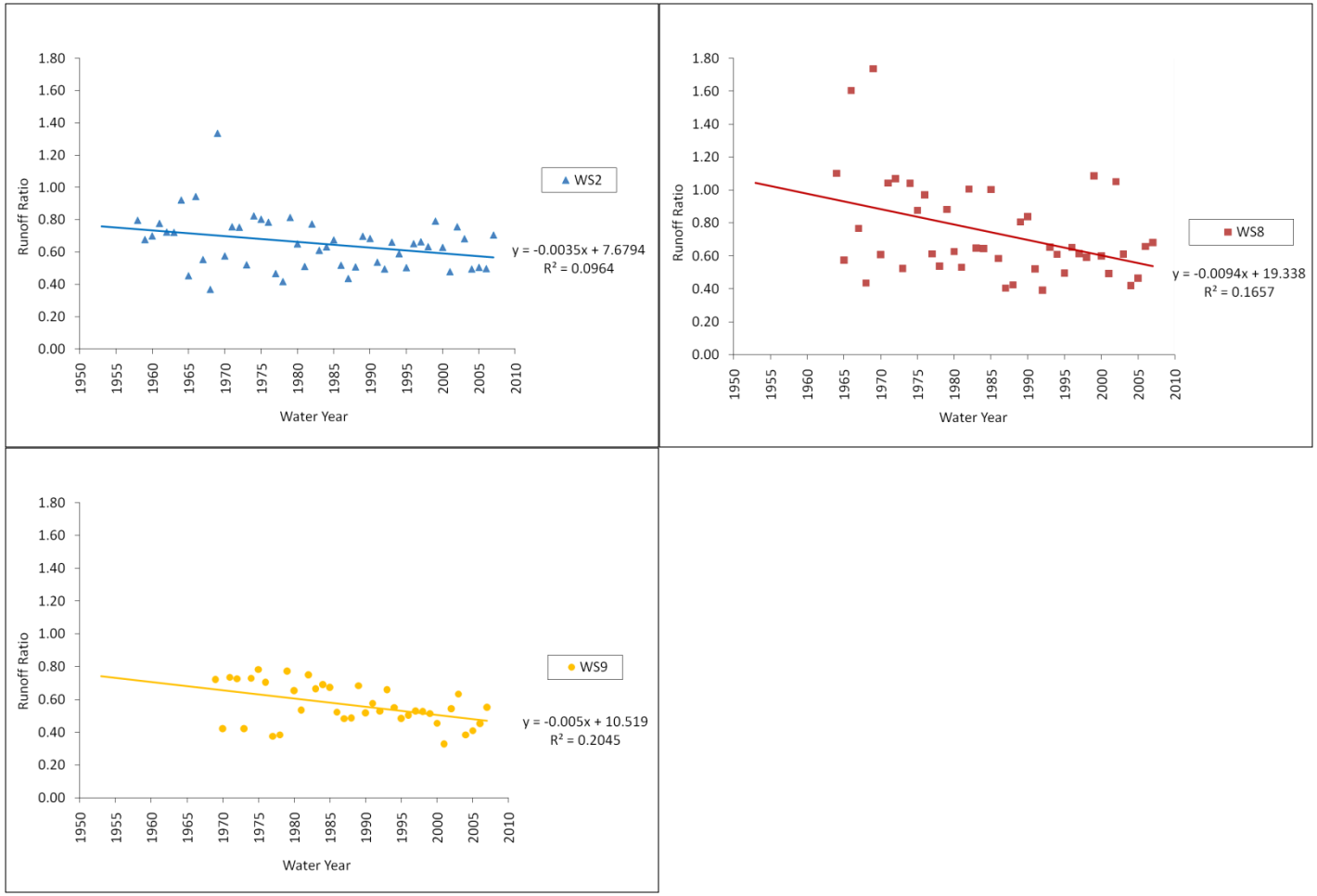

Figure G9. Trends in spring runoff ratio (using CS2MET precipitation) at (clockwise from bottom left) WS9, WS2, and WS8.

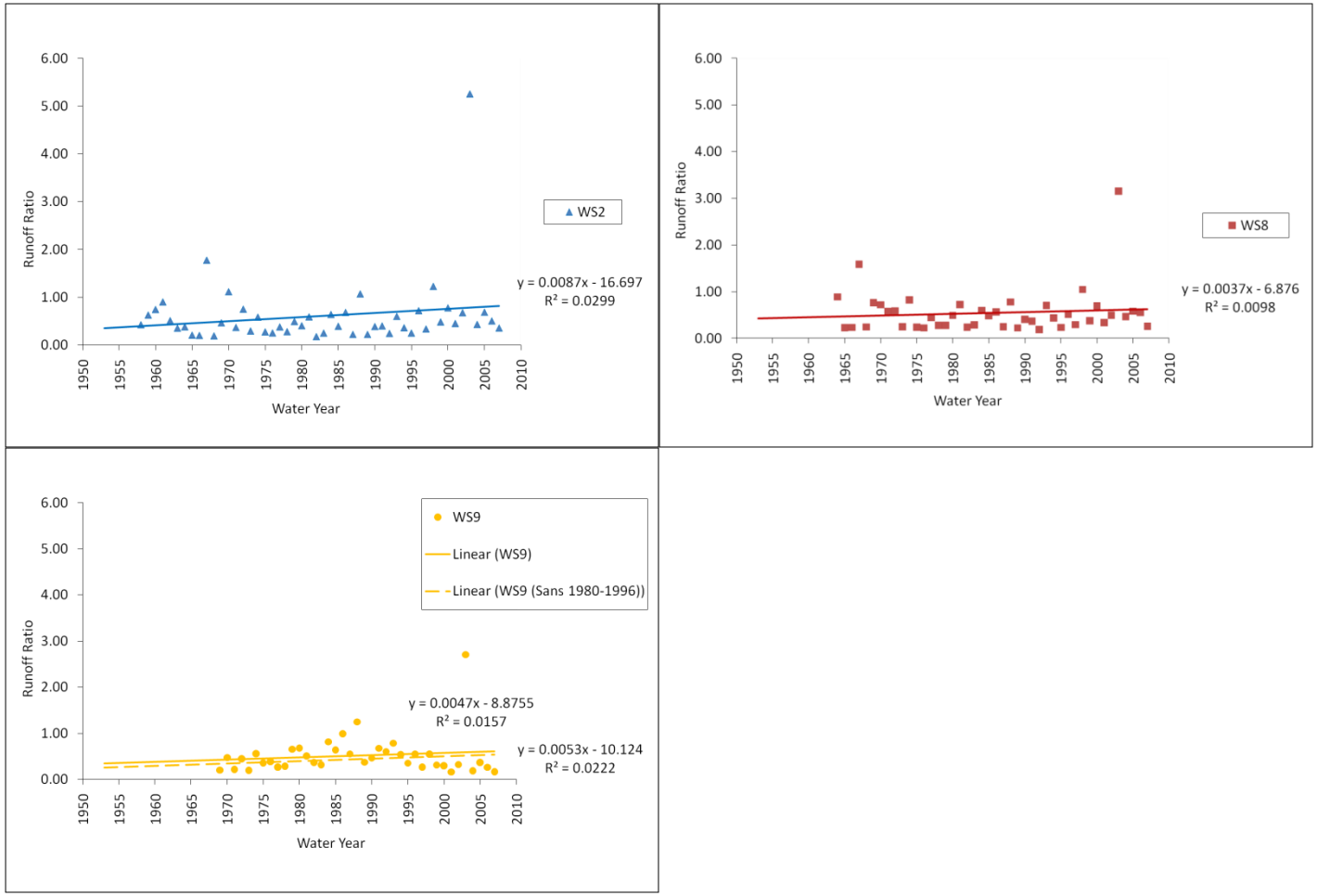

Figure G10. Trends in summer runoff ratio (using CS2MET precipitation) at (clockwise from bottom left) WS9, WS2, and WS8.

Table G1. Summary regression table of trends in runoff ratio (calculated using PRISM precipitation) at WS2, WS8, and WS9 for their respective periods of streamflow record.

Simple Linear Regression Model of Runoff Ratio (Discharge to PRISM Precipitation) over Time									
		Explanatory Variable Coefficients							
Dependent Variable		**Intercept**		**Year**		**P-value**		**R^2**	**N**
WS2 Annual Runoff Ratio		2.917		-0.001		0.127		0.043	55
WS8 Annual Runoff Ratio		5.921		-0.003		0.014	*	0.136	44
WS9 Annual Runoff Ratio		5.832		-0.003		0.080		0.081	39
WS2 Fall Runoff Ratio		2.463		-0.001		0.206		0.031	54
WS8 Fall Runoff Ratio		1.113		0.000		0.723		0.003	43
WS9 Fall Runoff Ratio		3.153		-0.001		0.324		0.027	38
WS2 Winter Runoff Ratio		1.144		0.000		0.852		0.001	55
WS8 Winter Runoff Ratio		2.553		-0.001		0.617		0.006	44
WS9 Winter Runoff Ratio		4.014		-0.002		0.469		0.014	39
WS2 Spring Runoff Ratio		7.523		-0.003		0.015	*	0.106	55
WS8 Spring Runoff Ratio		18.025		-0.009		0.007	**	0.163	44
WS9 Spring Runoff Ratio		11.847		-0.006		0.006	**	0.186	39
WS2 Summer Runoff Ratio		-2.854		0.002		0.441		0.011	55
WS8 Summer Runoff Ratio		-1.472		0.001		0.641		0.005	44
WS9 Summer Runoff Ratio		1.852		-0.001		0.836		0.001	39

Table G2. Summary regression table of trends in runoff ratio (calculated using CS2MET precipitation) at WS2, WS8, and WS9 for their respective periods of streamflow record.

Simple Linear Regression Model of Runoff Ratio (Discharge to CS2MET Precipitation) over Time									
		Explanatory Variable Coefficients							
Dependent Variable		**Intercept**		**Year**		**P-value**		**R^2**	**N**
WS2 Annual Runoff Ratio		2.631		-0.001		0.205		0.033	50
WS8 Annual Runoff Ratio		6.252		-0.003		0.003	**	0.194	44
WS9 Annual Runoff Ratio		5.616		-0.003		0.064		0.090	39
WS2 Fall Runoff Ratio		2.188		-0.001		0.334		0.020	49
WS8 Fall Runoff Ratio		1.007		0.000		0.733		0.003	43
WS9 Fall Runoff Ratio		2.464		-0.001		0.417		0.018	38
WS2 Winter Runoff Ratio		2.083		-0.001		0.594		0.006	50
WS8 Winter Runoff Ratio		3.846		-0.002		0.368		0.019	44
WS9 Winter Runoff Ratio		4.970		-0.002		0.321		0.027	39
WS2 Spring Runoff Ratio		7.679		-0.004		0.028	*	0.096	50
WS8 Spring Runoff Ratio		19.338		-0.009		0.006	**	0.166	44
WS9 Spring Runoff Ratio		10.519		-0.005		0.004	**	0.205	39
WS2 Summer Runoff Ratio		-16.697		0.009		0.230		0.030	50
WS8 Summer Runoff Ratio		-6.876		0.004		0.523		0.010	44
WS9 Summer Runoff Ratio		-8.876		0.005		0.447		0.016	39

Table G3. Summary regression table of trends in runoff ratio (calculated using PRISM precipitation) at WS2, WS8, and WS9 for the period of overlapping streamflow record from 1969-2007.

Simple Linear Regression Model of Runoff Ratio (Discharge to PRISM Precipitation) over Time, 1969-2007									
		Explanatory Variable Coefficients							
Dependent Variable		**Intercept**		**Year**		**P-value**		**R^2**	**N**
WS2 Annual Runoff Ratio		2.573		-0.001		0.471		0.014	39
WS8 Annual Runoff Ratio		7.135		-0.003		0.014	*	0.152	39
WS9 Annual Runoff Ratio		5.832		-0.003		0.080		0.081	39
WS2 Fall Runoff Ratio		2.169		-0.001		0.537		0.010	39
WS8 Fall Runoff Ratio		2.899		-0.001		0.379		0.021	39
WS9 Fall Runoff Ratio		3.153		-0.001		0.324		0.027	38
WS2 Winter Runoff Ratio		-0.797		0.001		0.740		0.003	39
WS8 Winter Runoff Ratio		3.405		-0.001		0.536		0.010	39
WS9 Winter Runoff Ratio		4.014		-0.002		0.469		0.014	39
WS2 Spring Runoff Ratio		11.141		-0.005		0.023	*	0.133	39
WS8 Spring Runoff Ratio		21.547		-0.010		0.004	**	0.203	39
WS9 Spring Runoff Ratio		11.847		-0.006		0.006	**	0.186	39
WS2 Summer Runoff Ratio		-11.720		0.006		0.115		0.066	39
WS8 Summer Runoff Ratio		-1.335		0.001		0.719		0.004	39
WS9 Summer Runoff Ratio		1.852		-0.001		0.836		0.001	39

Table G4. Summary regression table of trends in runoff ratio (calculated using CS2MET precipitation) at WS2, WS8, and WS9 for the period of overlapping streamflow record from 1969-2007.

Simple Linear Regression Model of Runoff Ratio (Discharge to CS2MET Precipitation) over Time 1969-2007									
		Explanatory Variable Coefficients							
Dependent Variable		**Intercept**		**Year**		**P-value**		**R^2**	**N**
WS2 Annual Runoff Ratio		2.532		-0.001		0.437		0.016	39
WS8 Annual Runoff Ratio		7.282		-0.003		0.004	**	0.199	39
WS9 Annual Runoff Ratio		5.616		-0.003		0.064		0.090	39
WS2 Fall Runoff Ratio		0.076		0.000		0.958		0.000	38
WS8 Fall Runoff Ratio		1.574		-0.001		0.630		0.007	38
WS9 Fall Runoff Ratio		2.464		-0.001		0.417		0.018	38
WS2 Winter Runoff Ratio		0.767		0.000		0.985		0.000	39
WS8 Winter Runoff Ratio		4.593		-0.002		0.333		0.025	39
WS9 Winter Runoff Ratio		4.970		-0.002		0.321		0.027	39
WS2 Spring Runoff Ratio		10.004		-0.005		0.041	*	0.108	39
WS8 Spring Runoff Ratio		20.018		-0.010		0.009	**	0.170	39
WS9 Spring Runoff Ratio		10.519		-0.005		0.004	**	0.205	39
WS2 Summer Runoff Ratio		-32.210		0.017		0.150		0.055	39
WS8 Summer Runoff Ratio		-13.991		0.007		0.288		0.030	39
WS9 Summer Runoff Ratio		-8.876		0.005		0.447		0.016	39

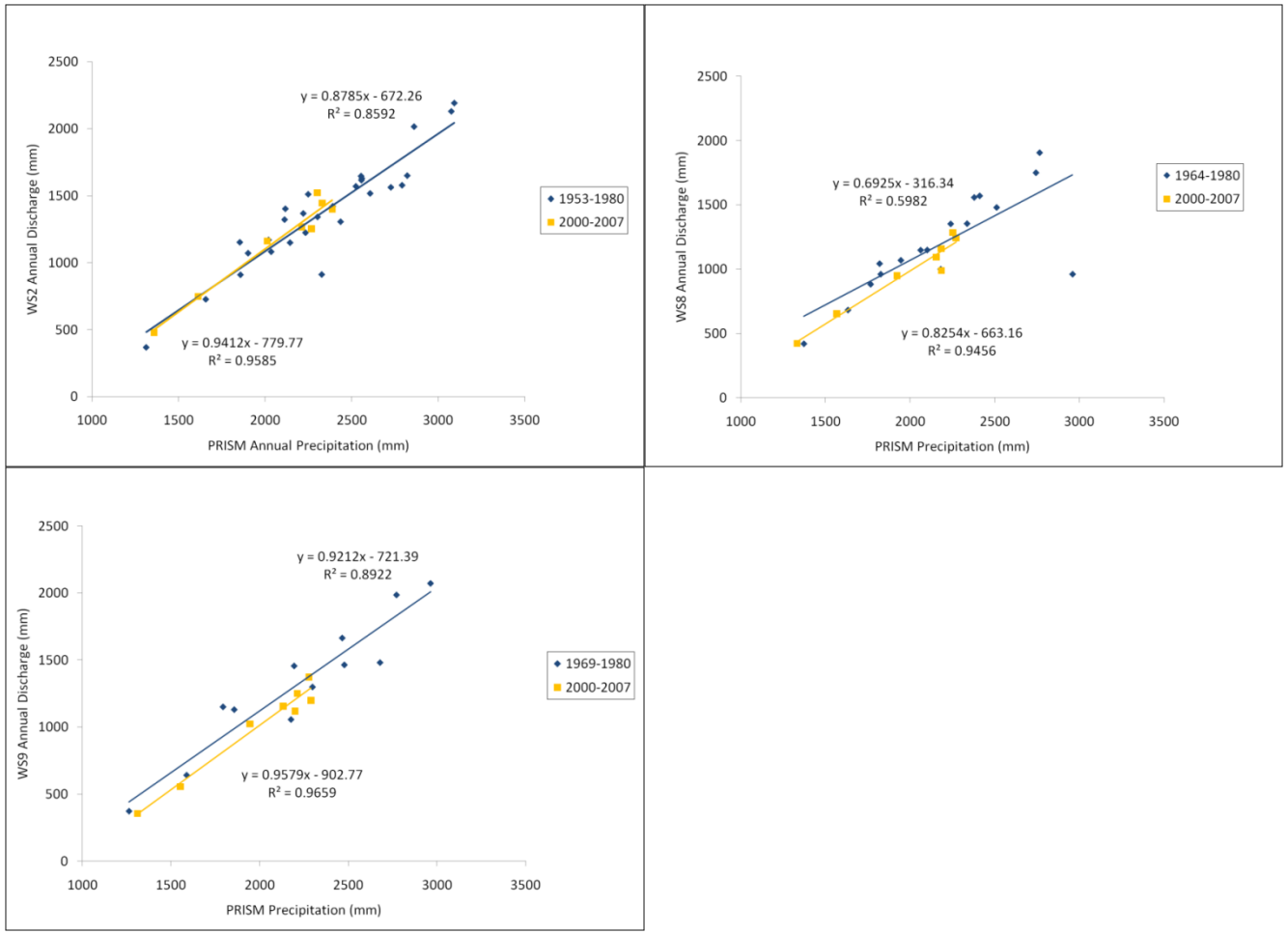

Figure G11. Annual discharge versus precipitation at (clockwise from bottom left) WS9, WS2, and WS8, for the period of record prior to 1981 and the period of record from 2000-2007.

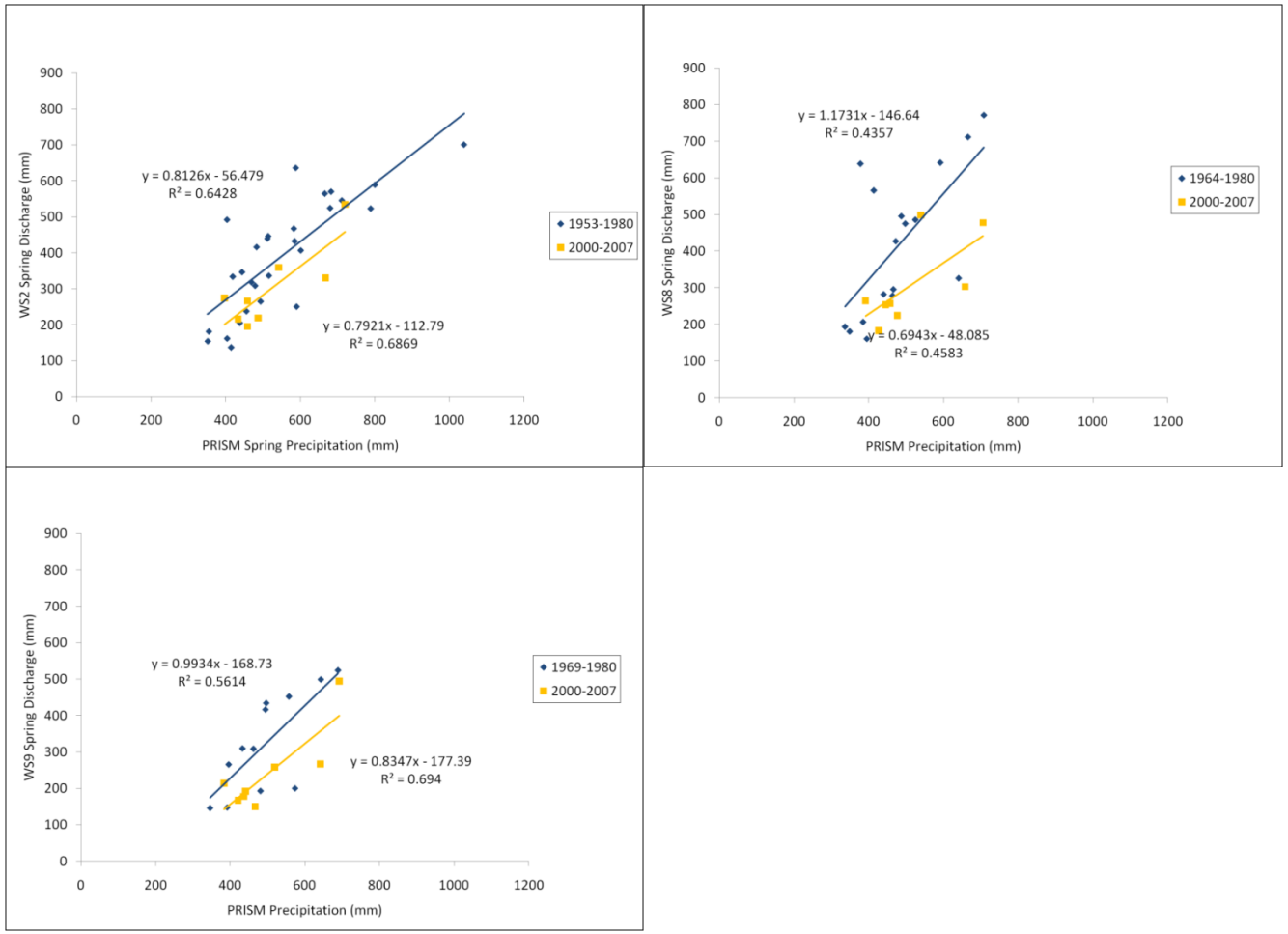

Figure G12. Spring discharge versus precipitation at (clockwise from bottom left) WS9, WS2, and WS8, for the period of record prior to 1981 and the period of record from 2000-2007.

Appendix H: Baseflow

Baseflows exhibit significant declines on an annual basis for WS8 and WS9 and during the spring for WS2 and WS8 (Table H1). The WS8 annual baseflow exhibits a decline of -4.584mm per year ($p<0.05$) for a net decline of 33.6% or 0.54mm/day over the 44 year period of streamflows. The WS9 annual baseflow exhibits a decline of -4.833mm per year ($p<0.05$) for a net decline of 32.0% or 0.50mm/day over the 39 year period of streamflows. The WS2 spring baseflow exhibits a decline of -1.764mm per year ($p<0.01$) for a net decline of 38.7% or 1.04mm/day over the 55 year period of streamflows. The WS8 spring baseflow exhibits a decline of -2.685mm per year ($p<0.05$) for a net decline of 44.6% or 1.26mm/day over the 44 year period of streamflows. Figures H1-H5 show the trends in baseflow over time on an annual and seasonal basis for all three watersheds. Trend lines and equations are shown on the figures along with an R^2 goodness of fit estimate.

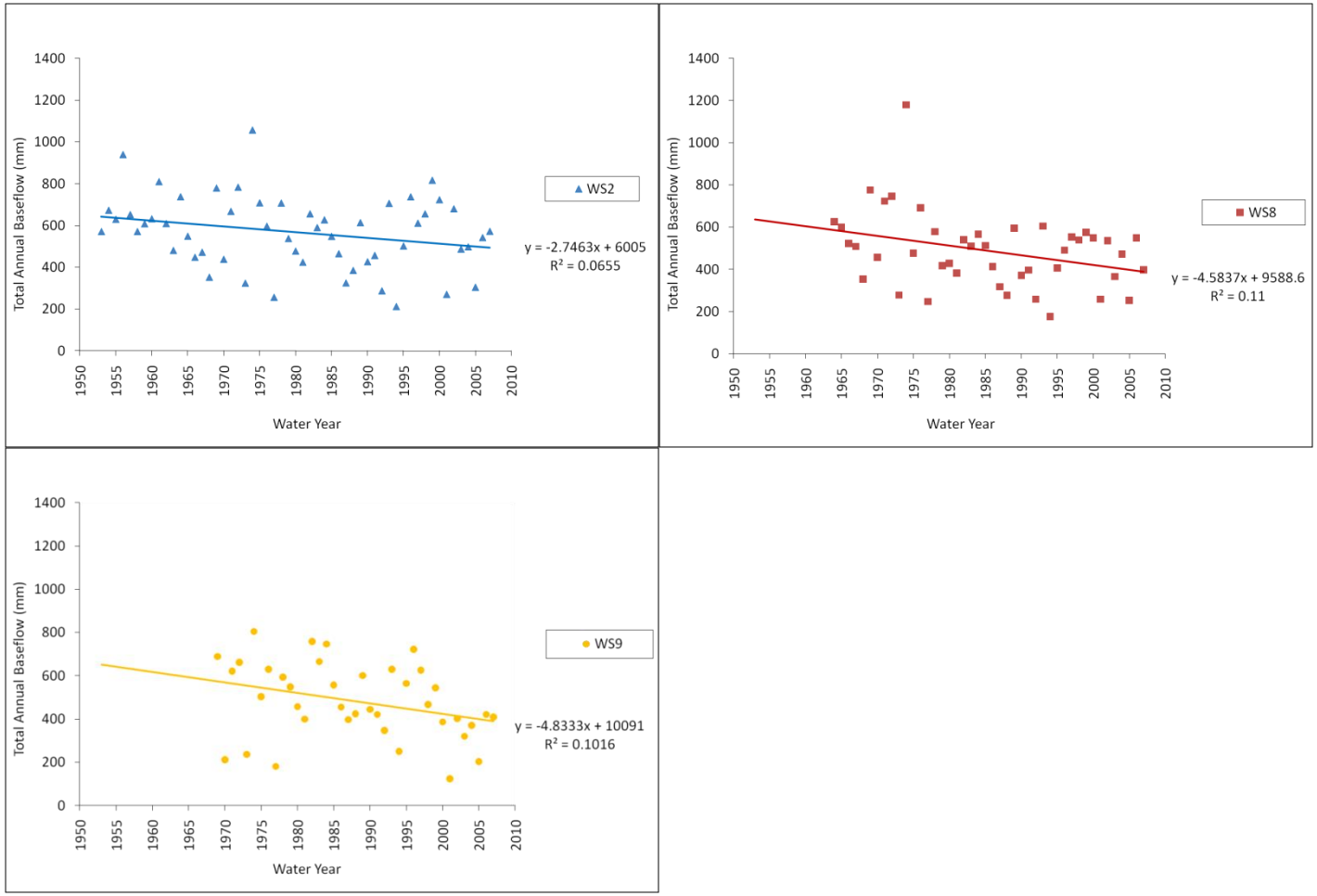

Figure H1. Annual baseflow at (clockwise from bottom left) WS9, WS2, and WS8.

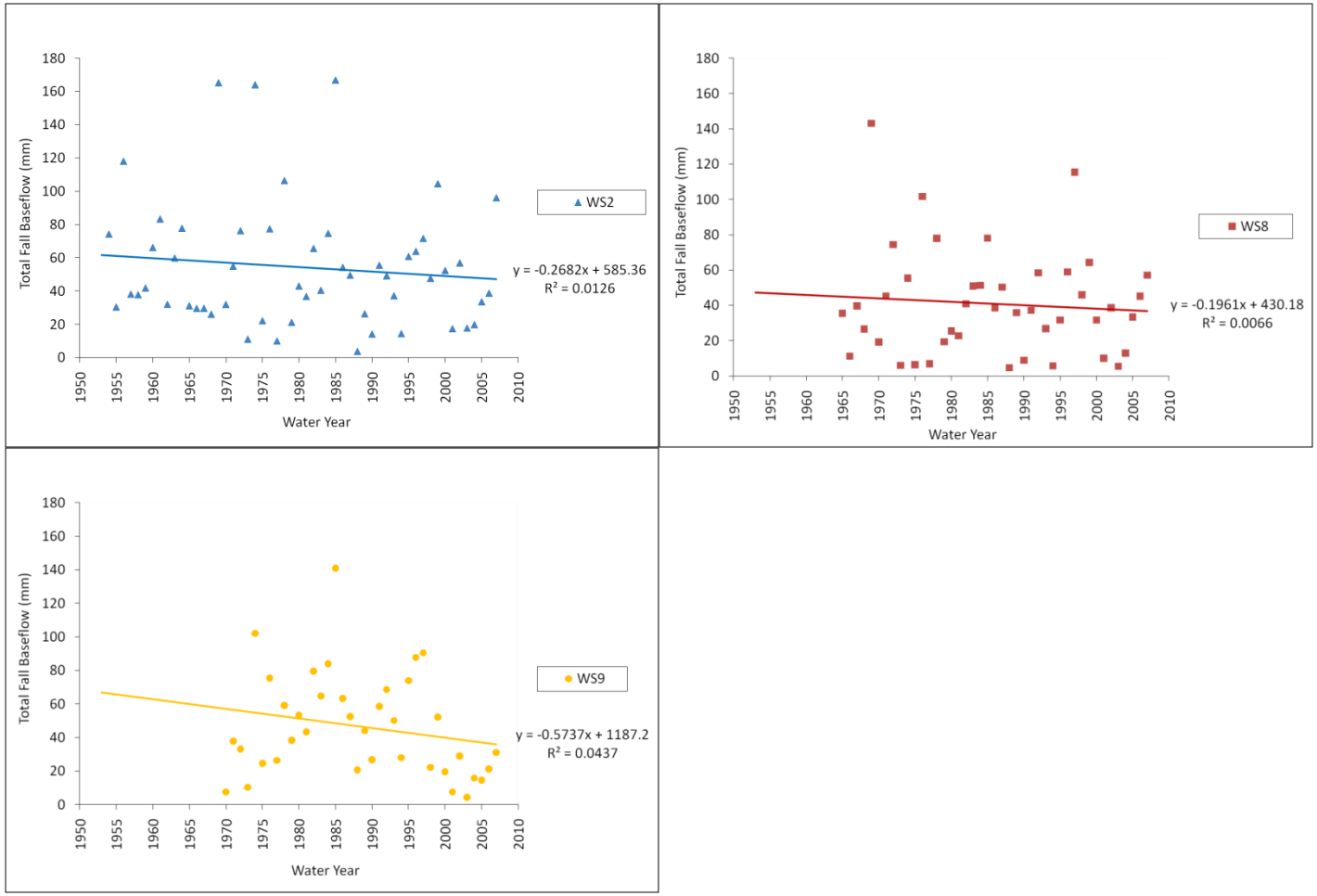

Figure H2. Fall baseflow at (clockwise from bottom left) WS9, WS2, and WS8.

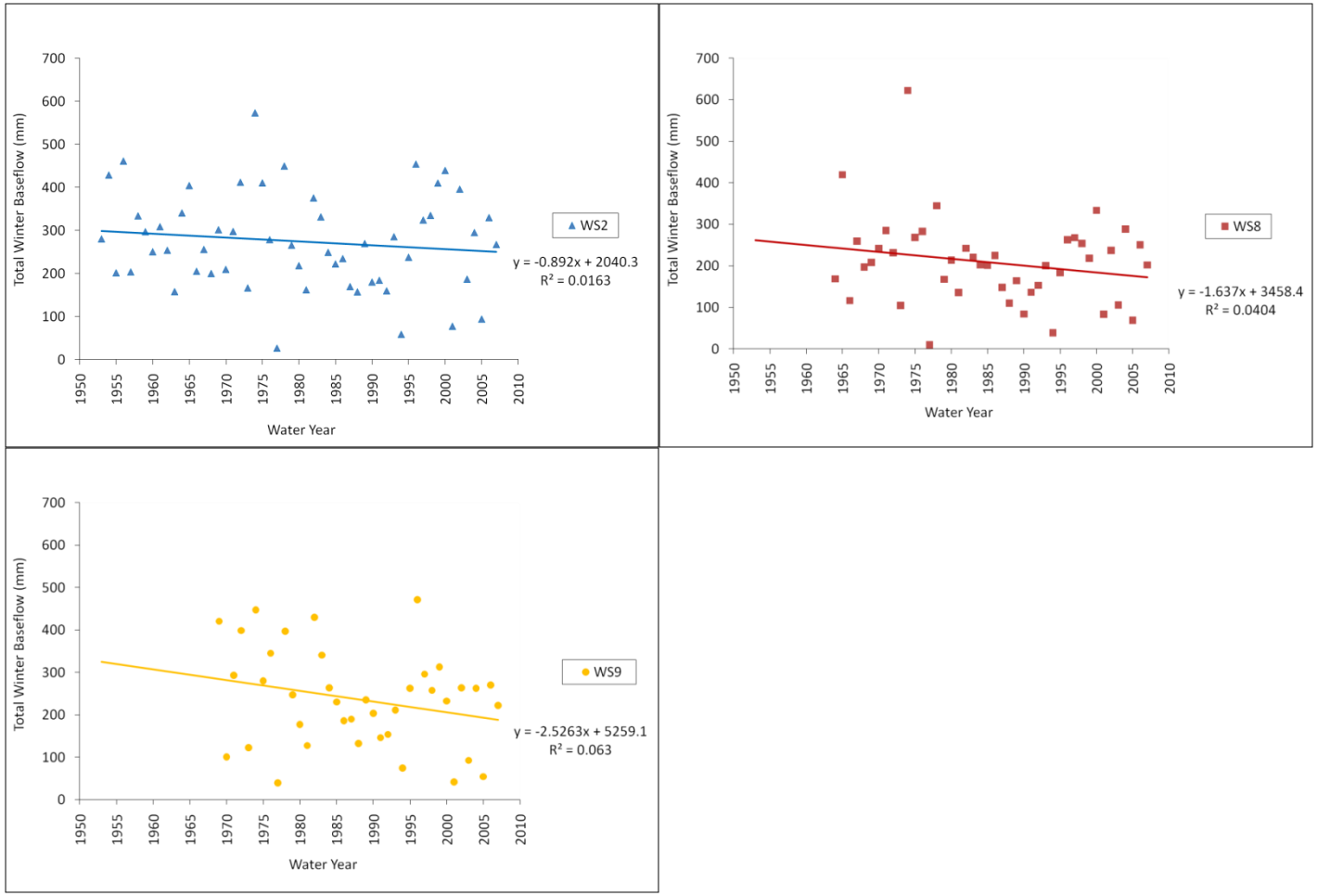

Figure H3. Winter baseflow at (clockwise from bottom left) WS9, WS2, and WS8.

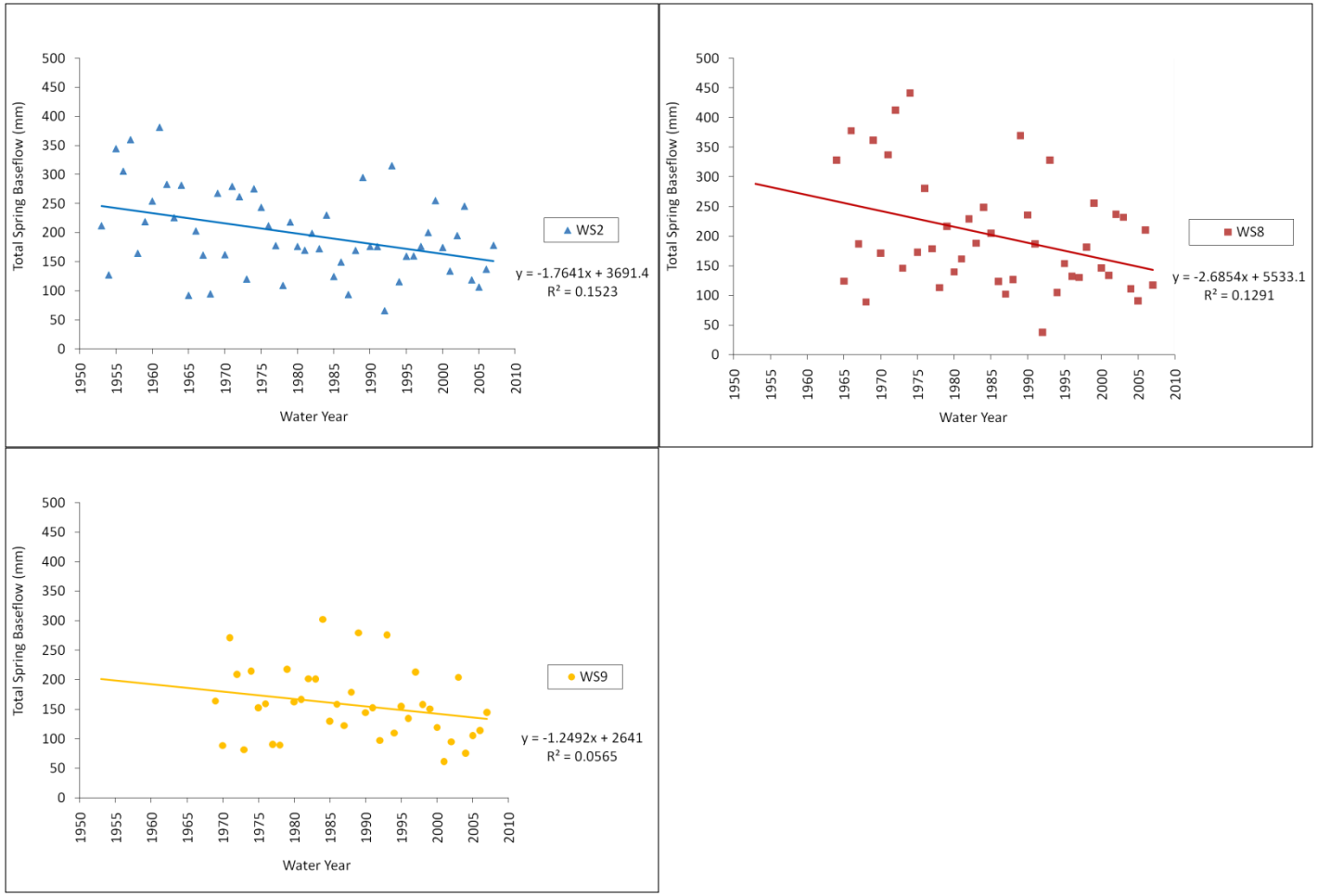

Figure H4. Spring baseflow at (clockwise from bottom left) WS9, WS2, and WS8.

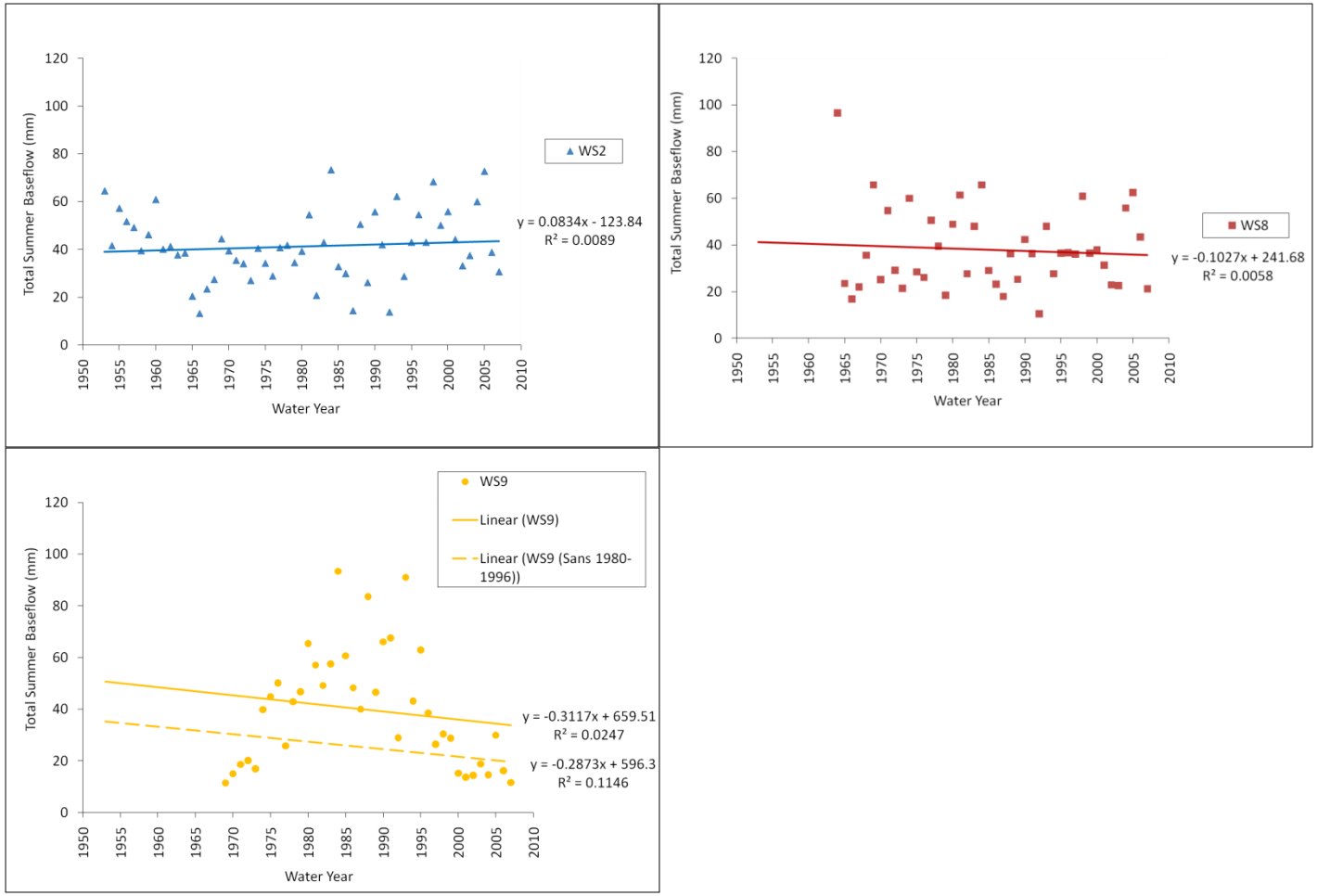

Figure H5. Summer baseflow at (clockwise from bottom left) WS9, WS2, and WS8.

Table H1. Summary regression table of trends in baseflow at WS2, WS8, and WS9 for their respective periods of record.

Simple Linear Regression Model of Baseflow over Time									
		Explanatory Variable Coefficients							
Dependent Variable		**Intercept**		**Year**		**P-value**		**R^2**	**N**
WS2 Annual Baseflow		6005.0		-2.746		0.059		0.065	55
WS8 Annual Baseflow		9588.6		-4.584		0.028	*	0.110	44
WS9 Annual Baseflow		10090.6		-4.833		0.048	*	0.102	39
WS2 Fall Baseflow		585.4		-0.268		0.419		0.013	54
WS8 Fall Baseflow		430.2		-0.196		0.606		0.007	43
WS9 Fall Baseflow		1187.2		-0.574		0.208		0.044	38
WS2 Winter Baseflow		2040.3		-0.892		0.352		0.016	55
WS8 Winter Baseflow		3458.4		-1.637		0.191		0.040	44
WS9 Winter Baseflow		5259.1		-2.526		0.123		0.063	39
WS2 Spring Baseflow		3691.4		-1.764		0.003	**	0.152	55
WS8 Spring Baseflow		5533.1		-2.685		0.017	*	0.129	44
WS9 Spring Baseflow		2641.0		-1.249		0.145		0.056	39
WS2 Summer Baseflow		-123.8		0.083		0.494		0.009	55
WS8 Summer Baseflow		241.7		-0.103		0.624		0.006	44
WS9 Summer Baseflow		659.5		-0.312		0.340		0.025	39

Sample Baseflow Program

```
      PROGRAM BASEFLOW
C
C
C     DESCRIPTION : This program    calculates the Baseflow Index
C
C     ARGUMENTS : NSAMP is INTEGER, FLOW and BFI are REAL*8.
C
C     LOCAL VARIABLES : MIN    - local minima (over 5 points)
C                       BLOCKS - total number of 5-point blocks
C                       TURN   - turning points
C                       TURNS  - total number of turning points
C                       AREA   - area under the baseflow curve
C
C
      INTEGER K,I,L,LA,M,day1(50000),month1(50000),year1(50000)
      INTEGER nsamp,BLOCKS,TURNS,MM,NN,day,month,year,JD,JDATE
      REAL*8 A,B,C,TEST
      REAL*8 FLOW(50000),MIN(10000,2),AREA,BASE,TOTA,BFI,TURN(10000,2)
c
      open(10,file='GSW09_input.csv')
      open(20,file='base.csv')
      open(30,file='flow.csv')
      nsamp=0
      do 100 n=1,50000
       read(10,*,end=200) flow(n),year1(n),month1(n),day1(n)
       nsamp=nsamp+1
100   continue
200   continue

c
      write(*,*) 'Please enter the first date in the file (DD,MM,YYYY)'
      read(5,*) day,month,year
      JD = JDATE(year,month,day)
      write(*,*) 'Number of samples = ',nsamp
      do 250 i=1,nsamp
       write(30,9200) jd+i-1,flow(i),i
250   continue
C
C     put minimum flows for each block of 5 into MIN(K,1) and the points
C     at which they occur into MIN(K,2),
C     put total number of blocks into BLOCKS
C
      K=0
      DO 1000 I=1,nsamp,5
            K=K+1
            TEST = FLOW(I)
            MIN(K,2) = I
            LA = I
            DO 1010 L=2,5
              LA=LA+1
              IF(FLOW(LA).GE.TEST) GOTO 1010
              TEST = FLOW(LA)
              MIN(K,2) = LA
```

```
1010    CONTINUE
            MIN(K,1) = TEST
1000  CONTINUE
      BLOCKS = K
C
C     put flow at each turning point into TURN(I,1)
C     and the points at which they occur into TURN(I,2),
C     put total number of turning points into TURNS
C
      I=0
      DO 2000 L=2,BLOCKS-1
            A = MIN(L-1,1)
            B = MIN(L,1)*0.9
            C = MIN(L+1,1)
            IF(B.GE.A) GOTO 2000
            IF(B.GE.C) GOTO 2000
            I=I+1
            TURN(I,1) = MIN(L,1)
            TURN(I,2) = MIN(L,2)
2000  CONTINUE
      TURNS = I
      IF(TURNS.LE.1) THEN
        BFI=0.0
        write(*,*) 'Too few samples to calculate a BFI!'
      ENDIF
c
c     Write the baseflow to base.q
c
      do 2500 i=1,turns
        write(20,9100) turn(i,2)+jd-1,turn(i,1),turn(i,2),
     &       day1(turn(i,2)),month1(turn(i,2)),year1(turn(i,2))
2500  continue
C
C     calculate volume of baseflow
C
      AREA=0.0
      DO 3000 L=1,TURNS-1
            BASE = TURN(L+1,2) - TURN(L,2)
            AREA = AREA + 0.5*BASE*(TURN(L,1)+TURN(L+1,1))
3000  CONTINUE
C
C     calculate volume of total flow
C
      MM = NINT(TURN(1,2))
      NN = NINT(TURN(TURNS,2))
      TOTA=0.0
      DO 4000 M=MM,NN
            TOTA = TOTA + FLOW(M)
4000  CONTINUE
C
C     calculate BFI
C
      BFI = AREA/TOTA
      write(*,*) 'Base flow index = ',BFI
C
9000  format(f8.3,4x,i4,4x,i4,4x,i4)
```

```
c 9000  format(8x,f12.3,13x,i4,i4,i4)
 9100  format(f12.0,f12.3,f12.0,3i5)
 9200  format(i12,f12.3,i12)
      STOP
      END
c
      FUNCTION JDATE(I,J,K)
      JDATE=K-32075+1461*(I+4800+(J-14)/12)/4
     ++367*(J-2-(J-14)/12*12)/12-3*((I+4900+(J-14)/12)/100)/4
      RETURN
      END
```

Appendix I: Cross Regressions

1 Winter Average Minimum Temperature as the Explanatory Variable

Modeled winter VPD at CS2MET has a significant positive relationship to PRISM winter average minimum temperature, estimated for each watershed (Table I1). A degree increase in WS2 PRISM winter average minimum temperature is associated with a 0.249 mbar increase ($p<0.01$) in modeled winter VPD at CS2MET. A degree increase in WS8 PRISM winter average minimum temperature is associated with a 0.242 mbar increase ($p<0.01$) in modeled winter VPD at CS2MET. A degree increase in WS9 PRISM winter average minimum temperature is associated with a 0.184 mbar increase ($p<0.01$) in modeled winter VPD at CS2MET.

April 1st SWE at Santiam Junction has a significant negative relationship to winter average minimum temperature as estimated by WS2 PRISM, WS8 PRISM, and WS9 PRISM (Table I1). A degree increase in WS2 PRISM winter average minimum temperature is associated with a 104.995 mm reduction ($p<0.01$) in April 1st SWE at Santiam Junction. A degree increase in WS8 PRISM winter average minimum temperature is associated with a 132.170 mm reduction ($p<0.01$) in April 1st SWE at Santiam Junction. A degree increase in WS9 PRISM winter average minimum temperature is associated with a 128.430 mm reduction ($p<0.01$) in April 1st SWE at Santiam Junction.

Winter runoff ratios for all three watersheds are not significantly associated with PRISM winter average minimum temperature, estimated for each watershed (Table I1).

Spring runoff ratios for all three watersheds have a significant negative relationship with PRISM winter average minimum temperature, estimated for each watershed (Table I1). A degree increase in WS2 PRISM winter average minimum temperature is associated with a 0.069 reduction ($p<0.01$) in WS2 spring runoff ratio. A degree increase in WS8 PRISM winter average

minimum temperature is associated with a 0.138 reduction ($p<0.01$) in WS8 spring runoff ratio. A degree increase in WS9 PRISM winter average minimum temperature is associated with a 0.059 reduction ($p<0.01$) in WS9 spring runoff ratio.

Spring baseflows for all three watersheds have a significant negative relationship with PRISM winter average minimum temperature, estimated for each watershed (Table I1). A degree increase in WS2 PRISM winter average minimum temperature is associated with a 26.38 mm reduction ($p<0.01$) in WS2 spring baseflow. A degree increase in WS8 PRISM winter average minimum temperature is associated with a 46.73 mm reduction ($p<0.01$) in WS8 spring baseflow. A degree increase in WS9 PRISM winter average minimum temperature is associated with a 20.74 mm reduction ($p<0.05$) in WS9 spring baseflow.

Summer runoff ratios for all three watersheds are not significantly associated with PRISM winter average minimum temperature, estimated for each watershed (Table I1).

Summer baseflows for all three watersheds are not significantly associated with PRISM winter average minimum temperature, estimated for each watershed (Table I1).

2 Winter Average Maximum Temperature as the Explanatory Variable

Modeled winter VPD at CS2MET has a significant positive relationship to PRISM winter average maximum temperature, estimated for each watershed (Table I2). A degree increase in WS2 PRISM winter average maximum temperature is associated with a 0.297 mbar increase ($p<0.01$) in modeled winter VPD at CS2MET. A degree increase in WS8 PRISM winter average maximum temperature is associated with a 0.296 mbar increase ($p<0.01$) in modeled winter VPD at CS2MET. A degree increase in WS9 PRISM winter average maximum temperature is associated with a 0.340 mbar increase ($p<0.01$) in modeled winter VPD at CS2MET.

April 1st SWE at Santiam Junction has a significant negative relationship to winter average maximum temperature as estimated by WS2 PRISM, WS8 PRISM, and WS9 PRISM (Table I2). A degree increase in WS2 PRISM winter average maximum temperature is associated with a 96.78 mm reduction ($p<0.01$) in April 1st SWE at Santiam Junction. A degree increase in WS8 PRISM winter average maximum temperature is associated with a 124.99 mm reduction ($p<0.01$) in April 1st SWE at Santiam Junction. A degree increase in WS9 PRISM winter average maximum temperature is associated with a 156.17 mm reduction ($p<0.01$) in April 1st SWE at Santiam Junction.

Winter runoff ratios for WS2 and WS9 exhibit a significant negative relationship with PRISM winter average maximum temperature, estimated for each watershed respectively (Table I2). A degree increase in WS2 PRISM winter average maximum temperature is associated with a 0.031 reduction ($p<0.05$) in WS2 winter runoff ratio. A degree increase in WS9 PRISM winter average maximum temperature is associated with a 0.06 reduction ($p<0.01$) in WS9 winter runoff ratio.

Spring runoff ratios for all three watersheds have a significant negative relationship with PRISM winter average maximum temperature, estimated for each watershed (Table I2). A degree increase in WS2 PRISM winter average maximum temperature is associated with a 0.059 reduction ($p<0.01$) in WS2 spring runoff ratio. A degree increase in WS8 PRISM winter average maximum temperature is associated with a 0.131 reduction ($p<0.01$) in WS8 spring runoff ratio. A degree increase in WS9 PRISM winter average maximum temperature is associated with a 0.062 reduction ($p<0.01$) in WS9 spring runoff ratio.

Spring baseflows for all three watersheds have a significant negative relationship with PRISM winter average maximum temperature, estimated for each watershed (Table I2). A

degree increase in WS2 PRISM winter average maximum temperature is associated with a 15.88 mm reduction ($p<0.05$) in WS2 spring baseflow. A degree increase in WS8 PRISM winter average maximum temperature is associated with a 40.66 mm reduction ($p<0.01$) in WS8 spring baseflow. A degree increase in WS9 PRISM winter average maximum temperature is associated with a 22.36 mm reduction ($p<0.01$) in WS9 spring baseflow.

Summer runoff ratios for all three watersheds are not significantly associated with PRISM winter average maximum temperature, estimated for each watershed (Table I2).

Summer baseflows for all three watersheds are not significantly associated with PRISM winter average maximum temperature, estimated for each watershed (Table I2).

3 Spring Average Minimum Temperature as the Explanatory Variable

Modeled spring VPD at CS2MET exhibits no relationship to PRISM spring average minimum temperature, estimated for each watershed (Table I3).

Only spring runoff ratio for WS8 exhibits a significant relationship with PRISM spring average minimum temperature (Table I3). A degree increase in WS8 PRISM spring average minimum temperature is associated with a 0.116 reduction ($p<0.01$) in WS8 spring runoff ratio.

Spring baseflows for WS2 and WS8 show a significant relationship with PRISM spring average minimum temperature, estimated for each watershed respectively (Table I3). A degree increase in WS2 PRISM spring average minimum temperature is associated with a 24.05 mm reduction ($p<0.05$) in WS2 spring baseflow. A degree increase in WS8 PRISM spring average minimum temperature is associated with a 39.39 mm reduction ($p<0.01$) in WS8 spring baseflow.

4 Spring Average Maximum Temperature as the Explanatory Variable

Modeled spring VPD at CS2MET has a significant positive relationship to PRISM spring average maximum temperature, estimated for each watershed (Table I4). A degree increase in WS2 PRISM spring average maximum temperature is associated with a 0.708 mbar increase ($p<0.01$) in modeled spring VPD at CS2MET. A degree increase in WS8 PRISM spring average maximum temperature is associated with a 0.715 mbar increase ($p<0.01$) in modeled spring VPD at CS2MET. A degree increase in WS9 PRISM spring average maximum temperature is associated with a 0.706 mbar increase ($p<0.01$) in modeled spring VPD at CS2MET.

Spring runoff ratios are not significantly related to PRISM spring average maximum temperature for any of the watersheds (Table I4).

Spring baseflows for all three watersheds show a significant relationship with PRISM spring average maximum temperature, estimated for each watershed respectively (Table I4). A degree increase in WS2 PRISM spring average maximum temperature is associated with a 29.37 mm reduction ($p<0.01$) in WS2 spring baseflow. A degree increase in WS8 PRISM spring average maximum temperature is associated with a 23.98 mm reduction ($p<0.05$) in WS8 spring baseflow. A degree increase in WS9 PRISM spring average maximum temperature is associated with a 15.38 mm reduction ($p<0.05$) in WS9 spring baseflow.

5 Summer Average Minimum Temperature as the Explanatory Variable

Modeled summer VPD at CS2MET has a significant positive relationship to PRISM summer average minimum temperature, estimated for WS2 and WS8 (Table I5). A degree increase in WS2 PRISM summer average minimum temperature is associated with a 2.564 mbar increase ($p<0.01$) in modeled summer VPD at CS2MET. A degree increase in WS8 PRISM

summer average minimum temperature is associated with a 2.235 mbar increase ($p<0.01$) in modeled summer VPD at CS2MET.

Summer runoff ratios are not significantly related to PRISM summer average minimum temperature for any of the watersheds (Table I5).

Only summer baseflow for WS9 exhibits a significant relationship with PRISM summer average minimum temperature (Table I5). A degree increase in WS9 PRISM summer average minimum temperature is associated with an 11.96 reduction ($p<0.05$) in WS9 summer baseflow.

6 Summer Average Maximum Temperature as the Explanatory Variable

Modeled summer VPD at CS2MET has a significant positive relationship to PRISM summer average maximum temperature, estimated for each watershed (Table I6). A degree increase in WS2 PRISM summer average maximum temperature is associated with a 2.371 mbar increase ($p<0.01$) in modeled summer VPD at CS2MET. A degree increase in WS8 PRISM summer average maximum temperature is associated with a 2.292 mbar increase ($p<0.01$) in modeled summer VPD at CS2MET. A degree increase in WS9 PRISM summer average maximum temperature is associated with a 2.415 mbar increase ($p<0.01$) in modeled summer VPD at CS2MET.

Summer runoff ratios for WS2 and WS8 exhibit a significant relationship with PRISM summer average maximum temperature (Table I6). A degree increase in WS2 PRISM summer average maximum temperature is associated with a 0.087 increase ($p<0.01$) in WS2 summer runoff ratio. A degree increase in WS8 PRISM summer average maximum temperature is associated with a 0.048 increase ($p<0.05$) in WS8 summer runoff ratio.

Only summer baseflow for WS9 exhibits a significant relationship with PRISM summer average maximum temperature (Table I6). A degree increase in WS9 PRISM summer average maximum temperature is associated with an 8.403 reduction ($p<0.01$) in WS9 summer baseflow.

7 April 1st SWE at Santiam Junction as the Explanatory Variable

Spring runoff ratios for all three watersheds exhibit a significant positive relationship to April 1st SWE at Santiam Junction (Table I7). A millimeter increase in April 1st SWE at Santiam Junction is associated with a 0.0003 increase ($p<0.01$) in WS2 spring runoff ratio. A millimeter increase in April 1st SWE at Santiam Junction is associated with a 0.0006 increase ($p<0.01$) in WS8 spring runoff ratio. A millimeter increase in April 1st SWE at Santiam Junction is associated with a 0.0003 increase ($p<0.01$) in WS9 spring runoff ratio.

Summer runoff ratios are not significantly associated with April 1st SWE at Santiam Junction for any of the watersheds (Table I7).

Spring baseflows for all three watersheds exhibit a significant positive relationship to April 1st SWE at Santiam Junction (Table I7). A millimeter increase in April 1st SWE at Santiam Junction is associated with a 0.11 mm increase ($p<0.01$) in WS2 spring baseflows. A millimeter increase in April 1st SWE at Santiam Junction is associated with a 0.22 mm increase ($p<0.01$) in WS8 spring baseflow. A millimeter increase in April 1st SWE at Santiam Junction is associated with a 0.08 increase ($p<0.01$) in WS9 spring baseflow.

Summer baseflows are not significantly associated with April 1st SWE at Santiam Junction for any of the watersheds (Table I7).

8 Vapor Pressure Deficit at PRIMET as the Explanatory Variable

Fall runoff ratios, fall baseflows, winter runoff ratios and winter baseflows do not exhibit a significant relationship with VPD measured at PRIMET for any of the watersheds (Table I8, I9).

WS2 and WS9 spring runoff ratios exhibit a significant negative relationship with VPD at PRIMET (Table I8). A mbar increase in VPD at PRIMET is associated with a 0.024 reduction ($p<0.05$) in WS2 spring runoff ratio and a 0.03 reduction ($p<0.05$) in WS8 spring runoff ratio.

WS2 summer runoff ratio exhibits a significant positive relationship with VPD at PRIMET (Table I8). A mbar increase in VPD at PRIMET is associated with a 0.043 increase ($p<0.01$) in WS2 summer runoff ratio.

Spring baseflows for WS2 and WS9 exhibit a significant negative relationship with VPD at PRIMET (Table I9). A mbar increase in VPD at PRIMET is associated with a 15.10 mm reduction ($p<0.05$) in WS2 spring baseflow. A mbar increase in VPD at PRIMET is associated with a 14.48 mm reduction ($p<0.05$) in WS9 spring baseflow.

WS9 summer baseflow exhibits a significant negative relationship with VPD at PRIMET (Table I9). A mbar increase in VPD at PRIMET is associated with a 3.46 mm reduction ($p<0.01$) in WS2 summer baseflow.

9 Vapor Pressure Deficit at CS2MET as the Explanatory Variable

Fall runoff ratios for WS2 and WS8 exhibit a significant relationship with modeled VPD at CS2MET (Table I10). A mbar increase in modeled VPD at CS2MET is associated with a 0.023 reduction ($p<0.05$) in WS2 fall runoff ratio, and a 0.028 reduction ($p<0.01$) in WS8 fall runoff ratio.

Fall baseflows for WS2 and WS8 exhibit a significant relationship with modeled VPD at CS2MET (Table I11). A mbar increase in modeled VPD at CS2MET is associated with a 9.05 mm reduction ($p<0.05$) in WS2 fall baseflow, and a 7.53 mm reduction ($p<0.05$) in WS8 fall baseflow.

Winter runoff ratios for WS2 and WS9 exhibit a significant relationship with modeled VPD at CS2MET (Table I10). A mbar increase in modeled VPD at CS2MET is associated with a 0.084 reduction ($p<0.05$) in WS2 winter runoff ratio, and a 0.17 reduction ($p<0.01$) in WS9 winter runoff ratio.

Winter baseflows for all three watersheds exhibit a significant relationship with modeled VPD at CS2MET (Table I11). A mbar increase in modeled VPD at CS2MET is associated with a 108.57 mm reduction ($p<0.01$) in WS2 winter baseflow, a 70.82 mm reduction ($p<0.05$) in WS8 winter baseflow, and a 156.67 mm reduction ($p<0.01$) in WS9 winter baseflow.

Spring runoff ratios exhibit no significant relationships with modeled VPD at CS2MET (Table I10).

Spring baseflows for WS2 and WS9 exhibit a significant relationship with modeled VPD at CS2MET (Table I11). A mbar increase in modeled VPD at CS2MET is associated with a 20.67 mm reduction ($p<0.01$) in WS2 spring baseflow, and a 18.99 mm reduction ($p<0.01$) in WS9 spring baseflow.

Summer runoff ratios for WS2 and WS8 exhibit a significant relationship with modeled VPD at CS2MET (Table I10). A mbar increase in modeled VPD at CS2MET is associated with a 0.037 increase ($p<0.01$) in WS2 summer runoff ratio, and a 0.014 increase ($p<0.05$) in WS8 summer runoff ratio.

Summer baseflows for WS9 exhibit a significant relationship with modeled VPD at CS2MET (Table I11). A mbar increase in modeled VPD at CS2MET is associated with a 3.94 mm reduction ($p<0.01$) in WS9 summer baseflow.

10 Coefficient of Variation for Precipitation as the Explanatory Variable

Winter runoff ratios for all three watersheds are significantly negatively associated with the coefficient of variation for precipitation at CS2MET (Table I12). A unit increase in the coefficient of variation is associated with a -0.226 reduction ($p<0.01$) in the WS2 winter runoff ratio to CS2MET. A unit increase in the coefficient of variation is associated with a -0.225 reduction ($p<0.05$) in the WS8 winter runoff ratio to CS2MET. A unit increase in the coefficient of variation is associated with a -0.207 reduction ($p<0.05$) in the WS9 winter runoff ratio to CS2MET. Figure I1 shows the winter runoff ratio for the three watersheds versus the coefficient of variation for precipitation at CS2MET by season. Trend lines and equations are shown on the figure along with an R^2 goodness of fit estimate.

11 Winter Average Wind Speed as the Explanatory Variable

Winter runoff ratios for all three watersheds are not significantly associated with average winter wind speed (Tables I13, I14).

Table I1. Simple linear cross-regressions with winter average minimum temperature as the explanatory variable.

Simple Linear Cross-Regressions with Winter Average Minimum Temperature as the Explantory Variable

		Explanatory Variable Coefficients										
Dependent Variable		**Intercept**		**Winter Average Minimum Temperature WS2 PRISM**		**Winter Average Minimum Temperature WS8 PRISM**		**Winter Average Minimum Temperature WS9 PRISM**	**P-value**		**R^2**	**N**
Winter VPD Modeled at CS2MET		2.4		0.249					0.000	**	0.304	47
Winter VPD Modeled at CS2MET		2.8				0.242			0.000	**	0.292	47
Winter VPD Modeled at CS2MET		2.7						0.184	0.009	**	0.143	47
April 1st SWE Santiam Junction		451.4		-104.995					0.008	**	0.124	55
April 1st SWE Santiam Junction		199.0				-132.170			0.002	**	0.205	44
April 1st SWE Santiam Junction		207.7						-128.430	0.007	**	0.180	39
WS2 Winter Runoff Ratio		0.7		-0.003					0.842		0.001	55
WS8 Winter Runoff Ratio		0.6				0.026			0.221		0.035	44
WS9 Winter Runoff Ratio		0.7						-0.012	0.620		0.007	39
WS2 Spring Runoff Ratio		0.7		-0.069					0.000	**	0.224	55
WS8 Spring Runoff Ratio		0.5				-0.138			0.000	**	0.334	44
WS9 Spring Runoff Ratio		0.5						-0.059	0.006	**	0.184	39
WS2 Spring Baseflow		201.2		-26.380					0.001	**	0.180	55
WS8 Spring Baseflow		131.4				-46.730			0.000	**	0.322	44
WS9 Spring Baseflow		131.7						-20.737	0.017	*	0.144	39
WS2 Summer Runoff Ratio		0.5		0.031					0.303		0.020	55
WS8 Summer Runoff Ratio		0.4				0.006			0.791		0.002	44
WS9 Summer Runoff Ratio		0.4						-0.012	0.734		0.003	39
WS2 Summer Baseflow		41.3		-0.165					0.922		0.000	55
WS8 Summer Baseflow		37.5				-0.221			0.924		0.000	44
WS9 Summer Baseflow		34.9						-3.888	0.250		0.036	39

Table I2. Simple linear cross-regressions with winter average maximum temperature as the explanatory variable.

Simple Linear Cross-Regressions with Winter Average Maximum Temperature as the Explantory Variable												
		Explanatory Variable Coefficients										
Dependent Variable		**Intercept**		**Winter Average Maximum Temperature WS2 PRISM**		**Winter Average Maximum Temperature WS8 PRISM**		**Winter Average Maximum Temperature WS9 PRISM**	**P-value**		**R^2**	**N**
Winter VPD Modeled at CS2MET		0.1		0.297					0.000	**	0.591	47
Winter VPD Modeled at CS2MET		0.2				0.296			0.000	**	0.568	47
Winter VPD Modeled at CS2MET		0.2						0.340	0.000	**	0.609	47
April 1st SWE Santiam Junction		1200.3		-96.777					0.006	**	0.136	55
April 1st SWE Santiam Junction		1345.1				-124.994			0.001	**	0.216	44
April 1st SWE Santiam Junction		1368.0						-156.169	0.000	**	0.313	39
WS2 Winter Runoff Ratio		0.9		-0.031					0.029	*	0.087	55
WS8 Winter Runoff Ratio		0.7				-0.011			0.573		0.008	44
WS9 Winter Runoff Ratio		1.1						-0.060	0.004	**	0.205	39
WS2 Spring Runoff Ratio		1.1		-0.059					0.000	**	0.212	55
WS8 Spring Runoff Ratio		1.7				-0.131			0.000	**	0.355	44
WS9 Spring Runoff Ratio		1.0						-0.062	0.001	**	0.245	39
WS2 Spring Baseflow		323.1		-15.877					0.032	*	0.084	55
WS8 Spring Baseflow		509.8				-40.661			0.000	**	0.287	44
WS9 Spring Baseflow		300.8						-22.362	0.005	**	0.197	39
WS2 Summer Runoff Ratio		0.4		0.013					0.630		0.004	55
WS8 Summer Runoff Ratio		0.4				-0.001			0.942		0.000	44
WS9 Summer Runoff Ratio		0.3						0.030	0.356		0.023	39
WS2 Summer Baseflow		45.8		-0.578					0.696		0.003	55
WS8 Summer Baseflow		37.1				0.099			0.963		0.000	44
WS9 Summer Baseflow		36.8						0.477	0.880		0.001	39

Table I3. Simple linear cross-regressions with spring average minimum temperature as the explanatory variable.

Simple Linear Cross-Regressions with Spring Average Minimum Temperature as the Explantory Variable												
		Explanatory Variable Coefficients										
Dependent Variable		**Intercept**		**Spring Average Minimum Temperature WS2 PRISM**		**Spring Average Minimum Temperature WS8 PRISM**		**Spring Average Minimum Temperature WS9 PRISM**		**P-value**		**R^2**		**N**
Spring VPD Modeled at CS2MET		8.4		0.219						0.351		0.019		47
Spring VPD Modeled at CS2MET		8.6				0.304				0.189		0.038		47
Spring VPD Modeled at CS2MET		8.9						0.016		0.948		0.000		47
WS2 Spring Runoff Ratio		0.75		-0.039						0.107		0.048		55
WS8 Spring Runoff Ratio		0.87				-0.116				0.008	**	0.158		44
WS9 Spring Runoff Ratio		0.67						-0.045		0.104		0.070		39
WS2 Spring Baseflow		260.15		-24.048						0.019	**	0.100		55
WS8 Spring Baseflow		250.52				-39.384				0.009	**	0.153		44
WS9 Spring Baseflow		170.70						-5.920		0.598		0.008		39

Table I4. Simple linear cross-regressions with spring average maximum temperature as the explanatory variable.

Simple Linear Cross-Regressions with Spring Average Maximum Temperature as the Explantory Variable														
		Explanatory Variable Coefficients												
Dependent Variable		**Intercept**		**Spring Average Maximum Temperature WS2 PRISM**		**Spring Average Maximum Temperature WS8 PRISM**		**Spring Average Maximum Temperature WS9 PRISM**		**P-value**		**R^2**		**N**
Spring VPD Modeled at CS2MET		-1.0		0.708						0.000	**	0.405		47
Spring VPD Modeled at CS2MET		-1.0				0.715				0.000	**	0.420		47
Spring VPD Modeled at CS2MET		-2.3						0.706		0.000	**	0.398		47
WS2 Spring Runoff Ratio		1.05		-0.029						0.092		0.053		55
WS8 Spring Runoff Ratio		1.22				-0.036				0.267		0.029		44
WS9 Spring Runoff Ratio		1.15						-0.036		0.052		0.098		39
WS2 Spring Baseflow		607.10		-29.374						0.000	**	0.303		55
WS8 Spring Baseflow		535.06				-23.977				0.028	*	0.109		44
WS9 Spring Baseflow		403.57						-15.382		0.038	*	0.111		39

Table I5. Simple linear cross-regressions with summer average minimum temperature as the explanatory variable.

Simple Linear Cross-Regressions with Summer Average Minimum Temperature as the Explantory Variable												
		Explanatory Variable Coefficients										
Dependent Variable		**Intercept**		**Summer Average Minimum Temperature WS2 PRISM**		**Summer Average Minimum Temperature WS8 PRISM**		**Summer Average Minimum Temperature WS9 PRISM**		**P-value**		**R^2**		**N**
Summer VPD Modeled at CS2MET		-1.51		2.564						0.001	**	0.229		48
Summer VPD Modeled at CS2MET		5.08				2.235				0.002	**	0.190		48
Summer VPD Modeled at CS2MET		14.35						1.190		0.140		0.047		48
WS2 Summer Runoff Ratio		-0.29		0.079						0.098		0.051		55
WS8 Summer Runoff Ratio		0.13				0.028				0.447		0.014		44
WS9 Summer Runoff Ratio		1.06						-0.077		0.192		0.046		39
WS2 Summer Baseflow		55.46		-1.461						0.587		0.006		55
WS8 Summer Baseflow		59.04				-2.558				0.508		0.010		44
WS9 Summer Baseflow		133.21						-11.959		0.032	*	0.118		39

Table I6. Simple linear cross-regressions with summer average maximum temperature as the explanatory variable.

Simple Linear Cross-Regressions with Summer Average Maximum Temperature as the Explantory Variable												
		Explanatory Variable Coefficients										
Dependent Variable		**Intercept**		**Summer Average Maximum Temperature WS2 PRISM**		**Summer Average Maximum Temperature WS8 PRISM**		**Summer Average Maximum Temperature WS9 PRISM**		**P-value**		**R^2**		**N**
Summer VPD Modeled at CS2MET		-36.96		2.371						0.000	**	0.702		48
Summer VPD Modeled at CS2MET		-33.88				2.292				0.000	**	0.687		48
Summer VPD Modeled at CS2MET		-42.14						2.415		0.000	**	0.718		48
WS2 Summer Runoff Ratio		-1.71		0.087						0.000	**	0.249		55
WS8 Summer Runoff Ratio		-0.83				0.048				0.013	*	0.139		44
WS9 Summer Runoff Ratio		-0.35						0.030		0.359		0.023		39
WS2 Summer Baseflow		58.82		-0.694						0.602		0.005		55
WS8 Summer Baseflow		108.53				-2.828				0.174		0.044		44
WS9 Summer Baseflow		267.85						-8.403		0.005	**	0.197		39

Table I7. Simple linear cross-regressions with April 1st SWE at Santiam Junction as the explanatory variable.

Simple Linear Cross-Regression Models of Streamflow Variables to April 1st Snow Water Equivalent at Santiam Junction										
		Explanatory Variable Coefficients								
Dependent Variable[1]		**Intercept**		**Apr 1st SWE**		**P-value**		**R^2**	**Period**	**N**
WS2 Spring Runoff Ratio		0.51		0.0003		0.000	**	0.357	1953-2007	55
WS8 Spring Runoff Ratio		0.47		0.0006		0.000	**	0.609	1964-2007	44
WS9 Spring Runoff Ratio		0.48		0.0003		0.000	**	0.337	1969-2007	39
WS2 Summer Runoff Ratio		0.52		-0.0001		0.372		0.015	1953-2007	55
WS8 Summer Runoff Ratio		0.36		0.0000		0.769		0.002	1964-2007	44
WS9 Summer Runoff Ratio		0.49		-0.0001		0.426		0.017	1969-2007	39
WS2 Spring Baseflow		150.00		0.1101		0.000	**	0.278	1953-2007	55
WS8 Spring Baseflow		114.86		0.2178		0.000	**	0.595	1964-2007	44
WS9 Spring Baseflow		127.22		0.0827		0.003	**	0.210	1969-2007	39
WS2 Summer Baseflow		43.51		-0.0051		0.368		0.015	1953-2007	55
WS8 Summer Baseflow		34.99		0.0072		0.361		0.020	1964-2007	44
WS9 Summer Baseflow		41.00		-0.0032		0.775		0.002	1969-2007	39

Table I8. Simple linear cross-regressions of runoff ratio (discharge to PRISM precipitation) against VPD at PRIMET by season.

Simple Linear Cross-Regression Model of Runoff Ratio against Vapor Pressure Deficit (VPD) at PRIMET									
		Explanatory Variable Coefficients							
Dependent Variable		**Intercept**		**VPD**		**P-value**		**R^2**	**N**
WS2 Fall Runoff Ratio		0.23		-0.001		0.916		0.001	16
WS8 Fall Runoff Ratio		0.26		-0.008		0.388		0.054	16
WS9 Fall Runoff Ratio		0.20		0.005		0.581		0.022	16
WS2 Winter Runoff Ratio		0.67		0.027		0.702		0.010	17
WS8 Winter Runoff Ratio		0.51		0.040		0.487		0.033	17
WS9 Winter Runoff Ratio		0.72		-0.030		0.682		0.011	17
WS2 Spring Runoff Ratio		0.86		-0.024		0.026	*	0.290	17
WS8 Spring Runoff Ratio		0.96		-0.029		0.109		0.163	17
WS9 Spring Runoff Ratio		0.85		-0.030		0.010	**	0.368	17
WS2 Summer Runoff Ratio		-0.55		0.043		0.007	**	0.416	16
WS8 Summer Runoff Ratio		0.10		0.011		0.191		0.119	16
WS9 Summer Runoff Ratio		0.46		-0.001		0.940		0.000	16

Table I9. Simple linear cross-regressions of baseflows against VPD at PRIMET by season.

Simple Linear Cross-Regression Model of Baseflow against Vapor Pressure Deficit (VPD) at PRIMET									
		Explanatory Variable Coefficients							
Dependent Variable		**Intercept**		**VPD**		**P-value**		**R^2**	**N**
WS2 Fall Baseflow		52.61		-1.299		0.444		0.042	16
WS8 Fall Baseflow		65.23		-2.721		0.268		0.087	16
WS9 Fall Baseflow		55.71		-1.740		0.476		0.037	16
WS2 Winter Baseflow		286.15		-20.535		0.709		0.010	17
WS8 Winter Baseflow		184.57		0.452		0.991		0.000	17
WS9 Winter Baseflow		279.84		-62.529		0.175		0.119	17
WS2 Spring Baseflow		345.80		-15.104		0.017	*	0.323	17
WS8 Spring Baseflow		361.73		-16.173		0.055		0.224	17
WS9 Spring Baseflow		305.91		-14.481		0.015	*	0.334	17
WS2 Summer Baseflow		52.54		-0.308		0.716		0.010	16
WS8 Summer Baseflow		49.28		-0.533		0.456		0.040	16
WS9 Summer Baseflow		121.38		-3.459		0.001	**	0.547	16

Table I10. Simple linear cross-regressions of runoff ratio (discharge to PRISM precipitation) against modeled VPD at CS2MET by season

Simple Linear Cross-Regression Model of Runoff Ratio against Modeled Vapor Pressure Deficit (VPD) at CS2MET									
		Explanatory Variable Coefficients							
Dependent Variable		**Intercept**		**VPD**		**P-value**		**R^2**	**N**
WS2 Fall Runoff Ratio		0.41		-0.023		0.021	*	0.110	48
WS8 Fall Runoff Ratio		0.41		-0.028		0.007	**	0.167	42
WS9 Fall Runoff Ratio		0.35		-0.010		0.330		0.027	37
WS2 Winter Runoff Ratio		0.90		-0.084		0.035	*	0.095	47
WS8 Winter Runoff Ratio		0.74		-0.054		0.314		0.025	42
WS9 Winter Runoff Ratio		1.12		-0.170		0.001	**	0.277	37
WS2 Spring Runoff Ratio		0.72		-0.010		0.583		0.007	47
WS8 Spring Runoff Ratio		0.60		0.015		0.644		0.006	41
WS9 Spring Runoff Ratio		0.87		-0.032		0.084		0.085	36
WS2 Summer Runoff Ratio		-0.38		0.037		0.000	**	0.270	48
WS8 Summer Runoff Ratio		0.05		0.014		0.043	*	0.099	42
WS9 Summer Runoff Ratio		0.53		-0.003		0.815		0.002	37

Table I11. Simple linear cross-regressions of baseflows against modeled VPD at CS2MET by season

Simple Linear Regression Model of Baseflow against Modeled Vapor Pressure Deficit (VPD) at CS2MET									
		Explanatory Variable Coefficients							
Dependent Variable		**Intercept**		**VPD**		**P-value**		**R^2**	**N**
WS2 Fall Baseflow		121.89		-9.053		0.015	*	0.122	48
WS8 Fall Baseflow		97.24		-7.534		0.014	*	0.141	42
WS9 Fall Baseflow		89.52		-5.750		0.072		0.089	37
WS2 Winter Baseflow		531.10		-108.568		0.000	**	0.257	47
WS8 Winter Baseflow		374.84		-70.822		0.036	*	0.106	42
WS9 Winter Baseflow		612.90		-156.670		0.000	**	0.436	37
WS2 Spring Baseflow		376.60		-20.671		0.003	**	0.183	47
WS8 Spring Baseflow		269.27		-7.102		0.523		0.011	41
WS9 Spring Baseflow		328.45		-18.990		0.008	**	0.187	36
WS2 Summer Baseflow		50.69		-0.449		0.422		0.014	48
WS8 Summer Baseflow		67.61		-1.261		0.081		0.074	42
WS9 Summer Baseflow		131.77		-3.935		0.000	**	0.393	37

Table I12. Simple linear cross-regressions of winter runoff ratios (calculated with PRISM precipitation) at WS2, WS8, and WS9, against the coefficient of variation for precipitation at CS2MET.

Simple Linear Cross-Regression Model of Winter Runoff Ratio by Watershed against the Coefficient of Variation (COV) for Precipitation at CS2MET											
		Explanatory Variable Coefficients									
Dependent Variable		**Intercept**		**COV**		**P-value**		**R^2**		**Period**	**N**
WS2 Winter Runoff Ratio		1.05		-0.226		0.002	**	0.179		1958-2007	50
WS8 Winter Runoff Ratio		0.92		-0.225		0.012	*	0.140		1964-2007	44
WS9 Winter Runoff Ratio		1.00		-0.207		0.022	*	0.134		1969-2007	39

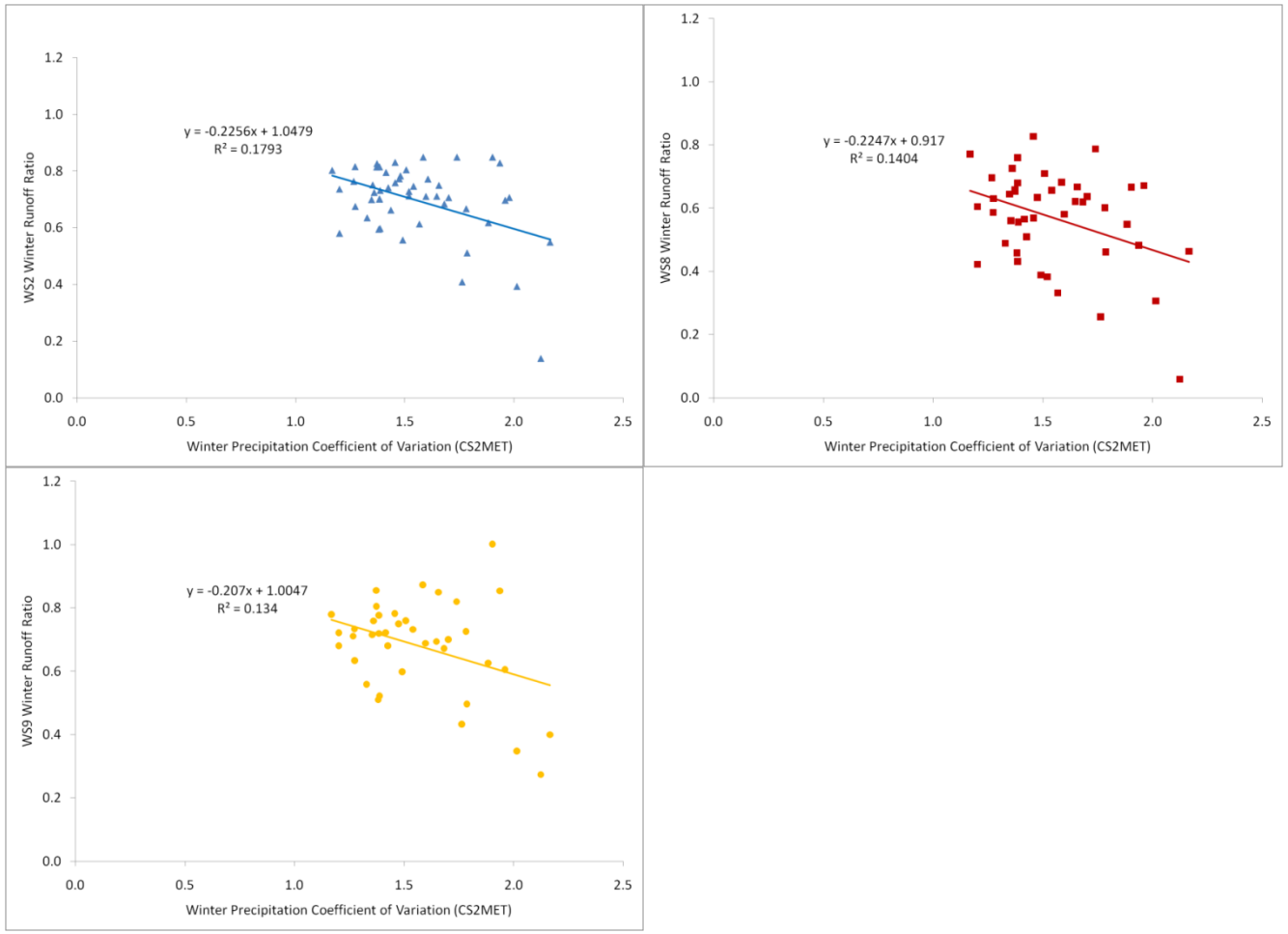

Figure I1. Winter runoff ratios (calculated using PRISM precipitation) for (clockwise from bottom left) WS9, WS2, and WS8, versus the coefficient of variation for precipitation at CS2MET.

Table I13. Simple linear cross-regressions of winter runoff ratios (calculated with PRISM precipitation) for WS2, WS8, and WS9, against winter average wind speed at PRIMET.

Simple Linear Cross-Regression Models of Winter Runoff Ratio by Watershed against Winter Average Wind Speed											
		Explanatory Variable Coefficients									
Dependent Variable		**Intercept**		**Winter Average Wind Speed**		**P-value**		**R^2**		**Period**	**N**
WS2 Winter Runoff Ratio		0.77		-0.213		0.208		0.060		1974-2006	28
WS8 Winter Runoff Ratio		0.64		-0.113		0.513		0.017		1974-2006	28
WS9 Winter Runoff Ratio		0.72		-0.023		0.904		0.001		1974-2006	28

Table I14. Simple linear cross-regressions of winter runoff ratios (calculated with PRISM precipitation) for WS2, WS8, and WS9, against winter average wind speed at PRIMET for the period since 1981.

Simple Linear Cross-Regression Models of Winter Runoff Ratio by Watershed against Winter Average Wind Speed since 1981											
		Explanatory Variable Coefficients									
Dependent Variable		**Intercept**		**Winter Average Wind Speed**		**P-value**		**R^2**		**Period**	**N**
WS2 Winter Runoff Ratio		0.76		-0.200		0.266		0.051		1981-2006	26
WS8 Winter Runoff Ratio		0.62		-0.075		0.674		0.007		1981-2006	26
WS9 Winter Runoff Ratio		0.72		-0.012		0.952		0.000		1981-2006	26

.

References

Aguado, E., Cayan, D., Riddle, L., and M. Roos, 1992: Climatic fluctuations and the timing of West Coast streamflow. Journal of Climate, 5, 1468-1493.

Barnard, H. R., 2009: Inter-relationships of Vegetation, Hydrology and Micro-climate in a Yong Douglas-fir forest. PhD dissertation, Oregon State University.

Barnett, T. P., Pierce, D. W., Hidalgo, H. G., Bonfils, C., Santer, B. D., Das, T., Bala, G., Wood, A. W., Nozawa, T., Mirin, A. A., Cayan, D. R., and M. D. Dettinger, 2008: Human-Induced Changes in the Hydrology of the Western United States. Science, 319, 5866, 1080–1083, 10.1126/science.1152538.

Black, B. A., Copenheaver, C. A., Frank, D. C., Stuckey, M. J., and R. E. Kormanyos, 2009: Multi-proxy reconstructions of northeastern Pacific sea surface temperature data from trees and Pacific geoduck. Palaeogeography Palaeoclimatology Palaeoecology, 278, 40-47.

Bond, B. J., Jones, J. A., Moore, G., Phillips, N., Post, D., and J. J. McDonnell, 2002: The zone of vegetation influence on baseflow revealed by diel patterns of streamflow and vegetation water use in a headwater basin. Hydrological Processes, 16, 1671-1677.

Bond, B.J. and K. L. Kavanagh, 1999: Stomatal behavior of four woody species in relation to lear-specific hydraulic conductance and threshold water potential. Tree Physiology, 19, 502-510.

Bond, B. J., Meinzer, F. C., and J. R. Brooks, 2007: How trees influence the hydrological cycle in forest ecosystems. *In*: Wood, Paul J; Hannah, David M; Sadler, Jonathan, eds. Hydroecology and ecohydrology: past, present and future. John Wiley & Sons. Ltd.: 7-35.

Brooks, J. R., Barnard, H. R., Coulombe, R., and J. J. McDonnell, 2010: Ecohydrologic separation of water between trees and streams in a Mediterranean climate. Nature Geoscience, 3, 100-104, 10.1038/NGEO722.

Cayan, D. R., Kammerdiener, S. A., Dettinger, M. D., Caprio, J. M., and D. H. Peterson, 2001: Changes in the onset of spring in the western United States. Bulletin of the American Meteorological Society, 82, 399–415.

Chen, J., Paw U, K. T., Ustin, S. L., Suchanek, T. H., Bond, B. J., Brosofske, K. D. and M. Falk, 2004: Net ecosystem exchanges of carbon, water and energy in young and old-growth Douglas-fir forests. Ecosystems 7, 534-544.

Christensen, J. H., Hewitson, B., Busuioc, A., Chen, A., Gao, X., Held, I., Jones, R., Kolli, R. K., Kwon, W-T., Laprise, R., Magaña Rueda, V., Mearns, C. G., Menéndez

J, Räisänen, J., Rinke, A., Sarr, A., and P. Whetton, 2007: Regional climate projections. *In* Climate Change 2007: The Physical Science Basis. Contribution of Working Group I to the Fourth Assessment Report of the Intergovernmental Panel on Climate Change, Solomon, S., Qin, D., Manning, M., Chen, Z., Marquis, M., Averyt, K. B., Tignor, M., and H. L. Miller (eds). Cambridge University Press: Cambridge; 847–940.

Christensen, L., Tague, C., and J. S. Baron, 2008: Spatial patterns of simulated transpiration response to climate variability in a snow dominated mountain ecosystem. Hydrological Processes, 22, 3576-3588, 10.1002/hyp.6961.

Daly, C., and W. McKee, 2009: Meteorological data from benchmark stations at the Andrews Experimental Forest. Long-Term Ecological Research, Forest Science Data Bank, Corvallis, OR. [Database]. Available: http://andrewsforest.oregonstate.edu/data/abstract.cfm?dbcode=MS001 (9 March 2010).

Das, T., Hidalgo, H. G., Dettinger, M. D., Cayan, D. R., Pierce, D. W., Bonfils, C., Barnett, T. P., Bala, G., and A. Mirin, 2009: Structure and detectability of trends in hydrological measures over the Western United States. Journal of Hydrometeorology, 10, 871-892.

Dettinger, M. D., and D. R. Cayan, 1995: Large-scale atmospheric forcing of recent trends toward early snowmelt runoff in California. Journal of Climate, 8, 606–623.

Dyrness, C. T. and G. Hawk, 1972: Vegetation and soils of the Hi-15 watersheds, H.J. Andrews Experimental Forest. Seattle: University of Washington; Coniferous Forest Biome Internal Report, 43, 28.

Emmingham, W. H., and R. H. Waring, 1977: An index of photosynthesis for comparing forest sites in western Oregon. Canadian Journal of Forest Research, 7, 165-174.

Emmingham, W.H. 1982. Ecological indexes as a means of evaluating climate, species distribution, and primary production, pp. 45-67 in R.L. Edmonds, ed. Analysis of coniferous forest ecosystems in the western United States Hutchinson Ross, Stroudsburg, PA.

Hawk, G., and C. T. Dyrness, 1972: Vegetation and soils of watersheds 2 and 3, H.J. Andrews Experimental Forest. Seattle: University of Washington; Coniferous For. Biome Internal Rep. 49. 48.

Hamlet, A. F., and D. P. Lettenmaier, 2005: Production of temporally consistent gridded precipitation and temperature fields for the continental United States. Journal of Hydrometeorology, 6, 330–336.

Hamlet, A.F., and D. P. Lettenmaier, 2007: Effects of 20th century warming and climate variability on flood risk in the western U.S.. Water Resources Research, 43, W06427, 10.1029/2006WR005099.

Hamlet, A. F., Mote, P. W., Clark, M. P., and D. P. Lettenmaier, 2005: Effects of temperature and precipitation variability on snowpack trends in the western U.S. Journal of Climate, 18, 4545–4561.

Hamlet, A. F., Mote, P. W., Clark, M. P., and D. P. Lettenmaier, 2007: 20th Century trends in runoff, evapotranspiration, and soil moisture in the western U.S. Journal of Climate, 20(8), 1468-1486.

Henshaw, D., and C. Creel, 2005: Meterological station locations, Andrews Experimental Forest. Long-Term Ecological Research, Forest Science Data Bank, Corvallis, OR. [Database]. Available: http://andrewsforest.oregonstate.edu/data/abstract.cfm?dbcode=MS026 (12 March 2010).

Hewlett, J. D., 1982: Principles of forest hydrology. University of Georgia Press, Athens, GA.

H. J. Andrews Experimental Forest Metadata Report (AND), p1-44, copyright Dante Da Sheperd, 2006. http://lterweb.forestry.oregonstate.edu/climhy//temp/AND.pdf

Jefferson, A., 2006: Hydrology and Geomorphic Evolution of Basaltic Landscapes, High Cascades, Oregon. PhD dissertation, Oregon State University.

Jefferson, A., Nolin, A., Lewis, S., and C. Tague, 2008: Hydrogeologic controls on streamflow sensitivity to climate variation. Hydrological Processes, 22, 4371–4385.

Johnson, S., and G. Lienkaemper, 2005: Experimental watershed boundaries and gaging station locations, Andrews Experimental Forest. Long-Term Ecological Research, Forest Science Data Bank, Corvallis, OR. [Database]. Available: http://andrewsforest.oregonstate.edu/data/abstract.cfm?dbcode=HF014 (12 March 2010).

Johnson, S., and J. Rothacher, 2009: Small watershed streamflow summaries at the Andrews Experimental Forest. Long-Term Ecological Research, Forest Science Data Bank, Corvallis, OR. [Database]. Available: http://andrewsforest.oregonstate.edu/data/abstract.cfm?dbcode=HF004 (9 March 2010).

Jones, J. A. and D. A. Post, 2004: Seasonal and successional streamflow response to forest cutting and regrowth in the northwest and eastern United States, Water Resources Research, 40, W05203, 10.1029/2003WR002952.

Knowles, N., Dettinger, M. D., and D. R. Cayan, 2006: Trends in Snowfall versus Rainfall in the Western United States. Journal of Climate. 19, 4545- 4559.

Law, B. E., Williams, M., Anthoni, P. M., Baldocchi, D. D., and M. H. Unsworth, 2000: Measuring and modelling seasonal variation of carbon dioxide and water vapour exchange of a Pinus ponderosa forest subject to soil water deficit. Global Change Biology 6: 613–630.

Link, T. E., Unsworth, M. H., and D. Marks, 2004: The dynamics of rainfall interception by a seasonal temperate rainforest. Agricultural and Forest Meteorology, 124, 171-191.

Little, J. S., Peterson, D. L., and M. Tjoelker, 2008: Douglas-fir growth in mountain ecosystems: water limits tree growth from stand to region. Ecological Monographs, 78, 349-368.

Luce, C. H. and Z. A. Holden, 2009: Declining annual streamflow distributions in the Pacific Northwest United States, 1948–2006. Geophysical Research Letters, 36, L16401, 10.1029/2009GL039407.

Mantgem, P. J. van, Stephenson, N. L., Byrne, J. C., Daniels, L. D., Franklin, J. F., Fulé, P. Z., Harmon, M. E., Larson, A. J., Smith, J. M., Taylor, A. H., and T. T. Veblen, 2009: Widespread Increase of Tree Mortality Rates in the Western United States, Science, 323, 5913, 521–524, 10.1126/science.1165000.

McCabe, G. J., and M. P. Clark, 2005: Trends and Variability in Snowmelt Runoff in the Western United States. Journal of Hydrometeorology, 6, 476–482.

Moore, G. W., Bond, B. J., Jones, J. A., Phillips, N., and F. C. Meinzer, 2004: Structural and compositional controls on transpiration in 40- and 450-year-old riparian forests in western Oregon, USA. Tree Physiology, 24, 481-491.

Mote, P. W., 2003: Trends in snow water equivalent in the Pacific Northwest and their climatic causes. Geophysical Research Letters, 30, 1601, 10.1029/2003GL017258.

Mote, P. W., 2006: Climate-driven variability and trends in mountain snowpack in western North America. Journal of Climate, 19, 6209–6220.

Mote, P. W., Hamlet, A. F., Clark, M. P., and D. P. Lettenmaier, 2005: Declining mountain snowpack in western North America. Bulletin of American Meteorological Society, 86, 39–49.

Nakawatase, J. M., and D. L. Peterson, 2006: Spatial variability in forest growth—climate relationships in the Olympic Mountains, Washington. Canadian Journal of Forest Research. 36, 77-91.

National Research Council, 2008: Hydrologic Effects of a Changing Forest Landscape. Water Science and Technology Board. National Academies Press, Washington, DC.

Nolin, A., and C. Daly C, 2006: Mapping "At Risk" snow in the Pacific Northwest. Journal of Hydrometeorology, 7, 1164–1171.

Perkins, R. M., 1997: Climatic and physiographic controls on peakflow generation in the western Cascades, Oregon. PhD thesis, Oregon State University, Corvallis, Oregon.

Perkins, R. M. and J. A. Jones, 2008: Climate variability, snow, and physiographic controls on storm hydrographs in small forested basins, western Cascades, Oregon. Hydrological Processes, 22, 4949–4964.

Post, D. A., and J. A. Jones, 2001: Hydrologic regimes of forested, mountainous, headwater basins in New Hampshire, North Carolina, Oregon, and Puerto Rico. Advances in Water Resources, 24, 1195-1210.

PRISM Climate Group, Oregon State University, http://www.prismclimate.org (5/28/09).

Regonda, S. K., Rajagopalan, B., Clark, M., and J. Pitlick, 2005: Seasonal Cycle Shifts in Hydroclimatology over the Western United States. Journal of Climate, 18, 372-384.

Royce, E. B., and M. G. Barbour, 2001: Mediterranean climate effects. I. Conifer water use across a Sierra Nevada ecotone. American Journal of Botany, 88, 911–918.

Soule, P.T., and P. A. Knapp, 2006: Radial growth rate increases in naturally occurring ponderosa pine trees: a late-20th century CO2 fertilization effect? New Phytologist, 171, 379–390.

Stewart, I. T., 2009: Changes in snowpack and snowmelt runoff for key mountain regions. Hydrological Processes, 23, 78-94, 10.1002/hyp.7128.

Stewart, I. T., Cayan, D. R., and M. D. Dettinger, 2005: Changes toward earlier streamflow timing across western North America. Journal of Climate, 18, 1136–1155.

Tague, C., and G. Grant, 2009: Groundwater dynamics mediate low-flow response to global warming in snow-dominated alpine regions. Water Resources Research, 45, W07421, 10.1029/2008WR007179.

Tague, C., Heyn, K., and L. Christensen, 2009: Topographic controls on spatial patterns of conifer transpiration and net primary productivity under climate warming in mountain ecosystems. Ecohydrology, 2, 541–554.

Taiz, L. and E. Zeiger, 1991: Plant Physiology. The Benjamin/Cummings Publishing Company, Inc, New York.

Tyree, M. T. and J. S. Sperry, 1998: Do woody plants operate near the point of catastrophic xylem dysfunction caused by dynamic water stress? Plant Physiology, 88, 574-580.

Unsworth, M.H., Phillips, N., Link, T., Bond, B.J., Falk, M., Harmon, M.E., Hinckley, T.M., Marks, D., and K. Tha Paw U, 2004: Components and controls of water flux in an old-growth Douglas-fir—western hemlock ecosystem. Ecosystems, 7, 468-481.

Valentine, T., and G. Lienkaemper, 2005: 30 meter digital elevation model (DEM) clipped to the Andrews Experimental Forest. Long-Term Ecological Research, Forest Science Data Bank, Corvallis, OR. [Database]. Available: http://andrewsforest.oregonstate.edu/data/abstract.cfm?dbcode=GI002 (12 March 2010).

Whitehead, D., 1998: Regulation of stomatal conductance and transpiration in forest canopies. Tree Physiology, 18, 633-644.

Wilson, K. B., Hanson, P. J., Mulholland, P. J., Baldocchi, D. D., and S. D. Wullschleger, 2001: A comparison of methods for determining forest evapotranspiration and its components: sap-flow, soil water budget, eddy covariance and catchment water balance. Agricultural and Forest Meteorology, 106, 153–168.

Winner, W. E., Berry, J., Bond, B. J., Cooper, C., Hinckley, T., Ehleringer, J., Fessenden, J., Lamb, B., McCarthy, S., McDowell, N., Phillips, N., Thomas, S.C., and M. Williams, 2004: Canopy carbon gain and water use: Analysis of old growth conifers in the Pacific Northwest. Ecosystems, 7, 482-497.

Wondzell, S. M., Gooseff, M. N., and B. L. McGlynn, 2007. Flow velocity and the hydrologic behavior of streams during baseflow. Geophysical Research Letters, 34, L24404, 10.1029/2007GL31256.

Wondzell, S. M., Gooseff, M. N., and B. L. McGlynn, 2010: An analysis of alternative conceptual models relating hyporheic exchange flow to diel fluctuations in discharge during baseflow recession. Hydrological Processes, 24, 686-694.

Zhao, F., Zhang, L., Xu, Z., and D. F. Scott, 2010: Evaluation of methods for estimating the effects of vegetation change and climate variability on streamflow. Water Resources Research, 46, W03505, 10.1029/2009WR007702.